

Stem Cell Expansion and Bioreactor Development

Anil Shiva Ramlogan

2010

Stem Cell Expansion and Bioreactor Development

Anil Shiva Ramlogan

2010

School of Engineering and Materials Science
Queen Mary University of London

**This thesis is submitted for the degree of Doctor of Philosophy, University of
London**

Abstract

A major challenge to the clinical success of cell-based tissue engineering strategies is the ability to obtain sufficient numbers of cells within an acceptable time frame. The expansion of cells on microcarriers within spinner flask bioreactor has shown promise in meeting that challenge. Spinner flask microcarrier technology is space-saving and media utilisation efficient. However, further optimisation in terms of, for example, seeding efficiency, expansion rates and harvest efficiency is necessary to realise the clinical potential of this technology. The present work is designed to improve cell expansion rates. It involves investigation of microcarrier composition and surface structure and spinner flask shear stress on cell growth.

BMSC growth on PHBV microcarriers was superior to PCL and PLGA microcarriers and comparable to Cytodex 1 microcarriers. Lower density PHBV microcarriers showed promise as a superior alternative to Cytodex 1. Two different impeller designs employed in the w/o/w method of microcarrier synthesis resulted in smoother and rougher PCL microcarriers with $R_a = 1.77 \pm 0.42 \mu\text{m}$ to $6.4 \pm 1.48 \mu\text{m}$ respectively. Superior BMSC growth was observed on the rougher PCL microcarriers. Differentiation potential along the osteogenic and adipogenic lineages of BMSCs expanded on the microcarrier types was retained.

Particle Image Velocimetry was used to quantify shear stress within a spinner flask bioreactor. It was found that 80% of the shear stress was localised within the impeller region which occupied 55% of the bioreactor working volume. Shear stress increased as Cytodex 1 microcarrier concentration and impeller rotational speed increased. Superior BMSC growth rates on microcarriers were observed for the lowest shear stress experimental group ($3.4 \times 10^{-3} \text{ N/m}^2 \leq \text{impeller region mean shear stress} \leq 4.6 \times 10^{-3} \text{ N/m}^2$) as compared to the three higher shear stress groups ($5.5 \times 10^{-3} \text{ N/m}^2 \leq \text{mean shear stress} \leq 1.3 \times 10^{-2} \text{ N/m}^2$). Expanded BMSCs on the cytodex 1 microcarriers retained multipotentiality for the range of shear stresses investigated.

Acknowledgements

Firstly, the author praises the Almighty God for facing the challenges of scientific research. Without His help, there would be no understanding. In addition, special thanks are in order for his family, with members both near and far.

The author wishes to thank the students and staff of Queen Mary University of London, Royal London Hospital, Progentix B.V. (The Netherlands), Progentix Orthobiology B.V. (The Netherlands) and Xpand Biotechnology B.V. (The Netherlands) for their kind and generous support throughout this project. The author would like to thank Prof. Joost D. de Bruijn for his guidance over the years. Many thanks are due to Prof. Chris Lawn and Dr. Catherine Gardner, for guidance with respect to the Particle Image Velocimetry studies. Special thanks to group members: Dr. Raheleh Ahmadi and Dr. Kruba Shankar Sivasubramanyam.

IOM³ Andrew Carnegie Research Fund, Armourers and Brasiers Company and a joint Armourers and Brasiers Company – Corus fund sponsored presentation of work (oral and poster) at the following conferences: Tissue Engineering International & Regenerative Medicine Society (TERMIS), European Society for Biomaterials (ESB). The Royal Academy of Engineering (grant reference F7-612) and the Society of Chemical Industry (SCI) sponsored a three-week overseas research visit. The Institute of Chemical Engineers (IChemE) short-listed aspects of this work for the Bioprocessing Award at the 2010 IChemE Awards of Innovation and Excellence. The School of Engineering and Materials Science sponsored the trip to the ceremony in Manchester.

Inspiration and encouragement on the pursuit of the PhD came from Prof. Dietmar W. Huttmacher and Assist. Prof. Tong Yen-Wah. The author is grateful for the year spent

under their supervision prior to the commencement of this PhD project. Special thanks are due to my examiners, Dr. Richard A. Black and Prof. Gary J. Lye. The former travelled through the snowfalls in Glasgow to examine me; the latter prepared me for my exchange year in Singapore during my undergraduate degree, which led to the creation of this thesis.

a.s.ramlogan@qmul.ac.uk

<http://www.sems.qmul.ac.uk/news/?eid=2342>

Table of Contents

Abstract	3
Acknowledgements	4
Table of Contents	6
Nomenclature	16
List of Figures	18
List of Tables.....	30
List of Equations	32
1 Literature Review	33
1.1 Introduction	33
1.2 Stem Cells.....	33
1.2.1 Stem Cell Hierarchy	34
1.2.2 Stem Cell Niches.....	36
1.2.3 Dedifferentiation, Redifferentiation, Transdifferentiation and Plasticity .	36
1.3 Mesenchymal Stem Cells	37
1.3.1 Characteristics	38
1.3.2 Identification	40
1.3.3 Differentiation	41

1.3.3.1	Osteogenic Lineage.....	41
1.3.3.2	Adipogenic Lineage.....	41
1.3.3.3	Chondrogenic Lineage.....	41
1.4	Scaffolds.....	42
1.4.1	Scaffolds and Cell Expansion Techniques.....	42
1.4.2	Scaffold Manufacture.....	43
1.4.3	Polymers.....	43
1.4.4	Polymer Candidates.....	44
1.4.4.1	PHBV [poly (3-hydroxybutyrate-co-3-hydroxyvalerate)].....	45
1.4.4.2	PCL [poly (ϵ -caprolactone)].....	46
1.4.4.3	PLGA [polyglycolide-co-lactide].....	47
1.5	Bioreactors.....	48
1.5.1	Static Systems.....	48
1.5.2	Spinner Flasks and Stirred-tanks.....	48
1.5.3	Rotating Wall Vessel.....	51
1.5.4	Biowave Reactor.....	52
1.5.5	Perfusion Bioreactor.....	53
1.6	Fluid Flow.....	56

1.7	Particle Image Velocimetry	58
1.8	Aims and Objectives of the Thesis	61
2	The Preparation and Characterisation of PHBV, PCL and PLGA microcarriers for cell expansion.....	62
2.1	Abstract	62
2.2	Introduction	63
2.3	Materials and Method.....	66
2.3.1	Polymeric Raw Materials.....	66
2.3.2	Microcarrier Synthesis	66
2.3.3	Surface area measurements	68
2.3.4	Spectroscopy	68
2.3.5	Scanning Electron Microscopy	69
2.4	Results	70
2.4.1	Spectroscopy	70
2.4.1.1	PHBV.....	70
2.4.1.2	PCL	72
2.4.1.3	PLGA.....	73
2.4.2	Scanning Electron Microscopy	75
2.4.3	Microcarrier Surface Area.....	78

2.5	Discussion	79
2.6	Conclusion.....	82
3	PHBV, PCL and PLGA Microcarriers support the Attachment and Proliferation of Human BMSCs	83
3.1	Abstract	83
3.2	Introduction	84
3.3	Materials and Method.....	86
3.3.1	Human BMSC Sources	86
3.3.2	Proliferation Medium for Human BMSCs.....	86
3.3.3	Osteogenic Medium for Human BMSCs	87
3.3.4	Adipogenic Medium for Human BMSCs	87
3.3.5	Pre-culture	87
3.3.6	Microcarrier Sterilisation, Cleaning and Pre-conditioning	88
3.3.7	Cell Seeding	88
3.3.8	BMSC Growth Analysis	89
3.3.9	Human BMSC Harvest	90
3.3.10	Differentiation of harvested human BMSCs.....	91
3.3.10.1	Osteogenic Differentiation.....	91
3.3.10.2	Adipogenic Differentiation.....	91

3.3.11	Microscopy.....	92
3.3.12	Statistical Analysis	92
3.4	Results	94
3.5	Discussion	100
3.6	Conclusion.....	103
4	BMSC Expansion on Microcarriers: The Effect of Surface Microstructure.....	104
4.1	Abstract	104
4.2	Introduction	105
4.3	Materials and Method.....	108
4.3.1	Microcarrier Synthesis and Surface Roughness Alteration	108
4.3.2	Scanning Electron Microscopy	109
4.3.3	Laser Profilometry	109
4.3.4	Human BMSC Sources	110
4.3.5	MSC Pre-cultivation, Culture, Population Monitor, Harvest and Differentiation	111
4.3.6	Microscopy.....	111
4.3.7	Statistical Analyses	111
4.4	Results	112
4.4.1	Scanning Electron Microscopy	114

4.4.2	Environmental SEM.....	115
4.4.3	Laser Profilometry	116
4.4.4	Human BMSC Population Analyses.....	118
4.4.5	Differentiation into the osteogenic and adipogenic lineages	121
4.5	Discussion	122
4.6	Conclusion.....	125
5	The Use of Particle Imaging Velocimetry to assess shear stress within a Spinner Flask Bioreactor	126
5.1	Abstract	126
5.2	Introduction	127
5.3	Materials and Method.....	130
5.3.1	Experimental Groups	130
5.3.2	Rheometer	130
5.3.3	Identification of Aqueous Glycerol Solutions with Matching Experimental Group Viscosities	131
5.3.4	PIV Replica and Impeller.....	131
5.3.5	Tracers.....	133
5.3.6	PIV Set-up and Procedure.....	134
5.3.7	PIV Data Processing	136

5.3.8	Shear stress, Fluid Regime and Relaxation Time	137
5.3.9	Statistical Analysis	139
5.4	Results and Discussion	140
5.4.1	Determination of PIV conditions which reflect the bioreactor conditions 140	
5.4.2	Relaxation Times and Reynolds Number	142
5.4.3	Cytodex 1 microcarrier as tracers	144
5.4.4	Evaluation of Shear Stress within Spinner Flask Bioreactor	145
5.5	Conclusion.....	155
6	The Effect of Cytodex 1 Microcarrier Concentration and Impeller Speed on the expansion of BMSCs within a Spinner Flask Bioreactor.....	156
6.1	Abstract	156
6.2	Introduction	157
6.3	Materials and Method.....	160
6.3.1	Human BMSC Sources	160
6.3.2	Proliferation Medium for Human BMSCs.....	160
6.3.3	Osteogenic Medium for Human BMSCs	160
6.3.4	Adipogenic Medium for Human BMSCs	160

6.3.5	Standard Medium for the Differentiation of Human BMSCs along the Chondrogenic Lineage	160
6.3.6	Spinner Flask/Microcarrier Sterilisation	161
6.3.7	Pre-culture	161
6.3.8	Cell Seeding	161
6.3.9	BMSC Growth Analysis	162
6.3.10	BMSC Harvest	163
6.3.11	Multipotency	163
6.3.11.1	Osteogenic lineage	163
6.3.11.2	Adipogenic lineage	165
6.3.11.3	Chondrogenic lineage	165
6.3.12	Statistical Analysis	166
6.4	Results	167
6.4.1	BMSC Expansion	167
6.4.2	BMSC Multipotency	172
6.5	Discussion	176
6.6	Conclusion	180
7	General Discussion	181

7.1	The Characterisation of PHBV, PCL and PLGA microcarriers and their support of the attachment and proliferation of BMSCs	181
7.2	BMSC Expansion on Microcarriers: The Effect of Surface Microstructure ..	184
7.3	The Use of Particle Imaging Velocimetry to assess shear within a Spinner Flask Bioreactor	186
7.4	The Effect of Cytodex 1 Microcarrier Concentration and Impeller Speed on the expansion of BMSCs within a Spinner Flask Bioreactor.....	187
7.5	Future Work and General Considerations	190
7.6	Concluding Remarks	191
8	Appendices.....	193
8.1	Sample calculation of Microcarrier Surface Area	193
8.2	Pilot Study quantitatively assessing the growth of Goat BMSCs on PHBV, PCL and PLGA microcarriers	195
8.3	The alamarBlue™ assay to construct a Standard Curve for the quantification of cell numbers	198
8.4	Rough and Smooth Microcarriers	200
8.5	Data for two other donors supplementary to chapter 3	203
8.6	Data for two other donors supplementary to chapter 4	207
8.7	Analysis of raw PIV data.....	211
9	Promotion of Research.....	213

9.1	List of Award Shortlists	213
9.2	List of Publications.....	213
9.3	List of Presentations (*presenting author).....	214
9.4	List of Travel Grant Awards.....	215
9.5	Student Research Management	216
10	References	218

Nomenclature

2D	Two-dimensional
3D	Three-dimensional
BMSC	Bone Marrow Stromal Cells
DMEM	Dulbecco's Modified Eagle's Medium
ES cells	Embryonic Stem cells
EPC	Endothelial Progenitor Cells
FGF	Fibroblast Growth Factors
FTIR	Fourier Transform InfraRed
HSC	Hematopoietic Stem Cells
IMS	Industrial Methylated Spirit
MSC	Mesenchymal Stem Cells
PBS	Phosphate Buffered Saline
PCL	Poly (ϵ -caprolactone)
PHB	Poly(3-hydroxybutyrate)
PHBV	Poly(3-hydroxybutyrate- <i>co</i> -3-hydroxyvalerate)
PHBV (5%)	Poly(3-hydroxybutyrate- <i>co</i> -3-hydroxyvalerate) (5% HV content)
PLGA	Polyglycolide- <i>co</i> -lactide

PVA	Polyvinyl alcohol
TGF	Transforming Growth Factor
SEM	Scanning Electron Microscopy
UV	Ultraviolet

Symbol	Definition	Units
μ	specific growth rate	s^{-1}, h^{-1}
t_d	doubling time	hours
x_t	cell population at time-point t	cells
x_0	cell population at time-point 0	cells
Δt	time-frame	hours
τ	shear stress	N/m^2
N_i	impeller speed	rpm, rps, s^{-1}
D_i	impeller diameter	mm, cm, m
Re	reynolds number	n/a
ρ	ρ = density	$kg/m^{-3}, g/l, g/ml$
μ	viscosity	$N s/m^2, kg/ms$
$\nu,$	kinematic viscosity	m^2/s
$t_{residence}$	fluid residence time	s
$t_{relaxation}$	particle relaxation or response time	s
V	reactor size	m^3
F	flow rate	m^3/s
ρ_p	particle density	$kg/m^{-3}, g/l, g/ml$
d_p	particle diameter	microns
$\dot{\gamma}$	shear rate	s^{-1}

List of Figures

FIGURE 1: THE PATH OF THE EMBRYO WHICH IS TRANSPORTED ALONG THE FALLOPIAN TUBE AND THEN IMPLANTED IN THE UTERINE WALL. ON THE RIGHT HAND SIDE OF THE DIAGRAM, A SPERMATOOZA HAS FERTILISED THE OOCYTE (FERTILIZATION). THIS IS KNOWN AS THE ZYGOTE AND IS TOTIPOTENT. THE FIRST MITOTIC DIVISION AT 36 HOURS HAS YIELDED TWO DAUGHTER CELLS WHICH ARE STILL TOTIPOTENT, EACH OF WHICH DIVIDE AGAIN TO FORM TOTIPOTENT STEM CELLS. SPECIALISATION OCCURS WHICH RESULTS IN A HOLLOW BALL OF CELLS (BLASTOCYST) AND A CLUSTER OF CELLS (ICM), WHICH ARE THE EMBRYONIC STEM CELLS. (DRIFE 2004)	35
FIGURE 2: THE MESENGENIC PROCESS. A DEPICTION OF A MESENCHYMAL STEM CELL PROLIFERATING, AND THEN DIFFERENTIATING INTO SEVERAL LINEAGES WHICH RESULT IN THE FORMATION OF BONE, CARTILAGE, MUSCLE, MARROW, TENDON/LIGAMENT AND CONNECTIVE TISSUE. (CAPLAN AND BRUDER 2001).....	39
FIGURE 3: CHEMICAL STRUCTURE OF PHBV, WHICH IS MADE UP OF THE CO-POLYMERS PHB (PORTION 1) AND HV (PORTION 2).....	45
FIGURE 4: CHEMICAL STRUCTURE OF PCL	46
FIGURE 5: CHEMICAL STRUCTURE OF PLGA WHICH IS A CO-POLYMER OF LACTIC ACID (PORTION 1) AND GLYCOLIC ACID (PORTION 2).....	47
FIGURE 6: SPINNER FLASK MANUFACTURED BY BELLCO GLASS INC (USA). IT IS USED SPECIFICALLY FOR MICROCARRIER CULTURE AND HAS A WORKING VOLUME OF UP TO 100 ML. THE IMPELLER IS COLOURED WHITE AND HAS A MAGNET ATTACHED TO IT. A MAGNETIC STIRRER IS USED TO ROTATE THE IMPELLER.	49
FIGURE 7: BASIC MAKE-UP OF A ROTATING-WALL VESSEL REACTOR TAKEN FROM (HAMMOND AND HAMMOND 2001) AND ORIGINATING FROM THE ARTICLE OF	

(GOODWIN ET AL. 1993A). BASICALLY THE BIOREACTOR FROM THE LEFT-HAND SIDE IS ATTACHED HORIZONTALLY TO THE END-PIECE ON THE RIGHT-HAND SIDE. ROTATION IS RELATIVE TO THE HORIZONTAL AXIS; ROTATION IN THE SPINNER FLASK FROM THE PRECEDING SECTION IS ALONG THE VERTICAL AXIS. 51

FIGURE 8: PICTURE OF A BIOWAVE REACTOR TAKEN AT XPAND BIOTECHNOLOGY BV (THE NETHERLANDS). THE RED LIQUID IS MEDIUM LOCATED IN A BAG. BELOW THE BAG LIES THE ROCKING UNIT WHICH MOVES THE TRAY FROM SIDE-TO-SIDE THEREBY CREATING A DYNAMIC ENVIRONMENT WITHIN THE MEDIUM. 52

FIGURE 9: THE PERFUSION SYSTEM CONSISTS OF THE ANCILLARY EQUIPMENT AND THE PERFUSION BIOREACTOR. THERE ARE TWO PERFUSION BIOREACTORS IN THIS PICTURE AND THEY ARE THE TWO PETRIDISHES LOCATED IN THE MIDDLE OF THE TWO RELATIVELY LARGE PUMPS. THE DURAN BOTTLES REPRESENT THE CULTURE MEDIUM RESERVOIR AND THE WASTE RESERVOIR. HUMAN EMBRYONIC STEM CELLS WERE EXPANDED IN THE PERFUSION BIOREACTORS. (FONG ET AL. 2005)..... 54

FIGURE 10: MEDIUM FLOWS IN A DOWNWARD DIRECTION THROUGH A SCAFFOLD WITH ATTACHED CELLS. THIS SCAFFOLD IS HELD IN PLACE BY THE SCAFFOLD AND DOES NOT MOVE WHATSOEVER. HENCE, THE CULTURE MEDIUM FLOWS THROUGH OR PERFUSES THE SCAFFOLD. (BANCROFT ET AL. 2003) 55

FIGURE 11: IN (A) PLUG FLOW, THE FLUID STREAMS HAVE EQUAL VELOCITY RESULTING IN A STRAIGHT LINE PROFILE. THE STREAM VELOCITIES DIFFER IN (B) TURBULENT FLOW AND (C) LAMINAR FLOW RESULTING IN MORE PARABOLIC PROFILES. (DORAN 2002)57

FIGURE 12: AN EXAMPLE OF AN EXPERIMENTAL ARRANGEMENT FOR PIV (RAFFEL ET AL. 2007). 58

FIGURE 13: THE SURFACE AREA OF MICROCARRIERS WITHIN THE SPINNER FLASK ON THE RIGHT IS EQUIVALENT TO THE SURFACE AREA OF THE T-FLASKS WITHIN THE INCUBATOR.63

FIGURE 14: MICROCARRIER SYNTHESIS67

FIGURE 15: SPECTRA OF THE RAW AND SYNTHESISED MICROCARRIER PHBV.....70

FIGURE 16: PHBV. 1 – PHB (POLYHYDROXYBUTYRATE) PORTION; 2 – HV (HYDROXYVALERATE) PORTION.71

FIGURE 17: COMPARISON OF SPECTRA FOR THE RAW STARTING MATERIAL AND PCL MICROCARRIERS.....72

FIGURE 18: CHEMICAL STRUCTURE OF PCL72

FIGURE 19: COMPARISON OF THE SPECTRA OF RAW STARTING MATERIAL AND PLGA MICROCARRIERS.....73

FIGURE 20: CHEMICAL STRUCTURE OF PLGA. IT IS A CO-POLYMER OF LACTIC ACID (PORTION 1) AND GLYCOLIC ACID (PORTION 2).....73

FIGURE 21: SURFACE TOPOGRAPHY OF DRY PHBV, PCL, PLGA AND CYTODEX 1 MICROCARRIERS. THE WORKING DISTANCE WAS 10 MM AND THE MAGNIFICATION WAS SET AT X 1000 WITH A WORKING DISTANCE OF 9.9 MM.....75

FIGURE 22: SURFACE TOPOGRAPHY OF DRY PHBV, PCL, PLGA AND CYTODEX 1 MICROCARRIERS. PHBV, PCL AND PLGA WERE AT X 15000 WITH A WORKING DISTANCE OF 19.0 MM. THE CYTODEX 1 MICROCARRIER WAS AT X 120000 WITH A WORKING DISTANCE OF 10.1 MM.76

FIGURE 23: PHBV, PCL AND PLGA MICROCARRIERS SUBJECTED TO DIFFERENT TEMPERATURES AND HUMIDITIES USING THE ENVIRONMENTAL SEM (WORKING DISTANCE OF 5.4 MM AND MAGNIFICATION OF X 400). THE WET CYTODEX 1 IMAGE

<p>WAS OBTAINED USING THE LIGHT MICROSCOPE; THE DRY CYTODEX 1 IMAGE WAS OBTAINED USING SEM.</p>	77
<p>FIGURE 24: HUMAN BMSC GROWTH ON THE DIFFERENT SCAFFOLD TYPES OVER A 120-HOUR PERIOD. NOTE THAT THE SEEDING DENSITY APPLIED WAS 2000 BMSCs/CM² AT TIME 0 HOURS.....</p>	94
<p>FIGURE 25: HUMAN BMSC POPULATION DOUBLINGS ON THE SCAFFOLD TYPES. THE DATA WAS CALCULATED UTILISING BMSC POPULATION NUMBERS AT TIME-POINTS 24 AND 120 HOURS.</p>	96
<p>FIGURE 26: HUMAN BMSC DOUBLING TIMES ON THE SCAFFOLD TYPES. THE DATA WAS CALCULATED UTILISING BMSC POPULATION NUMBERS AT TIME-POINTS 24 AND 120 HOURS.</p>	96
<p>FIGURE 27: LIGHT (L) AND FLUORESCENCE (F) MICROGRAPHS OF HUMAN BMSCs ON MICROCARRIERS AND WELL-PLATES AFTER 24 AND 120 HOURS AFTER SEEDING. THE GREEN COLOUR IN THE FLUORESCENT MICROGRAPHS INDICATES LIVE CELLS, WHICH CORRESPONDINGLY SHOWS THE LOCATION OF THE CELLS IN LIGHT MICROGRAPHS. THE WHITE SCALE BAR REPRESENTS 200µM. MAGNIFICATION WAS AT X100. ONLY LIGHT MICROGRAPHS ARE SHOWN FOR THE 2D CONTROL.....</p>	97
<p>FIGURE 28: DAY 12 ALP STAINING ON THE THREE EXPERIMENTAL GROUPS (PHBV, PCL AND PLGA) AND THE TWO CONTROL GROUPS (CYTODEX 1 AND 2D WELL-PLATES), WHICH WERE ALL HARVESTED BMSCs SUBJECTED TO OSTEOGENIC MEDIUM (PLUS DEXAMETHASONE). A 2D WELL-PLATE GROUP SUBJECTED TO PROLIFERATION MEDIUM (MINUS DEXAMETHASONE) WAS INTRODUCED AS A NEGATIVE CONTROL. ..</p>	98
<p>FIGURE 29: DAY 21 LIGHT MICROGRAPHS OF HARVESTED BMSCs FROM THE EXPERIMENTAL (PHBV, PCL AND PLGA MICROCARRIERS) AND CONTROL</p>	

(CYTODEX 1 AND 2D) GROUPS SUBJECTED TO ADIPOGENIC MEDIA AND THE 2D GROUP SUBJECTED TO PROLIFERATION MEDIA (NEGATIVE CONTROL)..... 99

FIGURE 30: PROPELLER-DESIGN IMPELLER (30 MM DIAMETER) ON THE LEFT-HAND SIDE FOR THE PRODUCTION OF SMOOTHER PCL MICROCARRIER SURFACES. PITCH-BLADE IMPELLER (49 MM DIAMETER) ON THE RIGHT-HAND SIDE FOR THE PRODUCTION OF ROUGHER PCL MICROCARRIER SURFACES..... 108

FIGURE 31: THE VARIABLE COMPONENTS OF THE SURFACE ROUGHNESS PARAMETERS. X REPRESENTS THE MICROCARRIER DIAMETER AND L REPRESENTS DIAMETER INTERVALS. $Z(x)$ REPRESENTS THE AMPLITUDE..... 109

FIGURE 32: EXTERNAL MORPHOLOGIES OF PCL-S (LEFT-HAND SIDE) AND PCL-R (RIGHT-HAND SIDE) MICROCARRIERS AT TWO DIFFERENT MAGNIFICATIONS AT 10kV. THE WORKING DISTANCE AND MAGNIFICATION OF THE TOP IMAGES WERE 10 MM AND X1000 RESPECTIVELY, AND OF THE BOTTOM IMAGES WERE 19 MM AND X1500 RESPECTIVELY..... 114

FIGURE 33: PCL-S AND PCL-R SUBJECTED TO DIFFERENT TEMPERATURES AND HUMIDITIES USING THE ENVIRONMENTAL SEM..... 115

FIGURE 34: LASER PROFIOMETRY SCANS OF PCL-S AND PCL-R MICROCARRIERS..... 116

FIGURE 35: SURFACE ROUGHNESS PARAMETERS (R_A , R_Q AND R_{ZDIN}) OF PCL-R AND PCL-S WHICH WERE OBTAINED FROM THE LASER PROFILOMETER SCANS. 117

FIGURE 36: HUMAN BMSC POPULATIONS ON THE DIFFERENT SCAFFOLD TYPES OVER A 120-HOUR PERIOD. CYTODEX 1 IS THE 3D CONTROL AND WELL-PLATES ARE THE 2D CONTROL. THE SEEDING DENSITY OF 2000 BMSCs/cm² WAS APPLIED AT TIME 0 HOURS..... 118

FIGURE 37: HUMAN BMSC POPULATION DOUBLINGS ON THE SCAFFOLD TYPES. THE DATA WAS CALCULATED UTILISING BMSC POPULATION NUMBERS AT TIME-POINTS 24 AND 120 HOURS. 119

FIGURE 38: HUMAN BMSC DOUBLING TIMES ON THE SCAFFOLD TYPES. THE DATA WAS CALCULATED UTILISING BMSC POPULATION NUMBERS AT TIME-POINTS 24 AND 120 HOURS. 119

FIGURE 39: LIGHT (L) AND FLUORESCENCE (F) MICROGRAPHS OF HUMAN BMSCs ON MICROCARRIERS AND WELL-PLATES AFTER 24 AND 120 HOURS AFTER SEEDING. THE GREEN COLOUR IN THE FLUORESCENT MICROGRAPHS INDICATES LIVE CELLS, WHICH CORRESPONDINGLY SHOWS THE LOCATION OF THE CELLS IN LIGHT MICROGRAPHS. THE WHITE SCALE BAR REPRESENTS 200 μ m. MAGNIFICATION WAS AT X100. ONLY LIGHT MICROGRAPHS ARE SHOWN FOR THE 2D CONTROL. 120

FIGURE 40: DAY 12 ALP AND OIL RED O STAINING ON THE TWO EXPERIMENTAL GROUPS (PCL-S AND PCL-R) AND THE TWO CONTROL GROUPS (CYTODEX 1 AND 2D WELL-PLATES), WHICH WERE ALL HARVESTED BMSCs SUBJECTED TO OSTEOGENIC MEDIUM (PLUS DEXAMETHASONE) OR ADIPOGENIC MEDIUM. A 2D WELL-PLATE GROUP SUBJECTED TO PROLIFERATION MEDIUM WAS INTRODUCED AS A NEGATIVE CONTROL. THE WHITE SCALE BAR REPRESENTS 200 μ m. 121

FIGURE 41: PIV REPLICA (LEFT) AND THE SPINNER FLASK (RIGHT). 133

FIGURE 42: THE PARTICLE-IMAGE VELOCIMETRY SYSTEM. 134

FIGURE 43: HEIGHT IN LEVELS OF THE PIV REPLICA WHERE DATA WAS SOURCED. 136

FIGURE 44: VISCOSITY OF CELL CULTURE MEDIA AT DIFFERENT MICROCARRIER CONCENTRATIONS AND ROTATIONAL SPEEDS AS REVEALED BY THE RHEOMETER AT 37°C. THE VISCOSITY VALUES WERE USED TO OBTAIN AQUEOUS GLYCEROL

CONCENTRATIONS AND TEMPERATURES (FIGURE 45) WHICH WERE USED FOR THE PIV STUDY. 140

FIGURE 45: LITERATURE VALUES (KAYE AND LABY 1995) ILLUSTRATING HOW THE VISCOSITY OF GLYCEROL VARIES WITH WATER CONCENTRATION AND TEMPERATURE. THE VISCOSITY VALUES OBTAINED BY THE RHEOMETER (FIGURE 44) WERE USED TO OBTAIN THE AQUEOUS GLYCEROL CONCENTRATION (GRAPH ON THE LEFT-HAND SIDE) AND THE TEMPERATURE (GRAPH ON THE RIGHT-HAND SIDE FOR 100% GLYCEROL ONLY). THE OBTAINED AQUEOUS GLYCEROL CONCENTRATION AND THE TEMPERATURE MATCHED THE CELL CULTURE CONDITIONS IN TERMS OF VISCOSITY. 141

FIGURE 46: TWO HORIZONTAL ORIENTATIONS OF THE IMPELLER (IMPELLER BLADE UPRIGHT ON THE LEFT-HAND SIDE AND MAGNET UPRIGHT ON THE RIGHT-HAND SIDE AS SEEN ON THIS PAGE) WHICH SHOWS THE CYTODEX 1 MICROCARRIERS SCATTERING THE LASER LIGHT. 144

FIGURE 47: A CLOSE-UP OF THE REGION OF INTEREST SHOWING THE CYTODEX 1 MICROCARRIERS SCATTERING THE LASER ENERGY. 144

FIGURE 48: COMPARISON OF THE ENSEMBLE MEAN SHEAR STRESS AGAINST LEVELS OF HEIGHT WITHIN THE SPINNER FLASK REPLICA. THE ENSEMBLE MEAN SHEAR STRESS WAS CALCULATED BASED ON 100 IMAGE PAIRS PER TWO IMPELLER ORIENTATIONS PER HEIGHT LEVEL PER EXPERIMENTAL GROUP TAKEN BY THE CAMERA. REFER TO FIGURE 43 FOR A DESCRIPTION OF THE LEVELS. THE DIFFERENCE BETWEEN EACH LEVEL WAS 4 MM. LEVEL 1 WAS 6.5 MM FROM THE BOTTOM OF THE REPLICA; LEVEL 7 WAS 13.5 MM FROM THE TOP OF THE WORKING VOLUME; LEVEL 3 REPRESENTS THE BOUNDARY BETWEEN THE IMPELLER AND NON-IMPELLER REGIONS. 146

FIGURE 49: THE MAXIMUM SHEAR STRESS RECORDED AT DIFFERENT HEIGHTS OF THE SPINNER FLASK BIOREACTOR FOR GIVEN IMPELLER SPEEDS AND MICROCARRIER CONCENTRATIONS. 147

FIGURE 50: THE MINIMUM SHEAR STRESS RECORDED AT DIFFERENT HEIGHTS OF THE SPINNER FLASK BIOREACTOR FOR GIVEN IMPELLER SPEEDS AND MICROCARRIER CONCENTRATIONS. 147

FIGURE 51: DISTRIBUTION OF MEAN SHEAR STRESS AT THE IMPELLER AND NON-IMPELLER REGIONS OF SPINNER FLASK BIOREACTOR FOR GIVEN IMPELLER SPEEDS AND MICROCARRIER CONCENTRATIONS. THIS DISTRIBUTION WAS BASED ON THE AVERAGE SHEAR STRESS OF THE IMPELLER REGION (LEVELS 4-7) AND THE NON-IMPELLER REGION (LEVELS 1-2). 148

FIGURE 52: VELOCITY MAGNITUDES (A, C) AND STRAIN RATES (B, D) OF HORIZONTAL ORIENTATED IMPELLER OF THE 45 RPM, 20 CM²/ML GROUP (A, B) AND OF THE 45 RPM, 60 CM²/ML GROUP (C, D) AT LEVEL 6. NOTE THAT THE POSITIVE AND NEGATIVE STRAIN RATES REPRESENT DIRECTION AS WELL AS MAGNITUDE. THE FLUID IS MOVING IN AN ANTI-CLOCKWISE DIRECTION. 149

FIGURE 53: VELOCITY MAGNITUDES (A, C) AND STRAIN RATES (B, D) OF HORIZONTAL ORIENTATED IMPELLER OF THE 60 RPM, 20 CM²/ML GROUP (A, B) AND OF THE 60 RPM, 60 CM²/ML GROUP (C, D) AT LEVEL 6. NOTE THAT THE POSITIVE AND NEGATIVE STRAIN RATES REPRESENT DIRECTION AS WELL AS MAGNITUDE. THE FLUID IS MOVING IN AN ANTI-CLOCKWISE DIRECTION. 150

FIGURE 54: VELOCITY MAGNITUDE MAP AT THE NON-IMPELLER REGION. IT WAS POSSIBLE TO OBTAIN A MAP OF THE ENTIRE REGION, AND NOT JUST THE SEMI-CIRCLE. THIS MAP WAS TAKEN FROM THE 60 RPM, 60 CM² GROUP, LEVEL 2. THE FLUID IS MOVING ANTI-CLOCKWISE AS THE IMPELLER ROTATES. 151

FIGURE 55: STRAIN RATE MAP OF NON-IMPELLER REGION (LEVEL 2) OF THE THE 60 RPM, 60 CM² GROUP. 151

FIGURE 56: DONOR 2 BMSC POPULATION GROWTH UNDER BIOREACTOR CONDITIONS (MICROCARRIER CONCENTRATION, IMPELLER SPEED) OVER 9 DAYS. BMSC SEEDING AT DAY 0 WAS 2000 BMSCs/cm² (4.0E+05 CELLS FOR THE SPINNER FLASK AND 2.0E+04 CELL FOR EACH WELL OF THE 2D CONTROL). THE LEGEND SHOWS THE MEAN SPATIAL ENSEMBLE-HEIGHT SHEAR STRESS FOR THE IMPELLER REGION (I) AND THE NON-IMPELLER REGION (NI) WHICH WAS EVALUATED IN THE PREVIOUS CHAPTER. 168

FIGURE 57: NUMBER OF POPULATION DOUBLINGS DURING DAYS 3 TO 6 FOR DONOR 2. 169

FIGURE 58: NUMBER OF POPULATION DOUBLINGS FOR THE ENTIRE 9-DAY PERIOD FOR DONOR 2..... 169

FIGURE 59: THE DONOR 2 BMSC POPULATION DOUBLINGS BETWEEN DAYS 3 TO 6 FOR BIOREACTOR CONDITIONS IN TERMS OF MICROCARRIER CONCENTRATION AND IMPELLER SPEED. THE SHEAR STRESS FOR THE IMPELLER AND NON-IMPELLER REGIONS, WHICH WAS EVALUATED IN THE PREVIOUS CHAPTER, IS DISPLAYED FOR GIVEN MICROCARRIER CONCENTRATIONS AND IMPELLER SPEEDS. 170

FIGURE 60: MICROGRAPHS OF THE MICROCARRIERS AND WELL-PLATES AT TIME-POINTS DAY 1 AND DAY 6. ON DAYS 1 & 6, THERE ARE FEWER CELLS VISIBLE ON THE HIGHER MICROCARRIER CONCENTRATION GROUPS. ON DAY 6, THE LOWEST SHEAR STRESS GROUP HAS THE HIGHEST CELL CONCENTRATION. 171

FIGURE 61: HARVESTED HUMAN BMSCS FROM DIFFERENT EXPERIMENTAL GROUPS SUBJECTED TO OSTEOGENIC MEDIA (PLUS DEXAMETHASONE) OVER A 21-DAY PERIOD. ALSO SHOWN IS THE IMPELLER AND NON-IMPELLER REGIONAL SHEAR STRESS EXPERIENCED BY THE BMSCS IN THE PREVIOUS NINE DAYS OF CULTURE IN SPINNER

FLASK BIOREACTORS WITH DIFFERENT MICROCARRIER CONCENTRATIONS (CM ² /ML) AND IMPELLER SPEEDS (RPM).	173
FIGURE 62: DAY 12 ALP ACTIVITY (TAKEN FROM FIGURE 61) FOR THE HARVESTED BMSCs WHICH WERE PREVIOUSLY SUBJECTED TO NINE DAYS OF CULTURE WITHIN SPINNER FLASK BIOREACTORS AT DIFFERENT MICROCARRIER CONCENTRATIONS (CM ² /ML) AND IMPELLER SPEEDS (RPM). THE SHEAR STRESS EXPERIENCED BY THE BMSCs DURING SPINNER FLASK BIOREACTOR CULTURE IS SHOWN.	174
FIGURE 63: MULTIPOTENCY RESULTS ALONG THE OSTEOGENIC (DAY 12), ADIPOGENIC (DAY 21) AND CHONDROGENIC (DAY 21) LINEAGES. NOTE THAT FOR THE "EXPANSION ONLY" SECTION OF CHONDROGENESIS, CHONDROGENIC MEDIUM MINUS TGFb1 WAS EMPLOYED.	175
FIGURE 64: LIGHT MICROGRAPH IMAGES OF MICROCARRIERS SIEVED INTO THE 212 -300 MM DIAMETER RANGES, ILLUSTRATING THE RANGE OF DIAMETERS MEASURED BY LEICA APPLICATION SOFTWARE (LAS).	194
FIGURE 65: GOAT BMSC EXPANSION ON DIFFERENT SCAFFOLD TYPES OVER A 120-HOUR PERIOD. SEEDING WAS PERFORMED AT TIME 0 HOURS AT A DENSITY OF 2000 BMSCs/CM ²	196
FIGURE 66: NUMBER OF POPULATION DOUBLINGS USING GOAT BMSC POPULATION NUMBERS FROM TIME-POINTS 24 AND 120 HOURS.	197
FIGURE 67: BMSC DOUBLING TIMES ON THE SCAFFOLD TYPES USING GOAT BMSC POPULATION NUMBERS FROM TIME-POINTS 24 AND 120 HOURS.	197
FIGURE 68: SEM MICROGRAPH OF UNSIEVED PCL-S MICROCARRIERS. THEY ALL APPEAR SMOOTH FOR A VARIETY OF DIAMETERS.	200
FIGURE 69: SEM MICROGRAPHS OF UNSIEVED PCL-R MICROCARRIERS. IT APPEARS THAT SURFACE ROUGHNESS INCREASES AS MICROCARRIER DIAMETER INCREASES.	200

FIGURE 70: SEM IMAGES OF PCL-S (LEFT) AND PCL-R (RIGHT) MICROCARRIERS WITHIN THE 212-300 MM RANGE.	201
FIGURE 71: SNAPSHOT OF THE SOFTWARE WHEN MEASURING THE SURFACE ROUGHNESS OF THE MICROCARRIERS.	202
FIGURE 72: HUMAN BMSC GROWTH (DONOR 2) ON THE DIFFERENT SCAFFOLD TYPES OVER A 120-HOUR PERIOD. NOTE THAT THE SEEDING DENSITY APPLIED WAS 2000 BMSCs/cm ² AT TIME 0 HOURS.	203
FIGURE 73: HUMAN BMSC POPULATION DOUBLINGS (DONOR 2) ON THE SCAFFOLD TYPES. THE DATA WAS CALCULATED UTILISING BMSC POPULATION NUMBERS AT TIME-POINTS 24 AND 120 HOURS.	204
FIGURE 74: HUMAN BMSC DOUBLING TIMES (DONOR 2) ON THE SCAFFOLD TYPES. THE DATA WAS CALCULATED UTILISING BMSC POPULATION NUMBERS AT TIME-POINTS 24 AND 120 HOURS.	204
FIGURE 75: HUMAN BMSC GROWTH (DONOR 3) ON THE DIFFERENT SCAFFOLD TYPES OVER A 120-HOUR PERIOD. NOTE THAT THE SEEDING DENSITY APPLIED WAS 2000 BMSCs/cm ² AT TIME 0 HOURS.	205
FIGURE 76: HUMAN BMSC POPULATION DOUBLINGS (DONOR 3) ON THE SCAFFOLD TYPES. THE DATA WAS CALCULATED UTILISING BMSC POPULATION NUMBERS AT TIME-POINTS 24 AND 120 HOURS.	206
FIGURE 77: HUMAN BMSC DOUBLING TIMES (DONOR 3) ON THE SCAFFOLD TYPES. THE DATA WAS CALCULATED UTILISING BMSC POPULATION NUMBERS AT TIME-POINTS 24 AND 120 HOURS.	206
FIGURE 78: HUMAN BMSC POPULATIONS (DONOR 2) ON THE DIFFERENT SCAFFOLD TYPES OVER A 120-HOUR PERIOD. CYTODEX 1 IS THE 3D CONTROL AND WELL-PLATES ARE	

THE 2D CONTROL. THE SEEDING DENSITY OF 2000 BMSCs/cm² WAS APPLIED AT TIME 0 HOURS.....207

FIGURE 79: HUMAN BMSC POPULATION DOUBLINGS (DONOR 2) ON THE SCAFFOLD TYPES. THE DATA WAS CALCULATED UTILISING BMSC POPULATION NUMBERS AT TIME-POINTS 24 AND 120 HOURS.....208

FIGURE 80: HUMAN BMSC DOUBLING TIMES (DONOR 2) ON THE SCAFFOLD TYPES. THE DATA WAS CALCULATED UTILISING BMSC POPULATION NUMBERS AT TIME-POINTS 24 AND 120 HOURS.....208

FIGURE 81: HUMAN BMSC POPULATIONS (DONOR 3) ON THE DIFFERENT SCAFFOLD TYPES OVER A 120-HOUR PERIOD. CYTODEX 1 IS THE 3D CONTROL AND WELL-PLATES ARE THE 2D CONTROL. THE SEEDING DENSITY OF 2000 BMSCs/cm² WAS APPLIED AT TIME 0 HOURS.....209

FIGURE 82: HUMAN BMSC POPULATION DOUBLINGS (DONOR 3) ON THE SCAFFOLD TYPES. THE DATA WAS CALCULATED UTILISING BMSC POPULATION NUMBERS AT TIME-POINTS 24 AND 120 HOURS.....210

FIGURE 83: HUMAN BMSC DOUBLING TIMES (DONOR 3) ON THE SCAFFOLD TYPES. THE DATA WAS CALCULATED UTILISING BMSC POPULATION NUMBERS AT TIME-POINTS 24 AND 120 HOURS.....210

List of Tables

TABLE 1: CHEMICAL GROUPS OF PHBV, PCL AND PLGA AND THE CORRESPONDING WAVELENGTHS.....	74
TABLE 2: DIAMETER RANGES AND SURFACE AREAS OF THE MICROCARRIERS. * DENOTES GE HEALTHCARE MANUFACTURER DATA IN TERMS OF WET SURFACE AREA PER DRY MASS OF CYTODEX 1.....	78
TABLE 3: TABLE OF SURFACE ROUGHNESS PARAMETER DEFINITIONS. THEY ARE AMPLITUDE PARAMETERS WHICH ARE MEASURES OF THE VERTICAL CHARACTERISTICS OF THE MICROCARRIER SURFACE.....	110
TABLE 4: DESCRIPTION OF THE EXPERIMENTAL GROUPS WITHIN THIS STUDY.....	130
TABLE 5: A COMPARISON OF THE PHYSICAL DIMENSIONS OF THE SPINNER FLASK AND THE PIV REPLICA.....	132
TABLE 6: EQUIVALENT PIV (IMPELLER SPEED, AQUEOUS GLYCEROL CONCENTRATION, TEMPERATURE) CONDITIONS FOR THE BIOREACTOR CONDITIONS (IMPELLER SPEED, MICROCARRIER SURFACE CONCENTRATION, TEMPERATURE) BASED ON THE RESULTS OF FIGURE 44 AND FIGURE 45.....	141
TABLE 7: CALCULATED PARAMETERS OF IMPELLER SPEED, TIP SPEED AND REYNOLDS' NUMBER FOR GIVEN IMPELLER SPEEDS AND MICROCARRIER CONCENTRATION.....	143
TABLE 8: COMPARISON OF THE RELAXATION TIMES OF BOTH THE PARTICLE AND OF THE FLUID.....	143
TABLE 9: DESCRIPTION OF THE EXPERIMENTAL GROUPS USED IN THIS STUDY. THE SPINNER FLASK REGIONAL SHEAR IS DIVIDED INTO THE IMPELLER REGION (I) AND NON-IMPELLER REGION (NI). EACH SHEAR STRESS VALUE REPRESENTS THE MEAN SPATIAL ENSEMBLE-HEIGHT SHEAR STRESS FOR THE GIVEN REGION AS SEEN IN FIGURE 48 AND	

IS WITHIN THE SHEAR STRESS RANGE STATED IN THE HYPOTHESIS OF THE
INTRODUCTION OF CHAPTER 6..... 162

List of Equations

EQUATION 1: NEWTON'S LAW OF VISCOSITY	59
EQUATION 2: REYNOLDS NUMBER.....	60
EQUATION 3: EXPONENTIAL GROWTH	90
EQUATION 4: SPECIFIC GROWTH RATE	90
EQUATION 5: DOUBLING TIME	90
EQUATION 6: POPULATION DOUBLINGS	90
EQUATION 7: NEWTON'S LAW OF VISCOSITY	137
EQUATION 8: TIP SPEED	137
EQUATION 9: REYNOLDS NUMBER.....	138
EQUATION 10: KINEMATIC VISCOSITY	138
EQUATION 11: FLUID RESIDENCE TIME.....	138
EQUATION 12: PARTICLE RELAXATION TIME.....	138

1 Literature Review

1.1 Introduction

Over a decade ago, there was great excitement about the future impact of tissue engineering (Cao et al. 1997; Fischman 1999; Langer and Vacanti 1999; Jacobs 2001), which was a field that was initiated barely a dozen years earlier (Skalak and Fox 1988). This multidisciplinary science promises to regenerate damaged/diseased tissues and organs, and reduce the US\$800 billion healthcare costs associated with Americans suffering from tissue loss or end-stage organ failure (Langer and Vacanti 1993). Whilst significant advancements have been made in tissue engineering (Muschler et al. 2004), there are scarce examples of human application (Horwitz et al. 2002). Next to the issue of cell survival (Meijer et al. 2007), a major challenge to the clinical success of cell-based tissue engineering strategies is the ability to obtain sufficient numbers of cells within an acceptable time frame (Vacanti 2006) with minimal handling, reproducibility and better online monitoring of the culture process. This thesis investigates the expansion of cells on microcarriers, and in particular, explores the effect of microcarrier composition and surface structure on cell growth, and shear stress on cell growth within a spinner flask bioreactor.

1.2 Stem Cells

“It is the great prerogative of Mankind above other Creatures, that we are not only able to behold the works of Nature, or barely to sustain our lives by them, but we have also the power of considering, comparing, altering, assisting, and improving them to various uses.” This is the opening line to the book, “Micrographia” (Hooke 1667) by English scientist, Robert Hooke, who first coined the term, “cell”. It is intriguing that this line

from the 17th century perfectly describes how the global scientific community functions today. The cell, in particular, stem cells, evokes such public dialogue, religious debate, political drama and perhaps most importantly, medical determination.

Stem cells possess the ability to self-renew and make at least one identical copy of itself (Till et al. 1964). They have the ability to differentiate or form other cell types. Stem cells may be divided into two groups: embryonic and adult (somatic) stem cells (Melton and Cowan 2004). Embryonic stem cells are derived from the embryo and can give rise to progeny from all three germ layers (endoderm, mesoderm and ectoderm) (Melton and Cowan 2004). Adult stem cells are undifferentiated stem cells which reside in differentiated tissues which are responsible for the growth, tissue maintenance and regeneration of diseased or damaged tissue (Melton and Cowan 2004). Alternatively, stem cells may be divided on the basis of potency (toti-, pluri-, multi-, uni-), which will be discussed in the next section.

1.2.1 Stem Cell Hierarchy

The stem cell hierarchy consists of the following in decreasing order of differentiation potential: totipotent stem cells, pluripotent stem cells, multipotent stem cells, unipotent stem cells. Totipotent stem cells have unlimited capability as they can specialise into extra-embryonic membranes and tissues, the embryo and all postembryonic tissues and organs. The fertilised oocyte (the zygote) and the descendants of the first two cell divisions are examples of totipotent stem cells (refer to Figure 1). The blastocyst contains a cluster of cells called the inner cell mass (ICM). The cells within the ICM are considered pluripotent and are referred to as embryonic stem cells. Pluripotent stem cells are capable of giving rise to most tissues of an organism, including those from the ectodermal, endodermal and mesodermal lineages. Pluripotent stems cells are unable to

give rise to the placenta and supporting tissues. Multipotent stem cells are capable of producing a limited range of differentiated cell lineages appropriate to their own germ layer, for example, bone marrow-derived stromal cells (BMSCs) and hematopoietic stem cells (HSCs) from the bone marrow. Unipotent stem cells, such as spermatogonial stem cells, form cells from a single lineage. (Alison et al. 2002; Macdonald et al. 2002; Jukes et al. 2008)

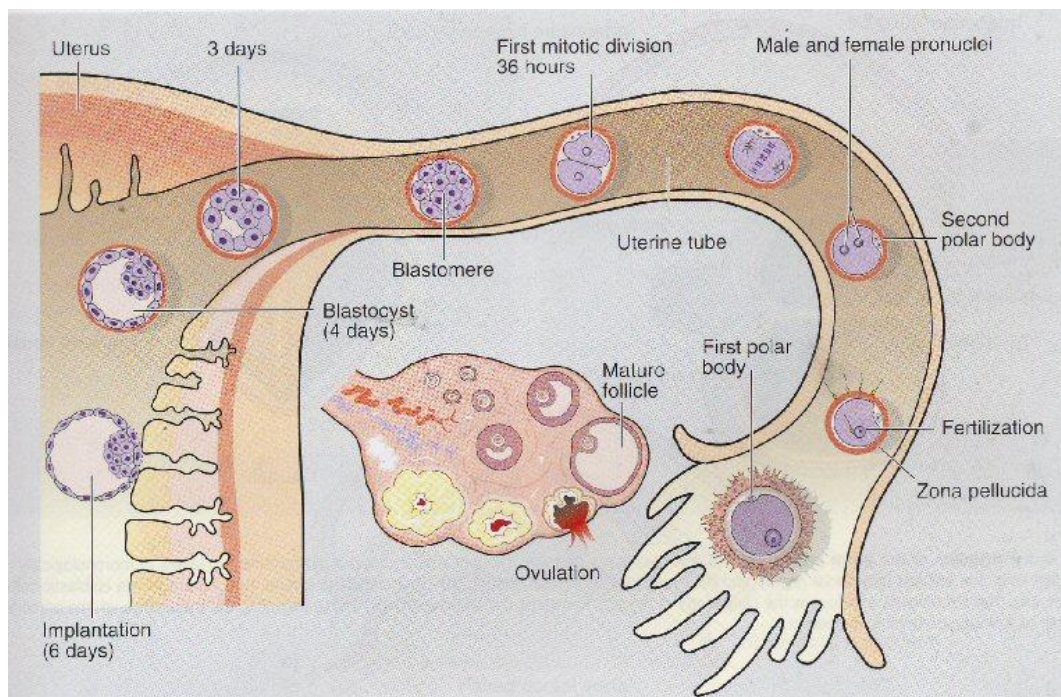


Figure 1: The path of the embryo which is transported along the fallopian tube and then implanted in the uterine wall. On the right hand side of the diagram, a spermatozoa has fertilised the oocyte (fertilization). This is known as the zygote and is totipotent. The first mitotic division at 36 hours has yielded two daughter cells which are still totipotent, each of which divide again to form totipotent stem cells. Specialisation occurs which results in a hollow ball of cells (blastocyst) and a cluster of cells (ICM), which are the embryonic stem cells. (Drife 2004)

1.2.2 Stem Cell Niches

Stem cell niches are composed of microenvironments that nurture stem cells and enable them to maintain tissue homeostasis (Schofield 1978). An appropriate spatiotemporal dialog occurs between stem and niche cells in order to fulfil lifelong demands for differentiated cells. Niche cells provide a sheltering environment that sequesters stem cells from differentiation stimuli, apoptotic stimuli and other stimuli that would challenge stem cell reserves. The niche also safeguards against excessive stem cell production that could lead to cancer. Stem cells must periodically activate to produce progenitor or transit amplifying (TA) cells that are committed to produce mature cell lineages. Hence, maintaining a balance of stem cell quiescence and activity is a hallmark of a functional niche (Moore and Lemischka 2006). *In vivo*, the homeostatic microenvironment of the niche ensures that stem cells retain their phenotype (Ohlstein et al. 2004).

1.2.3 Dedifferentiation, Redifferentiation, Transdifferentiation and Plasticity

Dedifferentiation is basically the reverse of differentiation, where differentiated cells can change into a less mature phenotype. For example, chondrocytes lose their phenotype when cultured *in vitro* on tissue culture plastic as they stop expressing the cartilage-specific marker collagen type II (von der Mark et al. 1977). However, in the presence of growth factors, such as TGF β , they redifferentiate into chondrocytes and express collagen II markers. Transdifferentiation is a switch of a cell into another cell, of the same or completely different tissue, of the same or different germ layer (Reh et al. 1987; Lagasse et al. 2000). The conversion of pancreatic cells to hepatocytes is an example of transdifferentiation (Slack and Tosh 2001). There are studies (Terada et al.

2002; Ying et al. 2002) which have demonstrated spontaneous cell fusion which raised the possibility that earlier findings were the result of cell fusion, rather than transdifferentiation. In other words, transdifferentiation may not actually happen.

Stem cell plasticity has been defined as “the ability of adult stem cells to acquire mature phenotypes that are different from their tissue of origin” (Grove et al. 2004). Hematopoietic stem cells have been shown to differentiate into hepatocytes *in vivo* (Lagasse et al. 2000). Skeletal muscle satellite cells have the capacity to form hematopoietic cells (Jackson et al. 1999). However, claims of plasticity have proven controversial. Firstly, hematopoietic stem cells and bone marrow-derived stromal cells may demonstrate plasticity, but they are essentially heterogeneous cell populations that are not fully defined. Consequently, it is unclear which cells give rise to originally sourced and unrelated cell types (Slayton and Spangrude 2004). Secondly, it cannot be ascertained whether the plasticity of cells resulting from *in vitro* culture is due to native plasticity or epigenetic modification (Slayton and Spangrude 2004). Epigenetics examines how genotypes give rise to phenotypes through an investigation of causal interactions rather than of the DNA sequence (Waddington 1962; Waddington 1966; Bird 2007). Epigenetics has alternatively been defined as “the study of mitotically and/or meiotically heritable changes in gene function that cannot be explained by changes in DNA sequence” (Russo et al. 1996).

1.3 Mesenchymal Stem Cells

Mesenchymal stem cells (MSCs) were discovered during the 1960s (Friedenstein et al. 1966; Friedenstein et al. 1970) where they were first described as colony-forming unit-fibroblasts (CFU-f). MSCs have been called bone marrow stromal cells (Ashton et al. 1980) and are found in the bone marrow and peripheral blood, in a 20:1 ratio in rabbits

(Wan et al. 2006). Recent evidence suggests that they are also found in the subcutaneous fat (Zuk et al. 2002; Tepliashin et al. 2005), umbilical cord blood (Lee et al. 2004), amniotic fluid (In 't Anker et al. 2003), synovial membrane of the knee (De Bari et al. 2001), hair follicles (Van Exan and Hardy 1980), muscle (Ferrari et al. 1998), trabecular bone (Noth et al. 2002) and foetal liver (Gotherstrom et al. 2003).

1.3.1 Characteristics

Bone marrow-derived stromal cell (BMSC) populations are heterogeneous (Bartl and Frisch 2003; Yin and Li 2006). MSCs are one of a number of BMSC populations, with a concentration of less than 1 MSC in 100,000 to 500,000 nucleated cells in the bone marrow (Caplan 2005).

Within the stem cell hierarchy, MSCs are designated as multipotent (Caplan 1991; Caplan 1994). MSCs have the potential to differentiate into mesenchymal tissues including bone, cartilage, muscle, tendon and fat (Figure 2). Recent research suggest that MSCs may in fact be pluripotent, rather than just multipotent (Jiang et al. 2002; Salingarnboriboon et al. 2003). These studies underline the ability of MSCs to differentiate into many lineages and consequently demonstrate potential in regenerative strategies.

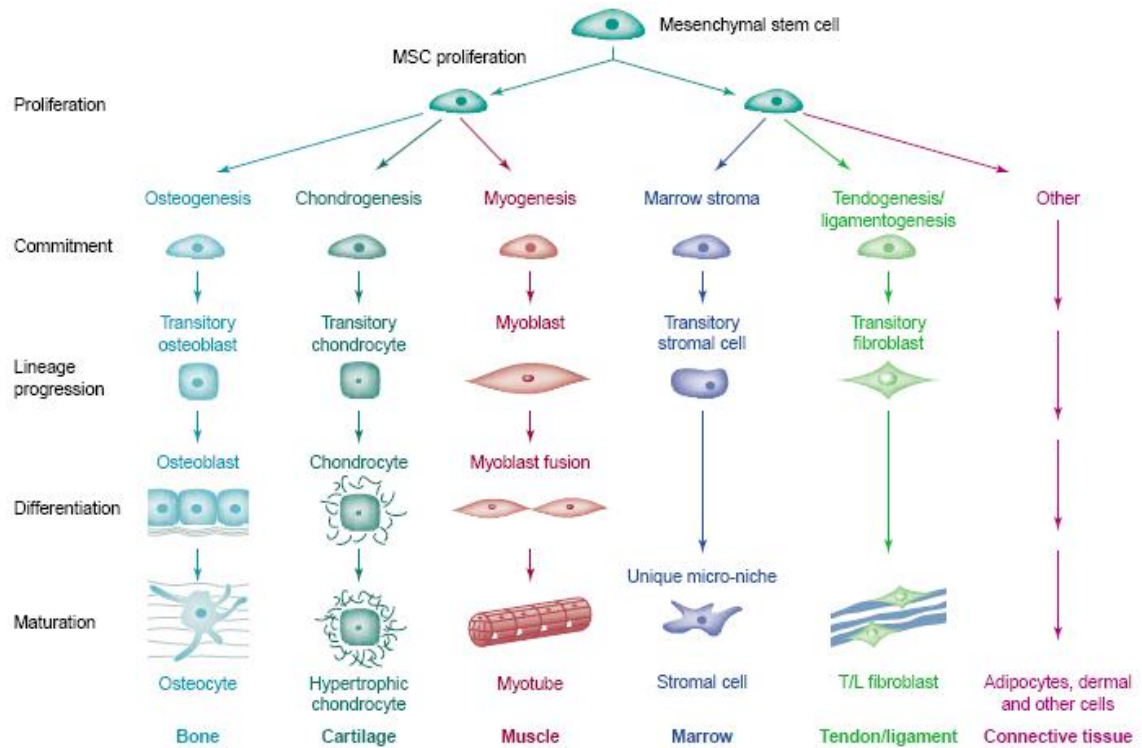


Figure 2: The Mesenchymal Process. A depiction of a mesenchymal stem cell proliferating, and then differentiating into several lineages which result in the formation of bone, cartilage, muscle, marrow, tendon/ligament and connective tissue. (Caplan and Bruder 2001)

MSCs are anchorage-dependent, which means that any successful *in vitro* expansion requires the cell to attach to a surface. *In vitro*, it has been shown that as these cells age, the number of population doublings decrease (Zimmermann et al. 2003; Delorme et al. 2009). Studies (Bruder et al. 1997; Zimmermann et al. 2003) have revealed that MSC proliferation remains within Hayflick's limit of 50 ± 10 cell doublings (Hayflick 1979). The *in vitro* lifespan of human MSCs plated at 3000-6000 cells/cm² was found to be 18.7 ± 2.5 population doublings (Zimmermann et al. 2003). An earlier study found that human MSCs from bone marrow plated at 5000 cells/cm² had an average lifespan of 38 ± 4 population doublings (Bruder et al. 1997).

1.3.2 Identification

There is no single method to identify MSCs. The methods of MSC identification include morphology, differentiation potential and antigenic markers. The morphology of MSCs, when viewed under a microscope, cannot be used as concrete proof of identification. However, it is well-documented that they are fibroblastic and plastic-adherent in culture (Colter et al. 2000; Dominici et al. 2006). Another means of identification is through differentiation potential (Jiang et al. 2002; Dominici et al. 2006; Schop et al. 2009b). This is a method which usually involves differentiation along the osteogenic, adipogenic and chondrogenic lineages.

Flow cytometry has been used to detect antigens on MSCs. Human MSCs have tested positive for SH2, SH3, CD29, CD44, CD71, CD90, CD106 and CD120a and negative for CD14, CD34 and CD45 (Pittenger et al. 1999). Recent work identified the expression of integrins: alpha1, alpha2, alpha3, alpha5, alpha6, alphav, beta1, beta3 and beta4, in addition to ICAM-1, ICAM-2, VCAM-1, CD72 and LFA-3 (Conget and Minguell 1999; Majumdar et al. 2003). Furthermore, CD105 has become the most used marker of MSCs (Bussolati et al. 2008; Odabas et al. 2008; Smiler et al. 2008). There is no single exclusive marker for MSCs, which hinders comparison of study outcomes which involve different approaches to cell characterisation (Dominici et al. 2006). In 2006, the Mesenchymal and Tissue Stem Cell Committee of the International Society for Cellular Therapy proposed minimum criteria for the antigenic identification of MSCs through expression ($\geq 95\%$ of MSC population) of CD105, CD73 and CD90, and the lack of expression ($\leq 2\%$ positive) of CD45, CD34, CD14 or CD11b, CD79 α or CD19 and HLA class II surface molecules (Dominici et al. 2006).

1.3.3 Differentiation

In the previous section, it was established that *in vitro* differentiation along multiple lineages was a means of identifying MSCs. This section examines the osteogenic, adipogenic and chondrogenic lineages in terms of markers.

1.3.3.1 Osteogenic Lineage

Osteogenesis is the process of bone formation. The constituents of the bone extracellular matrix, and hence the markers, are collagen I, biglycan, decorin, osteonectin, thrombospondin, fibronectin, osteopontin, bone sialoprotein and osteocalcin. Alkaline Phosphatase is an enzyme found in high concentrations in bone cells and is an early marker for bone formation (Jaiswal et al. 1997; Tonomura et al. 2007).

1.3.3.2 Adipogenic Lineage

Adipogenesis is the process of adipocyte or fat cell production. Oil red O staining (Koopman et al. 2001) is a technique used to identify lipid droplets of fat cells. Mest/Peg1 imprinted gene enlarges adipocytes and has been demonstrated as a marker for adipocyte size (Takahashi et al. 2005). Activin receptor-like kinase 7 (ALK7) is a novel marker for late phase adipocyte differentiation (Kogame et al. 2006).

1.3.3.3 Chondrogenic Lineage

Chondrogenesis is the process of cartilage formation. The markers of articular cartilage include collagen II (the predominant collagen type), VI, IX, X, XI, XII & XIV, proteoglycans (aggrecan, leucine-rich core proteins, decorin, fibromodulin, lumican, biglycan, perlecan), cartilage oligomeric protein, link protein, matrix- γ -carboxyglutamic acid protein, fibrillin-1, hyaluronic acid, superficial zone protein, chondroadherin and

CD44 (Poole et al. 2001). Safranin O is a method of staining the proteoglycan (Shepard and Mitchell 1976). Alcian blue staining at acidic pH is used to test for the presence of sulphated aggrecan (Lemare et al. 1998).

1.4 Scaffolds

MSCs are anchorage-dependent. They require support in order to expand. This section seeks to explore certain varieties of scaffolds and focuses upon the polymers which will be used in this project.

1.4.1 Scaffolds and Cell Expansion Techniques

T-flasks and well-plates are examples of two-dimensional (2-D) scaffolds which support proliferation of anchorage-dependent cells. Tissue culture plastic has proven beneficial for cell attachment, proliferation and harvest. However, laboratory procedures are labour-intensive and susceptible to contamination (Freshney 2000a). There are several routes to contamination when a laboratory operator has to handle multiple T-flasks over a period of weeks. Some routes include air particulates (spores and dust), faulty laminar hoods and poor technique (Freshney 2000a).

Microcarriers are examples of three-dimensional (3-D) scaffolds which support the proliferation of MSCs. 3-D scaffolds provide a greater surface area to volume ratio than 2-D scaffolds for expansion purposes. The 3-D structure allows for more efficient utilisation of culture media and is a space-saving technique (Malda and Frondoza 2006). If a seeding density of 2000 MSCs/cm² were applied to a 100 ml spinner flask containing a microcarrier concentration of 20 cm²/ml, then in order to achieve a target of 60 million MSCs, an equivalent of 12 T175-flasks are required. Hence, a target of 60 million MSCs may be achieved using 1 100 ml spinner flask or 12 T-flasks (half the

space of the incubator). As a consequence, the employment of a spinner flask reduces media consumption by roughly two-thirds. The potential for contamination of a microcarrier spinner flask cell culture is lower than the employment of 12 T-flasks in terms of handling and media replenishment.

1.4.2 Scaffold Manufacture

A variety of processing techniques have been developed which synthesise scaffolds made from both natural and synthetic polymers. The techniques include solvent casting/particulate leaching, phase inversion, fiber bonding, melt-based technologies, freeze-drying and rapid prototyping technologies (Salgado et al. 2004).

There are several methods of microcarrier synthesis. Some of these methods include spinning disk atomisation (Senuma et al. 2000), spray drying technique (Wang et al. 2004) and the water-in-oil-in-water (w/o/w) double-emulsion solvent extraction/evaporation method (Yang et al. 2000). The basic principle of the spinning disk atomisation method involves the break-up of fluid at the rim of the spinning disk resulting in droplet formation, as a consequence of interfacial forces (Senuma et al. 2000). The spray-drying technique dries a liquid feed through hot gas and an atomiser produces fine droplets or microspheres (Wang et al. 2004). The w/o/w method is relatively simple and cheap, and is used for the encapsulation of proteins for growth factor release (Zhu et al. 2007a; Zhu et al. 2009). The w/o/w method will be used to synthesise microcarriers to achieve some of the objectives of this thesis.

1.4.3 Polymers

Polymers are long-chain molecules that consist of a number of small repeating units (monomers). Polymers differ from monomers through the loss of unsaturation or the

elimination of small molecules such as water or HCL during the process of polymerisation. Cellulose, starches, rubber and deoxyribonucleic acid are all varieties of polymers (Visser et al. 1996). For tissue engineering applications, synthetic polymers are mostly employed owing to their biocompatibility, biodegradability and bulk mechanical stiffness characteristics. These synthetic polymeric biomaterials include poly(lactic acid), poly(glycolic acid), poly(lactic-co-glycolic acid), poly(ϵ -caprolactone), multi-block co-polymers comprising poly(ethylene oxide) and butylenes terephthalate units, polyphospho-esters, polyphosphazenes, polyanhydrides, polyorthoesters, poly(propylene fumarate)-diacrylate networks and poly(ethylene glycol)-diacrylate networks (van Dijkhuizen-Radersma et al. 2008). There are several examples of polymers used for cell growth and proliferation. Poly (ethylene terephthalene) PET has been used to support long-term human MSC growth (Zhao and Ma 2005). A blend of corn starch and poly (ϵ -caprolactone) has also been developed and, in conjunction with growth factors, was used to seed marrow stromal cells to grow bone-like cells (Gomes et al. 2006). Cytodex 1 microcarriers, which is composed of a cross-linked dextran, has demonstrated increasing promise for the 3D expansion of MSCs (Frauenschuh et al. 2007; Schop et al. 2008; Schop et al. 2009a; Schop et al. 2009b).

1.4.4 Polymer Candidates

This section examines the polymers which will be used to expand MSCs. The polymers which will serve as scaffolds are PHBV, PCL and PLGA. As will be discussed in greater detail in the following sections, these polymers were chosen owing to their biocompatibility properties, ability to be synthesised as microcarriers and potential as scaffolds for MSC proliferation.

1.4.4.1 PHBV [poly (3-hydroxybutyrate-co-3-hydroxyvalerate)]

Polyhydroxybutyrate (PHB) was first isolated by Lemoigne in 1925 and identified as a naturally occurring β -hydroxyacid. PHB is relatively abundant, being found in many different microorganisms as energy storage granules (similar to glycogen function in humans) at 1-30% dry weight (Doyle et al. 1991; Gomes et al. 2006). PHB has demonstrated excellent biocompatibility as evident by lack of toxicity (Saito et al. 1991), compatibility in contact with tissue (Malm et al. 1992) and blood (Clarotti et al. 1992; Malm et al. 1994). However, PHB homopolymers, like all other PHA homopolymers, are highly crystalline, extremely brittle, and relatively hydrophobic, (Lanza et al. 2000) which lacked structural integrity for certain tissue engineering applications.

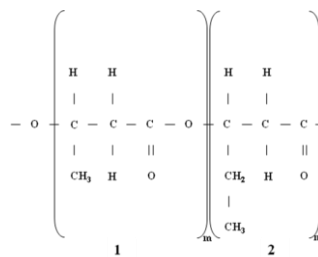


Figure 3: Chemical structure of PHBV, which is made up of the co-polymers PHB (portion 1) and HV (portion 2)

PHBV results when hydroxyvaleric acid (HV) is added to PHB (refer to Figure 3). Compared with PHB, PHBV exhibits reduced brittleness and enhanced flexibility (Yan Chen 2002). PHBV has been utilised in tissue engineering. Cartilage defects treated with chondrocyte-seeded PHBV showed better healing response than chondrocyte seeded CaP-Gelfix[®] matrices (Kose et al. 2005). PHBV has been shown to support *in*

vitro osteogenesis (Kumarasuriyar et al. 2005). It is expected that owing to the biocompatibility, reduced brittleness and ability to be synthesised as microcarriers, that PHBV microcarriers would support the attachment and proliferation of MSCs.

1.4.4.2 PCL [poly (ϵ -caprolactone)]

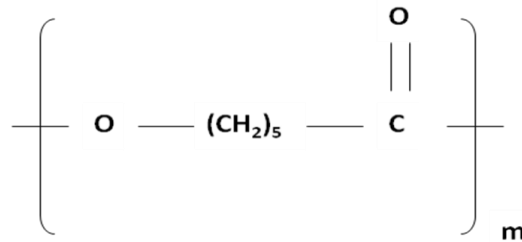


Figure 4: Chemical Structure of PCL

PCL is an organic biomaterial of synthetic origin (refer to Figure 4). It is a linear, aliphatic polyester formed by the ring-opening addition polymerisation of ϵ -caprolactone. The polymer has a regular structure and is crystallisable. The crystalline polymer has a melting point of approximately 63°C and the wholly amorphous polymer has a glass transition temperature of about -70°C (Klee et al. 1999). PCL (Lanza et al. 2000) has a high thermal stability. It is always in a rubbery state at room temperature, which contributes to the high permeability property for many therapeutic drug applications (Pitt et al. 1987). Extensive testing of the monomer and the polymer, PCL, has led to the general consensus that they are non-toxic and tissue-compatible materials. Osteoblasts have been seeded onto PCL-ceramic composites and in conjunction with rhBMP-2, significantly improved bone cell growth was noted (Rai et al. 2004). PCL-based hybrid scaffolds seeded with BMSC has shown promise for the treatment of large osteochondral defects in high-loading sites (Shao et al. 2006). It is expected that owing

to the biocompatibility and ability to be synthesised as microcarriers, that PCL microcarriers would support the attachment and proliferation of MSCs.

1.4.4.3 PLGA [polyglycolide-co-lactide]

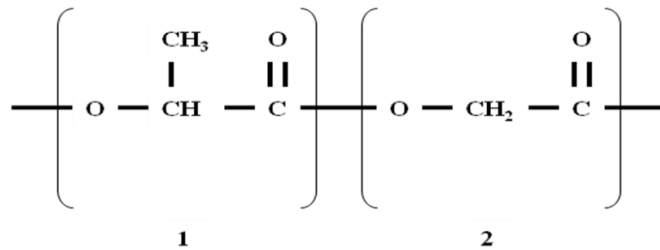


Figure 5: Chemical Structure of PLGA which is a co-polymer of lactic acid (portion 1) and glycolic acid (portion 2).

PLGA is a copolymer of polyglycolic acid (PGA) and polylactic acid (PLA) (refer to Figure 5). It is an organic biomaterial of synthetic origin. The degraded products of PLGA are lactic and glycolic acids which are both metabolites of the Krebs cycle (Gilding 1981); lactic acid is removed through aerobic respiration (Meisenberg and Simmons 2006b) and gluconeogenesis within the liver and kidneys (Meisenberg and Simmons 2006a). PLGA can be easily processed into a desired configuration owing to their chemical, physical, mechanical and degradative properties (Lu and Mikos 1996). PLGA copolymers are among the few synthetic polymers approved for human clinical uses (Kang et al. 2005). With regard to this project, it is expected that owing to the biocompatibility and ability to be synthesised as microcarriers, that PLGA microcarriers would support the attachment and proliferation of MSCs.

1.5 Bioreactors

“A bioreactor is a general term applied to a closed culture environment, that is usually mixed, that enables control of one or more environmental or operating variables that affect biological processes” (Ellis et al. 2005). Bioreactors currently used for tissue engineering applications include stirred-tank, perfusion, spinner flask, biowave, rotational wall, radial flow, packed-bed, fluidised-bed, and rotating (Goodwin et al. 1993b; Bancroft et al. 2003; Dang et al. 2004; Schroeder et al. 2005; Zhao and Ma 2005; Cameron et al. 2006). The aforementioned bioreactors have primarily been used for tissue culture; spinner flasks (Frauenschuh et al. 2007; Schop et al. 2008; Schop et al. 2009a; Schop et al. 2009b) and biowave (Schlaeppli et al. 2006; Eibl et al. 2010) bioreactors are gaining prominence in cell expansion.

1.5.1 Static Systems

Test tubes, T-flasks and well-plates are traditional means of facilitating static cultures. These represent a basis for the comparison of dynamic culture techniques. Dynamic systems offer many distinct advantages: superior rates of oxygen transfer, waste removal and nutrient supply; faster homogeneity achievement of nutrient concentration and temperature profiles; pH equilibrium more assured (Ellis et al. 2005).

1.5.2 Spinner Flasks and Stirred-tanks

Stirred culture systems have been extensively applied to the culture of microbial and mammalian cells. It is only recently that this type of system was applied to tissue engineering. This was driven by the need to develop human tissue repair strategies, which required significant quantities of cells (Vacanti 2006). The spinner flask and

stirred tank offered a dynamic environment which has been proven to improve cell yield and production rates (Kim et al. 2007; Stiehler et al. 2009).



Figure 6: Spinner Flask manufactured by Bellco Glass Inc (USA). It is used specifically for microcarrier culture and has a working volume of up to 100 ml. The impeller is coloured white and has a magnet attached to it. A magnetic stirrer is used to rotate the impeller.

There are several examples of stirred cultures being optimised for use in tissue culture. Encapsulated mouse embryonic stem cells with low-gelling temperature agarose placed in stirred-suspension bioreactors have produced scalable quantities of hematopoietic progenitor cells under controlled environmental conditions for potential short-term engraftment in host animals (Dang et al. 2004). A 15-fold expansion in the total number of human EB-derived cells cultured for 21 days in a stirred flask has been demonstrated, as compared to a 4-fold expansion in static culture; the initial inoculation cell concentration was $2-3 \times 10^6$ cells/ml, which highlighted the advantage of the dynamic compared to the static cultures (Cameron et al. 2006). A 2L stirred-tank bioreactor with a pitch-blade-turbine has been developed and optimised to yield high-density

genetically-engineered suspension cultures; for the production of cardiomyocytes (Schroeder et al. 2005).

The previous studies focussed on tissue culture. Recently, there has been research undertaken on the expansion of MSCs within spinner flask Cytodex 1 microcarrier cultures. As compared to cytodex 2 and 3, cytodex 1 has been demonstrated as the best 3D scaffold for the adherence of porcine MSCs (Frauensuh et al. 2007). This study postulated that MSCs migrated from the surface of the colonised less positively charged microcarriers to freshly-added non-colonised more positively charged microcarriers. Research has revealed information on the growth, metabolism and inhibitors of goat, rat and human MSCs (Schop et al. 2009a). Specifically, goat MSCs grew faster than rat and human MSCs, glucose consumption for cellular energy was through the glycolysis pathway for human and rat MSCs and the oxidative phosphorylation pathway and rat MSCs were more sensitive to lactate than human and goat MSCs. Information has been revealed on optimised feeding regimes as the longest proliferation phase of goat MSCs was noted when adding 30% fresh medium containing microcarriers as opposed to 30% fresh medium or no medium replenishment (Schop et al. 2008). This study indicated that the optimised feeding regime diluted the metabolites, added new energy sources (glucose and glutamine) and provided increased surface area for goat MSCs which tend to detach from one microcarrier to another during spinner flask culture.

1.5.3 Rotating Wall Vessel



Figure 7: Basic make-up of a rotating-wall vessel reactor taken from (Hammond and Hammond 2001) and originating from the article of (Goodwin et al. 1993a). Basically the bioreactor from the left-hand side is attached horizontally to the end-piece on the right-hand side. Rotation is relative to the horizontal axis; rotation in the spinner flask from the preceding section is along the vertical axis.

Features of a rotating-wall vessel reactor include a cylinder attached to a vertical surface or wall and rotation about a horizontal axis. This type of bioreactor has been used for the purposes of tissue culture and efforts have been devoted for optimisation purposes. The National Aeronautics and Space Administration (NASA) has worked on low shear stress, small turbulence microcarrier culture system for three-dimensional tissue culture. One experiment (Goodwin et al. 1993b) explored the co-cultivation of small intestine epithelium and MSCs on Cytodex 3 microcarriers. The conclusion of that experiment led to a new tissue culture model for further investigation. A review paper (Hammond and Hammond 2001) discussed the trade-offs of optimised cell culture within this type of bioreactor: minimise terminal velocity by selecting microcarrier beads and culture media with similar density, reduce coriolis and centrifugal forces, maximise nutrient flow. This paper found that (1) a reduction in gravity minimised terminal velocity (2) rotation induced coriolis and centrifugal forces, which in turn was directly proportional to terminal velocity and (3) nutrient mass transport to a cell was directly dependent on

terminal velocity and nutrient diffusion. Further to the third conclusion, it put forward that limitations to nutrient supply could be rectified through lower culture medium viscosity and/or providing a nutrient supply to form a concentration gradient.

1.5.4 Biowave Reactor

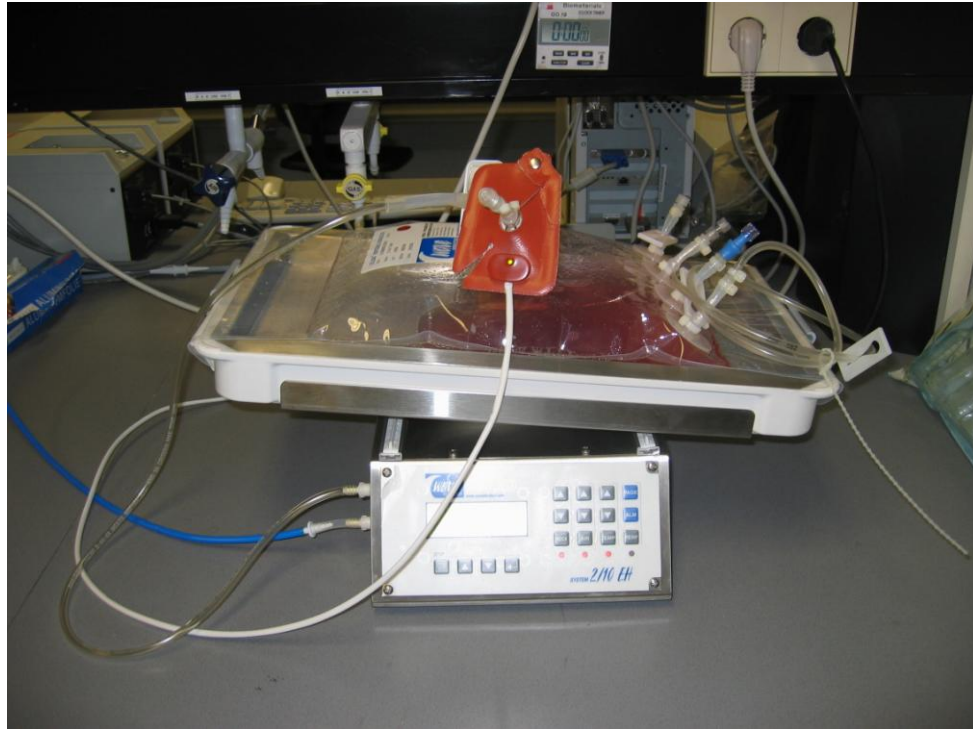


Figure 8: Picture of a Biowave Reactor taken at Xpand Biotechnology BV (The Netherlands). The red liquid is medium located in a bag. Below the bag lies the rocking unit which moves the tray from side-to-side thereby creating a dynamic environment within the medium.

Biowave reactors are relatively new technologies (Schlaeppli et al. 2006; Eibl et al. 2010). They have been used to process cells, bacteria and yeast. These bioreactors have been used mainly for cell expansion rather than for tissue culture. Wave Biotech AG is a company based in Switzerland which manufactures these bioreactors. Their design is based on a disposable Wave Bag[®] reactor and an accompanying rocking (agitation) unit, which together creates wave induced motion in order to achieve the desired degree of

mixing and oxygen transfer. Continuous aeration and de-aeration of the headspace guarantees an optimum supply of oxygen and the removal of metabolic gases. Sterilisation of the system is not required as the disposable reactor chambers are supplied pre-sterilised through gamma irradiation, which represents an alternative to maintenance-prone, time-intensive systems. The rocker facilitates wave motion which optimises nutrient transfer and prevents the cells from settling, simultaneously maintaining minimum shear stress and hence no requirement for aeration units or mechanical stirrers. There is some degree of unpredictability of fluid body formation and of the velocity and direction of bodies of fluid formation, which highlights the level of infancy of this developing technology.

1.5.5 Perfusion Bioreactor

Perfusion culture is the steady flow of media over or through a cell population/bed of cells (refer to Figure 9 and Figure 10). Common features of perfusion bioreactors include flow chambers, media reservoirs, peristaltic pumps, circulation loops and controls for temperature, pressure, carbon dioxide and oxygen. The flow chamber is the site for cell seeding, expansion and differentiation, depending on the environmental conditions. Perfusion bioreactors offer several advantages (Bancroft et al. 2003) for culturing scaffolds in tissue engineering. It provides enhanced delivery of nutrients throughout the entire scaffold by mitigating both external and internal diffusional limitations. Fluid shear stress provides mechanical stimulation to the cells which has proven convenient for research aims of stimulating bone cells (Hillsley and Frangos 1994). Cell shear stress may be varied by adjusting flow rates. The end-product advantage of the perfusion system is the 3-D layered scaffold of attached cells, made possible by enhanced nutrient delivery/waste removal.

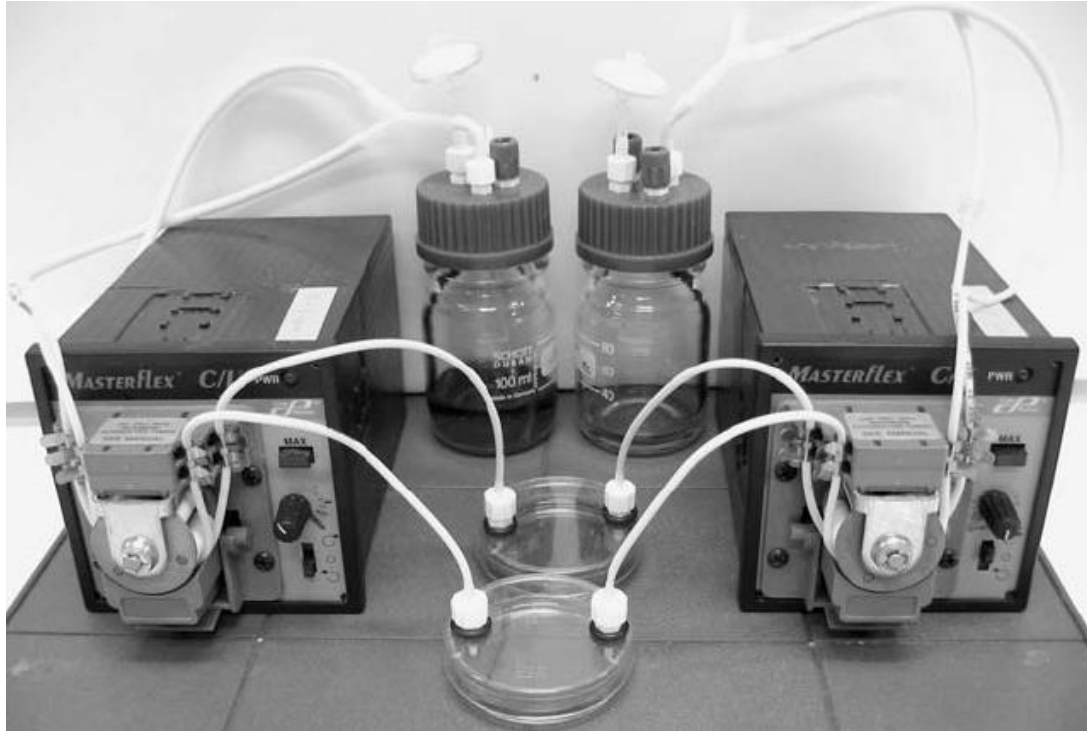


Figure 9: The perfusion system consists of the ancillary equipment and the perfusion bioreactor. There are two perfusion bioreactors in this picture and they are the two petridishes located in the middle of the two relatively large pumps. The Duran bottles represent the culture medium reservoir and the waste reservoir. Human embryonic stem cells were expanded in the perfusion bioreactors. (Fong et al. 2005)

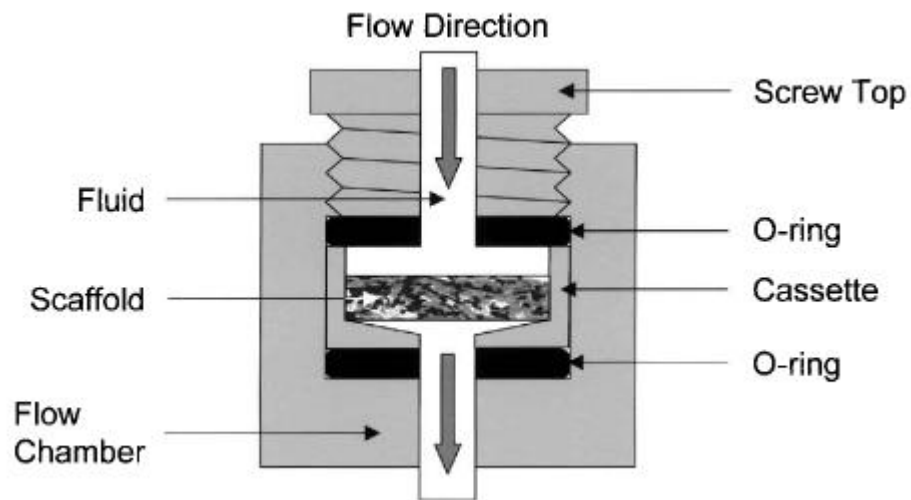


Figure 10: Medium flows in a downward direction through a scaffold with attached cells. This scaffold is held in place by the scaffold and does not move whatsoever. Hence, the culture medium flows through or perfuses the scaffold. (Bancroft et al. 2003)

A perfusion system has been designed using non-woven poly (ethylene terephthalate) (PET) matrices as scaffold for expansion and differentiation of human bone marrow-derived stromal cells (Zhao and Ma 2005). Braccini *et al.* engineered constructs by seeding, expansion and differentiation of bone marrow stromal cells (Braccini et al. 2005). This group maintained that the developed system may be used as a 3D *in vitro* model of bone marrow to study interactions between BMSCs and hematopoietic cells and also to streamline manufacture of osteoinductive grafts within the context of regenerative medicine. Fong *et al.* enhanced human embryonic cell numbers by 70% compared to a static conditions, through feeder conditioned media produced by mouse embryonic fibroblasts (Fong et al. 2005). The study was conducted in order to scale-up the bioprocess of undifferentiated human embryonic stem cells in sufficient quantities for tissue regeneration.

1.6 Fluid Flow

A fluid is a substance which undergoes continuous deformation when subjected to a shearing force (Doran 2002). In 1883, Osborne Reynolds first examined why the pattern of fluid flow, on a surface or through a pipe, varied with velocity, fluid physical properties and surface geometry (Coulson and Richardson 1999). His experiments categorised fluid flow based on velocity. Laminar or streamline flow is indicative of parallel streams which do not interact at low velocity, that is, no bulk movement at right angles to the major stream direction; however, some radial dispersion does take place owing to diffusion. Turbulent flow occurs at higher velocities and is featured by the lack of parallel streams, the presence of eddies and a higher level of radial mixing. Reynolds found that during turbulent flow in a pipe, a laminar sub-layer existed immediately adjacent to the wall.

Reynolds number (Re) is a parameter used to characterise fluid flow, so as to determine laminar, transition or turbulent flow regimes. The regimes are mathematically determined for fluid flow in a smooth pipe as $Re < 2100$ (laminar), $2100 \leq Re \leq 4000$ (transition) and $Re > 4000$ (turbulent) (Doran 2002). For stirred tank vessels, Re is dependent on a number of factors and mathematical determination is done on a case-by-case basis. But generally, Re (stirred vessels) ≤ 10 for laminar flow regimes (Doran 2002). It is important to establish Re in cell culture so as to evaluate fluid flow on cell growth.

Fluid flow regime (Riddle et al. 2006; Zhao et al. 2007) has a distinct influence on the MSC yield and phenotype. A shearing force is required to move fluid. Therefore, as mammalian cells are shear-sensitive (Chia et al. 2005), a flow regime with an optimum range of shear stress is preferred in order to maximise the MSC yield. For example,

Zhao *et al.* examined the effects of shear stress on 3-D human BMSC constructs within a perfusion bioreactor system (Zhao *et al.* 2007). That study involving laminar flow found higher proliferation rates at the lower end of the shear stress range of 1.0×10^{-4} N/m² to 1.0×10^{-5} N/m². This demonstrated improved growth rates when subjected to lower shear stress (1.0×10^{-4} N/m²).

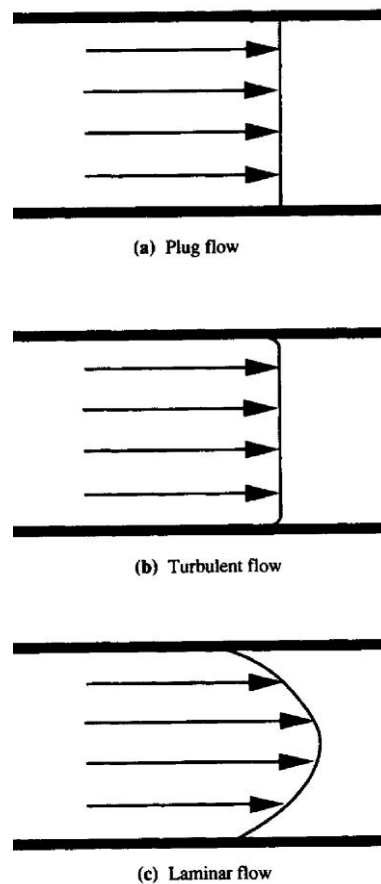


Figure 11: In (a) plug flow, the fluid streams have equal velocity resulting in a straight line profile. The stream velocities differ in (b) turbulent flow and (c) laminar flow resulting in more parabolic profiles. (Doran 2002)

An ideal plug flow reactor (refer to Figure 11) is characterised by fluid flow with no mixing whatsoever and fluid velocity is equal across the diameter of a pipe. Plug flow has been achieved in column or tubular reactors in an upward or downward manner at

high Re numbers. This type of flow is important when achieving continuous sterilisation, especially in the fermentation industry because contaminants reaching the outlet of the steriliser is not desirable (Doran 2002).

Viscosity is a measure of the resistance of a fluid to shear stress (Coulson and Richardson 1999; Doran 2002). It is determined by correlating the fluid velocity gradients to the shear forces. A Newtonian fluid may be defined as “one in which, provided that the temperature and pressure remain constant, the shear rate increases linearly with shear stress over a wide range of shear rates” (Coulson and Richardson 1999). In mathematical terms, both viscosity and shear rate are functions of shear stress; they are also both directly proportional to shear stress.

1.7 Particle Image Velocimetry

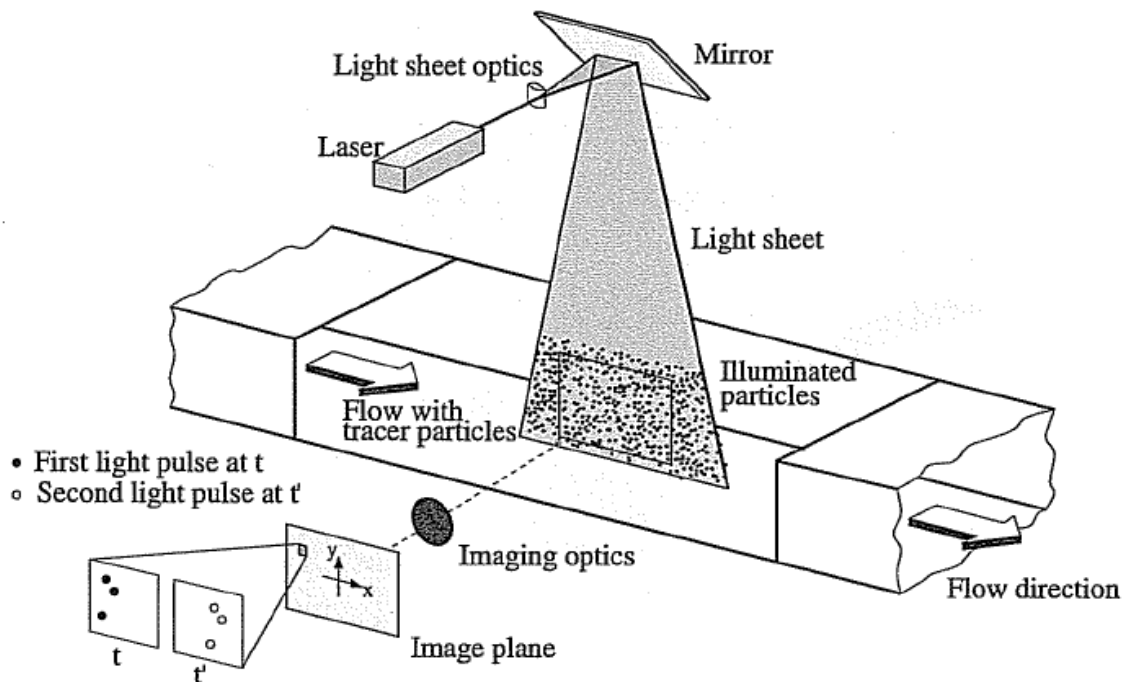


Figure 12: An example of an experimental arrangement for PIV (Raffel et al. 2007).

Particle Image Velocimetry (PIV) is a flow visualisation technique. With reference to Figure 12, in brief, fluid hydrodynamics may be assessed through the use of tracer particles, which follow fluid flow. These tracer particles scatter light which is recorded by a camera. A plane light sheet within the flow is illuminated twice by a laser. The time delay between the two illuminations forms the basis of quantitative analyses, for example, in terms of particle velocities, velocity magnitudes and shear distribution. (Raffel et al. 2007)

The employment of PIV to characterise the hydrodynamics of fluid flow in bioreactors is relatively new. Within regenerative medicine, PIV is used to develop tissue growth models relating hydrodynamic parameters to tissue properties (Sucosky et al. 2004; Bilgen et al. 2006; Disting et al. 2006; Bilgen and Barabino 2007). Given the requirements of the PIV set-up, researchers have faced tough practical challenges to replicate the stem cell culture environmental conditions and bioreactor dimensions (Sucosky et al. 2004; Bilgen and Barabino 2007). Often, significant changes have been made to those conditions and dimensions. However, valid conclusions were possible through established scale-up/scale-down models and careful material selection (Venkat et al. 1996; Sucosky et al. 2004).

In this project, the tracer particle velocities determined by the PIV will be used to evaluate Re and shear forces. Shear stress, τ , will be calculated using Equation 1, μ = viscosity and $\dot{\gamma}$ = shear rate. (Coulson and Richardson 1999)

Equation 1: Newton's Law of Viscosity

$$\tau = \mu \dot{\gamma}$$

The Reynolds number, Re , was calculated using Equation 2, where ρ = density, N_i = Impeller Speed and D_i = Impeller Diameter. (Doran 2002)

Equation 2: Reynolds Number

$$Re = \frac{(N_i D_i^2 \rho)}{\mu}$$

1.8 Aims and Objectives of the Thesis

A major challenge to the clinical success of cell-based tissue engineering strategies is the ability to obtain sufficient numbers of cells within an acceptable time frame. The expansion of BMSCs on 3D scaffolds has shown promise and the benefits compared to expansion on 2D scaffolds has been discussed within this literature review. Henceforth, the overall aim of this project is to further understand the expansion of BMSCs on 3D microcarriers, so as to maximise proliferation rates. This will be achieved through an examination of microcarrier polymer types and surface roughness and the effects of shear stress in dynamic culture. In consideration of the bioreactors, specifically those concerned with cell expansion rather than tissue growth, discussed within this chapter, spinner flasks will be employed to study the effects of shear stress on BMSC expansion on microcarriers in dynamic culture. This aim will be achieved by the following objectives:

- Preparation and characterisation of microcarrier polymeric types
- Investigation of the growth of BMSCs on different microcarrier polymeric types
- Evaluating BMSC growth on polymeric microcarriers with two levels of surface roughness
- Analysis of the shear stress within a spinner flask bioreactor for cell culture with the aid of PIV
- Examining the effects of shear stress on BMSC expansion on microcarriers within spinner flask bioreactors

2 The Preparation and Characterisation of PHBV, PCL and PLGA microcarriers for cell expansion

2.1 Abstract

Microcarriers have shown promise as scaffolds for cell expansion. This study focuses on the preparation and characterisation of three polymeric microcarriers in order to assess their suitability as scaffolds for the expansion of cells. PHBV [poly (3-hydroxybutyrate-co-3-hydroxyvalerate)], PCL [poly (ϵ -caprolactone)] and PLGA [polyglycolide-co-lactide] microcarriers were prepared employing the w/o/w (water in oil in water) method. Fourier transform infrared and raman data demonstrated that the synthesised microcarriers were all composed of the polymers. The scanning electron microscopy (SEM) results showed nanoporous PHBV and PLGA surfaces and a comparatively smooth PCL surface topography. The environmental SEM results indicated no microcarrier diameter changes when subjected to temperature and humidity changes.

2.2 Introduction

Cell expansion on two-dimensional (2-D) scaffolds is well-documented and has been in use for several decades (Freshney 2000b). T-flasks and well-plates are common examples of 2-D scaffolds. However, there exists a need to reduce the amount of incubator space occupied by the 2-D scaffolds (Figure 13) owing to the high usage of cell growth media and the potential of contamination associated with handling multiple T-flasks and well-plates over periods of weeks (Freshney 2000a). One promising alternative is the employment of 3-D microcarriers within a bioreactor. Cell expansion on these microcarriers has been proven to be more space-saving and media utilisation efficient (Malda and Frondoza 2006).



Figure 13: The surface area of microcarriers within the spinner flask on the right is equivalent to the surface area of the T-flasks within the incubator.

Cytodex 1 is manufactured by GE Healthcare and it is a positively-charged, cross-linked dextran microcarrier which expands in liquid from powder form by twenty times the

original volume. Recent literature has demonstrated promising data involving bone marrow stromal cell (BMSC) expansion on Cytodex 1 microcarriers (Frauensschuh et al. 2007; Weber et al. 2007; Schop et al. 2008; Schop et al. 2009a; Schop et al. 2009b). Whilst significant advances have been made in the optimisation of the bioprocessing of human BMSC spinner flask Cytodex 1 microcarrier culture, there is still a need to improve the seeding and harvesting efficiencies, as well as the expansion rates (Weber et al. 2007; Schop et al. 2008). It is therefore prudent that other microcarrier types should be explored to meet this need. It has previously been shown that surface topography affects cell growth (Degasne et al. 1999; Deligianni et al. 2001a; Deligianni et al. 2001b), where rougher surfaces significantly increased cell attachment and proliferation. In spinner flask culture, impeller rotation, which imparts shear stress, is necessary in order to suspend Cytodex 1 microcarriers. There is evidence which details the impact of shear stress on cells in terms of expansion, viability and morphology (Stathopoulos and Hellums 1985; Zeng et al. 2006; Zhao et al. 2007). Microcarrier types with lower densities than Cytodex 1 may conceivably require lower rotational speeds which would impart lower shear stress on cells.

PHBV [poly (3-hydroxybutyrate-co-3-hydroxyvalerate)], PCL [poly (ϵ -caprolactone)] and PLGA [polyglycolide-co-lactide] are three polymeric candidates for human BMSC microcarrier expansion. All three polymers have been demonstrated to be biocompatible (Doyle et al. 1991; Yagmurlu et al. 1999; Hutmacher et al. 2001; Kose et al. 2003; Dai et al. 2004; Kang et al. 2005; Kose et al. 2005; Kumarasuriyar et al. 2005; Shao et al. 2006). They can be processed into desired configurations (Lu and Mikos 1996; Yang et al. 2001; Zhu et al. 2007b; Zhu et al. 2009). It has previously been shown that lower crystalline/amorphous ratios within polymers favour cell attachment and growth (Park

and Cima 1996; Balasundaram et al. 2006; Czarnecki et al. 2008). Previous studies have shown that decreasing crystalline portions of polymeric blends (1) increase oxygen permeability (Deng et al. 2002) (2) maximise surface energy in order to maximise cell adhesion (Zheng et al. 2005) and (3) increases surface polarity which influences cell morphology on the scaffold (Zheng et al. 2005). PHBV has a lower crystallinity composition than PHB (polyhydroxybutyrate) owing to a higher HV (hydroxvalerate) content (Moore and Saunders 1998). PCL has high crystallinity, but its biodegradability and non-toxicity drive studies which aim to create PCL blends and co-polymers in order to control crystallinity (Jiang et al. 2001; Gomes et al. 2003). PLGA is far more amorphous than the semi-crystalline and more hydrophobic PLA (poly-L-lactide) owing to the lactic acid content (Çatiker et al. 2000; Tewes et al. 2006). On the basis of crystallinity content, it would be expected that BMSC expansion would be superior on PHBV and PLGA microcarriers, than on PCL microcarriers. However, the magnitude of influence of surface roughness as a competing factor in determining expansion rates is unknown.

The aims of this chapter are

- I. to synthesise microcarriers composed of PHBV, PCL and PLGA through the employment of the w/o/w method
- II. to examine the surface topography of the microcarriers through scanning electron microscopy (SEM) in order to evaluate its potential for cell attachment and proliferation
- III. to assess the impact of temperature and humidity changes on the microcarriers through environmental SEM.

2.3 Materials and Method

2.3.1 Polymeric Raw Materials

Poly (3-hydroxybutyrate-co-3-hydroxyvalerate) [PHBV] was purchased from Sigma Aldrich, United Kingdom. The poly (hydroxyvalerate) [PHV] content was 5% by weight of PHBV. The melting point is 165 °C.

Poly (ϵ -caprolactone) [PCL] was purchased from Sigma Aldrich, United Kingdom. The average M_w was 65000. The melting point is 60 °C.

Polyglycolide-co-lactide [PLGA] was purchased from Sigma Aldrich, United Kingdom. The lactide:glycolide ratio was 50:50 by percentage molecular weight. The average M_w was 40000 – 75000. The glass transition temperature is 45-50 °C.

2.3.2 Microcarrier Synthesis

The water in oil in water (w/o/w) method (Yang et al. 2000) was employed to synthesise the microcarriers from the polymers, PHBV, PCL and PLGA. Figure 14 is a basic illustration of the method.

Briefly, 0.60g polymer was dissolved in 12 ml of chloroform under mild stirring (“oil”). Stock solutions were composed of polyvinyl alcohol (PVA) (Sigma Aldrich, United Kingdom), dissolved in 0.01M PBS (Sigma Aldrich, United Kingdom) at 0.5 g/L for PHBV, 0.7 g/L for PCL and 0.7 g/L for PLGA. A 1.2 ml stock solution represented the first aqueous volume (“water”). A 300 ml stock solution represented the second aqueous volume (“water”).

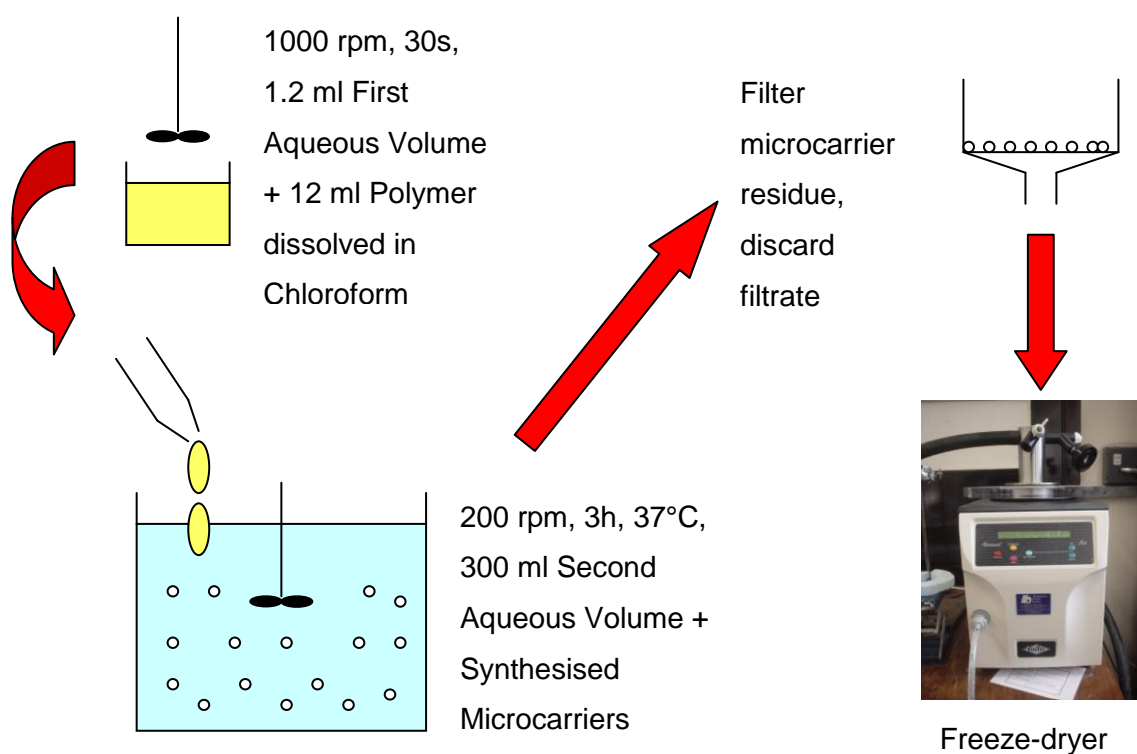


Figure 14: Microcarrier Synthesis

A 10/1 oil/water ratio was chosen, hence 1.2 ml of the first aqueous volume (“water”) was then added to the 12 ml organic solvent solution (“oil”) containing the completely dissolved polymer. Emulsification was carried out immediately using a homogenizer (Citenco F.H.P. motors LC9, England) for 30s at 1000 rpm. The emulsion was then transferred into the second aqueous volume (“water”). The solution was then placed under mechanical stirring at 200 rpm using a stirrer (Citenco F.H.P. motors LC9, England) for 3 hours to allow for the evaporation of residual chloroform. The temperature was kept constant at 37°C over a water bath. The final mixture was filtered with the residue collected and the filtrate discarded.

The residue which contained the microcarriers was washed with de-ionized water several times. Glass vials were weighed and then filled with the residual microcarriers produced by the w/o/w technique. The microcarriers were frozen in liquid nitrogen at -

196°C for 2 minutes, dried using a freeze-dryer (Biopharma Process Systems, United Kingdom) for 24 hours and weighed, repeatedly, until the mass was constant in order to completely remove moisture. The dried microcarriers were stored at 4°C.

2.3.3 Surface area measurements

Brass frame stainless steel meshes (Endecotts Limited, United Kingdom) were employed to separate the microcarriers into the 212-300 µm diameter size range. The mass of known volumes of sieved microcarriers was measured thrice as described in previous studies (Fischer et al. 2003; Ahmadi et al. 2009) assuming a spherical morphology. The average value was used to calculate the surface area of PHBV, PCL and PLGA microcarriers for a given diameter. Refer to appendix 8.1 for sample calculations. Light microscopy images of the diameter range are illustrated in that appendix.

2.3.4 Spectroscopy

Fourier transform infrared was necessary to determine the chemical structure (specifically, the functional groups) of the PHBV and PCL polymeric microcarriers. The sample was placed on a gold background and the spectra were obtained using the Nicolet 8700 FT-IR Continuum microscope (Thermo Fisher Corporation, USA). Nicolet Almega XR dispersive raman spectrometer equipped with a 785 nm laser, accumulating 1285 scans and an exposure time of 2s at 4 cm⁻¹ resolution, was used to determine the chemical structure of the PLGA polymeric microcarriers.

2.3.5 Scanning Electron Microscopy

The purpose of the Scanning Electron Microscopy (SEM) was to examine the surface topography of the microcarriers. The microcarriers were placed onto a stub with sticky carbon tape, coated with gold (20 nm thickness) and placed into the JEOL JSM 6300 scanning electron microscope. The accelerating voltage and working distance are stated beneath the images.

The purpose of environmental SEM was to assess the effects of humidity and temperature changes on the particle diameter and surface topography of the microcarriers. The QUANTA 3D FEG (The Netherlands) machine was utilised to adjust the humidity levels (10% and 100%) and the temperatures (4°C and 15°C). The microcarriers were placed on a stub and distilled water was used to keep the microcarriers on the stub. The accelerating voltage and working distance are stated beneath the images.

2.4 Results

2.4.1 Spectroscopy

Spectra of the raw polymers, PHBV, PCL and PLGA and synthesised microcarriers were compared. Based on the spectra, it was deduced that the microcarrier synthesis method had not affected the chemical constitutions of both the raw material and the synthesised microcarriers.

2.4.1.1 PHBV

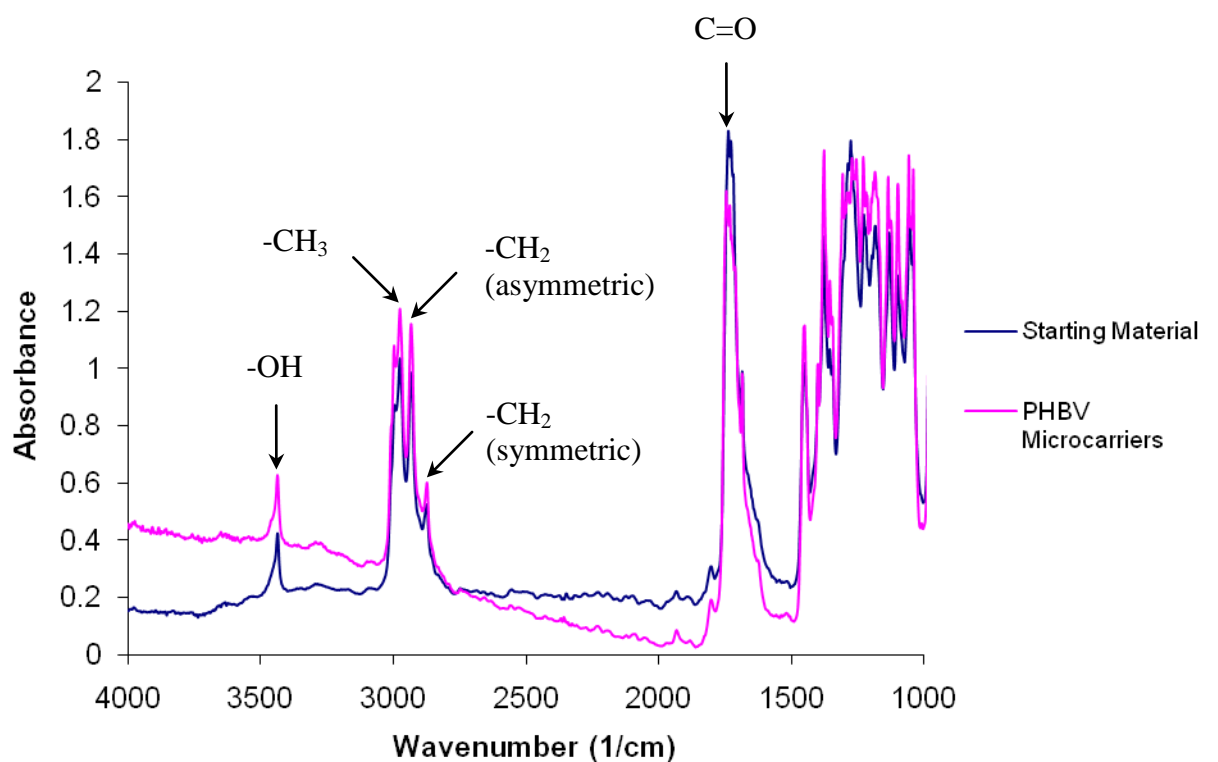


Figure 15: Spectra of the raw and synthesised microcarrier PHBV.

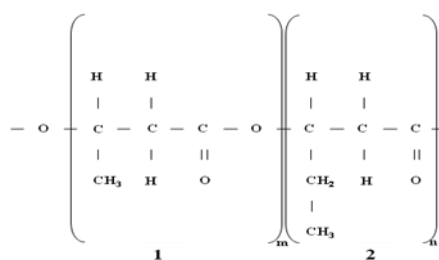


Figure 16: PHBV. 1 – PHB (polyhydroxybutyrate) portion; 2 – HV (hydroxyvalerate) portion.

Figure 15 illustrates the spectra of the raw PHBV starting material and of the synthesised PHBV microcarrier. Figure 16 illustrates the chemical structure of PHBV. Table 1 lists the chemical groups of PHBV and their corresponding wavelengths as seen in the spectra of Figure 15. As seen in Figure 15, the peaks of both the starting material and the synthesised microcarriers match. It was therefore concluded that they were constitutionally the same. Additionally, “-OH” was detected because the terminal carbon of the polymeric chain (Figure 16 – right-hand side connected to the C=O) must have four bonds to be chemically stable.

2.4.1.2 PCL

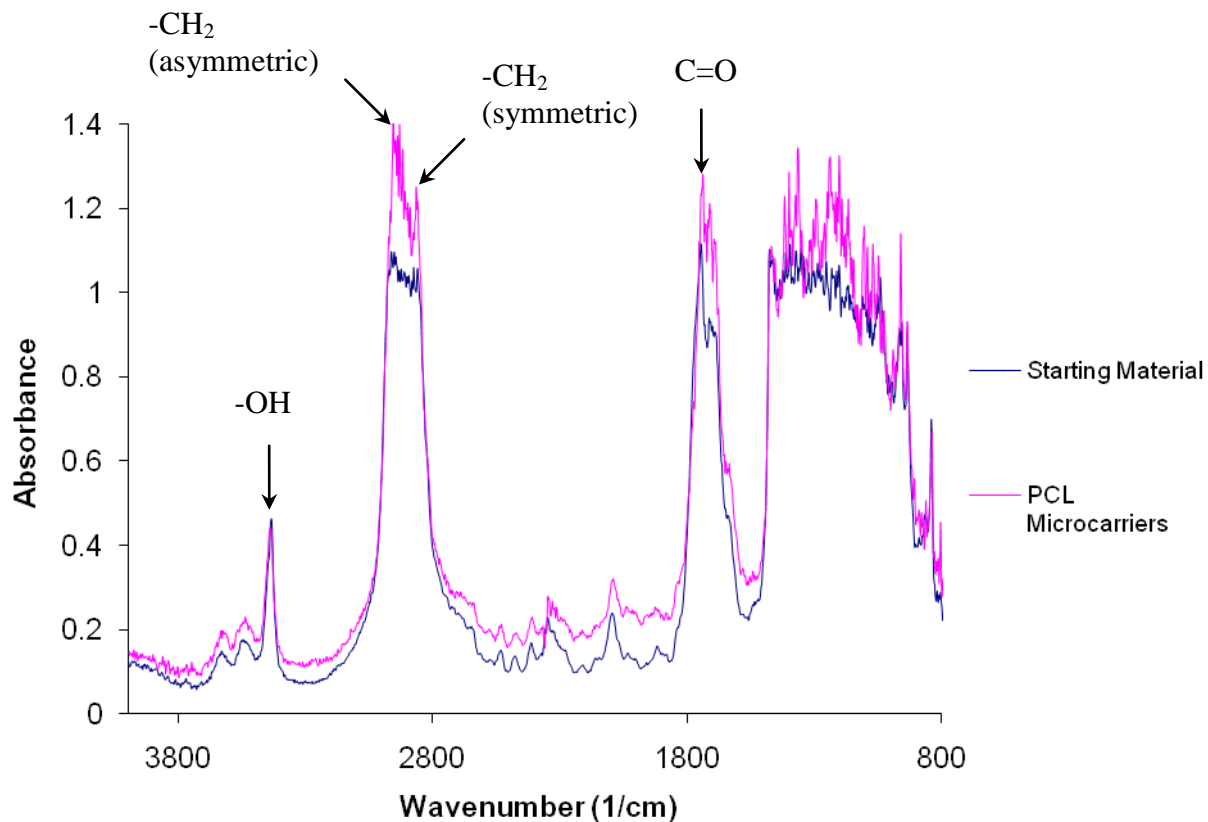


Figure 17: Comparison of Spectra for the raw starting material and PCL microcarriers.

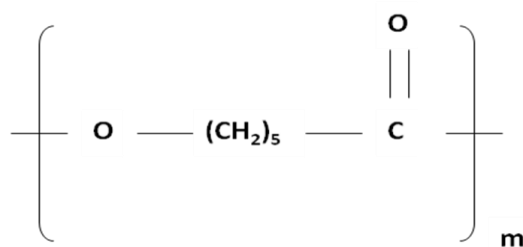


Figure 18: Chemical Structure of PCL

Figure 17 illustrates the spectra of the raw PCL starting material and of the synthesised PCL microcarrier. Figure 18 illustrates the chemical structure of PCL. Table 1 lists the chemical groups of PCL and their corresponding wavelengths as seen in the spectra of

Figure 17. As seen in Figure 21, the peaks of both the starting material and the synthesised microcarriers match. It was therefore concluded that they were constitutionally the same.

2.4.1.3 PLGA

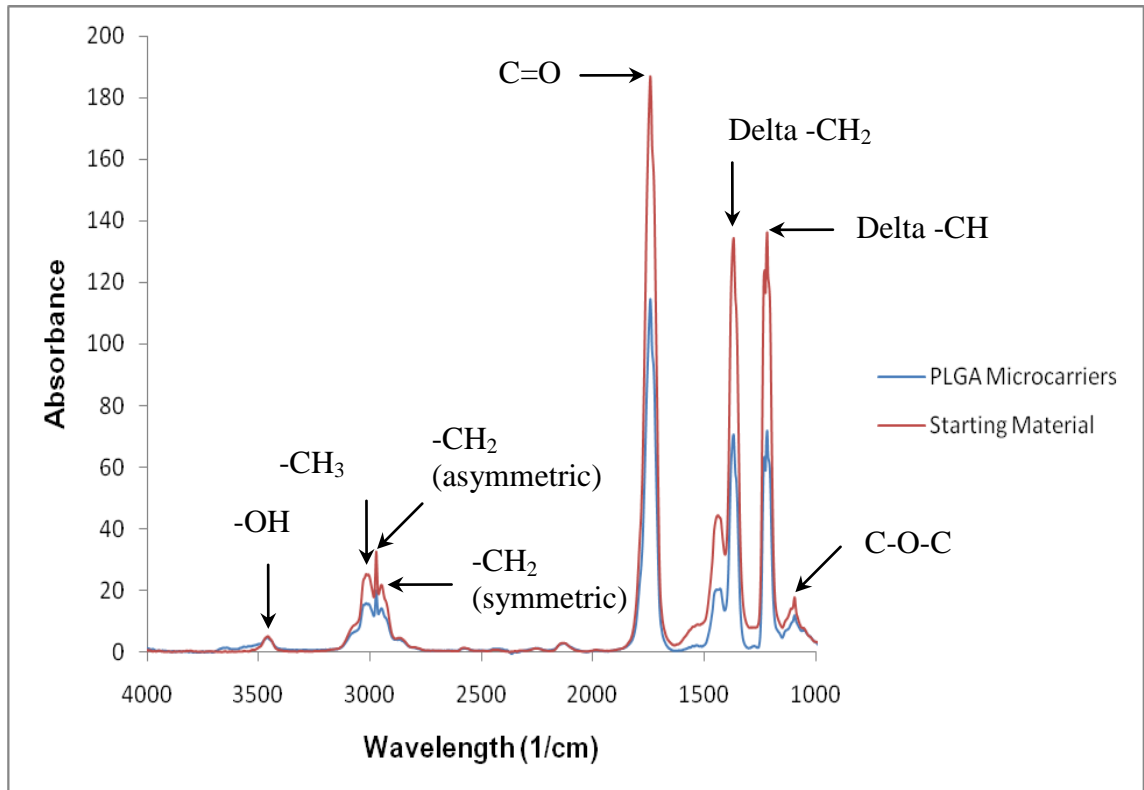


Figure 19: Comparison of the Spectra of raw starting material and PLGA microcarriers.

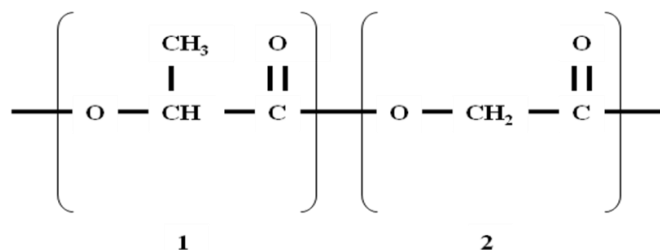


Figure 20: Chemical Structure of PLGA. It is a co-polymer of lactic acid (portion 1) and glycolic acid (portion 2).

Table 1: Chemical groups of PHBV, PCL and PLGA and the corresponding wavelengths.

Group	Wavenumber (cm⁻¹)	Reference
-OH	3600-3000	(George 1987)
-CH ₃	2960	(Nakanishi 1962b)
Asymmetric -CH ₂	2925	(Nakanishi 1962b)
Symmetric -CH ₂	2850	(Nakanishi 1962b)
Bonded carbonyl C=O	1850-1650	(George 1987)
Free carbonyl Ester	1735	(Nakanishi 1962a)
Delta -CH ₂	1434	(Nakanishi 1977b)
Delta -CH	1365	(Nakanishi 1977b)
C-O-C	1091	(Nakanishi 1977a)

Figure 19 illustrates the spectra of the raw PLGA starting material and of the synthesised PLGA microcarrier. Figure 20 illustrates the chemical structure of PLGA. Table 1 lists the chemical groups of PLGA and their corresponding wavelengths, as seen in the spectra of Figure 19. As seen in Figure 19, the peaks of both the starting material and the synthesised microcarriers match. It was therefore concluded that they were constitutionally the same. Additionally, “-OH” was detected because the terminal carbon of the polymeric chain (Figure 20 – the right-hand side adjacent to the C=O) must have four bonds to be chemically stable.

2.4.2 Scanning Electron Microscopy

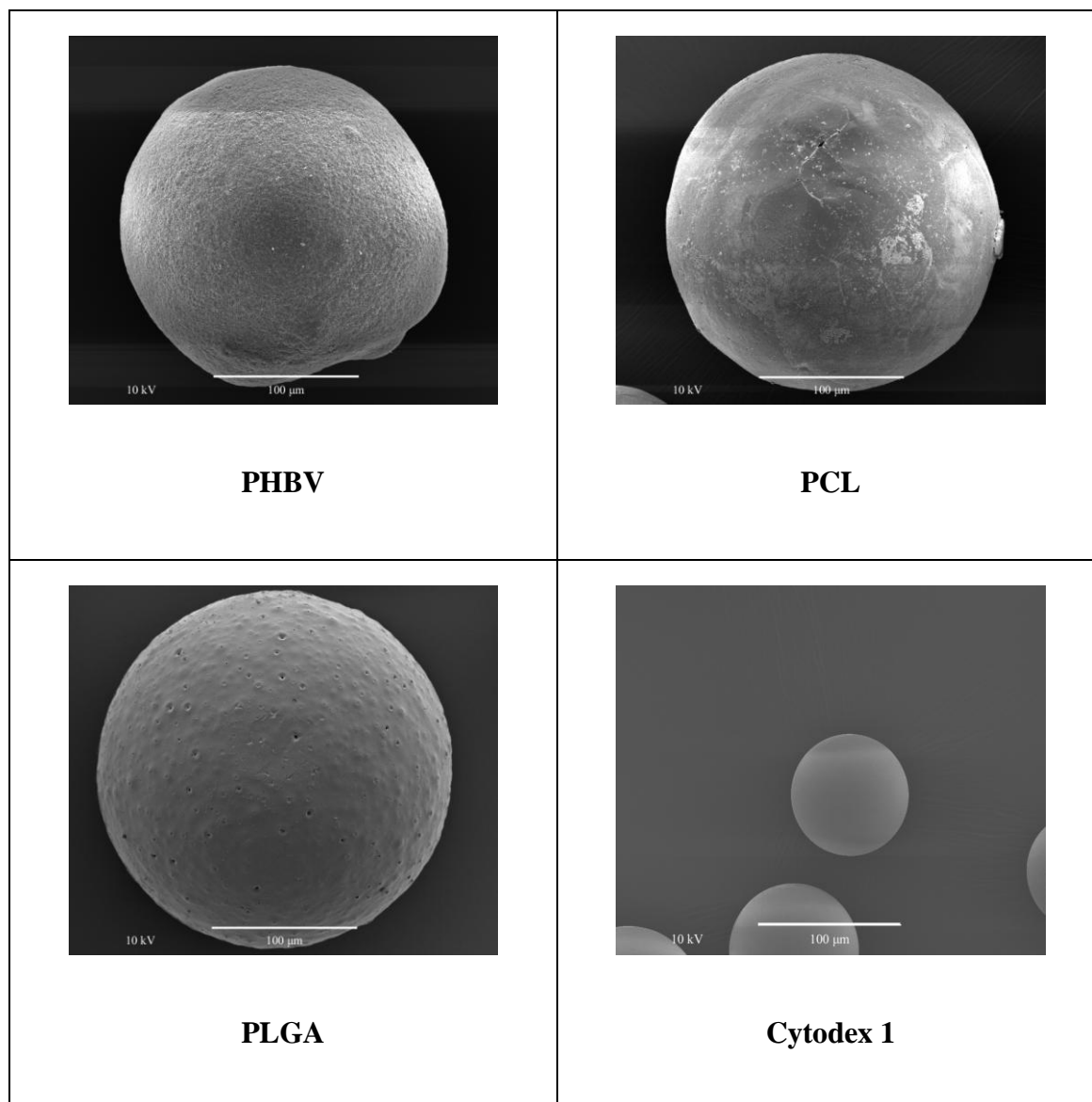


Figure 21: Surface topography of dry PHBV, PCL, PLGA and Cytodex 1 microcarriers. The working distance was 10 mm and the magnification was set at x 1000 with a working distance of 9.9 mm.

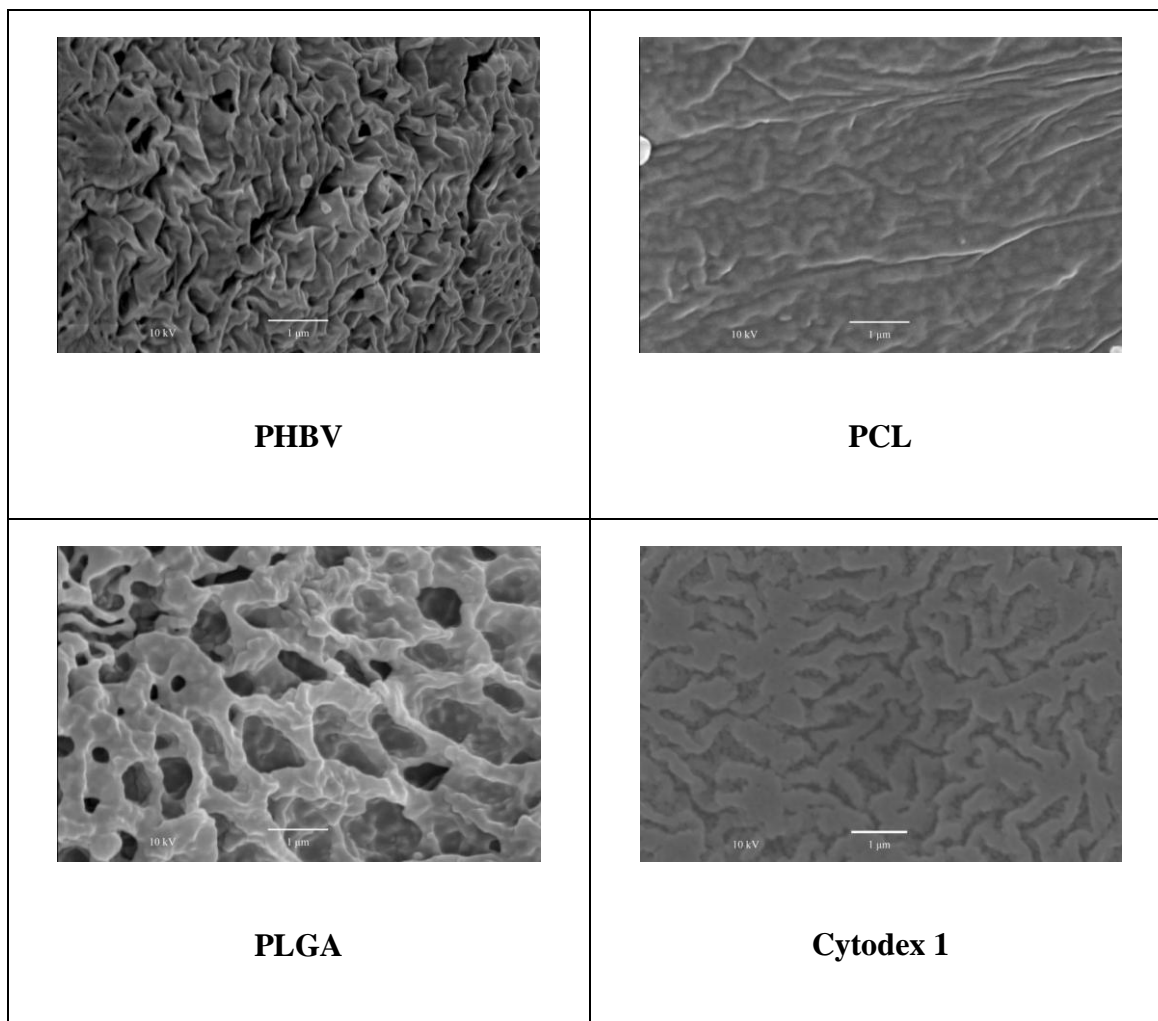


Figure 22: Surface topography of dry PHBV, PCL, PLGA and Cytodex 1 microcarriers. PHBV, PCL and PLGA were at x 15000 with a working distance of 19.0 mm. The cytodex 1 microcarrier was at x 120000 with a working distance of 10.1 mm.

Figure 21 illustrates the surface topographies of the microcarriers at low magnification. These images demonstrate the spherical appearance of the microcarriers with the PHBV microcarrier possessing a comparatively rough surface. Additionally, the Cytodex 1 microcarrier has a significantly smaller diameter. At higher magnification however, as seen in Figure 22, more detail emerges about the microcarrier surface topography. PHBV and PLGA microcarriers are nanoporous. PCL microcarriers possess surfaces

which are generally non-porous and exhibit ripples. Cytodex 1 microcarriers possess features which resemble ridges.

Figure 23 illustrates the morphology of the PHBV, PCL, PLGA and Cytodex 1 microcarriers when exposed to variations in temperature and humidity. As seen in the images, the microcarrier diameter does not significantly change with temperature and humidity variation. Internal porosity appears more visibly under 100% humidity, especially for the PHBV and PLGA microcarriers. The diameter of pores in PLGA appears to increase in size slightly as humidity was increased.

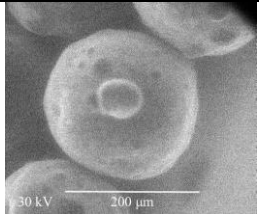
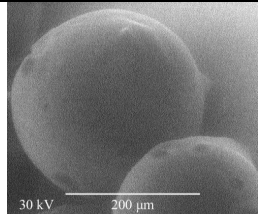
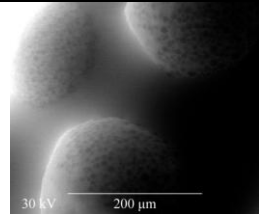
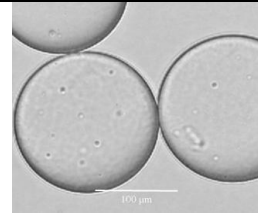
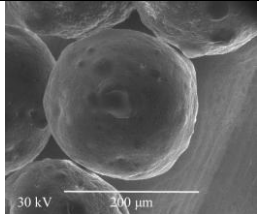
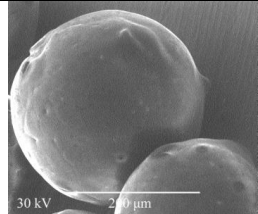
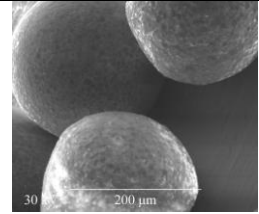
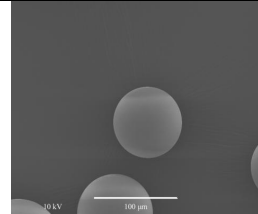
PHBV	PCL	PLGA	Cytodex 1
 <p data-bbox="347 1211 520 1283">15°C, 100% humidity</p>	 <p data-bbox="638 1211 810 1283">15°C, 100% humidity</p>	 <p data-bbox="928 1211 1101 1283">15°C, 100% humidity</p>	 <p data-bbox="1241 1211 1388 1245">25°C, wet</p>
 <p data-bbox="363 1554 507 1626">4°C, 10% humidity</p>	 <p data-bbox="654 1554 798 1626">4°C, 10% humidity</p>	 <p data-bbox="944 1554 1088 1626">4°C, 10% humidity</p>	 <p data-bbox="1241 1554 1388 1588">25°C, dry</p>

Figure 23: PHBV, PCL and PLGA microcarriers subjected to different temperatures and humidities using the environmental SEM (working distance of 5.4 mm and magnification of x 400). The wet Cytodex 1 image was obtained using the light microscope; the dry Cytodex 1 image was obtained using SEM.

2.4.3 Microcarrier Surface Area

Table 2 shows the surface area of PHBV, PCL and PLGA microcarriers of the diameter range 212-300 μm ; Cytodex 1 data was obtained from the manufacturer and its wet diameter range was 147-248 μm . Clearly, whilst the control, Cytodex 1 has the highest surface area, PLGA microcarriers possess the highest surface area of the three experimental groups. These data indicate that PLGA microcarriers are of the lowest density amongst the synthesised microcarriers.

Table 2: Diameter ranges and surface areas of the microcarriers. * denotes GE Healthcare manufacturer data in terms of wet surface area per dry mass of Cytodex 1.

Microcarrier	Dry Diameter Range (μm)	Dry Surface Area (cm^2/g)	Wet Diameter Range (μm)	Surface Area Available for Cell Attachment (cm^2/g)
PHBV	212 - 300	1429 ± 4	212 - 300	1429 ± 4
PCL	212 - 300	891 ± 10	212 - 300	891 ± 10
PLGA	212 - 300	1973 ± 7	212 - 300	1973 ± 7
Cytodex 1	54 - 86	991 ± 1	147 - 248	4400*

2.5 Discussion

The SEM images demonstrated distinct surface features of the synthesised microcarriers. PHBV and PLGA microcarriers possessed nanoporous surfaces whilst PCL surfaces were shown to be comparatively smooth. Polymeric microcarriers with similar surface topographies and diameter ranges have been shown to support the growth of different cell types (Shen et al. 2006; Jabbarzadeh et al. 2007; Zhu et al. 2007b; Zhu et al. 2009). Furthermore, coupled with evidence of biocompatibility (Doyle et al. 1991; Hutmacher et al. 2001; Dai et al. 2004; Kang et al. 2005; Shao et al. 2006), it is expected that PHBV, PCL and PLGA microcarriers will support the attachment and proliferation of BMSCs. Surface roughness on 2D scaffolds have been shown to significantly influence cell expansion (Degasne et al. 1999; Deligianni et al. 2001a; Deligianni et al. 2001b). In view of the smooth surface topography of the PCL microcarriers examined in this chapter, the level of surface roughness of this microcarrier type will be increased in order to evaluate the effect of microstructure on BMSC expansion in chapter 4.

In chapter 3, the BMSC proliferation rates on the microcarrier types will be assessed. The SEM images in this study have revealed rougher surfaces on PHBV and PLGA, as compared to the PCL microcarriers. Previous studies (Degasne et al. 1999; Deligianni et al. 2001a; Deligianni et al. 2001b) have reported superior expansion rates on 2D surfaces at the higher end of the surface roughness range: $0.3 \mu\text{m} \leq R_a \leq 5.1 \mu\text{m}$. Furthermore, higher amorphous and lower crystallinity content favours cell expansion (Park and Cima 1996; Balasundaram et al. 2006; Czarnecki et al. 2008). On the basis of crystallinity content and surface roughness, it would be expected that BMSC expansion would be superior on PHBV and PLGA as compared to PCL microcarriers.

These microcarriers are intended for use in spinner flasks bioreactors. The control, Cytodex 1 microcarriers, has shown promise in BMSC expansion (Frauenschuhr et al. 2007; Weber et al. 2007; Schop et al. 2008; Schop et al. 2009a; Schop et al. 2009b). It has previously been shown that as density differences between the microcarrier and the culture medium increased, so did the shear stress imparted on the microcarrier (Qiu et al. 1998). There is evidence which describes the impact of different levels of shear stress on cells in terms of expansion, viability and morphology (Stathopoulos and Hellums 1985; Zeng et al. 2006; Zhao et al. 2007). It is conceivable that microcarriers with lower densities than Cytodex 1 may require lower impeller rotational rates, thus imparting lower shear stress, in order to achieve suspension within spinner flask bioreactors. This study has provided surface area data, but there is no indication of the density consistency of the synthesised individual microcarriers. Hence, in chapter 3, the microcarrier density in culture medium will be qualitatively assessed.

The environmental SEM data indicated that the applied temperature and humidity changes resulted in no alterations in microcarrier diameter. The dry microcarriers are stored at 4°C after synthesis. As they are intended for cell culture work, they are subjected to incubating conditions of proliferation medium at 37°C. Whilst such conditions were not replicated exactly in the Environment SEM machine, an 11°C temperature rise, submergence in distilled water and 100% humidity resulted in no microcarrier diameter changes. The resistance of the polymeric microcarrier diameter under these conditions provided support for the method of surface area measurement (section 2.3.3 and appendix 8.1). This is a method which has been used successfully in previous studies (Fischer et al. 2003; Ahmadi et al. 2009), which assumes a spherical morphology. The measurements were performed thrice on each polymeric microcarrier

type and were compacted in eppendorf vials in order to improve data accuracy. This method will be employed in chapters 3 and 4.

2.6 Conclusion

PHBV, PCL and PLGA microcarriers were successfully synthesised and characterised by means of fourier transform infrared, scanning electron microscopy and environmental scanning electron microscopy. The SEM results showed nanoporous PHBV and PLGA surfaces and a comparatively smooth PCL surface morphology. Under humid conditions and temperature changes, the PHBV, PCL and PLGA microcarriers did not change in size. The diameter of the PLGA pores appeared to increase in size slightly when humidity was increased. The next step will be to examine the attachment and proliferation of bone marrow-derived mesenchymal stromal cells on the synthesised microcarriers.

3 PHBV, PCL and PLGA Microcarriers support the Attachment and Proliferation of Human BMSCs

3.1 Abstract

Previously, PHBV, PCL and PLGA microcarriers were characterised for their suitability as scaffolds for bone marrow stromal cell (BMSC), or mesenchymal stem cell expansion. In this study, the ability of these microcarriers to support human BMSC attachment and proliferation is evaluated. Human BMSCs were seeded on the microcarrier types and their numbers were assessed with the alamarBlue™ assay over a five-day period. Passage one BMSCs from three human donors were used in this experiment. Light and fluorescent microscopy was employed to monitor attachment and proliferation. The BMSCs were harvested from the microcarriers and evaluated for differentiation along the osteogenic and adipogenic lineages. BMSC expansion on the PHBV and Cytodex 1 microcarriers and the tissue culture plastic demonstrated no significant differences in proliferation rates and they were superior to PCL and PLGA microcarriers.

3.2 Introduction

PHBV [poly (3-hydroxybutyrate-co-3-hydroxyvalerate)], PCL [poly (ϵ -caprolactone)] and PLGA [polyglycolide-co-lactide] are examples of polymers which have been used in a wide variety of tissue engineering applications. Their biocompatibility has been established (Doyle et al. 1991; Hutmacher et al. 2001; Dai et al. 2004; Kang et al. 2005; Shao et al. 2006). The three polymers have been synthesised as 2D films and 3D discs for the purpose of evaluating *in vitro* growth, and also *in vivo* growth in animal models such as sheep and rabbits, in conjunction with BMSCs (Ren et al. 2005; Uematsu et al. 2005; Tang and Wu 2006; Curran et al. 2009). However, studies evaluating human BMSC growth on these three polymers are limited. Although, PLGA scaffolds, in particular, microcarriers, discs and nanofibers, have been utilised in conjunction with human BMSCs for pre-clinical studies (Moioli et al. 2007; Xin et al. 2007; Stiehler et al. 2009). To our knowledge, the employment of microcarriers composed of these three polymers have not been utilised for the purpose of human BMSC expansion.

Chapter 2 characterised PHBV, PCL and PLGA microcarriers which were prepared in-house. SEM images revealed that the surfaces of PHBV and PLGA microcarriers were nanoporous and that the PCL surfaces were comparatively smooth. From the literature, polymeric microcarriers with smooth and nanoporous topographies and diameter ranges have been shown to support the growth of different cell types (Shen et al. 2006; Jabbarzadeh et al. 2007; Zhu et al. 2007b; Zhu et al. 2009). Furthermore, pilot studies were conducted which successfully demonstrated the attachment and proliferation of goat BMSCs on the microcarriers; however, expanded BMSC harvests from the microcarriers resulted in dead cells (refer to appendix 8.2). It is therefore expected that human BMSCs will successfully attach and proliferate on the three microcarriers.

Human BMSCs expanded on 2D and 3D scaffolds have been shown to differentiate along more than one lineage (Pittenger et al. 1999; Schop et al. 2009a). Curran *et al.* demonstrated that adjustments in hydrophilicity, and the resultant surface chemistry, of PLGA-doped PCL films can induce human BMSC differentiation in the absence of biological stimuli (Curran et al. 2009). Furthermore, doping of PCL with PLGA increased the hydrophilic nature of PCL. As this study will be conducted over a relatively short time frame, the effect of the polymeric microcarrier differences in hydrophilicity on phenotypic retention is not expected to be significant.

As discussed in chapter 2, microcarriers possessing lower densities than Cytodex 1 would conceivably require lower impeller rotational rates in order to achieve suspension within spinner flask bioreactors. These lower rotational rates would impart lower shear stress on BMSCs.

The aims of this chapter are

- I. To demonstrate the attachment of BMSCs on the PHBV, PCL and PLGA microcarriers
- II. To evaluate and to compare the proliferation rates of human BMSCs on the microcarriers
- III. To harvest expanded human BMSCs from the microcarriers and to evaluate differentiation potential
- IV. To qualitatively assess the microcarrier densities of PHBV, PCL and PLGA.

3.3 Materials and Method

3.3.1 Human BMSC Sources

The human BMSCs were kindly donated by Xpand Biotechnology BV (The Netherlands). Three human donors were used. Bone marrow was obtained from three patients who underwent total hip arthroplasty in the Netherlands. The donors were: (1) female, aged 56, iliac crest, arthrodesis surgery, 59.8 million nucleated cells/cm³ bone marrow (2) female, aged 37, iliac crest, arthrodesis surgery, 25.0 million nucleated cells/cm³ bone marrow and (3) male, aged 45, acetabulum, total hip replacement surgery, 15.7 million nucleated cells/cm³ bone marrow. The bone marrow was placed in T-flasks at a density of 500,000 nucleated cells/cm², expanded in proliferation medium (refer to section 3.3.2) within a 5% CO₂, 37°C incubator, harvested and cryopreserved (Both et al. 2007). Passage one BMSCs were utilised for this study.

3.3.2 Proliferation Medium for Human BMSCs

The proliferation medium consisted of sterile α -Minimum Essential Medium (Invitrogen, United Kingdom) supplemented with 8.9% v/v heat inactivated Fetal Bovine Serum (Invitrogen, United Kingdom), 100 U/ml Penicillin (Sigma Aldrich, United Kingdom), 100 μ g/ml Streptomycin (Sigma Aldrich, United Kingdom), 2 mM L-glutamine (Sigma Aldrich, United Kingdom), 0.2 mM ascorbic acid (Sigma Aldrich, United Kingdom) and 1 ng/ml basic fibroblast growth factor (AbD Serotec, United Kingdom). The maximum shelf-life was one month and this medium was stored at 4°C. (Both et al. 2007; Ahmadi and de Bruijn 2008)

3.3.3 Osteogenic Medium for Human BMSCs

The osteogenic medium consisted of the proliferation medium (refer to section 3.3.2) without the basic fibroblast growth factor, but additionally supplemented with 10 mM β -glycerophosphate (Sigma Aldrich, United Kingdom) and 1×10^{-8} M dexamethasone (Sigma Aldrich, United Kingdom). The maximum shelf-life was one month and this medium was stored at 4°C (Jaiswal et al. 1997; Mendes et al. 1998; Both et al. 2007; Ahmadi et al. 2009).

3.3.4 Adipogenic Medium for Human BMSCs

The adipogenic medium consisted of sterile Dulbecco's Minimum Essential Medium (Invitrogen, United Kingdom) supplemented with 10% v/v heat inactivated Fetal Bovine Serum (Invitrogen, United Kingdom), 0.05 M 3-Isobutyl-1-methylxanthine (Sigma Aldrich, United Kingdom), 0.02 M Indomethacin (Sigma Aldrich, United Kingdom), 0.1 nM insulin (Sigma Aldrich, United Kingdom), 100 U/ml Penicillin (Sigma Aldrich, United Kingdom), 100 μ g/ml Streptomycin (Sigma Aldrich, United Kingdom), and 1 μ M dexamethasone (Sigma Aldrich, United Kingdom). The maximum shelf-life was one month and this medium was stored at 4°C. (Pittenger et al. 1999; Sekiya et al. 2002; Schop et al. 2009a)

3.3.5 Pre-culture

Cryopreserved Passage 1 human BMSCs were defrosted and plated on T-flasks at 2000 cells/cm². They were expanded in standard expansion medium until approximately 70% confluency.

3.3.6 Microcarrier Sterilisation, Cleaning and Pre-conditioning

Prior to cell seeding, 10 cm² of weighed synthesised microcarriers (refer to section 2.4.3), PHBV, PCL and PLGA, were placed into each well of 24 square well plates which does not allow cell attachment (Greiner Bio-One Limited, United Kingdom) in a fume cupboard for 10 minutes under uv light for sterilisation. After such time, the well-plate was shaken gently and then replaced into the fume cupboard for a further 10 minutes. The synthesised microcarriers were cleaned with pre-warmed, sterile phosphate-based saline solution (Sigma Aldrich, United Kingdom) in order to remove debris from the surface of the microcarriers to maximise cell attachment. Sterile Cytodex 1 microcarriers of 10 cm² surface area were then placed into wells. For pre-conditioning, 0.3 ml of pre-warmed standard expansion medium was placed into each well and the well-plates were then placed into a 5% CO₂, 37°C incubator for 30 minutes.

3.3.7 Cell Seeding

On Day 0, BMSCs were harvested from 70% confluent T-flasks using 0.25% trypsin w/v in 1 mM EDTA (Invitrogen, United Kingdom) and then seeded onto microcarriers and 6-well plates at a density of 2000 cells/cm². The volume of cells delivered to each well was 0.2 ml, thus increasing the volume to a total of 0.5 ml (0.2 ml cells and 0.3 ml conditioned medium containing microcarriers). This was shaken gently for 3 minutes and then left in the 5% CO₂, 37°C incubator for 4 hours to allow BMSC attachment to the microcarriers. After this period, the volume of each well was made up to 2 ml with standard expansion medium.

3.3.8 BMSC Growth Analysis

Two controls, in triplicate, were employed – Cytodex 1 microcarriers and tissue culture plastic well-plates. The experimental groups, again in triplicate, were (i) PHBV microcarriers, 212-300 micron diameter range (ii) PCL microcarriers, 212-300 micron diameter range (iii) PLGA microcarriers, 212-300 micron diameter range. The alamarBlue™ (Serotec, United Kingdom) assay was used to calculate the number of cells at 24, 72 and 120 hours.

At each time-point, the standard expansion medium was removed and 1 ml of 10% v/v alamarBlue™ in medium was added to each well. The well-plates were then placed into the incubator for 4 hours. After this period, 200 µl of each group was pipetted into 96 well-plates (VWR, United Kingdom). The fluorimeter (FLUOstar Galaxy, Germany) was used to measure the fluorescence at excitation and emission wavelengths of 544 nm and 590 nm respectively.

A standard curve of cell number versus wavelength was prepared per passage per donor specific to the BMSCs used in this study (refer to appendix 8.3). This curve was used to determine cell populations at different time-points and consequently to calculate the number of population doublings and the doubling times.

BMSC population growth curves were constructed based on the three time-point population measurements. The specific growth rate (μ) and doubling times (t_d) were calculated using Equation 3, Equation 4 and Equation 5, (Doran 2002), where x_t and x_0 represented the cell populations at different time-points. The number of population doublings for a given time-frame, Δt , was calculated using Equation 6.

Equation 3: Exponential Growth

$$x_t = x_0 e^{\mu t}$$

Equation 4: Specific Growth Rate

$$\mu = \frac{\ln(x_t) - \ln(x_0)}{\Delta t}$$

Equation 5: Doubling Time

$$t_d = \frac{\ln(2)}{\mu}$$

Equation 6: Population Doublings

$$\text{Doublings} = \frac{x_t}{x_0}$$

3.3.9 Human BMSC Harvest

At the final time-point of 120 hours, the microcarriers were placed on 100 μm pore size cell strainers (BD Falcon, United Kingdom) and washed thoroughly with pre-warmed, sterile Phosphate-based saline solution. The strainers containing the microcarriers were then placed into 6-well plates containing pre-warmed 0.25% trypsin-edta. The well-plates were placed into the incubator for 20 minutes. After such time, the standard expansion medium was added to stop the action of the enzyme trypsin, and the cells centrifuged at 300 x g. Pellets were obtained and the proliferation medium was discarded.

3.3.10 Differentiation of harvested human BMSCs

3.3.10.1 Osteogenic Differentiation

For osteogenic differentiation, human MSCs were seeded in 48-well plates at a density of 5000 cells/cm². Osteogenic medium (plus dexamethasone) represented the experimental group and the proliferation medium (minus dexamethasone) (section Proliferation Medium for Human BMSCs) represented the control. Medium was refreshed twice weekly. On day 12, the cells were fixed in 4 % w/v paraformaldehyde in PBS (Sigma Aldrich, United Kingdom). ALP staining was employed using the Alkaline Phosphatase Detection kit (Millipore[®], International).

ALP staining was employed to stain the alkaline phosphatase enzyme using the Alkaline Phosphatase Detection kit (Millipore[®], International). Briefly, the stain involved the fixation of cells for 1 minute, followed by rinse buffer TBST (20 mM Tris-HCL, pH 7.4, 0.15 M NaCl, 0.05 % v/v Tween, Millipore[®], International). Then, the cells were incubated with a solution of mix fast red violet solution (0.8 g/L stock), naphthol AS-BI phosphate solution (4 mg/L in 2 mol/L AMPD buffer, pH 9.5) and water (2:1:1 ratio) for 15 minutes in the dark at room temperature. Then, the solution was removed after incubation, rinsed again with TBST and finally the cells were covered with PBS. A false positive control (excluding naphthol AS-BI phosphate solution from the procedure) was used. A red precipitate confirmed the presence of ALP.

3.3.10.2 Adipogenic Differentiation

For adipogenic differentiation, human MSCs were seeded in 48-well plates at a density of 5000 cells/cm². Adipogenic media represented the experimental group and the

proliferation medium (section 3.3.2) represented the control. Medium was refreshed twice weekly. On day 21, the cells were fixed in 3.7 % formaldehyde. Oil Red O (Sigma Aldrich, United Kingdom) staining was employed to stain fat droplets.

Briefly, 3 mg/ml Oil Red O (Sigma Aldrich, United Kingdom) in isopropanol (Sigma Aldrich, United Kingdom) was diluted with deionised water (2:1 ratio). This working solution was filtered after 10 minutes and the resulting solution was used within 120 minutes. The formaldehyde was removed from the well-plates and the cells were washed gently with deionised water. Then, 60% isopropanol v/v was used to cover the cells for 5 minutes. The isopropanol was removed and the working solution of Oil Red O was allowed to cover the cells for 5 minutes. After this time, the well-plates were rinsed with deionised water. Fat droplets were stained in the colour of red. (Pittenger et al. 1999; Sekiya et al. 2002)

3.3.11 Microscopy

Light microscopy was used to qualitatively assess the cell attachment and proliferation. Fluorescent microscopy was used to assess live/dead cell proportions. Calcein AM dye (Invitrogen, United Kingdom) was used to stain live MSCs attached to the microcarriers. Ethidium homodymer (Invitrogen, United Kingdom) was used to stain dead cells.

3.3.12 Statistical Analysis

Statistical analyses were performed on the number of population doublings using Genstat version 10.1 software. An ANOVA was performed when comparing all three experimental groups and two control groups for significant differences. The number of independent replicates was 3. A student t-test was performed when comparing any

significant differences detected by the ANOVA. The level of significance was set at $p < 0.05$.

3.4 Results

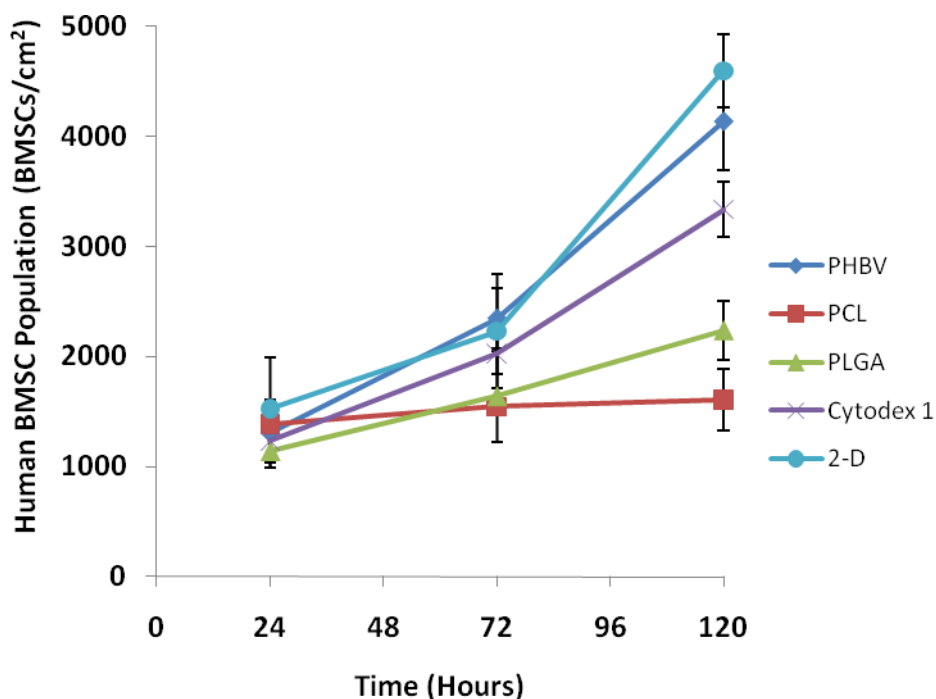


Figure 24: Human BMSC growth on the different scaffold types over a 120-hour period. Note that the seeding density applied was 2000 BMSCs/cm² at time 0 hours.

The human BMSC growth curves (Figure 24) showed general cell population increases on the different scaffold types over the 120-hour period. These cell population increases were also seen in the light and fluorescent micrographs (Figure 27). PHBV and Cytodex 1 microcarriers and the tissue culture plastic (2-D) scaffolds possessed superior final time-point BMSC populations as compared to the PLGA and PCL microcarriers.

The population doublings (Figure 25) and doubling time (Figure 26) graphical illustrations revealed that there were no significant differences in proliferation rates amongst the PHBV and Cytodex 1 microcarriers and the tissue culture plastic scaffolds over the 120-hour time period. PHBV microcarriers and the tissue culture plastic demonstrated superior BMSC proliferation rates as compared to the PCL and PLGA

microcarriers. Cytodex 1 microcarriers possessed superior BMSC proliferation rates over the PCL microcarriers; no significant differences were detected in the BMSC proliferations rates between Cytodex 1 and PLGA microcarriers.

At time-point 120 hours, harvested cells from the microcarriers and tissue culture plastic were subjected to osteogenic and adipogenic media. On day 12, ALP staining was performed and it was found that BMSCs harvested from the microcarriers and tissue culture plastic had differentiated into osteoblast-like cells owing to positive tests for ALP (Figure 28). On day 21, Oil red O staining was performed and it was found that BMSCs harvested from the microcarriers and tissue culture plastic had differentiated into adipocyte-like cells owing to positive tests for stained oil droplets (Figure 29). No differences in differentiation potential were seen.

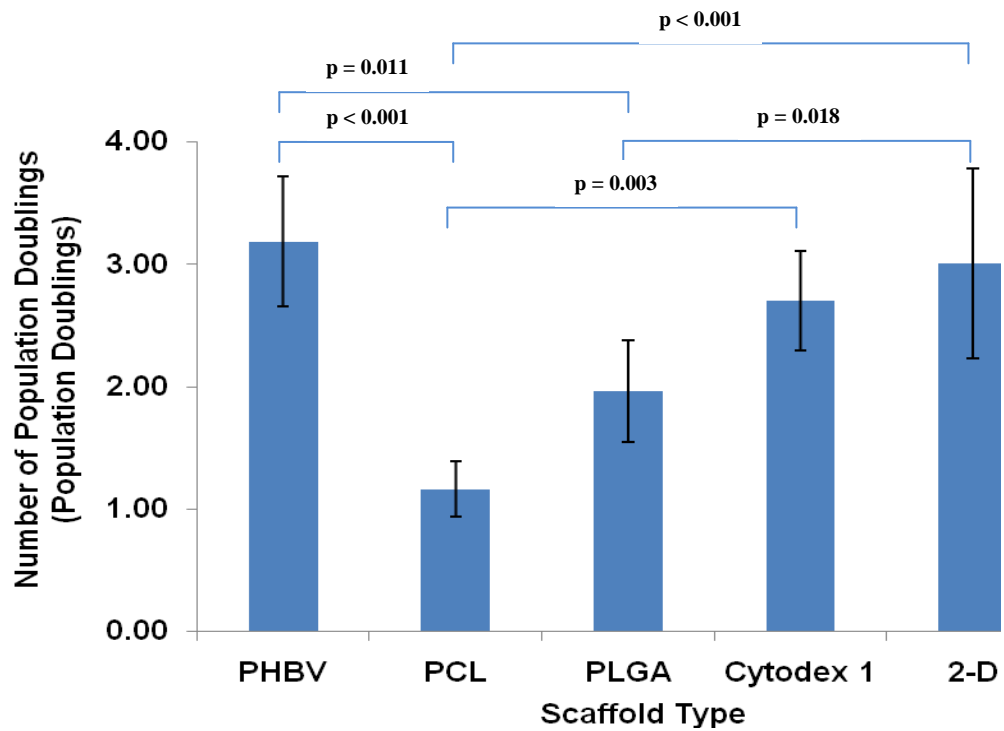


Figure 25: Human BMSC Population Doublings on the scaffold types. The data was calculated utilising BMSC population numbers at time-points 24 and 120 hours.

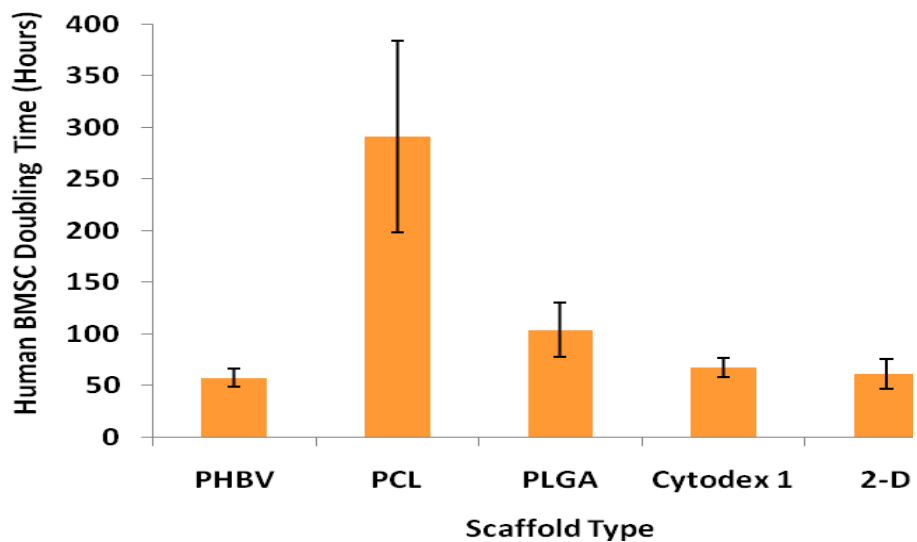


Figure 26: Human BMSC doubling times on the scaffold types. The data was calculated utilising BMSC population numbers at time-points 24 and 120 hours.

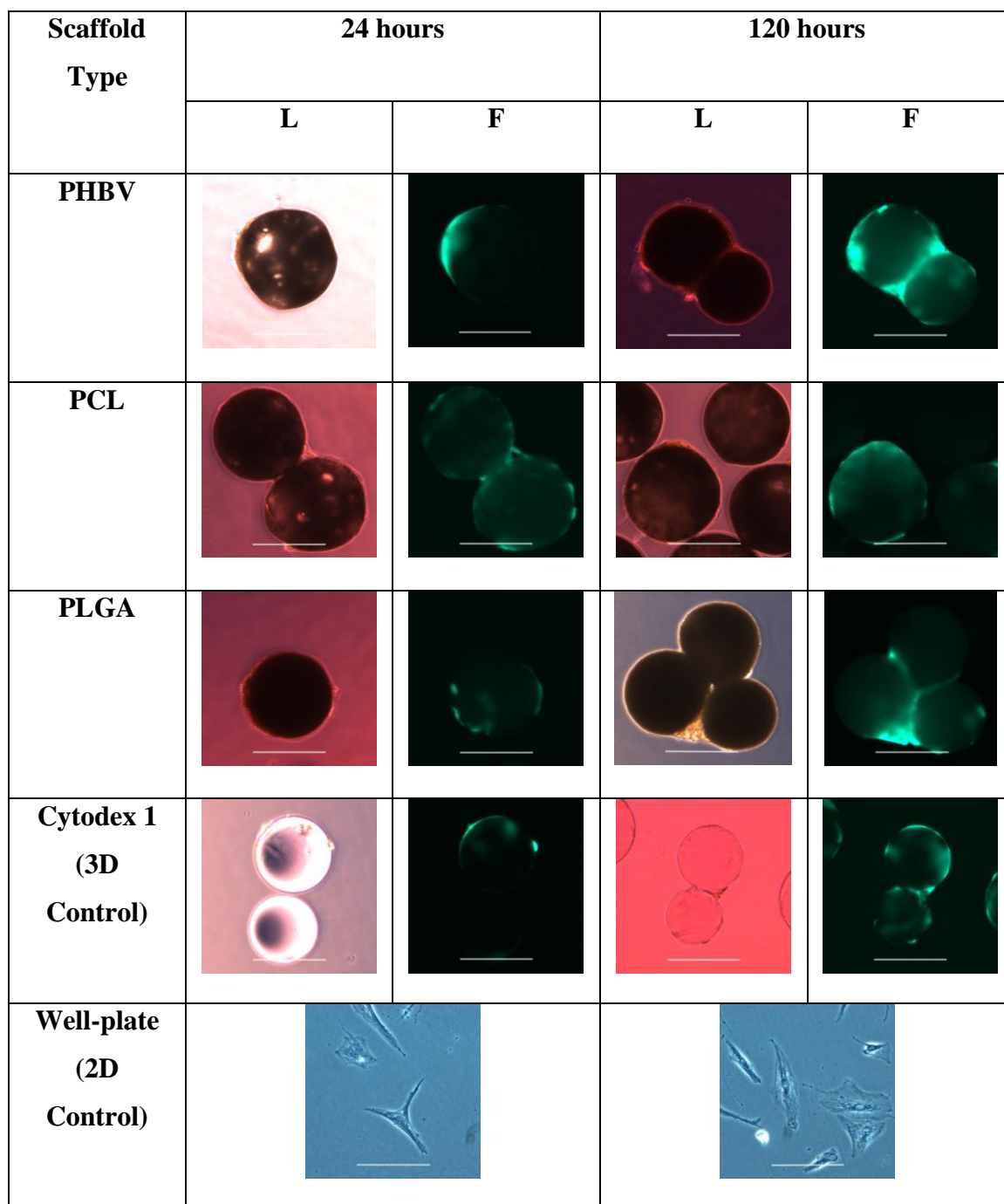


Figure 27: Light (L) and Fluorescence (F) micrographs of human BMSCs on microcarriers and well-plates after 24 and 120 hours after seeding. The green colour in the fluorescent micrographs indicates live cells, which correspondingly shows the location of the cells in light micrographs. The white scale bar represents 200µm. Magnification was at x100. Only light micrographs are shown for the 2D control.

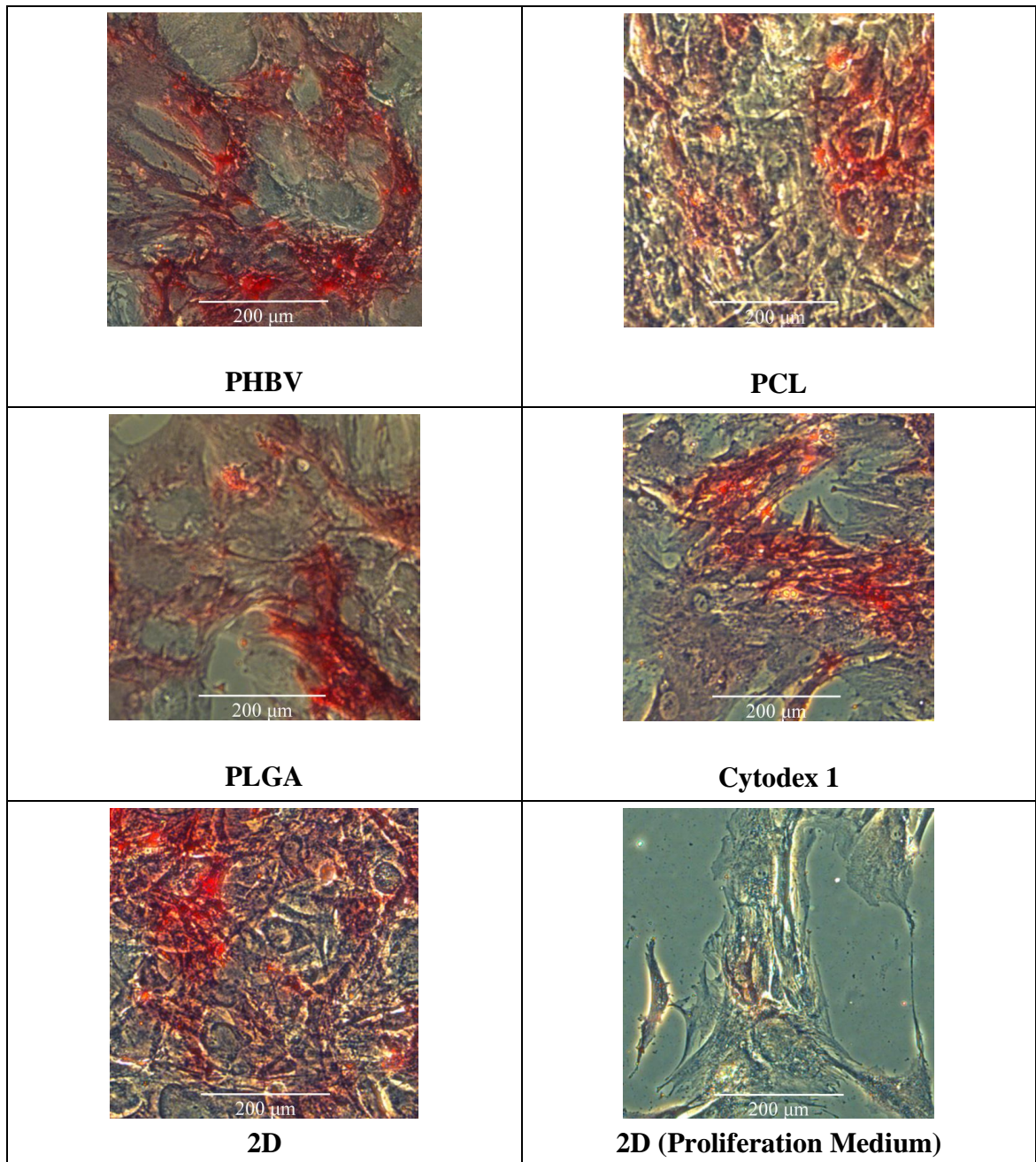


Figure 28: Day 12 ALP staining on the three experimental groups (PHBV, PCL and PLGA) and the two control groups (Cytodex 1 and 2D well-plates), which were all harvested BMSCs subjected to osteogenic medium (plus dexamethasone). A 2D well-plate group subjected to proliferation medium (minus dexamethasone) was introduced as a negative control.

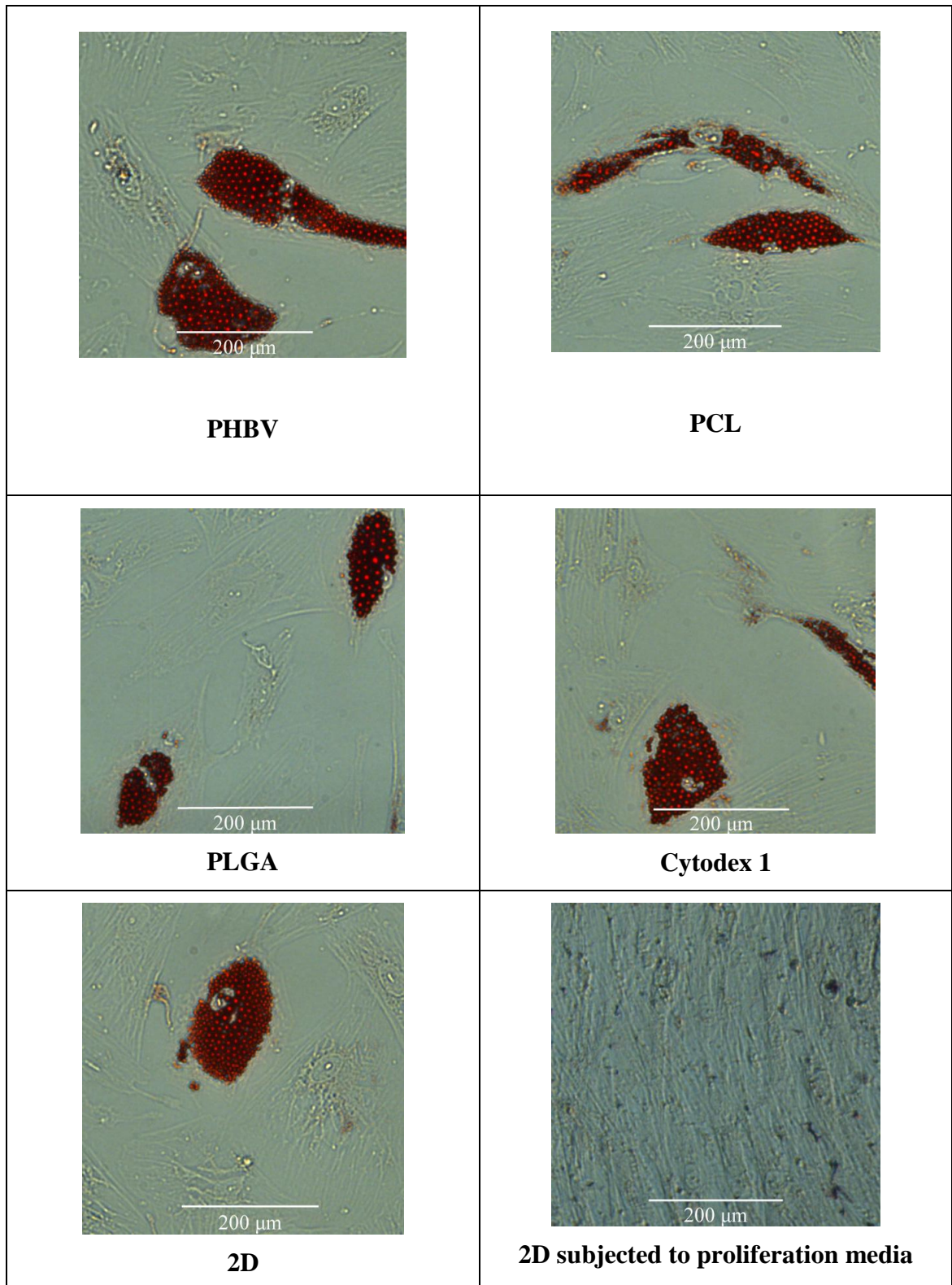


Figure 29: Day 21 light micrographs of harvested BMSCs from the experimental (PHBV, PCL and PLGA microcarriers) and control (Cytodex 1 and 2D) groups subjected to adipogenic media and the 2D group subjected to proliferation media (negative control).

3.5 Discussion

This study has demonstrated superior BMSC growth on PHBV microcarriers as compared to the PLGA and PCL microcarriers, and similar growth rates on Cytodex 1 and tissue culture plastic 2D control. Human BMSCs proliferated more on PHBV microcarriers (4.22 ± 0.68 population doublings) as compared to PCL (2.15 ± 0.42 population doublings) and PLGA (2.95 ± 0.34 population doublings) microcarriers. The statistics backed these trends indicating significant evidence of a difference ($p < 0.001$) between PHBV and PCL and of a difference ($p = 0.011$) between PHBV and PLGA. These trends were evident for BMSCs from the three human donors (see appendix 8.5). No significant differences were observed in the proliferation rates among the PHBV and Cytodex 1 microcarriers and the tissue culture plastic. This data demonstrated that BMSC expansion rates on microcarriers are comparable to those on 2D scaffolds, and thus microcarrier culture shows even more promise as an alternative to 2D culture. Additionally, PHBV microcarriers exhibited comparable, rather than superior, proliferation rates to Cytodex 1 microcarriers.

Chapter 2 and observations from this investigation revealed that during static culture, Cytodex 1 and PHBV microcarriers sank to the bottom of proliferation medium within the well-plates. The only exception was that a proportion of the PHBV microcarriers did not sink to the bottom, but occupied different levels of the proliferation medium. It is conceivable that within a spinner flask bioreactor culture, the lower density PHBV microcarriers may require lower impeller rotational rates as compared to the Cytodex 1 microcarriers. As previously discussed in chapter 2, there is evidence which details the impact of different levels of shear stress on cells in terms of expansion, viability and morphology (Stathopoulos and Hellums 1985; Zeng et al. 2006; Zhao et al. 2007).

Although beyond the scope of this thesis, BMSC expansion on the Cytodex 1 microcarriers, the higher density PHBV microcarrier and the lower density PHBV microcarriers should be investigated within a spinner flask culture environment to compare proliferation rates and to assess the impact of shear stress from different impeller rotational speeds. However, any such study must consider that the diameter ranges of Cytodex 1 (147 – 248 μm) and PHBV (212 - 300 μm) microcarriers would influence the magnitude of shear stress on the microcarriers, as Qiu *et al.* (1998) found that as the density difference between the microcarrier and the culture medium increased, so did the shear stress imparted on the microcarrier (Qiu *et al.* 1998).

This investigation revealed that the harvested BMSCs were successfully differentiated along the osteogenic and adipogenic lineages, and that no differences were detected between the experimental and control groups in terms of differentiation potential. This was expected as previous research (Li *et al.* 2002; Gauthaman *et al.* 2009) showed stem cells retaining their stemness on various polymeric scaffolds. Considering that ALP activity peaks between days 10-14 (Storrie and Stupp 2005) during *in vitro* osteogenesis and that the oil droplets were stained at day 21 during adipogenesis, the expansion of BMSCs on the polymeric microcarriers took place over 5 days which is a relatively short period of time. Curran *et al.* (2009) showed that PLGA doping of PCL affected the plastic potential of human BMSCs on films over a 28-day period (Curran *et al.* 2009). This study found that PCL containing 0 – 30 wt % PLGA enhanced chondrogenic potential both in basal and chondrogenic conditioned media, in particular 30 wt % PLGA showing the greatest enhanced chondrogenic potential. Furthermore, the osteogenic potential of these PCL/PLGA films were found to be lacking osteogenic potential (Marletta *et al.* 2007; Curran *et al.* 2009), with only PCL containing 20 wt %

PLGA facilitating osteogenic differentiation of BMSCs under osteogenic conditions. Any expansion strategy involving BMSC culture on polymeric microcarriers greater than 5 days may affect the differentiation potential of attached or harvested cells. Therefore, although outside the scope of this thesis, future work should focus on the differentiation potential of attached and harvested BMSCs from polymeric microcarrier cultures over longer periods of culture.

The SEM images from chapter 2 revealed differences in the surface topography of the polymeric microcarriers. As such and through this investigation, surface topography and chemical constitution are two of the variables which may explain the significant variation of human BMSC expansion rates on the three microcarrier types. Consequently, the effect of surface morphology will be investigated in the next chapter.

3.6 Conclusion

Human BMSCs successfully attached and proliferated on PHBV, PCL and PLGA microcarriers. This study has demonstrated superior BMSC growth on PHBV microcarriers as compared to the PLGA and PCL microcarriers, and similar growth rates on cytodex 1 and tissue culture plastic 2D control. This superiority was evident for all three human donors. Expanded BMSCs were harvested from the microcarriers and showed the ability to differentiate along the osteogenic and adipogenic lineages. This investigation demonstrated that human BMSC expansion rates on PHBV microcarriers is comparable to those on tissue culture plastic and therefore shows promise as an alternative to 2D-based culture. As compared to Cytodex 1 microcarriers, the lower density PHBV microcarriers would be expected to require lower spinner flask rotational rates, thus imparting lower shear stress on cells, in order to achieve suspension. Surface morphology and chemical constitution were identified as two variables which may have accounted for the different proliferation rates of the polymeric microcarriers. The next chapter shall focus on evaluating the effect of microcarrier surface morphology on human BMSC expansion.

4 BMSC Expansion on Microcarriers: The Effect of Surface Microstructure

4.1 Abstract

This chapter builds on the previous results by investigating the effect of microcarrier surface microstructure on BMSC expansion. The surface roughness of PCL microcarriers was altered by using two impeller designs during microcarrier synthesis. The effect of impeller design on surface microstructure was shown with SEM and laser profilometry. These two characterisation techniques revealed visual differences in the surface roughness of PCL-r (rough PCL) and PCL-s (smooth PCL) and R_a values of $1.8 \pm 0.5 \mu\text{m}$ and $6.4 \pm 1.5 \mu\text{m}$ respectively. BMSCs from all three human donors showed superior proliferation rates on PCL-r as opposed to PCL-s, and maintained their differentiation potential along the osteogenic and adipogenic lineages.

4.2 Introduction

Polymeric surface modification has been demonstrated to have an effect on biological processes (Sittinger et al. 1996; Park et al. 1998; Wan et al. 2004; Thissen et al. 2006). For example, oxygen plasma treatment on PLGA films increased hydrophilicity and surface roughness which resulted in increased mouse fibroblast cell adhesion and shear stress endurance within a parallel plate flow chamber (Wan et al. 2004). Emulsion solvent evaporation techniques are a common means of polymeric microcarrier synthesis (Yang et al. 2000; Zhu et al. 2007b). Variations of this method have been employed to manipulate their physical features (Crofts and Park 1998; Yang et al. 2000; Chun et al. 2004). Cationic composite microcarriers, synthesised by single emulsion, exhibited superior chondrogenic performance in attachment, proliferation and function compared to hydrophobic and anionic microcarriers (Chun et al. 2004). A higher water proportion in the first emulsion was shown to increase the porosity of PLGA microcarriers (Crofts and Park 1998). Qualitative results (Yang et al. 2000) have suggested that PLGA microcarriers synthesised at higher temperatures (38°C and 42°C) possessed a higher degree of surface roughness. Whilst thermal and chemical means have been used to alter surface roughness, to our knowledge, impeller designs have not been explored as an alternative. It is known that impeller design defines flow patterns which influence mixing regimes, levels of shear stress, the intensity of agitation and vortex frequency (Hooker et al. 1990; Doran 2002; Chua et al. 2008). However, impeller design effects on microcarrier surface roughness during the w/o/w method of preparation are unclear.

It has previously been shown that cell expansion rates on 2D surfaces increase as surface roughness, R_a , increases. Degasne *et al.* showed that human osteoblast-like cell

attachment and proliferation increased on titanium disks as the R_a increased from 0.30 ± 0.01 to 0.94 ± 0.09 μm (Degasne et al. 1999). This trend was seen in work by Deligianni *et al.* with human BMSCs on hydroxyapatite disks with R_a increasing from 0.733 ± 0.203 μm to 4.680 ± 0.433 μm (Deligianni et al. 2001b). Again, this was seen in work presented by Deligianni *et al.* with human BMSCs on Ti-6Al-4V disk surfaces with R_a increasing from 0.320 ± 0.065 μm to 0.874 ± 0.185 μm (Deligianni et al. 2001a). Chapters 2 and 3 revealed differences in surface microstructure as well as differences in BMSC expansion rates; superior expansion rates were noted on the rougher polymeric surfaces. To our knowledge, there are no studies of cell expansion rates on microcarriers with different levels of surface roughness. Based on the combined minimum and maximum levels of 2D surface roughness of previous studies (Degasne et al. 1999; Deligianni et al. 2001a; Deligianni et al. 2001b), $0.30 \mu\text{m} \leq R_a \leq 5.1 \mu\text{m}$, it would be expected that BMSC expansion on microcarriers with R_a at the higher end of the range would be higher than the lower end.

The aims and objectives of this study were:

- I. To prepare microcarriers of different surface microstructure roughness.
- II. To characterise the surface roughness of PCL microcarriers produced by the novel method of manufacture.
- III. To evaluate the growth of human BMSCs on PCL microcarriers and to test the hypothesis that increasing the degree of PCL microcarrier surface microstructure ($0.29 \mu\text{m} \leq R_a \leq 5.11 \mu\text{m}$) from the lower to higher end of the range would increase the expansion rates of human BMSCs.

- IV. To harvest expanded BMSCs from the PCL microcarriers and to evaluate retention of differentiation potential.

4.3 Materials and Method

4.3.1 Microcarrier Synthesis and Surface Roughness Alteration

The w/o/w method was employed to synthesise and prepare microcarriers as previously described in sections 2.3.2 and 2.3.3 using the polymer, PCL (section 2.3.1). A polyvinyl alcohol concentration of 0.6 g/l (for smoother PCL microcarriers) or 0.9 g/l (for rougher PCL microcarriers) was employed to ensure that the microcarriers were completely separated from each other.



Figure 30: Propeller-design impeller (30 mm diameter) on the left-hand side for the production of smoother PCL microcarrier surfaces. Pitch-blade impeller (49 mm diameter) on the right-hand side for the production of rougher PCL microcarrier surfaces.

4.3.2 Scanning Electron Microscopy

Scanning Electron Microscopy (SEM) was used to examine the surface topography of the microcarriers. Section 2.3.5 describes how this was performed.

4.3.3 Laser Profilometry

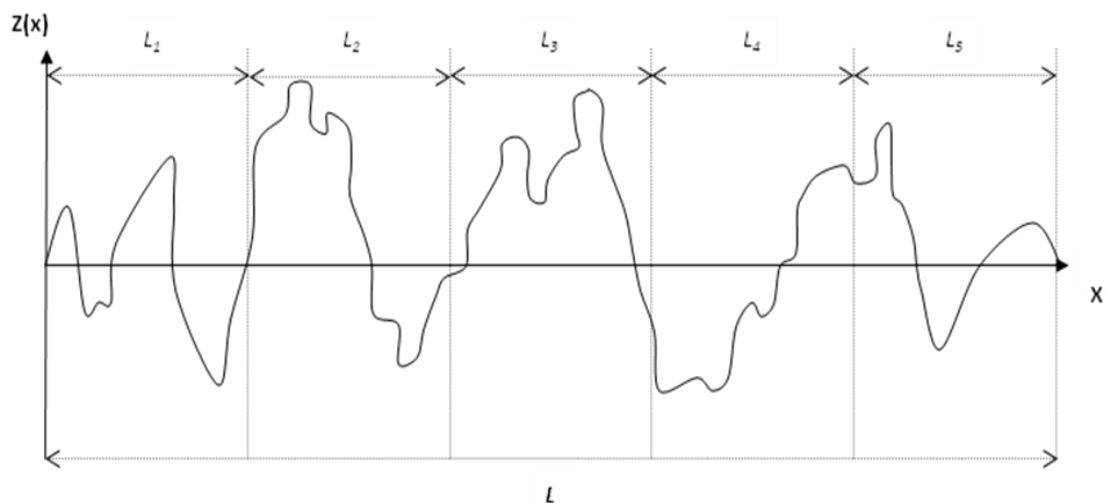


Figure 31: The variable components of the surface roughness parameters. x represents the microcarrier diameter and l represents diameter intervals. $Z(x)$ represents the amplitude.

The level of dry microcarrier surface roughness was measured with a laser profilometer (Proscan 2000A, Scantron Industrial Products Limited, England). The non-contact sensor head (model S29/12 Chromatic) possessed a measuring range of 12 mm, a stand-off distance of 29 mm, a resolution of 280 nm and a nominal spot size of 22 μm . Microcarrier surface roughness was measured using an area of 100 μm x 100 μm at 1 μm step size ($n = 6$). The surface filter was set to 1 so as to convert the spherical dimensions of the microcarriers into a 2D surface. The parameters evaluated were R_a , R_q and R_{zDIN} , which are amplitude characterisations. Figure 31 and Table 3 describe these parameters (Wieland 1999). Appendix 8.4 describes the method of surface roughness measurement.

Table 3: Table of surface roughness parameter definitions. They are amplitude parameters which are measures of the vertical characteristics of the microcarrier surface.

Parameter	Definition	Formula
R_a	Arithmetic mean of the absolute departures of the roughness profile from the mean line.	$\frac{1}{L} \int_0^L z(x) \cdot dx$
R_q	Root Mean Square. This parameter gives leverage to the extreme R_a values.	$\sqrt{\frac{1}{L} \int_0^L z^2(x) \cdot dx}$
R_{zDIN}	Numerically the average height difference between the five highest peaks (p) and the five lowest valleys (v) within the sampling length.	$\frac{1}{5} \left[\sum_{i=1}^{i=5} z_{pi} - \sum_{i=1}^{i=5} z_{vi} \right]$

4.3.4 Human BMSC Sources

The human BMSCs were provided by Xpand Biotechnology BV (The Netherlands). BMSCs from three human donors were used. Bone marrow was obtained from three patients who underwent total hip arthroplasty in the Netherlands. Their details are listed in section 3.3.1. The bone marrow was placed in T-flasks, expanded in proliferation medium (refer to section 3.3.2), harvested and either cryopreserved or replated. Passage two BMSCs were utilised for this study.

4.3.5 MSC Pre-cultivation, Culture, Population Monitor, Harvest and Differentiation

BMSC pre-cultivation, culture, population monitor, harvest and differentiation into more than one lineage were carried out as per sections 3.3.5, 3.3.6, 3.3.7, 3.3.8, 3.3.9 and 3.3.10. The experimental groups, conducted in triplicate, were smooth PCL (PCL-s) microcarriers and rough PCL (PCL-r) microcarriers. The control groups were Cytodex 1 microcarriers and expansion on plastic tissue culture well-plates (2D).

4.3.6 Microscopy

Light and fluorescent microscopy was used to qualitatively assess the cell attachment and proliferation on the microcarriers and tissue culture well-plates. Fluorescent microscopy was used to assess live/dead cell proportions on the microcarriers. Calcein AM dye (Invitrogen, United Kingdom) was used to stain live BMSCs attached to the microcarriers whilst Ethidium homodymer (Invitrogen, United Kingdom) was used to stain dead cells.

4.3.7 Statistical Analyses

Statistical analysis was performed on the number of population doublings and the surface roughness data using Genstat version 10.1 software. An ANOVA was selected when comparing all two experimental groups and two control groups for significant differences. The number of independent replicates was 3 (for cell culture studies) and 6 (for surface roughness studies). A student t-test was performed when comparing any significant differences detected by the ANOVA. A student t-test was performed for the surface roughness parameters. The level of significance was set at $p < 0.05$.

4.4 Results

The SEM images of PCL-s and of PCL-r, show visible differences in the surface roughness of the two microcarriers (Figure 32 and appendix 8.4). This observation was supported by the laser profilometry data (Figure 34 and Figure 35) which showed that PCL-r has a $R_a = 6.4 \pm 1.5$ microns and PCL-s has a $R_a = 1.8 \pm 0.5$ microns ($p = 0.025$). The root mean square (R_q) data showed that the surfaces of the PCL-r ($R_q = 17.9 \pm 5.7$ microns) and PCL-s ($R_q = 4.6 \pm 0.5$ microns) microcarriers do contain small areas of extreme surface roughness. The Environmental SEM results showed no changes in diameter as temperature and humidity increased by 11°C and 90% respectively (Figure 33).

The results of one human donor are presented within this section and the trends are representative of all three human donor BMSCs (see appendix 8.6). Cell population curves (Figure 36), population doublings (Figure 37), population doubling times (Figure 38) and light and fluorescent images (Figure 39) demonstrated BMSC cell growth and attachment on both surfaces. The PCL-r surface (2.16 ± 0.11 population doublings) favoured cell growth ($p = 0.02$) as compared to the PCL-s surface (1.33 ± 0.20 population doublings). Cell growth was superior on the control groups (tissue culture plastic and Cytodex 1) as compared to the experimental groups.

After harvesting, the BMSCs were successfully differentiated along the osteogenic and adipogenic lineages (Figure 40) for both the experimental and control groups which were subjected to the differentiation media. The ALP staining and lipid droplets were clearly visible as compared to the control groups which had been subjected to proliferation medium. These data showed that the expanded BMSCs have retained a differentiation potential to at least the osteogenic and adipogenic lineages. No

differences in differentiation potential were seen between the experimental and control groups.

4.4.1 Scanning Electron Microscopy

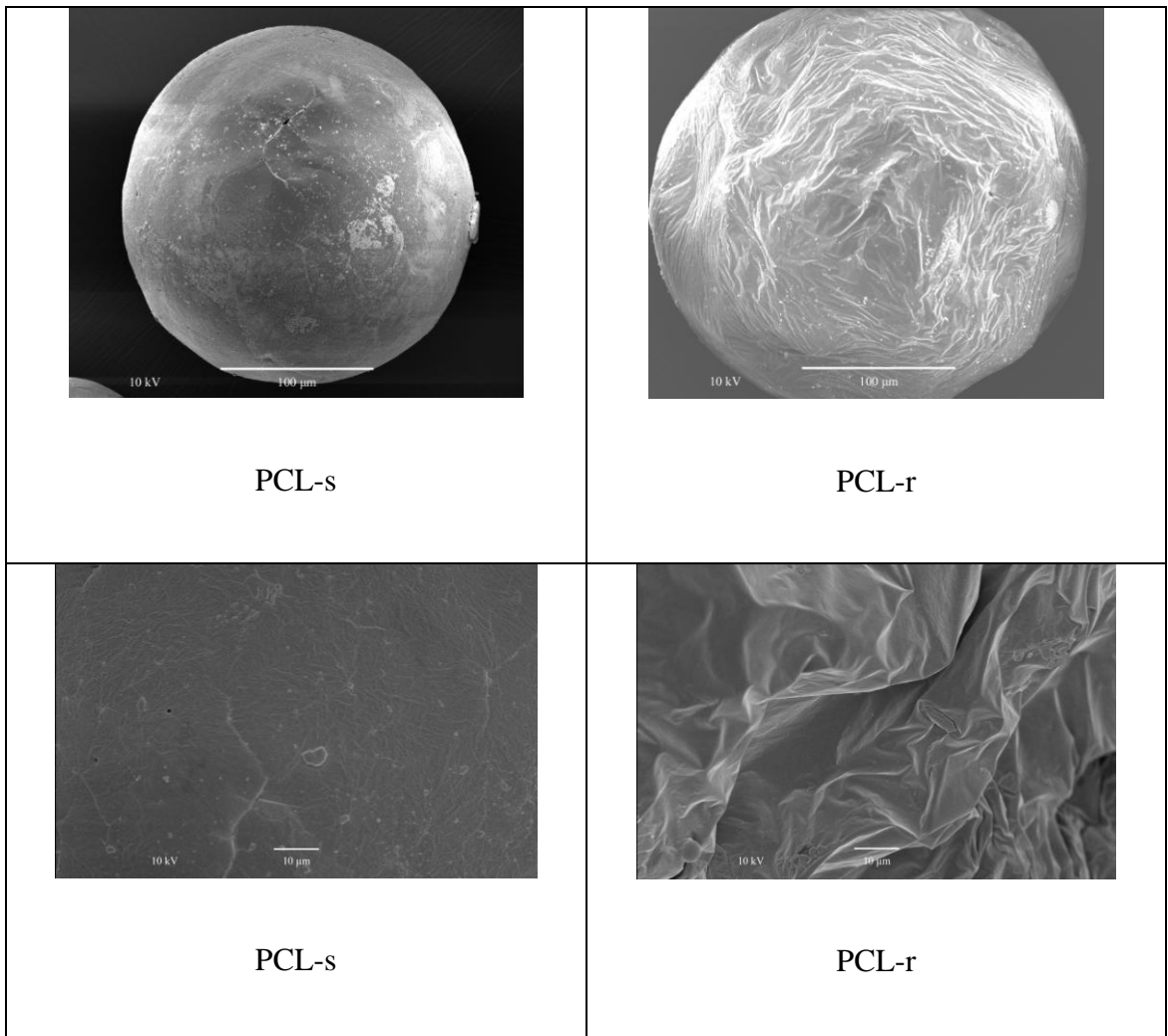


Figure 32: External morphologies of PCL-s (left-hand side) and PCL-r (right-hand side) microcarriers at two different magnifications at 10kV. The working distance and magnification of the top images were 10 mm and x1000 respectively, and of the bottom images were 19 mm and x1500 respectively.

4.4.2 Environmental SEM

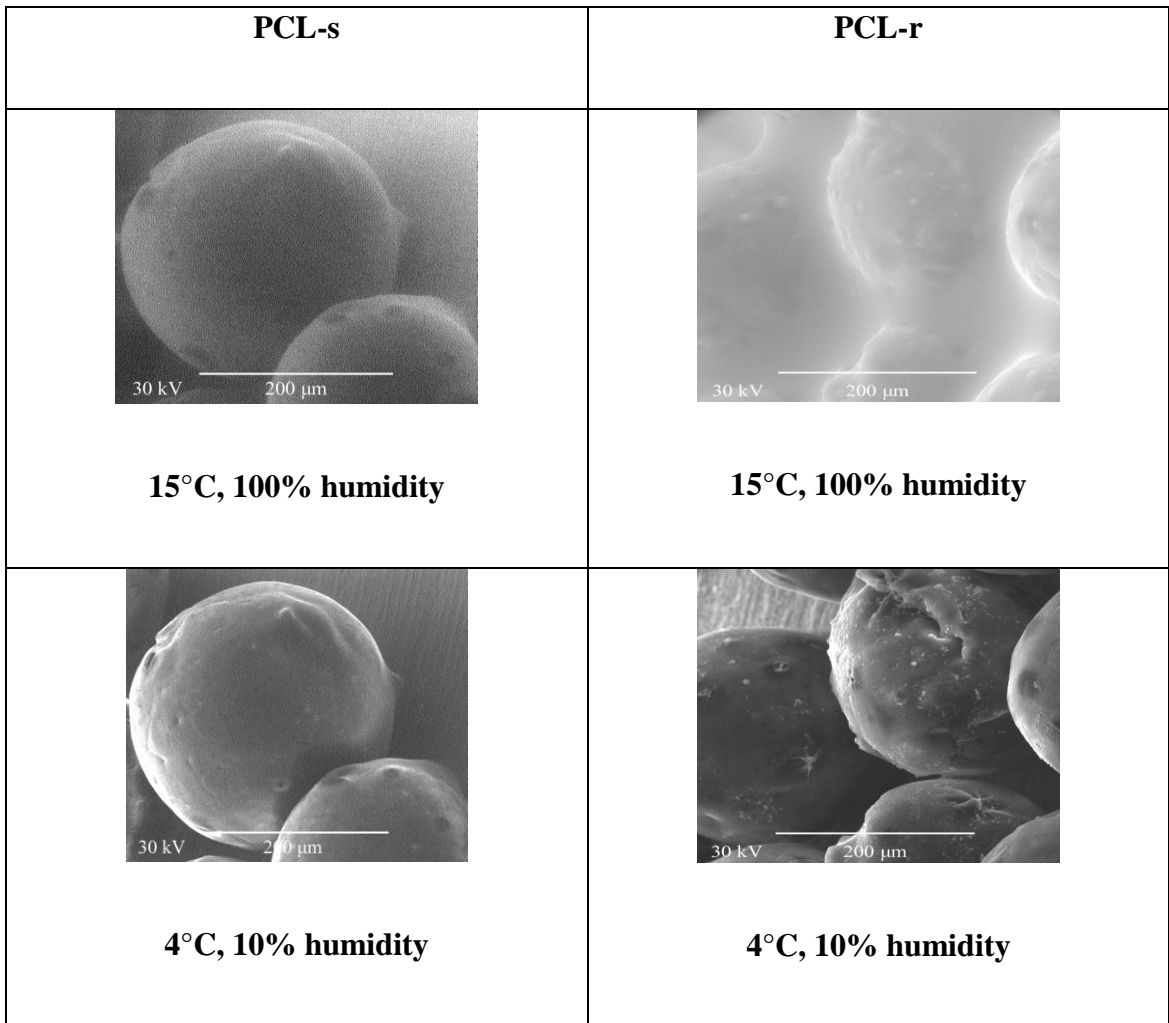
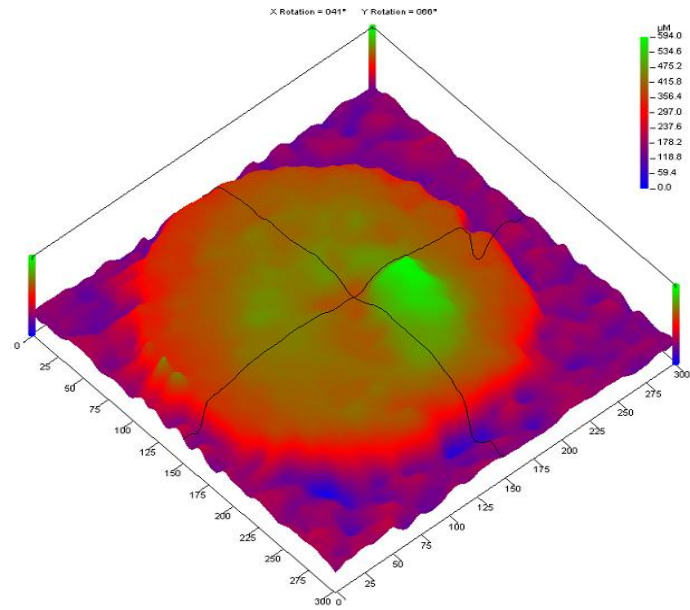
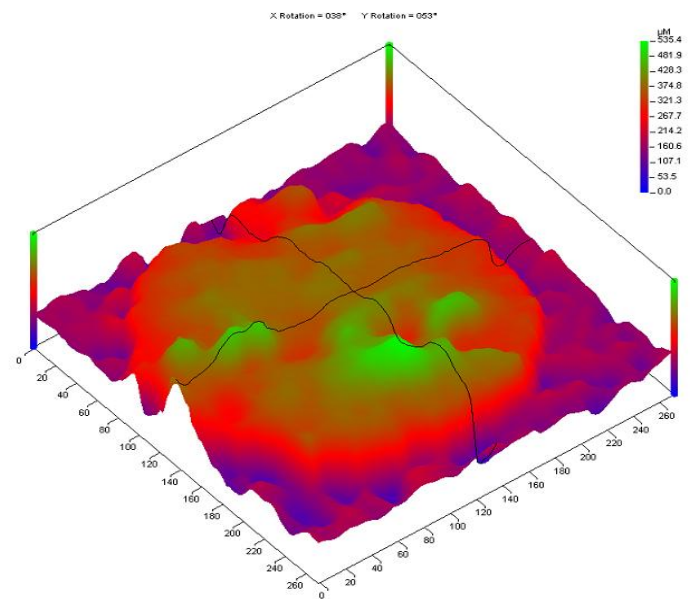


Figure 33: PCL-s and PCL-r subjected to different temperatures and humidities using the environmental SEM.

4.4.3 Laser Profilometry



PCL-s



PCL-r

Figure 34: Laser Profilometry Scans of PCL-s and PCL-r microcarriers.

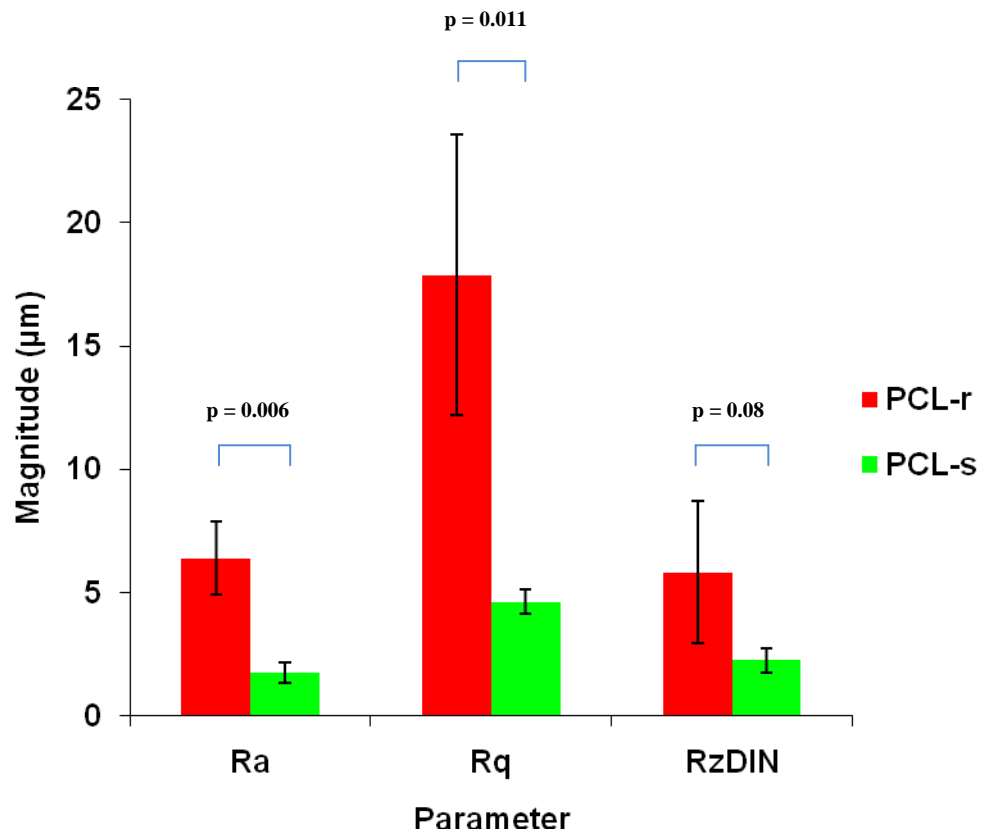


Figure 35: Surface roughness parameters (R_a , R_q and R_{zDIN}) of PCL-r and PCL-s which were obtained from the laser profilometer scans.

4.4.4 Human BMSC Population Analyses

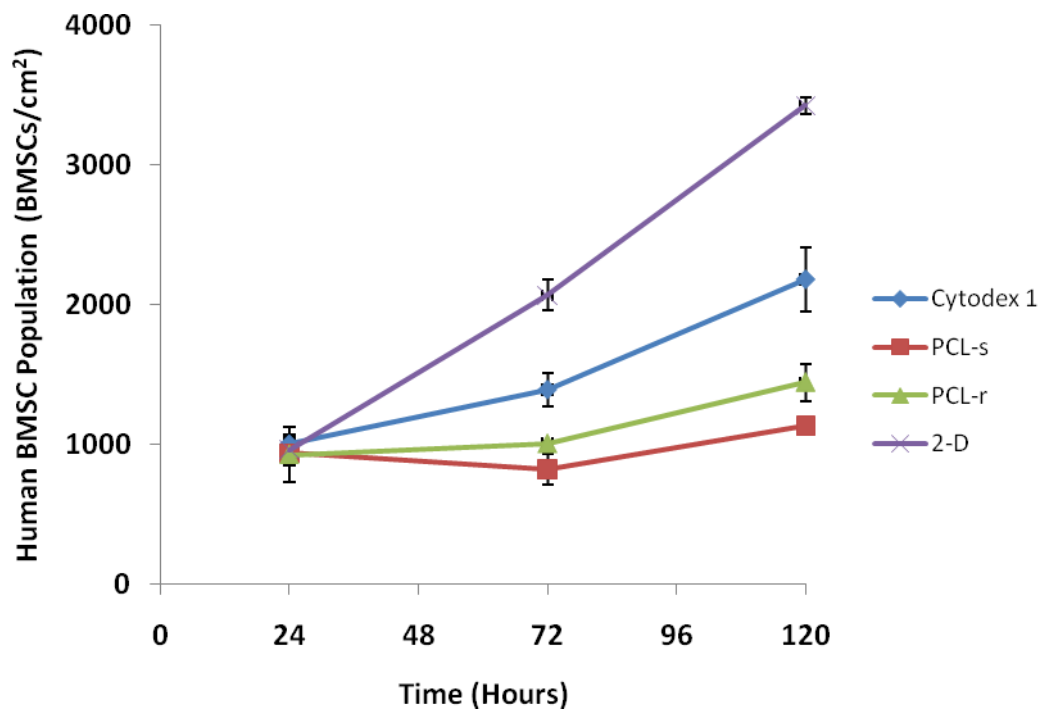


Figure 36: Human BMSC populations on the different scaffold types over a 120-hour period. Cytodex 1 is the 3D control and well-plates are the 2D control. The seeding density of 2000 BMSCs/cm² was applied at time 0 hours.

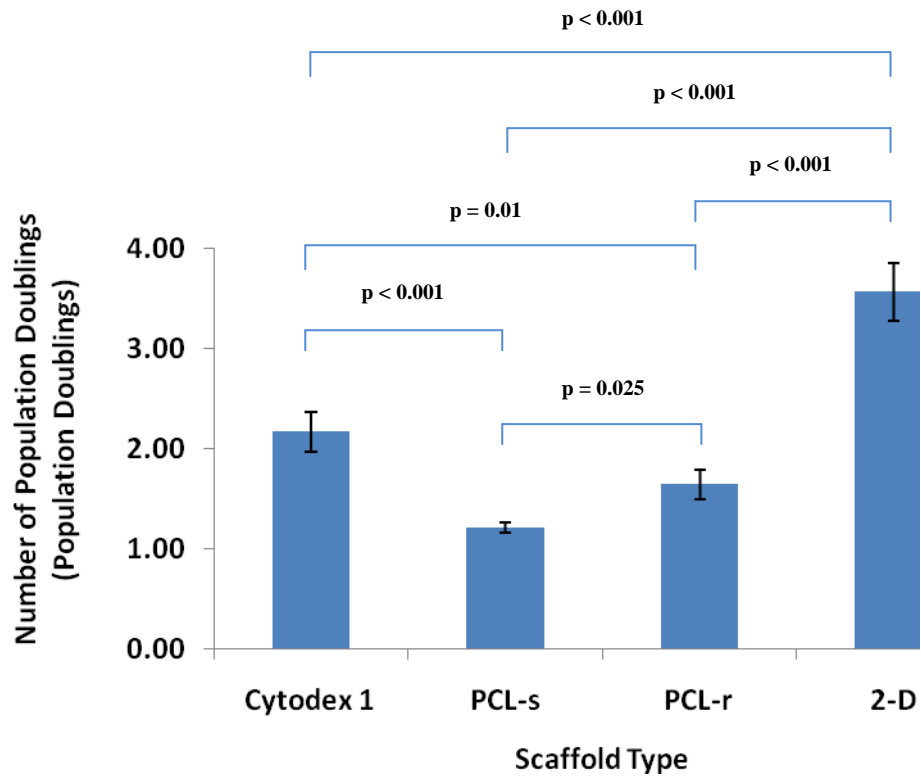


Figure 37: Human BMSC Population Doublings on the scaffold types. The data was calculated utilising BMSC population numbers at time-points 24 and 120 hours.

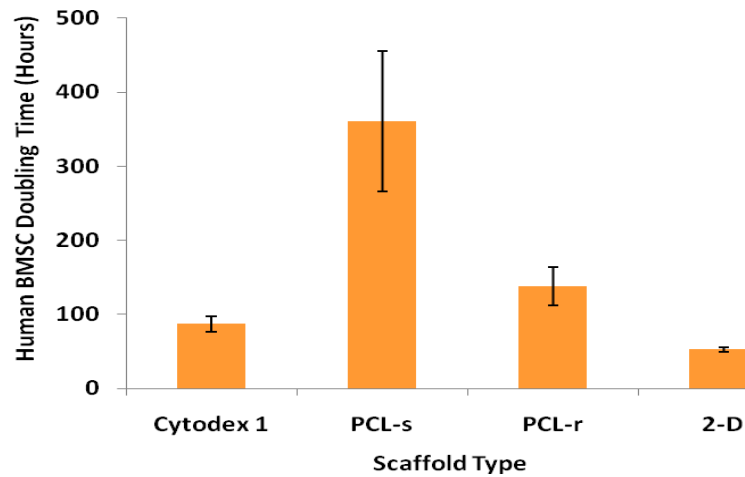


Figure 38: Human BMSC doubling times on the scaffold types. The data was calculated utilising BMSC population numbers at time-points 24 and 120 hours.

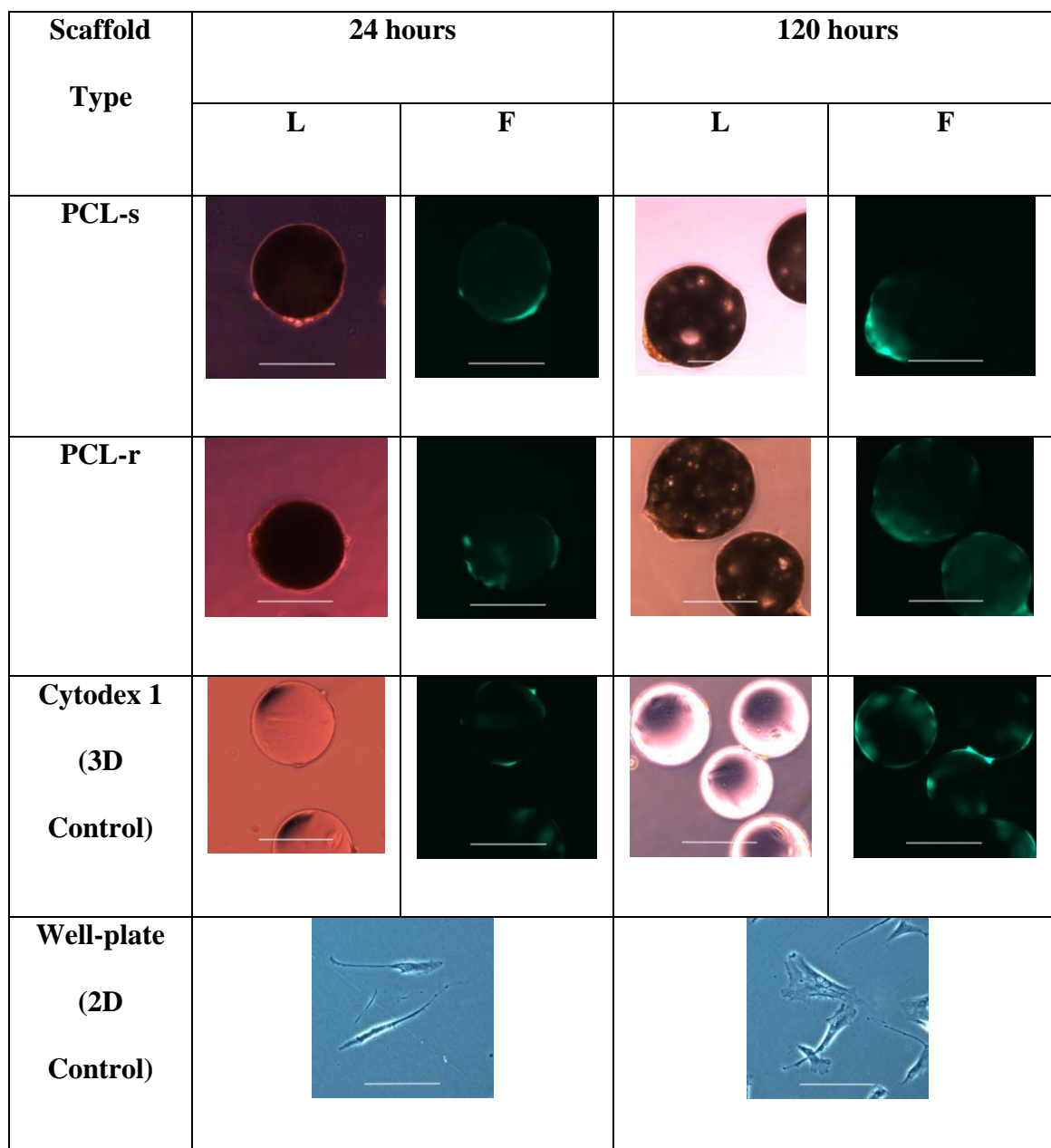


Figure 39: Light (L) and Fluorescence (F) micrographs of human BMSCs on microcarriers and well-plates after 24 and 120 hours after seeding. The green colour in the fluorescent micrographs indicates live cells, which correspondingly shows the location of the cells in light micrographs. The white scale bar represents 200µm. Magnification was at x100. Only light micrographs are shown for the 2D control.

4.4.5 Differentiation into the osteogenic and adipogenic lineages

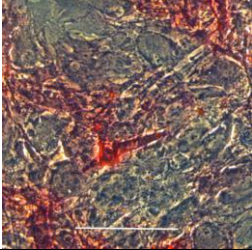
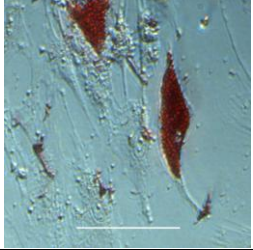
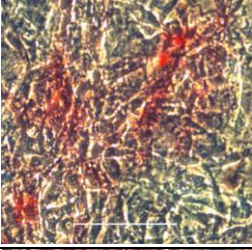

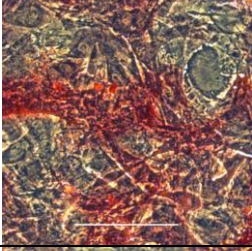

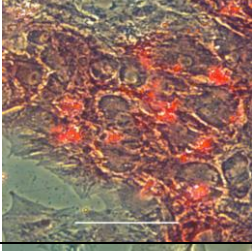
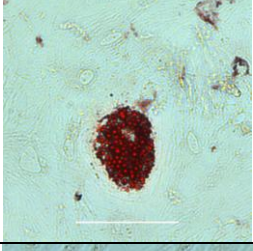

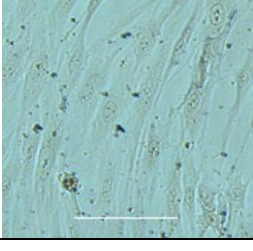
Scaffold Type	Osteogenesis	Adipogenesis
PCL-s		
PCL-r		
Cytodex 1		
2D		
2D (proliferation media only)		

Figure 40: Day 12 ALP and Oil Red O staining on the two experimental groups (PCL-s and PCL-r) and the two control groups (Cytodex 1 and 2D well-plates), which were all harvested BMSCs subjected to osteogenic medium (plus dexamethasone) or adipogenic medium. A 2D well-plate group subjected to proliferation medium was introduced as a negative control. The white scale bar represents 200µm.

4.5 Discussion

We have shown that two different impeller designs allow the synthesis of PCL microcarriers with different surface roughness. This was demonstrated by both SEM and laser profilometry. Based on laser profilometry, PCL-r microcarriers had $R_a = 6.4 \pm 1.5$ microns and PCL-s microcarriers had a $R_a = 1.7 \pm 0.4$ microns ($p = 0.006$). Although outside the scope of this thesis, the reason why the two designs produced PCL microcarriers of different surface roughness needs further investigation. We postulate that during the process of synthesis (refer to section 2.3.2), when the emulsion of dissolved PCL in chloroform is placed into the second aqueous volume and stirred for three hours, the mixing regimes differ significantly per impeller design, thereby altering the surface roughness of the microcarriers. On closer inspection of the three-hour stirring stage, it was noted that the circulating microcarriers (both PCL-s and PCL-r) did not reside within the impeller region. This suggested that different mixing regimes, rather than direct interaction of the PCL microcarriers with impeller blades, caused the difference in the microcarrier surface roughness. To support this postulation, it has previously been shown that impeller design defines the flow patterns which ultimately determine the mixing regime (Doran 2002). For the cultivation of plant cells in a stirred vessel, it has been shown that for a given impeller rotational speed, the intensity of agitation increased as the impeller diameter increased and a greater intensity of mixing was achieved throughout the vessel as the distance between the impeller and the air-liquid interface increased (Hooker et al. 1990). Within a biocentrifugal pump, it was found that for a given impeller rotational speed, a 16 forward-swept-blade impeller resulted in a lower frequency of vortices and high-shear-stress spots as compared to the

16-straight blade impeller, and differing velocity vector distribution and lower shear stress levels as compared to the 8-backward-swept blade impeller (Chua et al. 2008).

This study explored the effect of microcarrier surface roughness (R_a from $1.77 \pm 0.49 \mu\text{m}$ to $6.4 \pm 1.48 \mu\text{m}$) on human BMSC proliferation. Surface roughness measurements were taken on dry microcarriers. The drying effect may have led to artefacts owing to shrinkage. However, the environmental SEM images showed no changes in diameter and very little differences in surface roughness when subjected to temperature and humidity variations. BMSCs from all three human donors showed superior proliferation rates on PCL-r as opposed to PCL-s. For the human donor presented in this study, 2.16 ± 0.11 population doublings were recorded for PCL-r as compared to the 1.33 ± 0.20 population doublings for the PCL-s ($p = 0.025$) over the 120-hour culture period. This is consistent with previous findings (Degasne et al. 1999; Deligianni et al. 2001a; Deligianni et al. 2001b) where a variety of cell types were expanded on 2D surfaces with a combined range of degrees of surface roughness, $0.29 \mu\text{m} \leq R_a \leq 5.11 \mu\text{m}$.

The harvested BMSCs from the microcarriers were successfully shown to differentiate along the osteogenic and adipogenic lineages through qualitative analyses (ALP and Oil Red O staining respectively). There were no visual differences in the intensity of staining amongst the PCL-s, PCL-r and control groups. Cell culture on smooth and rough PCL surfaces over a 120-hour period had no effect on the BMSC differentiation potential as compared to the tissue culture plastic and Cytodex 1 control groups. Previous research has showed stem cells retaining their stemness on various polymeric scaffolds (Li et al. 2002; Gauthaman et al. 2009). MG 63 osteoblast-like cells have been cultured on smoother and rougher titanium disks ($0.22 \mu\text{m} \leq R_a \leq 4.37 \mu\text{m}$) and it has been found that the rougher surface resulted in higher concentrations of differentiation

markers (Lincks et al. 1998). Increased osteogenic differentiation potential has been supported by other studies (Martin et al. 1995; Lohmann et al. 1999). Furthermore, mesenchymal stem cell differentiation has been induced in the absence of biological stimuli, namely doping PCL with PLGA (Curran et al. 2009). Future research should therefore focus on the evaluation of differentiation potential of the harvested BMSCs, which have been cultured over a longer time frame on polymeric surfaces of different degrees of surface roughness.

4.6 Conclusion

A novel method of employing two impeller designs was used to prepare smooth and rough PCL microcarriers. The effect of impeller design on surface microstructure was shown with SEM and laser profilometry. These two characterisation techniques revealed visual differences in the surface roughness of PCL-r (rough PCL) and PCL-s (smooth PCL) and R_a values of $1.8 \pm 0.5 \mu\text{m}$ and $6.4 \pm 1.5 \mu\text{m}$ respectively. BMSCs from all three human donors showed superior proliferation rates on PCL-r as opposed to PCL-s, and maintained their differentiation potential along the osteogenic and adipogenic lineages. Future work is recommended to understand the mixing regimes which led to PCL microcarriers of significantly distinct microstructures, and to evaluate the effects of surface microstructure on differentiation potential over a longer cell culture period.

5 The Use of Particle Imaging Velocimetry to assess shear stress within a Spinner Flask Bioreactor

5.1 Abstract

The level of shear stress within a spinner flask bioreactor has been quantified with PIV (Particle Imaging Velocimetry). A PIV replica was constructed to closely mimic a spinner flask bioreactor used for 3D cell culture. With the aid of the PIV system, the shear was measured through systematically altering the microcarrier concentration and impeller speed. Cytodex 1 microcarriers were found to be adequate tracers within the PIV system. The mean shear stress within the impeller region was found to be approximately four times that within the non-impeller region. As expected, mean shear stress increased as microcarrier concentration and impeller speed increased.

5.2 Introduction

In the simplest terms, a bioreactor may be defined as any environment which supports biological activity. However, for the purposes of regenerative medicine, specifically stem cell production, this definition needs to be refined as environmental control is essential in any cell culture process. The variables that influence the viability and expansion of cells on microcarriers within a spinner flask bioreactor include stirring rate, microcarrier concentration, temperature, media pH, nutrients and metabolic waste concentration and dissolved gaseous pressures. This chapter focuses on quantifying shear stress within a spinner flask so that it may be used to determine its effect on cell culture.

Methods of shear stress measurement have proven vital in order to understand the nature of stem cells. Relatively simple laminar flow bioreactors have been utilised to measure shear stress based on flow rate and channel dimensions (Zeng et al. 2003; Zeng et al. 2006). Cell-based constructs in perfusion bioreactor systems, though laminar flow-based, have posed a greater challenge in terms of obtaining reliable shear stress data (Zhao et al. 2007). Shear stress measurements in such systems are based on flow rate and perfusion bioreactor channel dimensions, which involve complex mathematical modelling software and sophisticated equations such as Stokes' flow equations, Brinkman's equation and Poiseuille velocity profiles. Equally challenging was the determination of shear stress in spinner flask or stirred-tank bioreactor systems (Venkat et al. 1996; Aubin et al. 2004; Sucusky et al. 2004). PIV (Particle Imaging Velocimetry) is a flow visualisation technique (Raffel et al. 2007). The use of PIV is a relatively new tool for the assessment of shear stress in bioreactors for the purpose of expanding BMSCs. In this field, it has mainly been used for experimental studies relating to the

regeneration of cartilage (Bilgen et al. 2006; Bilgen and Barabino 2007) where velocity and shear profiles were established around cartilage constructs for bioreactor optimisation, and liver (Provin et al. 2008), where shear stress profiles provided recommendations for optimal liver construct geometry development. These studies have traditionally required the development of a bioreactor replica in terms of geometry and which accurately replicates cell culture conditions. To complement experimental results obtained by the previous studies, the shear stress was calculated through computational fluid dynamics (CFD) modelling, which was calculated as the area-weighted average at any given time.

Previous data (Stathopoulos and Hellums 1985; Zhao et al. 2007) have provided information on the shear stress that cells can withstand. This chapter not only measures shear stress under certain conditions, but it provides data which can determine optimal bioreactor design through impeller design, stirring speed and microcarrier concentration.

In this chapter, PIV will be employed to quantify shear stress within a spinner flask for the ultimate purpose of evaluating BMSC expansion within spinner flask microcarrier culture. The aims and objectives are:

- I. To build a PIV replica of a 100 ml spinner flask.
- II. To establish a viable PIV set-up in order to gather data.
- III. To determine the suitability of Cytodex 1 microcarriers as tracer particles.
- IV. To quantify shear stress levels at different horizontal positions of the spinner flask.

- V. To identify regions of high and low shear stress.
- VI. To perform a basic assessment of spinner flask hydrodynamics.

5.3 Materials and Method

5.3.1 Experimental Groups

The experimental groups within this study were based on impeller rotation rates and Cytodex 1 (GE Healthcare, United Kingdom) microcarrier concentrations. Table 4 describes the experimental groups in terms of impeller rates and microcarrier concentration. Microcarrier concentrations are described both in microcarrier surface area per unit volume of proliferation media and in microcarrier mass per unit volume of proliferation media.

Table 4: Description of the Experimental Groups within this study.

Group	Spinner Flask Impeller Rate (rpm)	Wet Microcarrier Concentration (cm ² /ml)	Dry Microcarrier Concentration	
			(g/ml)	(g/l)
1	45	20	0.0045	4.5
2	45	60	0.0136	13.5
3	60	20	0.0045	4.5
4	60	60	0.0136	13.5

5.3.2 Rheometer

In order to determine viscosity, a rheometer (TA Instruments, AR2000, USA) was employed to analyse proliferation medium (see section 3.3.2 for the constituents)

tailored to support the growth of human BMSCs. The purpose was to ensure that the cell culture conditions could be accurately reproduced in the PIV experiments using varying concentrations of glycerol. A 40 mm (2°) cone head was used in the set-up. Each experimental group was subjected to three runs. Each run consisted of 15 time-point samples of viscosity measurements within a 90 second period with the cone head rotating within the medium. Prior to each run, the samples were pre-warmed to 37°C and the equilibration time was 60 seconds. The cone head rotational speeds were 2π rad/s (60 rpm) and $3\pi/2$ rad/s (45 rpm). The average values from the three runs were taken as the viscosity of the experimental group.

5.3.3 Identification of Aqueous Glycerol Solutions with Matching Experimental Group Viscosities

Literature values (Kaye and Laby 1995) of aqueous solutions were sought to match the viscosity results of the experimental groups from the previous section (section 5.3.2), in order to use for the PIV experiments. Two graphs were plotted: (1) viscosity versus aqueous glycerol and (2) viscosity versus temperature (see Figure 45).

5.3.4 PIV Replica and Impeller

A PIV replica was constructed so as to match closely the dimensions of the working volume of the cell culture spinner flask as well as to facilitate PIV measurements. Table 5 and Figure 41 provide information on the differences between the PIV replica and the cell culture spinner flask. The geometry of the PIV replica bears insignificant differences to the spinner flask.

Table 5: A comparison of the physical dimensions of the spinner flask and the PIV replica.

Dimension	Spinner Flask	PIV Replica	Difference relative to Spinner Flask (%)
Internal Diameter (mm)	57.56	58.14	1.0
Outer Diameter (mm)	63.56	68.08	7.1
Working Volume Height (mm)	43.08	40.00	7.7
Working Volume (ml)	100	100	0
Impeller Height (mm)	25.50	25.50	0
Impeller Diameter (mm)	50.76	50.76	0
Shape of Flask Bottom	Curved Middle	Flat	n/a
Distance of magnet from top and bottom of impeller respectively (mm)	12.86, 3.32	12.86, 3.32	0, 0



Figure 41: PIV replica (left) and the spinner flask (right).

5.3.5 Tracers

Cytodex 1 microcarriers (GE Healthcare, United Kingdom) were utilised as tracers. A dry mass of 0.07g Cytodex 1 microcarriers (effective concentration of 0.007g dry mass/1 volume glycerol or 0.00007g dry mass/ml volume glycerol) was used for each experimental group (100 ml). The average diameter of the microcarriers was 147 – 248 microns.

5.3.6 PIV Set-up and Procedure

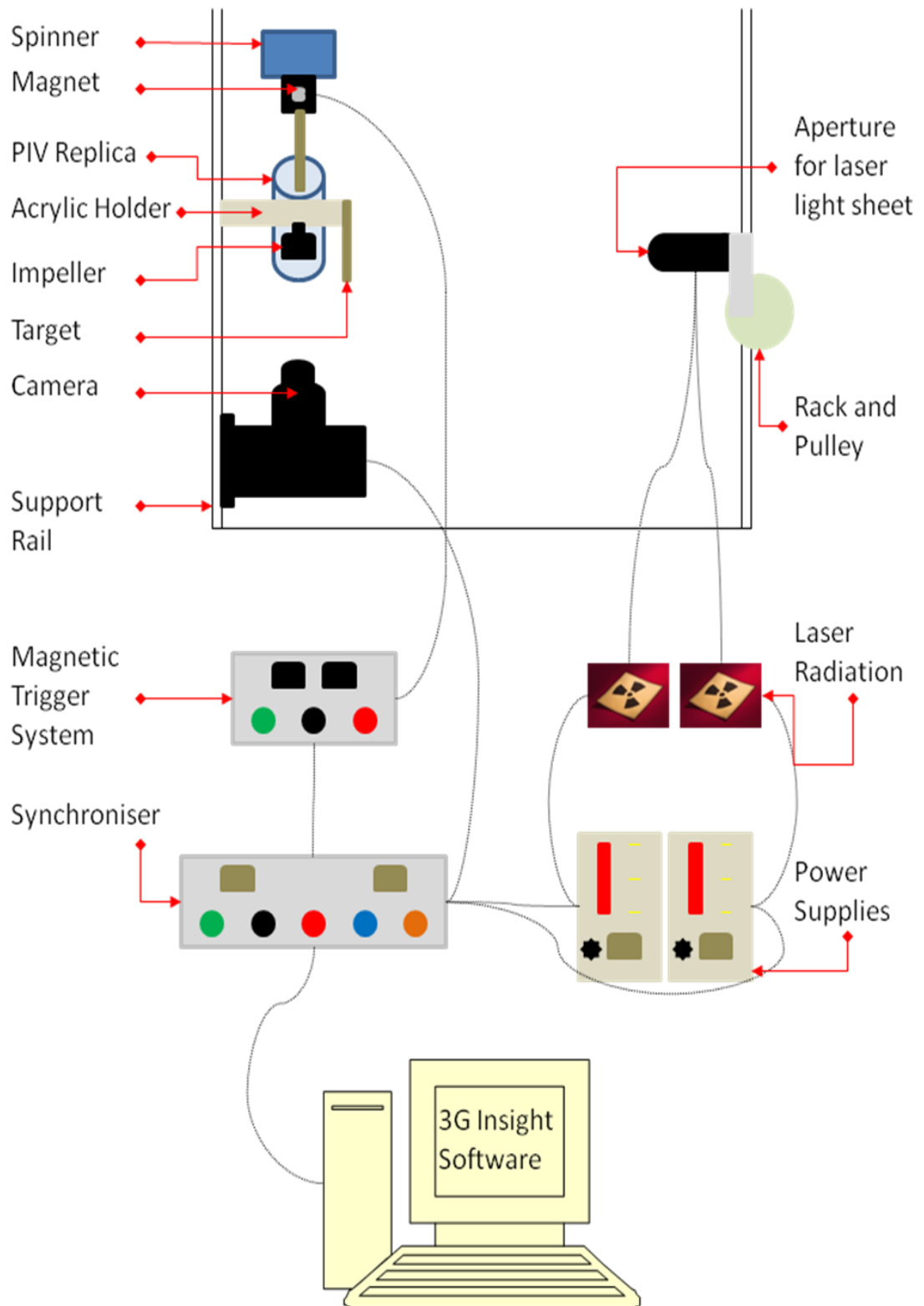


Figure 42: The Particle-Image Velocimetry system.

The TSI laser system was used to record Particle Image Velocimetry (PIV) data. It consisted of a 190 mJ Nd:Yag laser, maximum repetition rate 15 Hz and a 4 megapixel Power View Plus Camera fitted with a Nikon 105 mm lens. The laser light was diverted to the appropriate position for data acquisition by means of a light arm. The sheeting optics were attached to the light arm aperture so as to direct the light sheet across the PIV replica, illuminating a circular cross-section. In order to reduce specular reflections, the impeller surface was treated with matt black paint and the experimental area enclosed during data acquisition.

As shown in Figure 42, the PIV replica was placed in the acrylic holder which was held firmly by an 22.5 x 180 mm Optical Rail (Bosch Rexroth, United Kingdom). The Optical Rail was held perpendicularly through the use of 45 x 45 x 90 brackets (Bosch Rexroth, United Kingdom). A camera was attached to the perpendicular Bosch Rail such that the lens was in line with the bottom of the prototype flask. The machine spinner was positioned such that the impeller would occupy the working volume of the prototype flask and skim the surface, in order to mimic the impeller position used during cell culture experiments.

A magnetic trigger system was used to trigger the PIV system. The magnet was secured to the spinner to ensure data acquisition at identical positions during each cycle. This allowed a number of image pairs to be acquired and ensemble average velocity fields to be calculated. The PIV system was controlled through a computer interface, Insight 3G version 9.0.3.1 software (TSI, USA).

As the light sheet passed through the flask, the cytodex 1 microcarriers scattered the light such that the camera could record the movement of the particle images over two frames. Temperature control of the ambient air was possible using a portable 9k BTU

air conditioner of model number 636212 (Homebase, United Kingdom) and a thermocouple. Data collection took place within one hour of glycerol-tracer preparation.

5.3.7 PIV Data Processing

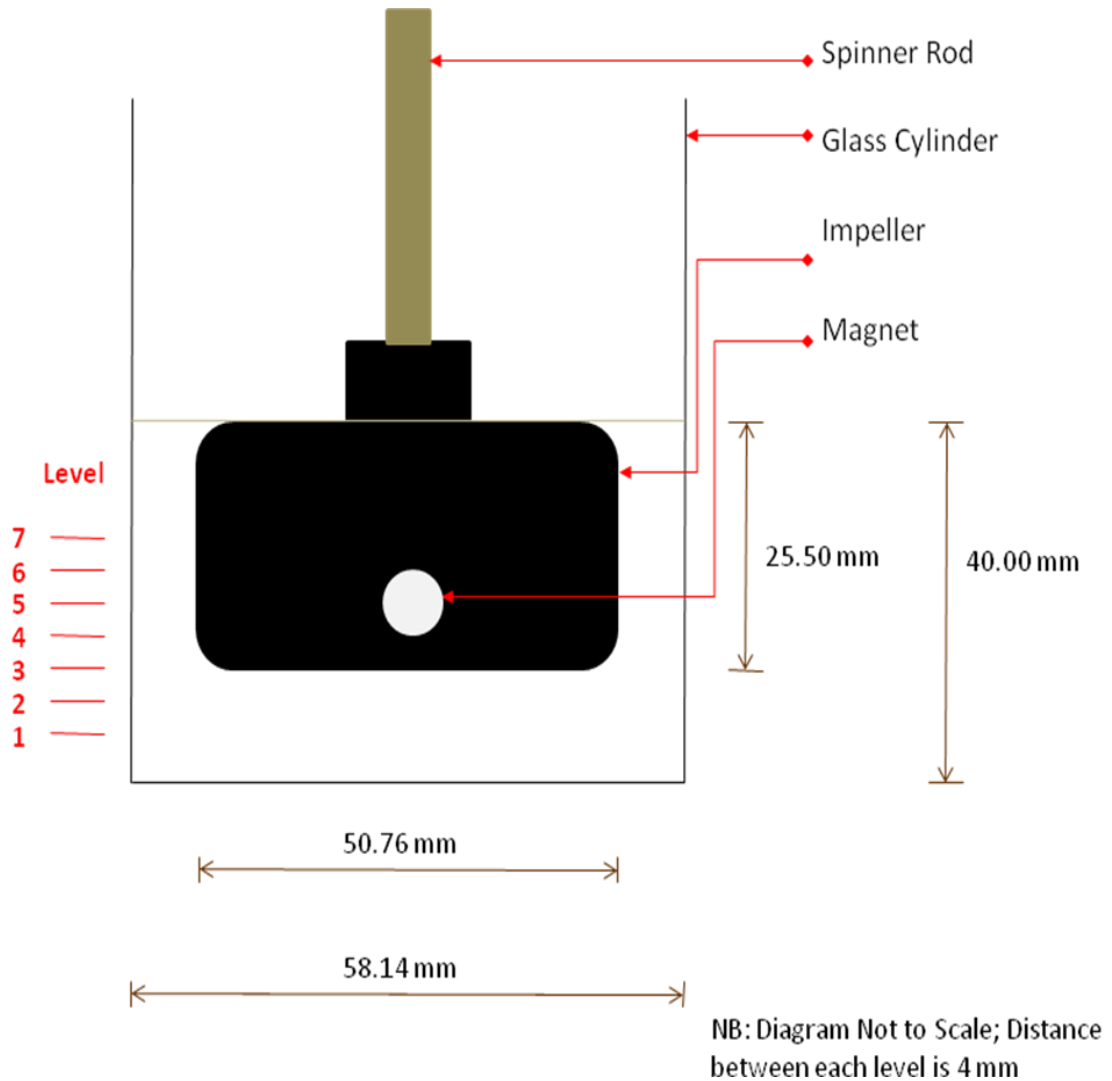


Figure 43: Height in levels of the PIV replica where data was sourced.

The region of interest was defined to ensure only valid data was included; the same region was applied at all heights of data acquisition (see Figure 43). A Fast Fourier Transform (FFT) cross-correlation algorithm was applied to image pairs to calculate velocity vectors. A recursive nyquist grid processed the images in multiple passes. The

displacement from the correlation data was carried out through the three-point estimator of a Gaussian peak (peak engine) fitting (Raffel et al. 2007). Data validation occurred through 3 x 3 median filtering (Westerweel 1994).

Ensemble-average data was calculated from 100 image pairs per impeller orientation, per height level, per experimental group (see appendix 8.7). Two impeller orientations were investigated in this study. Velocity magnitude and strain rate two-dimensional maps were constructed. Minimum, maximum, mean, standard deviation and standard error of the mean shear stress values were obtained (Freedman et al. 1998; Hines et al. 2003; Altman and Bland 2005; Bluman 2008). These parameters were plotted against PIV replica height levels for given experimental groups. Where mean shear stress was plotted against height, statistical analyses were performed using Genstat version 10.1 software.

5.3.8 Shear stress, Fluid Regime and Relaxation Time

Shear stress, τ , was calculated using Equation 7, μ = viscosity and γ = shear rate. (Coulson and Richardson 1999)

Equation 7: Newton's Law of Viscosity

$$\tau = \mu\dot{\gamma}$$

Tip Speed was calculated using Equation 8, where N_i = Impeller Speed and D_i = Impeller Diameter. (Doran 2002)

Equation 8: Tip Speed

$$Tip\ Speed = \pi N_i D_i$$

The Reynolds number, Re , was calculated using Equation 9, where ρ = density. This parameter defined flow regime. (Doran 2002)

Equation 9: Reynolds Number

$$Re = \frac{(N_i D_i^2 \rho)}{\mu}$$

Kinematic Viscosity, ν , was calculated using Equation 10. (Doran 2002)

Equation 10: Kinematic Viscosity

$$\nu = \frac{\mu}{\rho}$$

Fluid residence time, $t_{residence}$, was calculated using Equation 11, where V = reactor size and F = Flow rate. (Doran 2002)

Equation 11: Fluid Residence Time

$$t_{residence} = \frac{V}{F}$$

Particle Relaxation Time, $t_{relaxation}$, was calculated using Equation 12, where ρ_p = particle density and d_p = particle diameter. (Raffel et al. 2007)

Equation 12: Particle Relaxation Time

$$t_{relaxation} = \frac{\rho_p d_p^2}{18\nu}$$

5.3.9 Statistical Analysis

Statistical analyses were performed on regional shear stress using Genstat version 10.1 software. An ANOVA was performed when comparing all experimental groups for significant differences. Specifically, the number of independent replicates was 200 per level of the PIV replica. A student t-test was performed when comparing any significant differences detected by the ANOVA. The level of significance was set at $p < 0.05$.

5.4 Results and Discussion

5.4.1 Determination of PIV conditions which reflect the bioreactor conditions

The results of the rheometer experiments (Figure 44) showed that a three-fold increase in microcarrier concentration resulted in a roughly two-fold viscosity increase. Literature values (Kaye and Laby 1995) pertaining to the viscosity changes of aqueous glycerol were plotted (Figure 45) in order to determine concentrations of aqueous glycerol and temperature required to replicate cell culture viscosity conditions. The exact conditions are shown in Table 6.

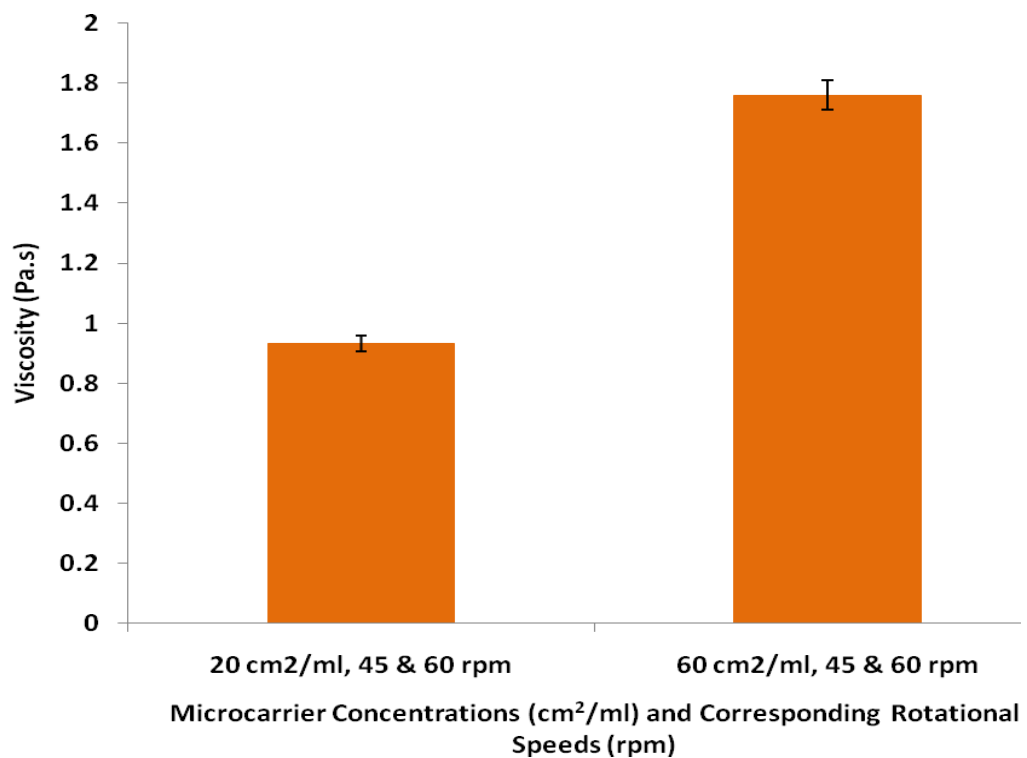


Figure 44: Viscosity of Cell Culture Media at different microcarrier concentrations and rotational speeds as revealed by the Rheometer at 37°C. The viscosity values were used to obtain aqueous glycerol concentrations and temperatures (Figure 45) which were used for the PIV study.

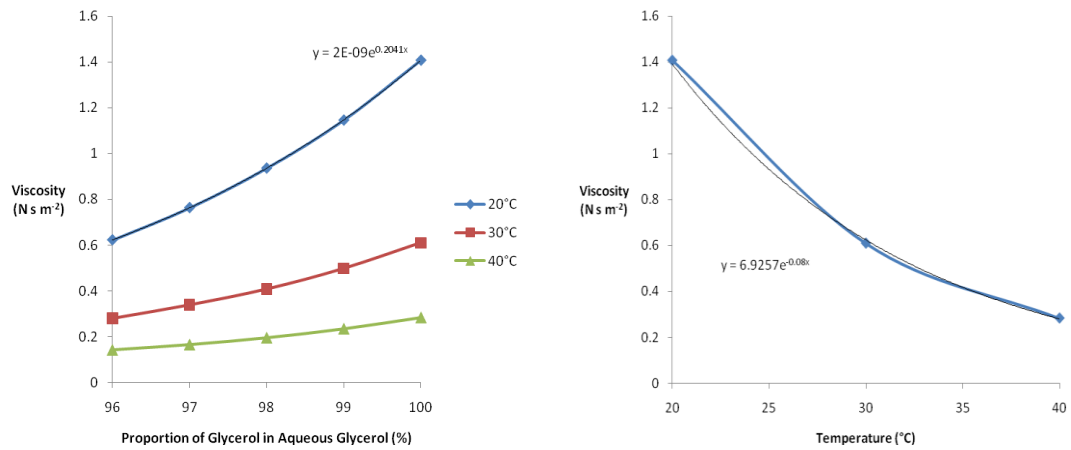


Figure 45: Literature values (Kaye and Laby 1995) illustrating how the viscosity of glycerol varies with water concentration and temperature. The viscosity values obtained by the rheometer (Figure 44) were used to obtain the aqueous glycerol concentration (graph on the left-hand side) and the temperature (graph on the right-hand side for 100% glycerol only). The obtained aqueous glycerol concentration and the temperature matched the cell culture conditions in terms of viscosity.

Table 6: Equivalent PIV (impeller speed, aqueous glycerol concentration, temperature) conditions for the bioreactor conditions (impeller speed, microcarrier surface concentration, temperature) based on the results of Figure 44 and Figure 45.

Bioreactor Condition	Equivalent PIV Condition
45 rpm, 20 cm ² /ml, 37°C	45 rpm, 98% Glycerol, 20°C
45 rpm, 60 cm ² /ml, 37°C	45 rpm, 100% Glycerol, 17.1°C
60 rpm, 20 cm ² /ml, 37°C	60 rpm, 98% Glycerol, 20°C
60 rpm, 60 cm ² /ml, 37°C	60 rpm, 100% Glycerol, 17.1°C

5.4.2 Relaxation Times and Reynolds Number

As seen in Table 7, $1.09 \leq Re \leq 2.72$ for all four experimental groups. This demonstrated that laminar flow was prevalent in the spinner flask bioreactor (Coulson et al. 1999; Dusting et al. 2006). Table 8 compares the relaxation time of the particle (Cytodex 1 microcarrier) and the residence time of the fluid. The relaxation time is a measure for the tendency of particles to attain velocity equilibrium with the fluid (Raffel et al. 2007). The result demonstrated that $t_{\text{relaxation}} < t_{\text{residence}}$ by five orders of magnitude. This proved that the Cytodex 1 microcarriers followed fluid flow and thus proved suitable as tracers.

The particle relaxation time (Equation 12) assumes a Stokes' regime ($Re < 1$). At greater Re , Equation 12 can overestimate the relaxation or response time (Micheletti and Yianneskis 2004). Neutrally buoyant particles are generally expected to have no influence on the continuous phase; however there are studies which demonstrate a significant influence as particle volumetric concentration increase (Zitoun et al. 2001; Micheletti and Yianneskis 2004). The experimental groups within our study demonstrated $1.09 \leq Re \leq 2.72$; generally, Re (stirred vessels) ≤ 10 for laminar flow regimes (Doran 2002). Therefore, it was assumed that the Cytodex 1 microcarriers still followed fluid flow.

Table 7: Calculated parameters of impeller speed, tip speed and Reynolds' number for given impeller speeds and microcarrier concentration.

Experimental Groups	Impeller Speed N_i (rps)	Tip Speed $\pi N_i D_i$ (m)	Reynolds Number Re
45 rpm, 20 cm ² /ml	0.75	0.12	2.04
45 rpm, 60 cm ² /ml	0.75	0.12	1.09
60 rpm, 20 cm ² /ml	1	0.16	2.72
60 rpm, 60 cm ² /ml	1	0.16	1.45

Table 8: Comparison of the relaxation times of both the particle and of the fluid.

Experimental Groups	Density of Fluid ρ_f (kg/m ³)	Kinematic Viscosity μ_k (m ² /s)	Relaxation Time Particle $t_{relaxation}$ (s)	Residence Time Fluid $t_{residence}$ (s)
45 rpm, 20 cm ² /ml	984.55	9.47×10^{-3}	2.39×10^{-6}	0.21
45 rpm, 60 cm ² /ml	993.64	1.77×10^{-4}	1.27×10^{-6}	0.16
60 rpm, 20 cm ² /ml	984.55	9.47×10^{-3}	2.39×10^{-6}	0.21
60 rpm, 60 cm ² /ml	993.64	1.77×10^{-4}	1.27×10^{-6}	0.16

5.4.3 Cytodex 1 microcarrier as tracers

Figure 46 shows two orientations of the impeller and the cytodex 1 microcarriers scattering the laser light. The presence of the impeller and magnet results in shadows. Hence, for the purpose of data extraction, the region of interest is in the form of a semi-circle (top half of the images in Figure 46). Figure 47 shows the microcarriers scattering light within the region of interest.

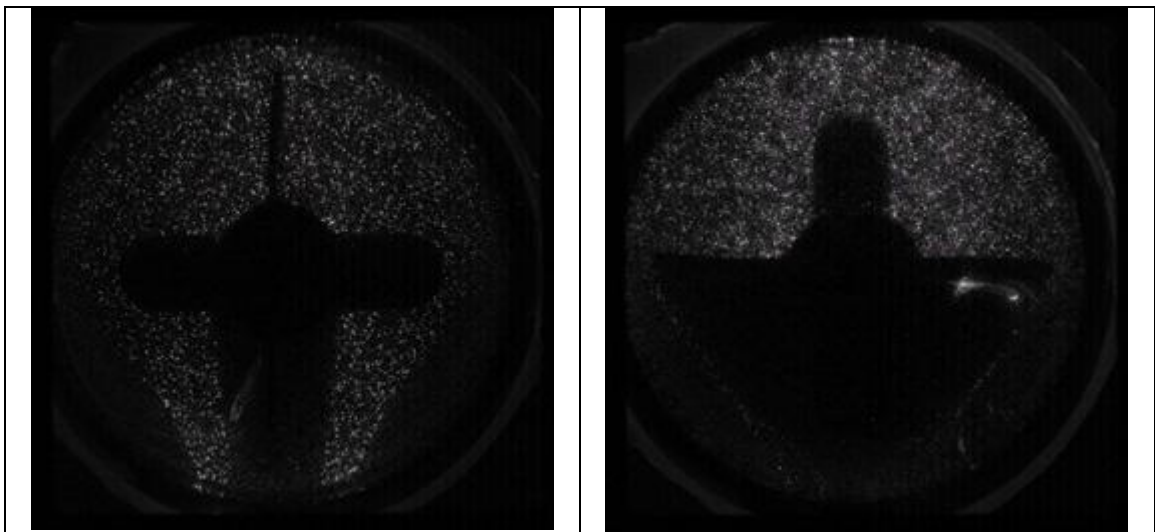


Figure 46: Two horizontal orientations of the impeller (impeller blade upright on the left-hand side and magnet upright on the right-hand side as seen on this page) which shows the cytodex 1 microcarriers scattering the laser light.

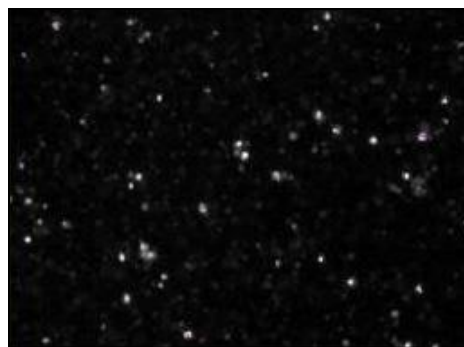


Figure 47: A close-up of the region of interest showing the cytodex 1 microcarriers scattering the laser energy.

5.4.4 Evaluation of Shear Stress within Spinner Flask Bioreactor

As shown in Figure 48, the magnitude of shear stress for all four groups is approximately four-fold higher within the impeller region (levels 4-7) as compared to below the impeller region (levels 1-2). The 45 rpm, 20 cm² group has a steady level of shear stress and no observable peak at the region of the impeller for all levels, whereas for the other groups, a peak is observed between levels 5-6. Furthermore, there is a distinct range of mean shear stress for the 45 rpm, 20 cm² group ($3.4 \times 10^{-3} \leq \text{shear stress} \leq 4.6 \times 10^{-3} \text{ N/m}^2$) as opposed to the close proximity of the other three groups ($5.5 \times 10^{-3} \leq \text{shear stress} \leq 1.3 \times 10^{-2} \text{ N/m}^2$).

The maximum and minimum spatial shear stress recorded respectively per level for given impeller speeds and microcarrier concentrations are shown in Figure 49 and Figure 50 respectively. They indicate maximum shear stress to be in the order of 10^{-2} to 10^{-1} N/m^2 , whereas minimum shear stress was found to be in the order of 10^{-7} to 10^{-6} N/m^2 .

The relative shear stress of the impeller versus the non-impeller regions is shown in Figure 51. It indicates that 80% of the shear stress by volume is localised at the levels of the impeller region. Between the groups, there were statistical differences ($p \leq 0.001$) which were noted at the impeller region. At the non-impeller region, there was no statistical difference with the two exceptions of a difference between 60 rpm, 60 cm²/ml and 45 rpm, 60 cm²/ml ($p = 0.01$) and a difference between 60 rpm, 60 cm²/ml and 60 rpm, 20 cm²/ml ($p = 0.037$). Figure 52, Figure 53, Figure 54 and Figure 55 show maps of the velocity and strains rates at the impeller and non-impeller regions.

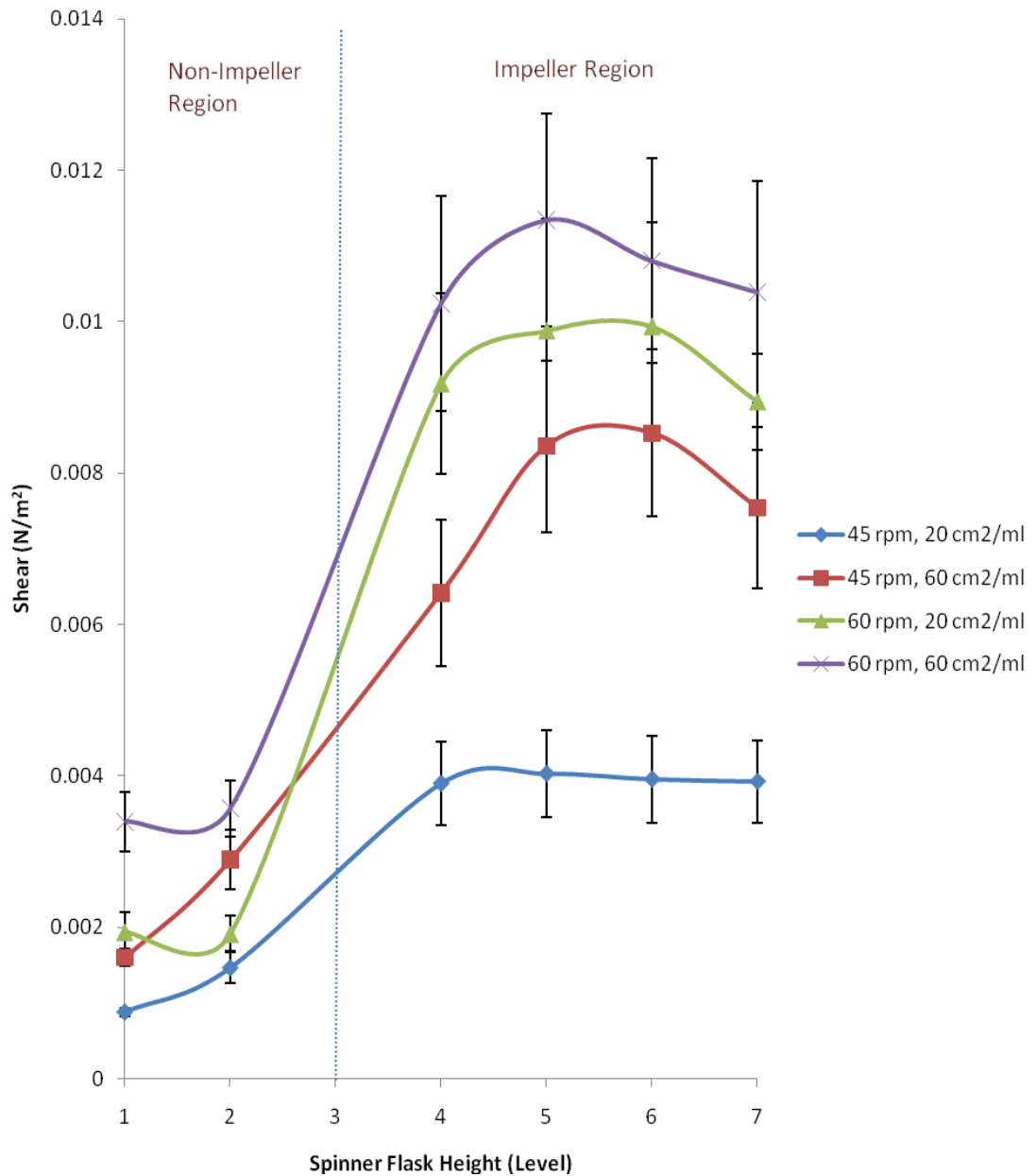


Figure 48: Comparison of the ensemble mean shear stress against levels of height within the Spinner Flask replica. The ensemble mean shear stress was calculated based on 100 image pairs per two impeller orientations per height level per experimental group taken by the camera. Refer to Figure 43 for a description of the levels. The difference between each level was 4 mm. Level 1 was 6.5 mm from the bottom of the replica; level 7 was 13.5 mm from the top of the working volume; level 3 represents the boundary between the impeller and non-impeller regions.

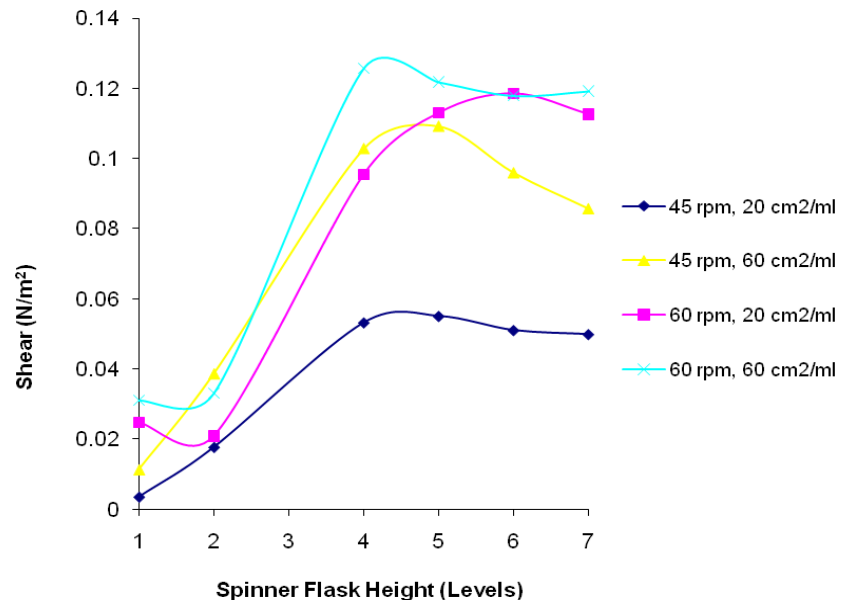


Figure 49: The maximum shear stress recorded at different heights of the spinner flask bioreactor for given impeller speeds and microcarrier concentrations.

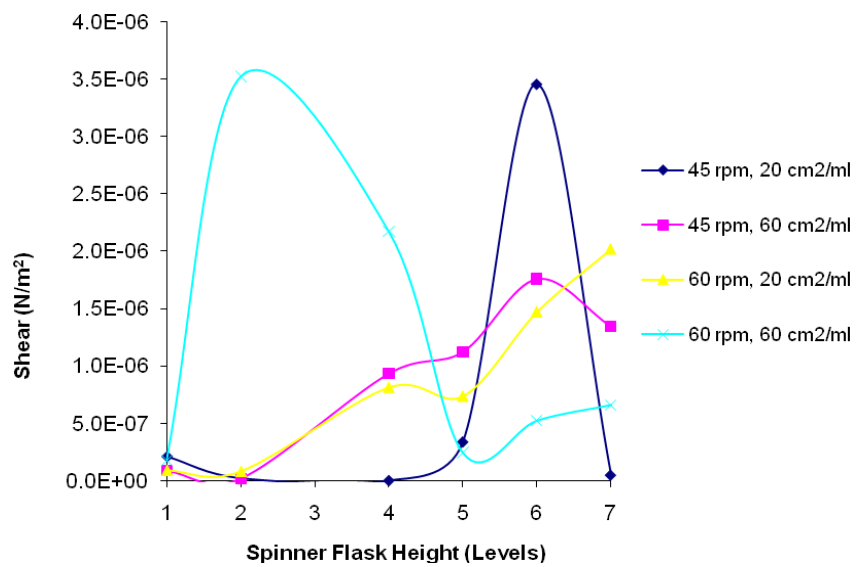


Figure 50: The minimum shear stress recorded at different heights of the spinner flask bioreactor for given impeller speeds and microcarrier concentrations.

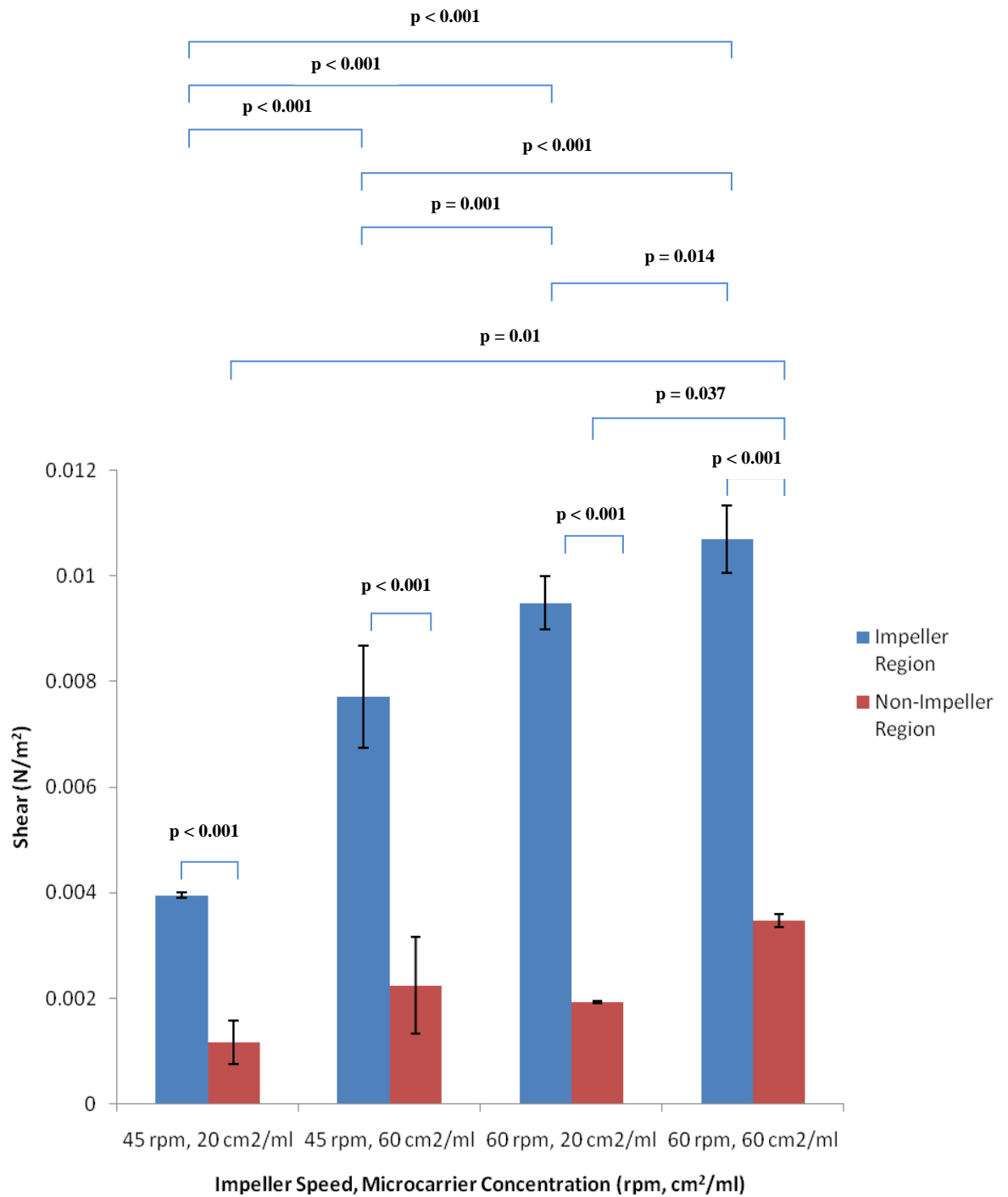


Figure 51: Distribution of mean shear stress at the impeller and non-impeller regions of spinner flask bioreactor for given impeller speeds and microcarrier concentrations. This distribution was based on the average shear stress of the impeller region (levels 4-7) and the non-impeller region (levels 1-2).

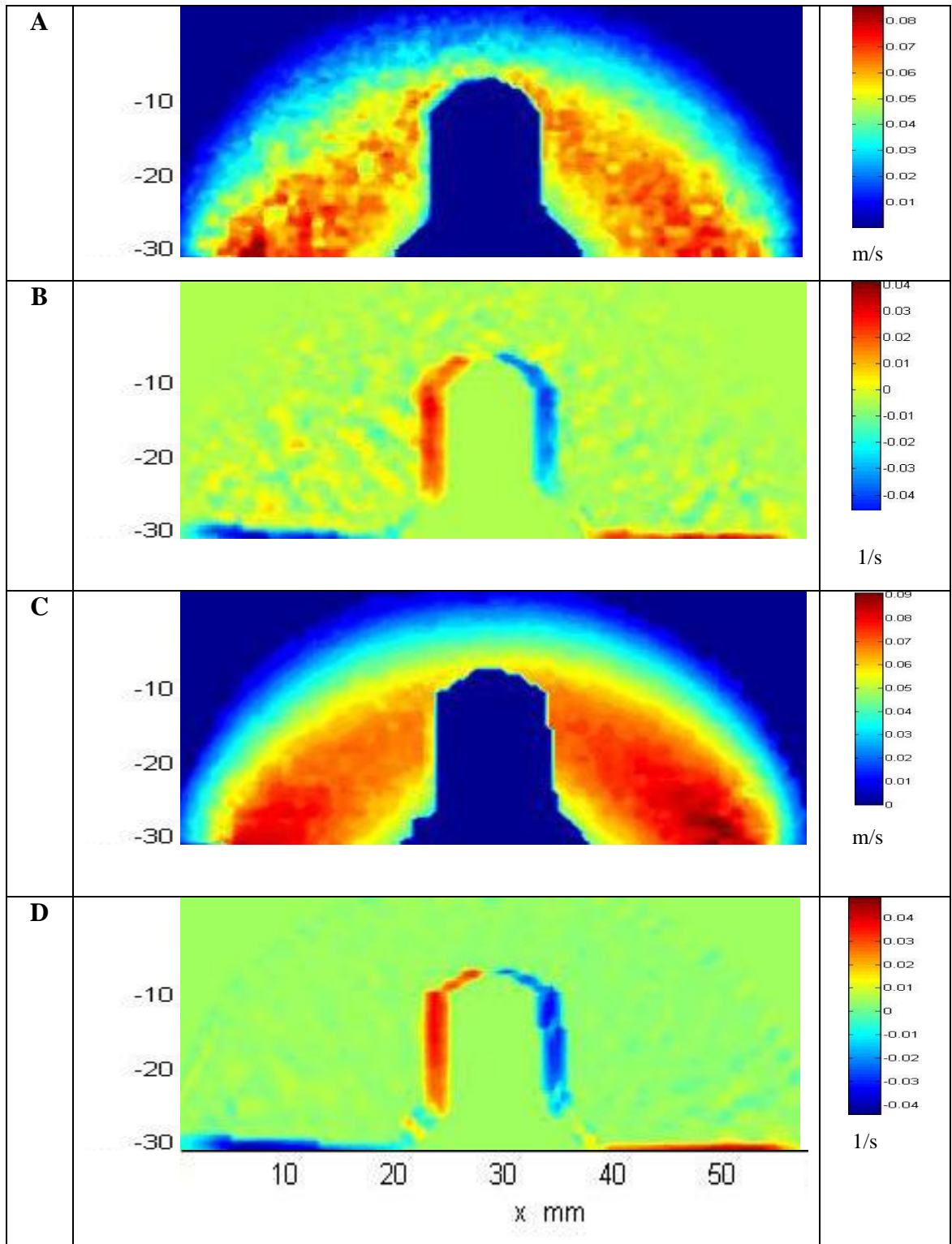


Figure 52: Velocity magnitudes (A, C) and strain rates (B, D) of horizontal orientated impeller of the 45 rpm, 20 cm²/ml group (A, B) and of the 45 rpm, 60 cm²/ml group (C, D) at level 6. Note that the positive and negative strain rates represent direction as well as magnitude. The fluid is moving in an anti-clockwise direction.

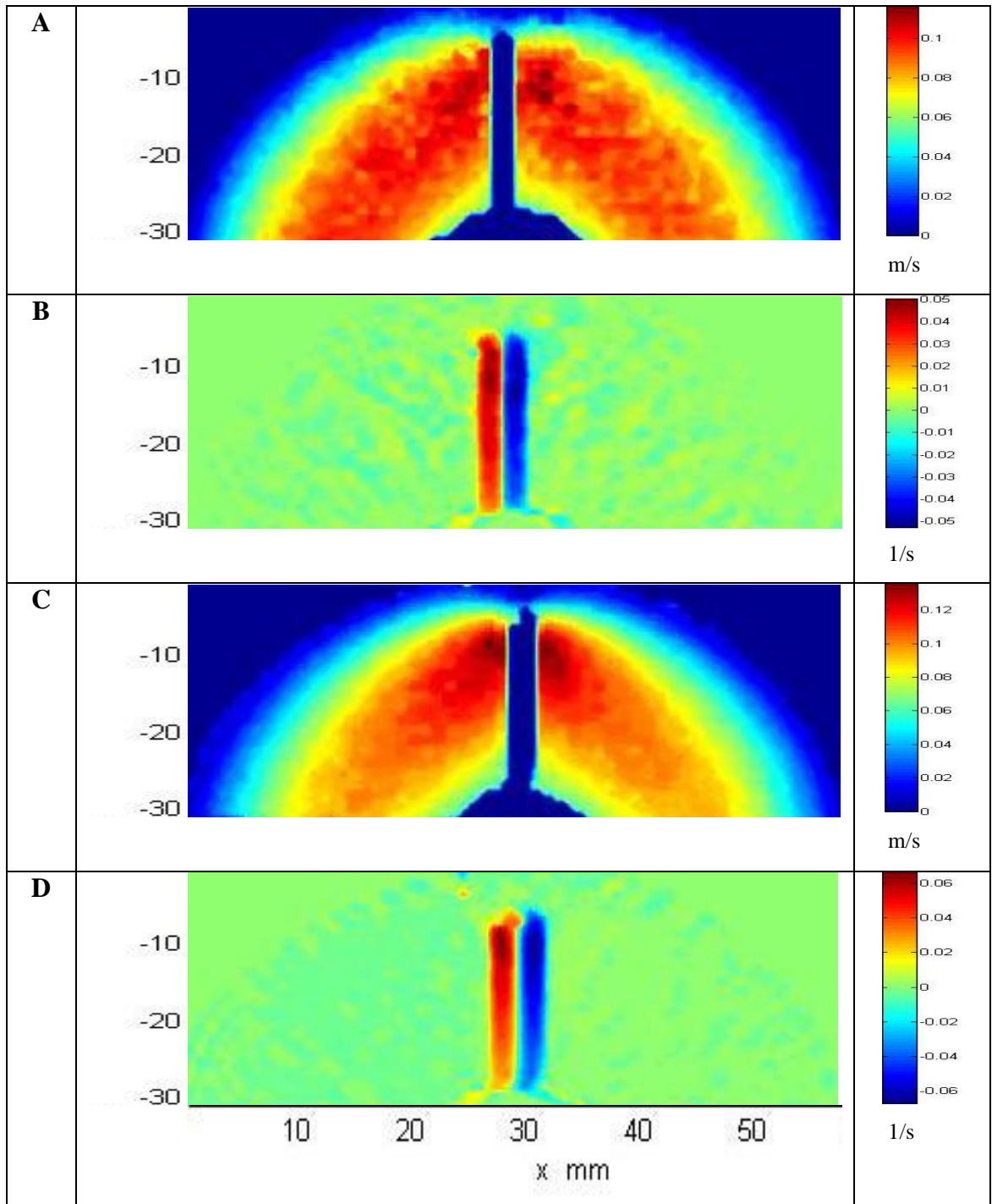


Figure 53: Velocity magnitudes (A, C) and strain rates (B, D) of horizontal orientated impeller of the 60 rpm, 20 cm²/ml group (A, B) and of the 60 rpm, 60 cm²/ml group (C, D) at level 6. Note that the positive and negative strain rates represent direction as well as magnitude. The fluid is moving in an anti-clockwise direction.

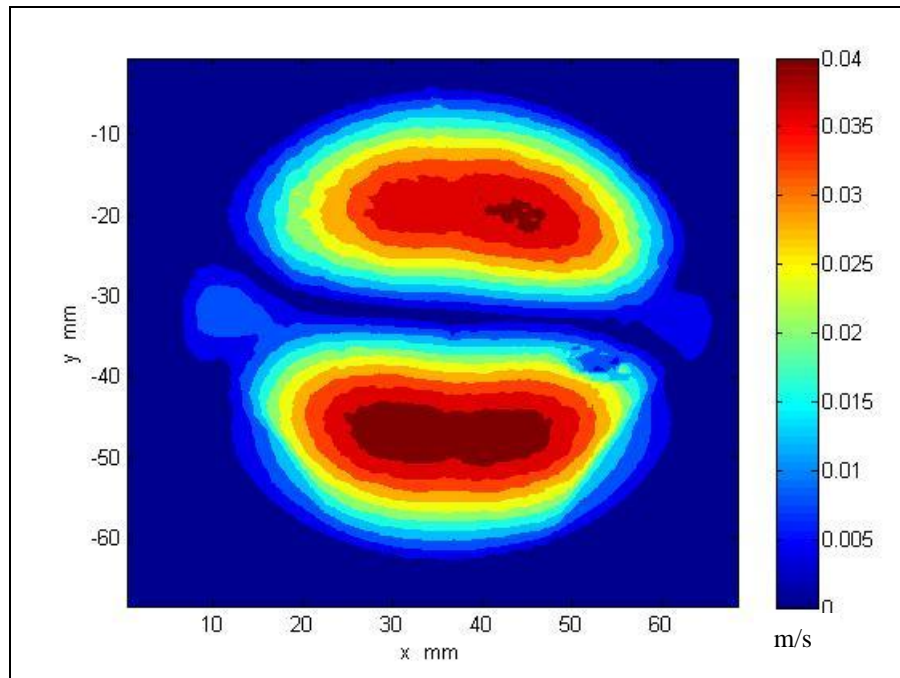


Figure 54: Velocity magnitude map at the non-impeller region. It was possible to obtain a map of the entire region, and not just the semi-circle. This map was taken from the 60 rpm, 60 cm² group, level 2. The fluid is moving anti-clockwise as the impeller rotates.

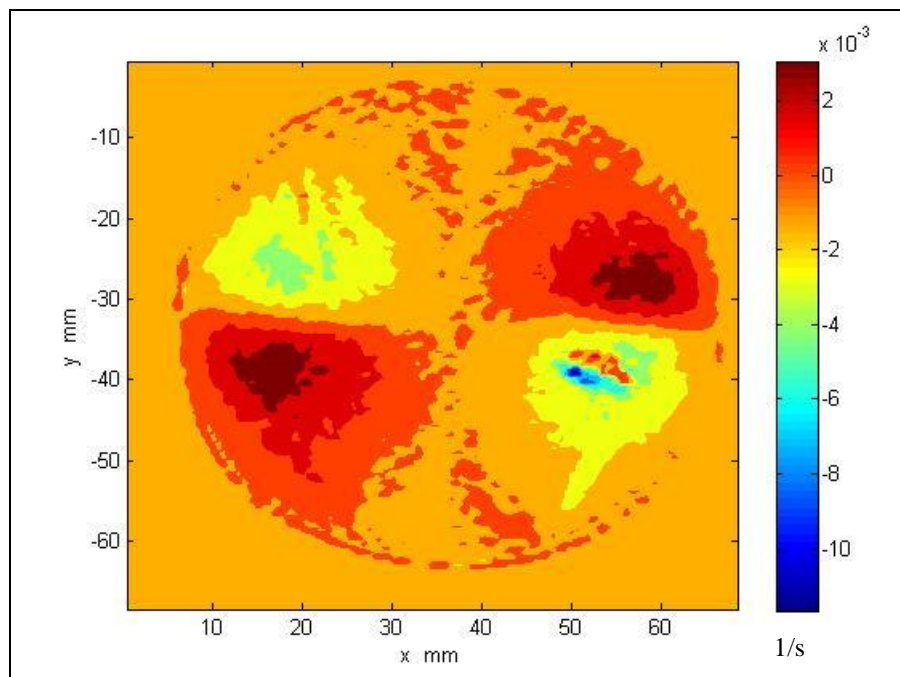


Figure 55: Strain rate map of non-impeller region (level 2) of the the 60 rpm, 60 cm² group.

Cytodex 1 microcarriers have traditionally been employed in cell culture strategies (Hirtenstein et al. 1980; Frauenschuh et al. 2007; Weber et al. 2007; Schop et al. 2008). But to our knowledge, this is the only study where these microcarriers have been utilised as tracers within a PIV system. Two main criteria (Somerscales et al. 1981; Raffel et al. 2007) were assessed for the suitability of cytodex 1 microcarriers as tracers: (1) ability to move with the fluid flow and (2) light scattering properties. The first criterion was satisfied as the relaxation time data showed that the fluid residence time exceeded the particle relaxation time by five orders of magnitude. The ability of the microcarrier to move with fluid flow was therefore a consequence of the fluid residence time exceeding the particle relaxation time. Additionally, the maximum velocity recorded by the PIV system was within, and did not exceed, the calculated tip speeds (

Table 7). This suggested that fluid flow was not disrupted by the microcarriers. The second criterion was satisfied by the qualitative data (Figure 46 and Figure 47) which clearly showed light scatter.

This study found that mean shear stress within the impeller region was approximately four times that within the non-impeller region, with significant statistical differences of $p < 0.001$ for all four experimental groups (Figure 51). With the impeller region occupying greater volume than the non-impeller region, it can be concluded that the microcarriers spend more than half of the time in regions of much higher mean shear stress. In general, when comparing the experimental groups, an increase in microcarrier concentration and rotational speed resulted in an increase in mean shear stress for the impeller region. However, for the non-impeller region, the increase in mean shear stress was far less pronounced as demonstrated by the statistical analyses. In fact, no statistical difference was observed when comparing the three lowest mean shear stress groups.

Work involving PIV and spinner flasks (Bilgen et al. 2006; Bilgen and Barabino 2007) has shown shear stress to be in the range of $0 - 0.06 \text{ N/m}^2$. However, in this study, absolute zero shear stress values were not found in any experimental group. This revealed that the PIV system in this study was capable of extracting data lower than 10^{-7} N/m^2 . There have been extensive studies on the effect of shear stress on stem cells (Sawae et al. 2004; Zeng et al. 2006; Grellier et al. 2009). Zhao *et al.* explored the effects of shear stress on human BMSCs within a perfusion bioreactor system (Zhao et al. 2007). Whilst PIV was not used to determine the shear stress, that study revealed higher BMSCs proliferation rates at the lower end of the shear stress range 1×10^{-5} to $1 \times 10^{-4} \text{ N/m}^2$. Our work revealed shear stress to be 1-2 orders of magnitude higher. In fact, there was a distinct level of impeller region mean shear stress for the 45 rpm, 20

cm² group ($3.4 \times 10^{-3} \leq \text{mean shear stress} \leq 4.6 \times 10^{-3} \text{ N/m}^2$) as opposed to the close proximity of the other three groups ($5.5 \times 10^{-3} \leq \text{mean shear stress} \leq 1.3 \times 10^{-2} \text{ N/m}^2$). As a consequence, it is hypothesised that ensemble mean spatial shear stress, within the impeller region of a 100 ml spinner flask bioreactor, of the range: $3.4 \times 10^{-3} \leq \text{mean shear stress} \leq 4.6 \times 10^{-3} \text{ N/m}^2$, would result in higher BMSC proliferation rates on Cytodex 1 microcarriers, as compared to the range: $5.5 \times 10^{-3} \leq \text{mean shear stress} \leq 1.3 \times 10^{-2} \text{ N/m}^2$.

5.5 Conclusion

Cytodex 1 microcarriers were found to be suitable tracers for the PIV system. The residence time of the fluid was found to be five orders of magnitude higher than the relaxation time of the microcarrier. Laser light scattering was found to be adequate for this study. The mean shear stress within the impeller region was approximately four times that within the non-impeller region, and this, coupled with the higher volumetric occupation of the impeller, suggested that microcarriers spent more than half of culture time exposed to the higher shear stress of the impeller region. Having measured the range of shear stress, it is expected that within the impeller region of a 100 ml spinner flask bioreactor, of the range: $3.4 \times 10^{-3} \text{ N/m}^2 \leq \text{mean shear stress} \leq 4.6 \times 10^{-3} \text{ N/m}^2$, would result in higher BMSC proliferation rates on Cytodex 1 microcarriers, as compared to the range: $5.5 \times 10^{-3} \text{ N/m}^2 \leq \text{mean shear stress} \leq 1.3 \times 10^{-2} \text{ N/m}^2$ (Zhao et al. 2007).

6 The Effect of Cytodex 1 Microcarrier Concentration and Impeller Speed on the expansion of BMSCs within a Spinner Flask Bioreactor

6.1 Abstract

Previously, a method of quantifying shear stress within a spinner flask bioreactor was established. It was hypothesised that mean shear stress settings with low shear stress, $3.4 - 4.6 \times 10^{-3} \text{ N/m}^2$, would result in higher BMSC proliferation rates on Cytodex 1 microcarriers, as compared to high shear stress, $5.5 - 13 \times 10^{-3} \text{ N/m}^2$. Lower microcarrier concentration was found to favour BMSC expansion. The results showed higher proliferation rates of BMSCs at low shear stress rates whilst maintaining multipotency. Interestingly, two experimental groups with similar shear stress resulted in significantly different proliferation rates, which were explained by one group having higher microcarrier concentrations and thus a higher frequency of microcarrier-microcarrier collisions.

6.2 Introduction

Within the last decade in the field of regenerative medicine, much effort has been devoted to the study of dynamic stem cell culture. Its superiority over static culture has been demonstrated through improved proliferation rates (Bancroft et al. 2002; Sikavitsas et al. 2002; Stiehler et al. 2009). The science behind dynamic 3D microcarrier-based cell culture is being investigated with attention paid to metabolism and growth inhibitors (Schop et al. 2008; Higuera et al. 2009; Schop et al. 2009a; Schop et al. 2009b). There is an abundance of literature dedicated to the effect of shear stress on stem cells (Sawae et al. 2004; Zeng et al. 2006; Grellier et al. 2009). For example, laminar flow shear stress was found to be a key regulator for mouse embryonic stem cell differentiation into endothelial cells when compared against static culture (Zeng et al. 2006). Another study showed that laminar flow shear stress on human BMSCs resulted in a significant increase in alkaline phosphatase expression and a substantial decrease in type 1 collagen, as compared to static culture (Grellier et al. 2009). However, the effect of shear stress in spinner flask bioreactor stem cell cultures is a relatively under-explored area (Sen et al. 2002; Fok and Zandstra 2005). Whilst shear stress in spinner flasks and stir-tanks has been explored extensively, it is widely related to animal cell culture systems (Cherry and Papoutsakis 1988; Cherry and Papoutsakis 1989b; Cherry and Kwon 1990; Cherry 1993).

The effect of shear stress on human embryonic kidney cells has been examined through laminar fluid flow within a flow channel (Stathopoulos and Hellums 1985). It was found that shear stresses of 0.26 N/m^2 had no apparent effect on cell viability. The shear stress range of $0.65 - 1.30 \text{ N/m}^2$ resulted in the loss of cell viability and an increase in post-shear stress urokinase enzyme release, indicating that the cell was functionally

capable of producing higher concentrations of enzyme. Shear stress within the range of 2.60 - 5.40 N/m² caused an even greater loss of cell viability, morphological changes of cell disruption and reduced levels of urokinase. Zhao *et al.* examined the effects of shear stress on 3-D human bone marrow-derived stromal cell constructs within a perfusion bioreactor system (Zhao et al. 2007). That study involving laminar flow found higher proliferation rates at the lower end of the shear stress range of 1.0×10^{-4} N/m² to 1.0×10^{-5} N/m². Furthermore, the higher shear stress resulted in an upregulated osteogenic potential. From chapter 5, different levels of shear stress are obtained by selecting different impeller speeds and microcarrier concentrations within a 100 ml spinner flask bioreactor. It is therefore hypothesised that mean shear stress, in the form of microcarrier concentration and impeller speed, within the impeller region of a 100 ml spinner flask bioreactor, of the range: $3.4 \times 10^{-3} \leq \text{mean shear stress} \leq 4.6 \times 10^{-3}$ N/m² (Figure 48), would result in higher BMSC proliferation rates on Cytodex 1 microcarriers, as compared to the range: $5.5 \times 10^{-3} \leq \text{mean shear stress} \leq 13 \times 10^{-3}$ N/m² (Figure 48). Shear stress in laminar flow bioreactors is unidirectional, whereas the shear stress is multidirectional in spinner flasks. However, the PIV results from chapter 5 have quantified different levels of shear stress within the spinner flask which provides a range of shear stress experienced by the proliferating BMSCs.

The aims and objectives of this study are:

- I. to investigate the effect of microcarrier concentration and impeller speed on BMSC proliferation
- II. to test the hypothesis that mean shear stress, in the form of microcarrier concentration and impeller speed, within the impeller region of a 100 ml spinner flask bioreactor, of the range: $3.4 \times 10^{-3} \leq \text{mean shear stress} \leq 4.6 \times 10^{-3}$ N/m²,

would result in higher BMSC proliferation rates on Cytodex 1 microcarriers, as compared to the range: $5.5 \times 10^{-3} \leq \text{mean shear stress} \leq 1.3 \times 10^{-2} \text{ N/m}^2$

III. to examine the impact of shear stress on BMSC multipotency.

6.3 Materials and Method

6.3.1 Human BMSC Sources

BMSCs from three human donors were used in this study. The bone marrow was taken from consenting patients undergoing total hip arthroplasty and the BMSCs were harvested and cryo-preserved. Passage 1 BMSCs were used for this study. The first human donor was male, 42 years old. The second donor was male, 19 years old. The third donor was male, 25 years old.

6.3.2 Proliferation Medium for Human BMSCs

Refer to section 3.3.2 for details of this medium.

6.3.3 Osteogenic Medium for Human BMSCs

Refer to section 3.3.3 for details of this medium.

6.3.4 Adipogenic Medium for Human BMSCs

Refer to section 3.3.4 for details of this medium.

6.3.5 Standard Medium for the Differentiation of Human BMSCs along the Chondrogenic Lineage

The chondrogenic medium consisted of sterile Dulbecco's Minimum Essential Medium (Invitrogen, United Kingdom) supplemented with 1% ITS v/v premix (Sigma Aldrich, United Kingdom), 50 µg/ml ascorbic acid (Sigma Aldrich, United Kingdom), 100 units/ml penicillin (Invitrogen, United Kingdom), 100 µg/ml streptomycin (Invitrogen, United Kingdom), 0.01 nM dexamethasone (Sigma Aldrich, United Kingdom), 40 µg/ml proline (Sigma Aldrich, United Kingdom), 100 µg/ml sodium pyruvate (Sigma

Aldrich, United Kingdom) and 0.01 $\mu\text{g/ml}$ TGF β 1 (Peprotech, United Kingdom). The medium was stored at 0°C to 5°C and the maximum shelf-life was one month. (Freshney 2005; Campbell et al. 2006; Schop et al. 2009a)

6.3.6 Spinner Flask/Microcarrier Sterilisation

Dry Cytodex 1 microcarriers (GE Healthcare, United Kingdom) were loaded into one 500 ml spinner flask (Bellco, USA). Phosphate-based saline solution (Sigma Aldrich, United Kingdom) was poured into the spinner flask at 50 ml/dry g Cytodex 1. The 500 ml spinner flask and four 100 ml spinner flasks, with side caps loosely open, were placed in autoclave bags and partially sealed with autoclave tape. They were then placed into an autoclave and exposed to 121°C for a minimum of 20 minutes. After cooling, the phosphate-based solution (PBS) was replenished from the 500 ml spinner flask without removing the microcarriers.

6.3.7 Pre-culture

Cryo-preserved passage 1 human BMSCs were defrosted and plated on T-flasks at 2000 cells/cm². They were expanded in proliferation medium until approximately 70 % confluency. The PBS was removed from the 500 ml spinner flask and the microcarriers were conditioned with proliferation medium.

6.3.8 Cell Seeding

In the 500 ml spinner flask, microcarrier surface area concentration was 20 cm²/ml. BMSCs, harvested from T-flasks, were seeded onto microcarriers of the 500 ml spinner flask at a density of 2000 BMSCs/cm². Partial dynamic seeding was employed for 4 hours by means of 2 minutes at 45 rpm and 30 minutes at 0 rpm on day 0. After such

time, the contents of the 500 ml spinner flask were divided such that there were 20 cm²/ml cell-seeded microcarriers in four sterile 100 ml spinner flasks. Fresh pre-conditioned microcarriers, which contained no BMSCs, were placed into two of the 100 ml spinner flasks such that the microcarrier concentration was 60 cm²/ml. A description of the experimental and control groups are displayed in Table 9.

Table 9: Description of the experimental groups used in this study. The spinner flask regional shear is divided into the impeller region (I) and non-impeller region (NI). Each shear stress value represents the mean spatial ensemble-height shear stress for the given region as seen in Figure 48 and is within the shear stress range stated in the hypothesis of the introduction of chapter 6.

Group	Microcarrier Concentration	Cell Culture Impeller Speed	Spinner Flask Regional Shear Stress	
	(cm ² /ml)	(rpm)	I (N/m ²)	NI (N/m ²)
1	20	45	3.9 x 10 ⁻³	1.1 x 10 ⁻³
2	60	45	7.7 x 10 ⁻³	2.2 x 10 ⁻³
3	20	60	9.4 x 10 ⁻³	1.9 x 10 ⁻³
4	60	60	10.7 x 10 ⁻³	3.5 x 10 ⁻³
Control	n/a	n/a	n/a	n/a

6.3.9 BMSC Growth Analysis

The four experimental groups were cultured at different impeller speeds (refer to Table 9) for a period of 9 days. At days 1, 3, 6 and 9, three samples were taken from each spinner flask and washed with pre-warmed PBS. The alamarBlueTM (Serotec, United Kingdom) assay was applied to the samples, as well as the 2D control, as described in section 3.3.8. On completion of the assay, the microcarriers were washed thoroughly,

dried in an oven and an equivalent number of fresh microcarriers were placed back into the spinner flasks. A standard curve of cell number versus wavelength was prepared per passage per donor specific to the BMSCs used in this study (appendix 8.3). This curve was used to determine cell populations at different time-points and consequently calculate the number of population doublings. BMSC population growth curves were constructed based on the four time-point population measurements and the formulae used were as per section 3.3.8. Donor 2 BMSC data is displayed in the results section as representative of all three human donors.

6.3.10 BMSC Harvest

At day 9, the BMSCs were harvested from the microcarriers and the well-plates as described in section 3.3.9.

6.3.11 Multipotency

The pellets were re-suspended and differentiated along the osteogenic, adipogenic and chondrogenic lineages. The next three sub-sections describe cell culture protocol and evaluation of lineage differentiation.

6.3.11.1 Osteogenic lineage

For osteogenic differentiation, human MSCs were seeded in 24-well plates at a density of 5000 cells/cm². Standard osteogenic media was used, with medium plus dexamethasone representing the experimental group and proliferation medium (minus dexamethasone) representing the control. Medium was refreshed twice weekly. On day 12, the cells were fixated in 3.7 % formaldehyde in PBS.

ALP staining was employed to stain the alkaline phosphatase enzyme using the Alkaline Phosphatase Detection kit (Millipore[®], International). The protocol is described in section 3.3.10.1.

An ALP assay (Randox Laboratories, United Kingdom) was performed as a form of quantitative analysis. Well-plates from timepoints of days 4, 8, 12 and 20 were kept at -80°C. Briefly, to measure the ALP concentration, the well-plates were defrosted at room temperature. Then, 0.2% triton was added to each well. An ultrasonic water bath filled with ice was used to further lyse the cells for 5 minutes. Standards of p-nitrophenol were prepared according to the instructions of the manufacturer. Then, 100 µl of samples were placed into 96-well plates, followed by 100 µl of PNP solution. Next, 200 µl standards were placed into another well-plate. The control was 0.2% triton only. The well-plates were incubated at 37°C for 1 hour and absorbance was measured at 405 nm.

Protein concentration was measured using the Pierce[®] BCA protein assay kit (Thermo Scientific, United Kingdom), which is “a detergent-compatible formulation based on bicinchonic acid (BCA) for the colorimetric detection and quantification of protein”. 25 µl of the samples prepared for the ALP assay were placed into 96-well plates. Briefly, dilute albumin (BSA) sample standards and working reagent (WR) were prepared according to the instructions of the manufacturer. Then, 25 µl of the samples prepared for the ALP assay and BSA standards were placed into 96-well plates. This was followed by 200 µl of the WR. The plates were shaken gently for 30 seconds and incubated for 30 minutes. After cooling to room temperature, the absorbance was measured at 562 nm.

Graphs were drawn with ALP activity against timepoints. They were used to analyse the osteogenic potential of the harvested BMSCs.

6.3.11.2 Adipogenic lineage

For adipogenic differentiation, human BMSCs were seeded in 24-well plates at a density of 5000 cells/cm². Standard adipogenic media was used, with adipogenic medium representing the experimental group and proliferation medium representing the control. Medium was refreshed twice weekly.

On day 21, the cells were fixated in 3.7 % formaldehyde. The Oil Red O staining procedure was performed as described in section 3.3.10.2.

6.3.11.3 Chondrogenic lineage

For chondrogenic differentiation, human MSCs were pelleted in centrifuge tubes at 500,000 cells/pellet. Standard chondrogenic media was used with chondrogenic medium representing the experimental group and chondrogenic medium minus TGFβ1 representing the control. The media was refreshed twice-weekly. On day 21, the pellets were placed in 3.7% formaldehyde.

The histology was carried out by the Institute of Cell and Molecular Sciences Core Pathology group of Queen Mary University of London. Briefly, a pellet section was dewaxed in xylene and placed in alcohol. It was rehydrated in distilled water, then stained with Weigerts Iron Haematoxylin (1:1 solution of 0.1 g/L haematoxylin in ethanol to 30% ferric chloride & 1% hydrochloric acid in distilled water) for 6 minutes and washed in tap water for 5 minutes. It was incubated with aqueous fast green FCF (1:5000 dilution) for 3 minutes and then washed in 1% acetic acid. It was then incubated with 0.1% aqueous Safranin O for 6 minutes. Subsequently, it was dehydrated

with ethanol. Xylene was used to remove the ethanol and it was finally mounted in xylene-based mountant. The glycosaminoglycan content of the chondrocyte-like cells was stained in the colour of red.

6.3.12 Statistical Analysis

Statistical analysis was performed on the number of population doublings using Genstat version 10.1 software. An ANOVA was performed when comparing all four experimental groups and one control group for significant differences. The number of independent replicates was 3. A student t-test was performed when comparing any significant differences detected by the ANOVA. The level of significance was set at $p < 0.05$.

6.4 Results

6.4.1 BMSC Expansion

As seen in Figure 56, higher shear stress (60 cm²/ml, 45 rpm and 60 cm²/ml, 60 rpm) generally results in a lower BMSC population as compared to the day 1 population. Higher microcarrier concentrations (60 cm²/ml) result in more pronounced differences between the initial and final time-point populations for any given experimental group. The lowest shear stress group (20 cm²/ml, 45 rpm) most closely resembles the growth curve of the 2D control, in terms of the day 9 BMSC population being greater than that of day 1. Interestingly, the average shear stress for the 60 cm²/ml, 45 rpm and 20 cm²/ml, 60 rpm groups were found to be I (Impeller Region) = 7.7×10^{-3} N/m², NI (Non-Impeller Region) = 2.2×10^{-3} N/m² and I = 9.4×10^{-3} N/m², NI = 1.9×10^{-3} N/m², respectively (Figure 56). These two groups had similar shear stress, yet the BMSC growth was superior on the lower microcarrier concentration group (20 cm²/ml).

The lowest shear stress group was superior ($p < 0.001$) to both the experimental and control groups in terms of the number of population doublings between days 3 to 6 (Figure 57 and Figure 59). Conversely, the control group was superior ($p < 0.001$) to all the experimental groups in terms of the number of population doublings for the entire cell culture period (Figure 58). Within the experimental groups, the higher microcarrier concentrations resulted in significantly lower population doublings. Micrographs provided qualitative proof of BMSC populations at different time-points (Figure 60) as lower microcarrier concentrations show higher numbers of attached cells, but with the lower rotational rate (20 cm²/ml, 45 rpm) being superior to the higher rotational rate (20 cm²/ml, 60 rpm). At day 6, the former shows some microcarriers with rounded cells whilst the latter shows flatter cells.

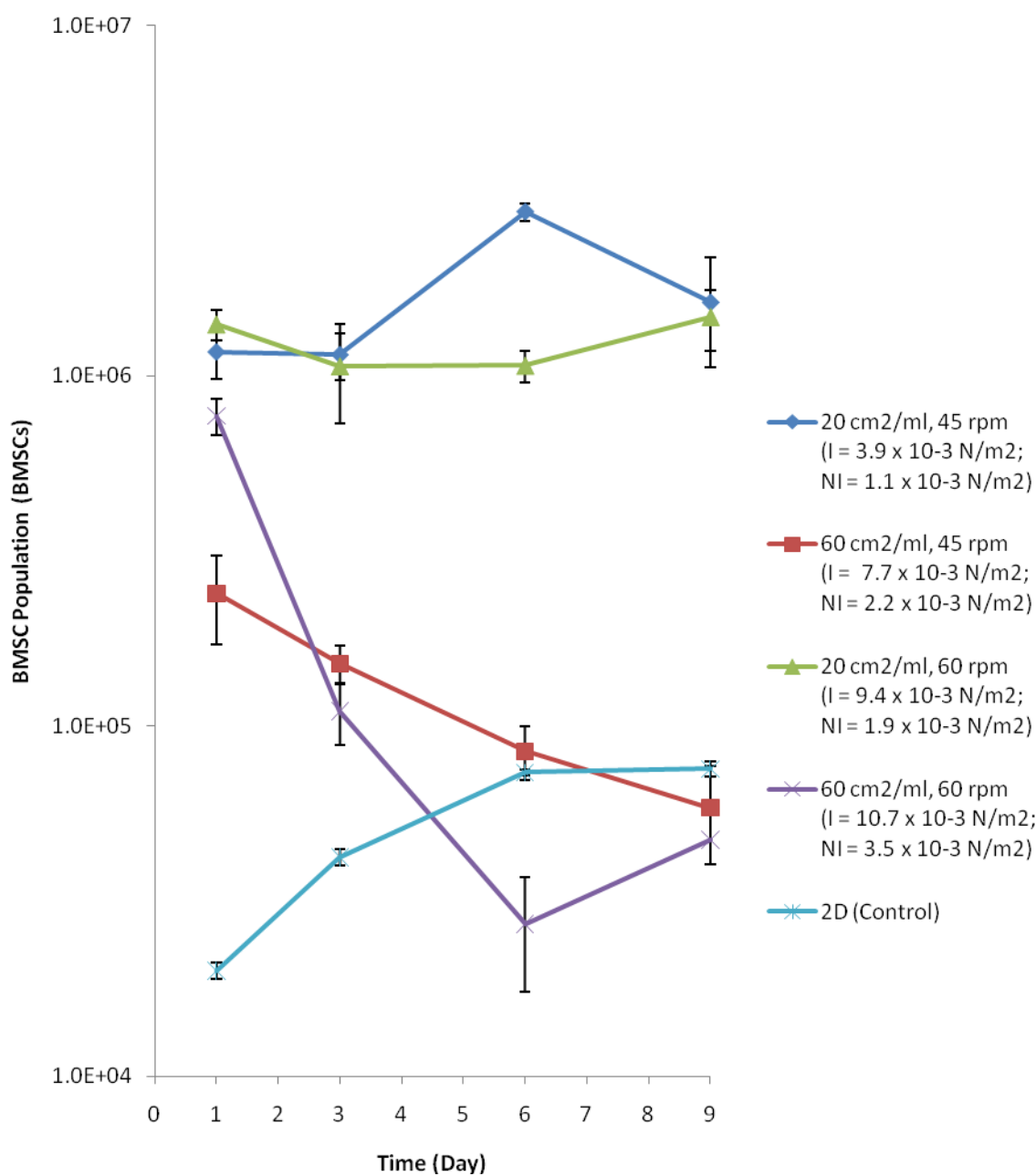


Figure 56: Donor 2 BMSC Population growth under bioreactor conditions (microcarrier concentration, impeller speed) over 9 days. BMSC seeding at day 0 was 2000 BMSCs/cm² (4.0E+05 cells for the spinner flask and 2.0E+04 cell for each well of the 2D control). The legend shows the mean spatial ensemble-height shear stress for the impeller region (I) and the non-impeller region (NI) which was evaluated in the previous chapter.

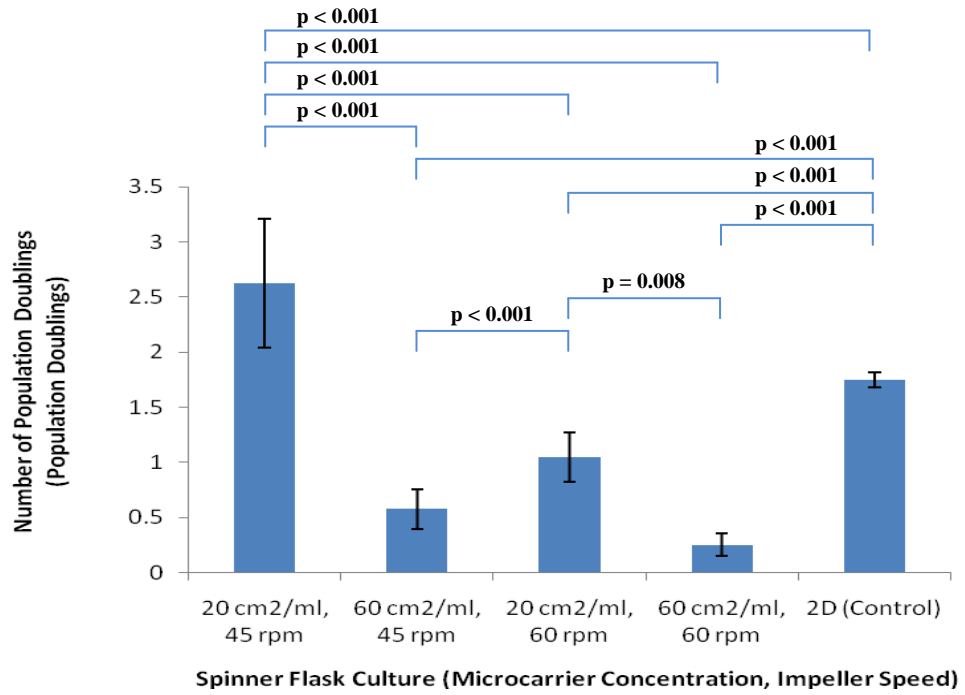


Figure 57: Number of Population Doublings during days 3 to 6 for donor 2.

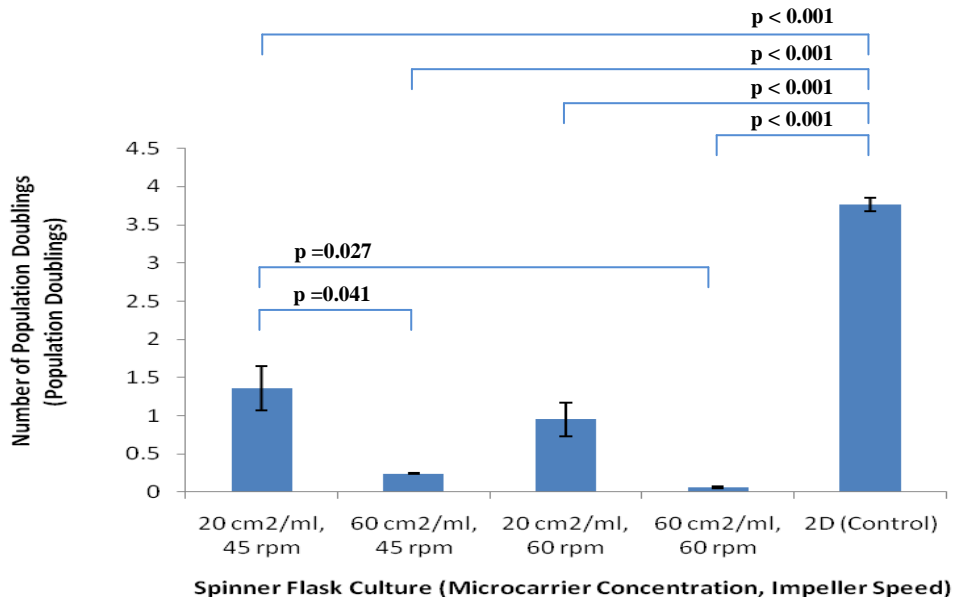


Figure 58: Number of population doublings for the entire 9-day period for donor 2.

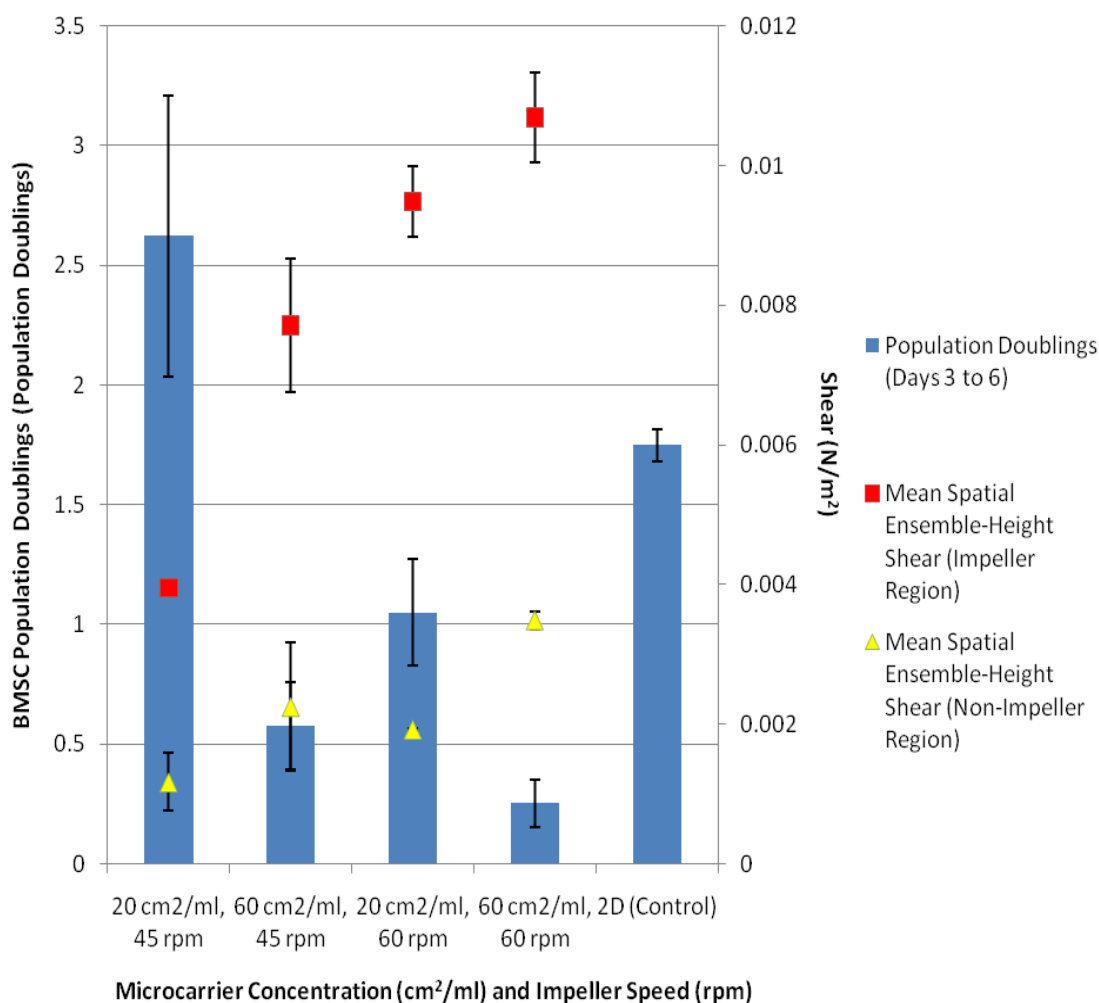


Figure 59: The donor 2 BMSC population doublings between days 3 to 6 for bioreactor conditions in terms of microcarrier concentration and impeller speed. The shear stress for the impeller and non-impeller regions, which was evaluated in the previous chapter, is displayed for given microcarrier concentrations and impeller speeds.

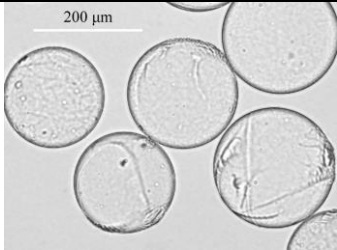

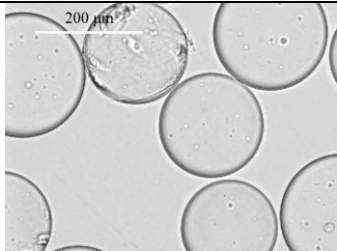
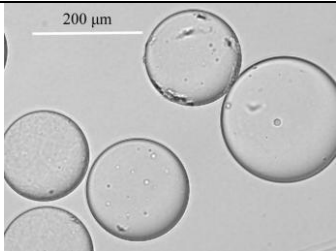
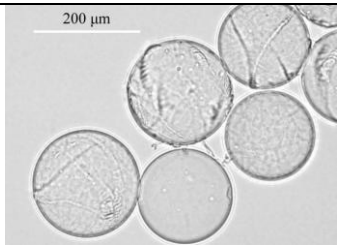
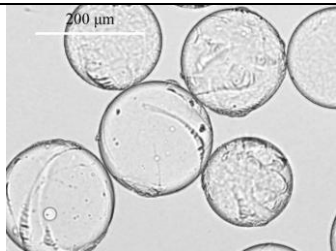
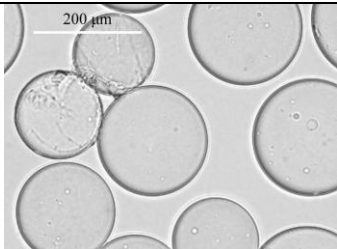
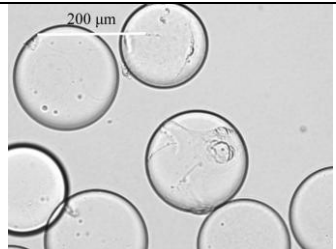
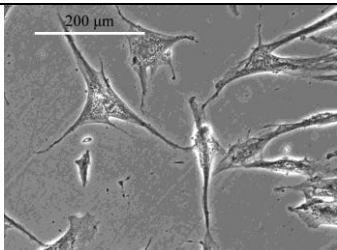
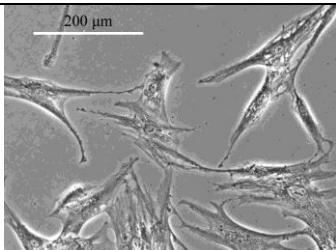
Group	Day 1	Day 6
45 rpm, 20 cm ² /ml		
45 rpm, 60 cm ² /ml		
60 rpm, 20 cm ² /ml		
60 rpm, 60 cm ² /ml		
2D Control		

Figure 60: Micrographs of the microcarriers and well-plates at time-points day 1 and day 6. On days 1 & 6, there are fewer cells visible on the higher microcarrier concentration groups. On day 6, the lowest shear stress group has the highest cell concentration.

6.4.2 BMSC Multipotency

On day 12 of osteogenic culture, the ALP activity of BMSCs which had been cultured on the control is superior ($p < 0.001$) to the experimental groups (Figure 61 and Figure 62). Within the experimental groups, the highest shear stress group shows the highest ALP activity. The other three lower shear stress groups show no significantly different levels of ALP activity. All experimental and control groups retained multipotentiality (Figure 63). No differences in the proportion of Oil Red O staining were seen between the 2D control and experimental groups for adipogenesis. No differences in the intensity of Safranin O staining were noted between the 2D control and experimental groups for chondrogenesis.

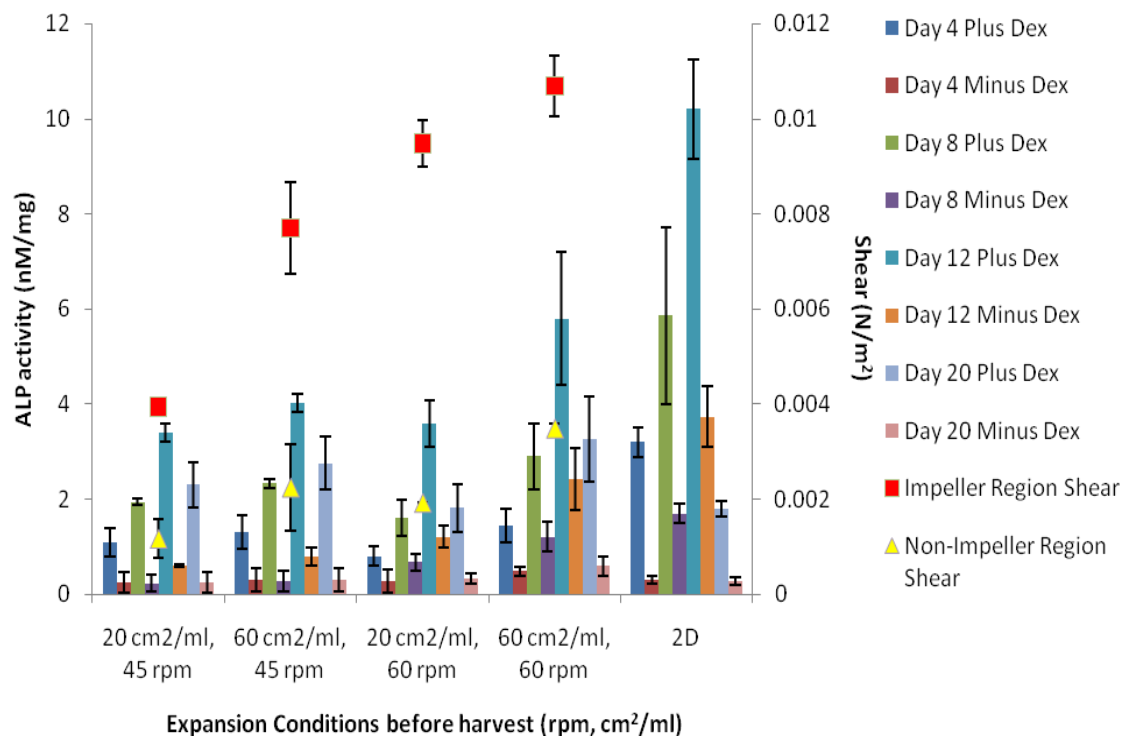


Figure 61: Harvested human BMSCs from different experimental groups subjected to osteogenic media (plus dexamethasone) over a 21-day period. Also shown is the impeller and non-impeller regional shear stress experienced by the BMSCs in the previous nine days of culture in spinner flask bioreactors with different microcarrier concentrations (cm²/ml) and impeller speeds (rpm).

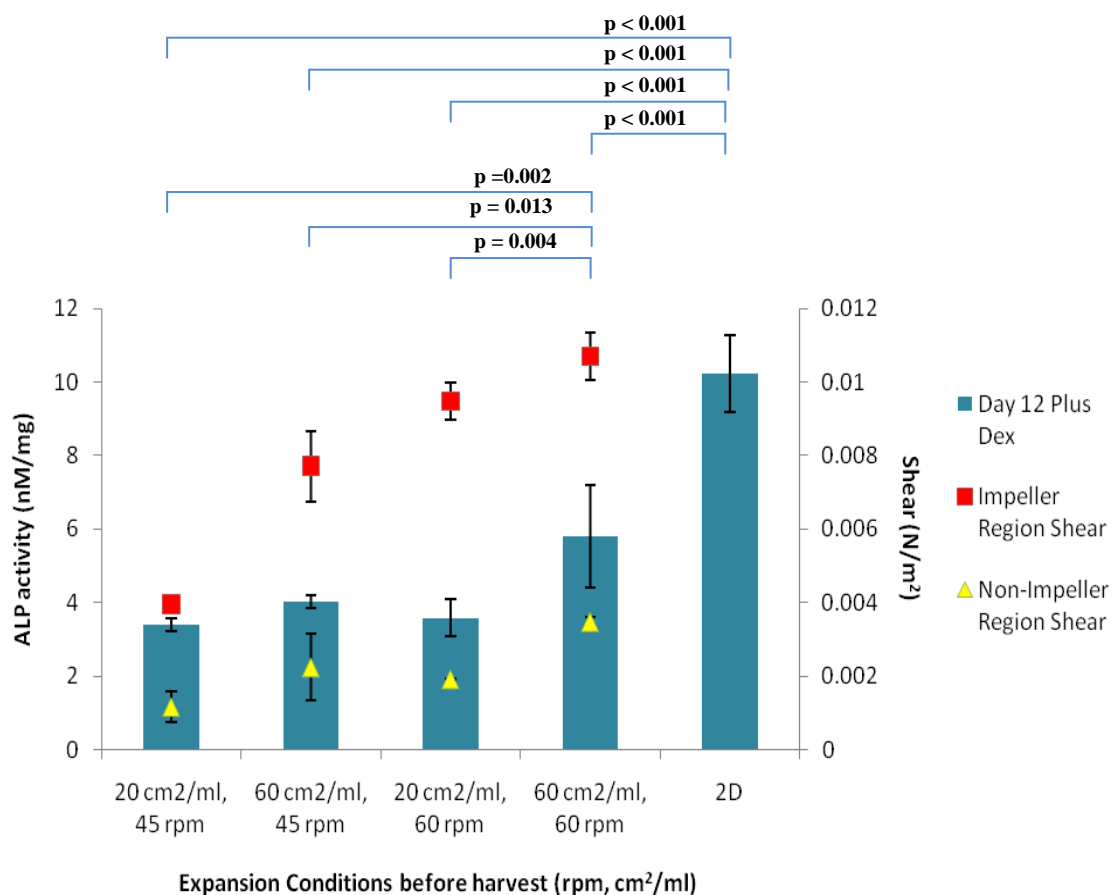


Figure 62: Day 12 ALP activity (taken from Figure 61) for the harvested BMSCs which were previously subjected to nine days of culture within spinner flask bioreactors at different microcarrier concentrations (cm²/ml) and impeller speeds (rpm). The shear stress experienced by the BMSCs during spinner flask bioreactor culture is shown.

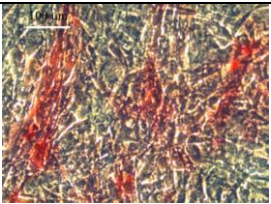

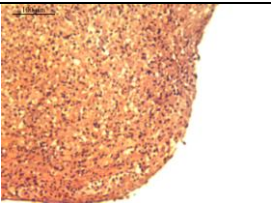
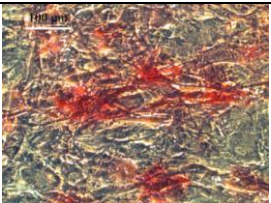

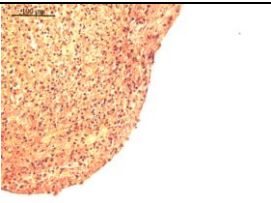
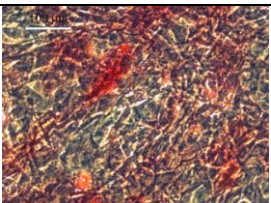


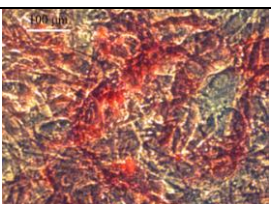


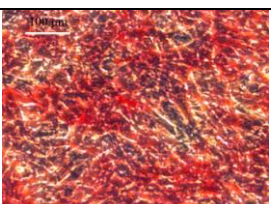
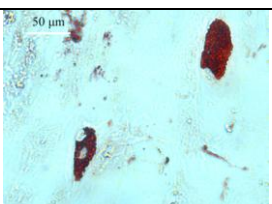
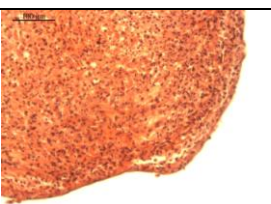
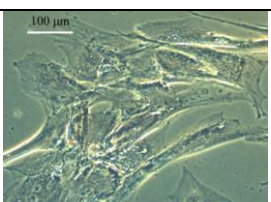
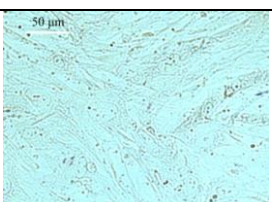
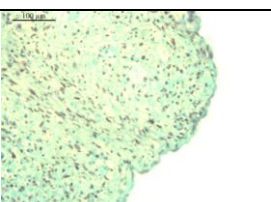
Group	Osteogenesis	Adipogenesis	Chondrogenesis
45 rpm, 20 cm ² /ml			
45 rpm, 60 cm ² /ml			
60 rpm, 20 cm ² /ml			
60 rpm, 60 cm ² /ml			
2D Control			
Expansion only			

Figure 63: Multipotency results along the osteogenic (day 12), adipogenic (day 21) and chondrogenic (day 21) lineages. Note that for the "Expansion only" section of chondrogenesis, chondrogenic medium minus TGFβ1 was employed.

6.5 Discussion

This study has shown that spinner flask BMSC growth within the lowest shear stress group ($3.4 \times 10^{-3} \text{ N/m}^2 \leq \text{impeller region mean shear stress} \leq 4.6 \times 10^{-3} \text{ N/m}^2$; $I = 3.9 \times 10^{-3} \text{ N/m}^2$, $NI = 1.1 \times 10^{-3} \text{ N/m}^2$) was superior to the highest shear stress group ($I = 10.7 \times 10^{-3} \text{ N/m}^2$, $NI = 3.5 \times 10^{-3} \text{ N/m}^2$) (Figure 56). This was consistent with a previous study where lower laminar flow-induced shear stress resulted in higher BMSC proliferation rates (Zhao et al. 2007). The apparent absence of a lag phase of the BMSC growth on the control is the result of four, rather than nine, time points within the 9-day period (Larson et al. 2008). The shorter lag phase is attributed to the stationary cell culture on 2D surfaces in the case of the control, as opposed to the longer lag phase being the result of centrifugal dynamic cell culture on 3D surfaces which was employed in the experimental groups.

As expected, significantly higher BMSC population doublings (2.6 ± 0.6 doublings) on microcarriers were noted in the lowest shear stress group ($3.4 \times 10^{-3} \text{ N/m}^2 \leq \text{impeller region mean shear stress} \leq 4.6 \times 10^{-3} \text{ N/m}^2$) as compared to the higher shear stress and the control group (Figure 57) during days 3-6. Future work should examine impeller design in order to optimise the mixing regime to maximise cell yield (Hooker et al. 1990; Doran 2002; Chua et al. 2008). Higher impeller speeds and microcarrier concentrations resulted in lower proliferation rates (Figure 57 and Figure 58). Generally, as shear stress decreased, the proliferation rates increased. However, there was an exception in the case of two groups ($60 \text{ cm}^2/\text{ml}$, 45 rpm and $20 \text{ cm}^2/\text{ml}$, 60 rpm) (Figure 56) with I (Impeller Region) = $7.7 \times 10^{-3} \text{ N/m}^2$, NI (Non-Impeller Region) = $2.2 \times 10^{-3} \text{ N/m}^2$ and $I = 9.4 \times 10^{-3} \text{ N/m}^2$, $NI = 1.9 \times 10^{-3} \text{ N/m}^2$, respectively. The group with $I = 9.4 \times 10^{-3} \text{ N/m}^2$ had a higher shear stress and superior growth rate as compared to the

group with $I = 7.7 \times 10^{-3} \text{ N/m}^2$. This may be attributed to the fact that the latter had a three-fold microcarrier concentration and thus conceivably higher microcarrier-microcarrier collisions (Cherry and Papoutsakis 1988; Papoutsakis 1991). Previous studies have provided insight on cell damage mechanisms within microcarrier cell cultures (Cherry and Papoutsakis 1986; Cherry and Papoutsakis 1988; Croughan et al. 1988). Microcarrier-bioreactor collisions may not have significantly contributed to the lower BMSC growth as, microcarriers are small, almost neutrally buoyant and can follow fluid flow (Croughan et al. 1988; Papoutsakis 1991), and previous studies have provided evidence of no substantial cell damage between microcarriers and well-designed impellers (Cherry and Papoutsakis 1988; Cherry and Papoutsakis 1989a). Moreover, for high levels of spinner flask agitation, it has been demonstrated that the microcarrier-microcarrier interaction becomes the dominant cause of cell damage at higher Cytodex 1 microcarrier concentration (Croughan et al. 1988). Additionally, it has been demonstrated that as packing fraction increases, the minimum separation distance between neighbour particles decreases within solid particle liquid suspensions (Mueller et al. 2010). As our study was conducted under a spinner flask laminar mixing regime, future work should focus on microcarrier-to-microcarrier collisions in order to assess BMSC damage.

Multipotency was assessed from harvested cells after nine days of cell culture. Harvested BMSCs were successfully shown to differentiate along the osteogenic, adipogenic and chondrogenic lineages. Hence, the expanded BMSCs retained their differentiation potential. ALP assays were performed on the osteogenic lineage. It was found that the 2D control group showed significantly higher ALP activity as compared to the experimental groups ($p < 0.001$). This demonstrated an apparent partial loss of

osteogenic potential. Cell bridges between microcarriers are known to occur within spinner flask culture which may aggregate (Cherry and Papoutsakis 1988; Papoutsakis 1991) and as seen in Figure 60, some individual microcarriers have almost full coverage of BMSCs. As differentiation of mesenchymal stem cells are known to be triggered by increasing cell density (Osdoby and Caplan 1979; Osdoby and Caplan 1981; Caplan et al. 1983), it is possible that a proportion of spinner flask BMSCs from our study began to differentiate along the osteogenic lineage during cell expansion, prior to osteogenic medium culture. This may have accounted for the lower ALP activity of the experimental groups relative to the control, given that ALP activity peaks at days 10-14 (Storrie and Stupp 2005). If this explanation is true, then the conclusion of partial loss of osteogenic potential would therefore not be valid. Future work should therefore examine the multipotency of harvested cells at earlier (< 9 days) and later (> 9 days) stages of the growth cycle. This would shed light on the variations of cell density and differentiation potential during the growth cycle. However, it must be considered that BMSC harvest after day 9 would increase the probability of multilayer cell formation and contact inhibition (Levine et al. 1965; Cherry and Papoutsakis 1989b); the former would inevitably decrease harvest efficiency. Additionally, age plays a role in expansion (Bruder et al. 1997; Kim et al. 2008) and differentiation (Bruder et al. 1997; Neuhuber et al. 2008). Human BMSC proliferation rates decrease as the cells achieve higher numbers of population doublings (Bruder et al. 1997). Loss of osteogenic potential has been shown to occur above 30 population doublings (Bruder et al. 1997).

The mechanotransduction mechanism by which the shear stress transduces the biochemical signals of the cell from membrane to nuclei is not well understood (Kapur et al. 2003). However, cell growth and differentiation responses to shear-induced

stimuli have been an effective means of improving that understanding (Goldstein et al. 2001; Sikavitsas et al. 2003). For example, significant differences in early and late marker expression of cell undergoing osteogenesis are known to occur when fluid flow shear stress are applied within a planar environment in the short-term (minutes to hours) (Bakker et al. 2001; You et al. 2001; Saunders et al. 2003) as opposed to the long-term (days to weeks) (Bancroft et al. 2002; van den Dolder et al. 2003). Our study has employed PIV to quantify shear-induced stimuli on medium-term spinner flask microcarrier culture (9 days). On inspection of the ALP activities of the experimental groups, post-culture, no significant differences were found between the three lower shear stress groups (Figure 61 and Figure 62). However, there were significant differences when comparing the highest shear stress group (impeller region mean shear stress of $1.1 \times 10^{-2} \text{ N/m}^2$). This higher ALP activity at higher shear stress was expected as it was in line with trends revealed in previous studies (Zhao et al. 2007; Stiehler et al. 2009).

6.6 Conclusion

This study has focused on the effect of microcarrier concentration and impeller speed on BMSC expansion within spinner flask bioreactor culture systems. It tested the hypothesis that the impeller spatial mean shear stress of the range, 3.4×10^{-3} to $4.6 \times 10^{-3} \text{ N/m}^2$, would result in higher BMSC population doublings on Cytodex 1 microcarriers, as compared to the range to the range of 5.45×10^{-3} to $1.27 \times 10^{-2} \text{ N/m}^2$. Growth rate was superior within the lower shear stress range as compared to the higher shear stress range. Lower microcarrier concentration was found to favour BMSC expansion. Interestingly, two experimental groups with similar shear stress resulted in significantly different proliferation rates, which were attributed to differences in microcarrier-microcarrier collision frequencies. Harvested BMSCs were shown to retain their multipotency.

7 General Discussion

This chapter reviews the studies undertaken to explore the effect of microcarrier composition, structure and shear stress on Bone Marrow Stromal Cell (BMSC) growth. Various studies within this thesis (chapters 3, 6) have shown that BMSC growth rates on microcarriers can match those on tissue culture plastic. BMSC growth on PHBV microcarriers was superior to PCL and PLGA microcarriers and comparable to Cytodex 1. The surface roughness of PCL microcarriers were altered by two different impeller designs during the w/o/w method of microcarrier synthesis. A higher level of microcarrier surface roughness was found to significantly improve cell proliferation rates (chapter 4). Particle-image velocimetry (PIV) was used to quantify shear stress within a spinner flask bioreactor (chapter 5) at different microcarrier concentrations and impeller rotational rates. Shear stress was found to increase as microcarrier concentration and impeller rotation increased. Superior BMSC proliferation rates were shown within the experimental group with the lowest level of shear stress (20 cm²/ml, 45 rpm). All BMSCs harvested from microcarriers these studies (chapters 2-3, 6) maintained their differentiation potential to at least two lineages.

7.1 The Characterisation of PHBV, PCL and PLGA microcarriers and their support of the attachment and proliferation of BMSCs

Cell expansion on microcarriers has proven to be more space-saving and media utilisation efficient as compared to tissue culture plastic (Malda and Frondoza 2006). Various studies have demonstrated promising data involving BMSC expansion on Cytodex 1 microcarriers (Frauenschuh et al. 2007; Weber et al. 2007; Schop et al. 2008; Schop et al. 2009a; Schop et al. 2009b). Whilst significant advances have been made in

the optimisation of the bioprocessing of human BMSC spinner flask Cytodex 1 microcarrier culture, there is still a need to improve the seeding and harvesting efficiencies, as well as the expansion rates (Weber et al. 2007; Schop et al. 2008). Alternatives to Cytodex 1 were investigated in chapters 2 and 3.

Our study showed that BMSC proliferation rates on PHBV microcarriers were superior ($p < 0.001$) to PCL and PLGA microcarriers and comparable to Cytodex 1 microcarriers. It has previously been shown that lower crystalline/amorphous ratios within polymers favour cell attachment and growth (Park and Cima 1996; Balasundaram et al. 2006; Czarnecki et al. 2008). Of the three polymers, PCL has the highest crystallinity (Jiang et al. 2001; Gomes et al. 2003). BMSC expansion rates on PCL microcarriers were significantly lower than the other two polymers on account of high crystallinity content. However, SEM images revealed rougher surfaces on PHBV and PLGA microcarriers as compared to PCL. Previous studies have reported superior expansion rates on 2D surfaces at the higher end of the surface roughness range: $0.3 \mu\text{m} \leq R_a \leq 5.1 \mu\text{m}$ (Degasne et al. 1999; Deligianni et al. 2001a; Deligianni et al. 2001b). The magnitude of influence of surface roughness as a competing factor in determining expansion rates is unknown. The effect of surface roughness on cell growth was evaluated in chapter 4.

These microcarriers are intended for use in spinner flask bioreactors. Observations from our work revealed that during static culture, Cytodex 1 and PHBV microcarriers sank to the bottom of proliferation medium within the well-plates. The only exception was that a proportion of the PHBV microcarriers did not sink to the bottom, but occupied different levels of the proliferation medium. It is conceivable that within a spinner flask bioreactor culture, the lower density PHBV microcarriers may require lower impeller

rotational rates as compared to the Cytodex 1 microcarriers. Various studies have detailed the impact of shear stress on cells in terms of expansion, viability and morphology (Stathopoulos and Hellums 1985; Zeng et al. 2006; Zhao et al. 2007). The lower density PHBV microcarriers therefore show promise as an alternative to Cytodex 1 microcarriers, especially as our study revealed no significant difference in BMSC expansion rates on these two microcarriers. Future work should compare cell proliferation rates on lower and higher density PHBV microcarriers and Cytodex 1 microcarriers within spinner flask culture and assess the impact of shear stress from different impeller rotational speeds. However, any such study must consider that the diameter ranges of Cytodex 1 (147 – 248 μm) and PHBV (212 - 300 μm) microcarriers would influence the magnitude of shear stress on the microcarriers, as Qiu *et al.* (1998) found that as the density difference between the microcarrier and the culture medium increased, so did the shear stress imparted on the microcarrier (Qiu et al. 1998).

Our study demonstrated that BMSCs expanded on the microcarrier types successfully retained their differentiation potential along the osteogenic and adipogenic lineages, and no differences were detected between the groups in terms of intensity of staining marker. The former observation was in line with previous studies which showed that stem cells retain their stemness on various polymeric scaffolds (Li et al. 2002; Gauthaman et al. 2009). Curran *et al.* (2009) demonstrated that PLGA doping of PCL affected the differentiation potential of human BMSCs on films over a 28-day period (Curran et al. 2009). That study found that PCL containing 0 – 30 wt % PLGA enhanced chondrogenic potential both in basal and chondrogenic conditioned media, in particular 30 wt % PLGA showing the greatest enhanced chondrogenic potential. Furthermore, the osteogenic potential of these PCL/PLGA films were found to be

lacking osteogenic potential (Marletta et al. 2007; Curran et al. 2009), with only PCL containing 20 wt % PLGA facilitating osteogenic differentiation of BMSCs under osteogenic conditions. Any expansion strategy involving BMSC culture on polymeric microcarriers greater than 5 days may affect the differentiation potential of attached or harvested cells, considering that ALP activity peaks between days 10-14 (Storrie and Stupp 2005) during in vitro osteogenesis and that the oil droplets were stained at day 21 during osteogenesis in our study. Therefore, future work should focus on the differentiation potential of attached and harvested BMSCs from polymeric microcarrier cultures over longer periods of culture.

7.2 BMSC Expansion on Microcarriers: The Effect of Surface Microstructure

The results from chapters 2 and 3 showed superior BMSC growth on the less crystalline microcarriers with higher levels of surface roughness. The magnitude of influence of microcarrier surface roughness as a competing factor in determining expansion rates is unknown. Chapter 4 evaluated the role of surface microstructure on cell growth.

We have shown that two different impeller designs (Figure 30), used during the w/o/w method (section 2.3.2), result in the synthesis of PCL microcarriers with different surface roughness. The difference in surface roughness was validated by both SEM and laser profilometry. Based on laser profilometry, PCL-r microcarriers had $R_a = 6.4 \pm 1.5$ microns and PCL-s microcarriers had a $R_a = 1.7 \pm 0.4$ microns ($p = 0.006$). Whilst thermal and chemical means have been used to alter surface roughness (Crotts and Park 1998; Yang et al. 2000; Chun et al. 2004), to our knowledge, impeller designs have not been explored as an alternative. On closer inspection of the three-hour stirring stage (section 2.3.2), it was noted that the circulating microcarriers (both PCL-s and PCL-r)

did not reside within the impeller region. This suggested that different mixing regimes, rather than direct interaction of the PCL microcarriers with impeller blades, caused the difference in the microcarrier surface roughness. It has previously been shown that impeller design defines the flow pattern which determine mixing regime (Doran 2002). As impeller diameter was increased for a given rotational speed within a stirred vessel, the intensity of agitation was also increased (Hooker et al. 1990). Within a biocentrifugal pump, a 16 forward-swept-blade impeller resulted in a lower frequency of vortices and high-shear-stress spots as compared to a 16-straight blade impeller; the velocity vector distribution and lower shear stress levels differed when a 8-backward-swept blade impeller was compared to the 16 forward-swept-blade impeller (Chua et al. 2008).

BMSCs from all three human donors showed superior proliferation rates on PCL-r as opposed to PCL-s. For the human donor presented in this study, 2.16 ± 0.11 population doublings were recorded for PCL-r as compared to the 1.33 ± 0.20 population doublings for the PCL-s ($p = 0.025$). This was consistent with previous findings (Degasne et al. 1999; Deligianni et al. 2001a; Deligianni et al. 2001b) where a variety of cell types were expanded on 2D surfaces with a combined range of degrees of surface roughness, $0.29 \mu\text{m} \leq R_a \leq 5.11 \mu\text{m}$.

The harvested BMSCs from the microcarriers retained their differentiation potential to the osteogenic and adipogenic lineages. This was expected as previous studies have demonstrated stem cells retaining their stemness on a variety of polymeric scaffolds (Li et al. 2002; Gauthaman et al. 2009). Osteoblast-like cells have been cultured on smoother and rougher titanium disks ($0.22 \mu\text{m} \leq R_a \leq 4.37 \mu\text{m}$) and it has been shown that the rougher surface resulted in higher concentrations of differentiation markers

(Lincks et al. 1998). Increased osteogenic differentiation potential has been supported by other studies (Martin et al. 1995; Lohmann et al. 1999). Future studies should evaluate the differentiation potential of harvested BMSCs which have been cultured over a longer period of time on polymeric surfaces of different levels of surface roughness.

7.3 The Use of Particle Imaging Velocimetry to assess shear within a Spinner Flask Bioreactor

Shear stress measurement has proven integral in order to understand the nature of stem cells. However, the complexities of different bioreactors have posed challenges to gaining reliable shear stress data. PIV is a flow visualisation technique (Raffel et al. 2007), which is a relatively new tool in the evaluation of shear stress in spinner flask bioreactors. This technique was used in chapter 5 to quantify shear stress within a spinner flask so that it may be used to determine its effect on cell culture (chapter 6).

To our knowledge, this is the only study where Cytodex 1 microcarriers have been used as tracers for PIV systems. These microcarriers were suitable as tracers as they were able to move with the fluid flow and to scatter light (Somerscales et al. 1981; Raffel et al. 2007). The relaxation time data showed that the fluid residence time exceeded the particle relaxation time by five orders of magnitude (

Table 8). Furthermore, the maximum velocity recorded by the system did not exceed the calculated tip speed. Images taken using the PIV system software showed light scatter from the microcarriers (Figure 47). No absolute zero shear stress values were found in any experimental group, which bear testimony to the accuracy and sensitivity of PIV. The Cytodex 1 microcarriers show promise as tracers for PIV systems for the assessment of velocity flow fields and shear stress distribution.

Our study found that mean shear stress within the impeller region was approximately four times that within the non-impeller region ($p < 0.001$ for all four experimental groups). With the impeller region occupying approximately 55% of the working volume, it can be concluded that the microcarriers spend more than half of the culture time in regions of much higher mean shear stress. In general, when comparing the experimental groups, an increase in microcarrier concentration and rotational speed resulted in an increase in mean shear stress for the impeller region. However, for the non-impeller region, the increase in mean shear stress was far less pronounced as demonstrated by the statistical analyses. In fact, no statistical difference was observed when comparing the three lowest mean shear stress groups.

7.4 The Effect of Cytodex 1 Microcarrier Concentration and Impeller Speed on the expansion of BMSCs within a Spinner Flask Bioreactor

Zhao *et al.* (2007) demonstrated higher BMSC proliferation rates within a perfusion bioreactor at the lower end of the shear stress range: $1.0 \times 10^{-4} \text{ N/m}^2$ to $1.0 \times 10^{-5} \text{ N/m}^2$ (Zhao et al. 2007). In consideration of these data and the results of chapter 5, it was hypothesised that impeller spatial ensemble mean shear stress of a 100 ml spinner flask bioreactor, of the range, 3.4×10^{-3} to $4.6 \times 10^{-3} \text{ N/m}^2$, would result in higher BMSC culture on Cytodex 1 microcarrier proliferation rates, as compared to the range of 5.5×10^{-3} to $1.3 \times 10^{-2} \text{ N/m}^2$.

Our study has shown that spinner flask BMSC growth within the lowest shear stress group ($3.4 \times 10^{-3} \leq \text{mean impeller shear stress} \leq 4.6 \times 10^{-3} \text{ N/m}^2$; $I = 3.9 \times 10^{-3} \text{ N/m}^2$, $NI = 1.1 \times 10^{-3} \text{ N/m}^2$) was superior to the highest shear stress group ($I = 10.7 \times 10^{-3} \text{ N/m}^2$, $NI = 3.5 \times 10^{-3} \text{ N/m}^2$) (Figure 56). As expected, significantly higher BMSC population

doublings (2.6 ± 0.6 doublings) on microcarriers were noted in the lowest shear stress group ($3.4 \times 10^{-3} \leq \text{impeller region mean shear stress} \leq 4.6 \times 10^{-3} \text{ N/m}^2$) as compared to the higher shear stress and the control group during days 3-6. Higher impeller speeds (60 rpm versus 45 rpm) and microcarrier concentrations ($60 \text{ cm}^2/\text{ml}$ versus $20 \text{ cm}^2/\text{ml}$) resulted in lower proliferation rates. Generally as shear stress decreased, the proliferation rates increased. However, there was an exception in the case of two groups ($60 \text{ cm}^2/\text{ml}$, 45 rpm and $20 \text{ cm}^2/\text{ml}$, 60 rpm) (Figure 56) with I (Impeller Region) = $7.7 \times 10^{-3} \text{ N/m}^2$, NI (Non-Impeller Region) = $2.2 \times 10^{-3} \text{ N/m}^2$ and I = $9.4 \times 10^{-3} \text{ N/m}^2$, NI = $1.9 \times 10^{-3} \text{ N/m}^2$, respectively. The group with I = $9.4 \times 10^{-3} \text{ N/m}^2$ had a slightly higher shear stress and superior growth rate as compared to the group with I = $7.7 \times 10^{-3} \text{ N/m}^2$. This may be attributed to the fact that the latter had a three-fold microcarrier concentration and thus conceivably higher microcarrier-microcarrier collisions (Cherry and Papoutsakis 1988; Papoutsakis 1991). Microcarriers are small, almost neutrally buoyant and can follow fluid flow (Cherry and Papoutsakis 1988; Papoutsakis 1991) and previous studies have provided evidence of no substantial cell damage between microcarriers and well-designed impellers (Cherry and Papoutsakis 1989a; Cherry and Papoutsakis 1989b). Consequently, microcarrier-bioreactor collisions may not have significantly contributed to the lower BMSC growth of higher microcarrier concentration group. It is more likely that microcarrier-microcarrier collisions was the cause of that lower BMSC growth, as it has been demonstrated that at higher levels of agitation, the microcarrier-microcarrier interaction becomes the dominant cause of cell damage at higher Cytodex 1 microcarrier concentration (Croughan et al. 1988). As our study was conducted under a spinner flask laminar mixing regime, future work should focus on microcarrier-to-microcarrier collisions in order to assess BMSC damage.

Harvested BMSCs from microcarriers which had undergone 9 days of culture were demonstrated to retain their multipotency in our study. In comparing the experimental groups, the ALP activity was found to be significantly higher for the group (60 cm²/ml, 60 rpm) which underwent the highest level of shear stress ($I = 10.7 \times 10^{-3} \text{ N/m}^2$, $NI = 3.5 \times 10^{-3} \text{ N/m}^2$) as compared to the others. There were no significant differences amongst the three other groups. Higher ALP activity at higher shear stress has been demonstrated in perfusion and spinner flask systems (Zhao et al. 2007; Stiehler et al. 2009). The ALP activity of the control was significantly higher than the experimental groups. One possible reason for this observation may have been high cell density triggering the osteogenic differentiation during cell culture, prior to cell harvest. Cell bridges between microcarriers are known to occur within spinner flask culture which may aggregate (Cherry and Papoutsakis 1988; Papoutsakis 1991) and as seen in Figure 60, some individual microcarriers have almost full coverage of BMSCs. As differentiation of mesenchymal stem cells are known to be triggered by increasing cell density (Osdoby and Caplan 1979; Osdoby and Caplan 1981; Caplan et al. 1983), it is possible that a proportion of spinner flask BMSCs from our study began to differentiate along the osteogenic and adipogenic lineages during cell culture, prior to osteogenic medium culture. This would account for the lower ALP activity of the experimental groups relative to the control, given that ALP activity peaks at days 10-14 (Storrie and Stupp 2005). Future work should evaluate the multipotency of harvested cells at earlier and later stages of the growth cycle. This would provide information on the variations of cell density and differentiation potential on the growth cycle.

7.5 Future Work and General Considerations

Microcarrier cell culture within spinner flask bioreactors has demonstrated great promise as an alternative scaffold to tissue culture plastic. As a means of expanding large numbers of cells, it is space-saving, more media utilisation efficient and potentially useful in reducing the risk of contamination as compared to multiple well-plates and T-flasks in several incubators (Freshney 2000a; Malda and Frondoza 2006). Spinner flask microcarrier technology could be used in cell-based tissue engineering strategies for clinical application.

Many interesting novel facts were discovered during this thesis with regard to polymeric microcarrier composition and surface structure and spinner flask shear stress on BMSC proliferation. However, more experiments are necessary in order to establish spinner flask microcarrier technology for clinical application. BMSC expansion on Cytodex 1 and PHBV microcarriers were found to be comparable. Yet, the lower density PHBV microcarriers show promise as an alternative to Cytodex 1 as they may require lower impeller rotational rates, thus lower shear stress, to achieve suspension within a spinner flask. Differentiation potential was retained along the osteogenic and adipogenic lineages of harvested BMSC which were cultured on microcarrier types of PHBV, PCL and PLGA over a 5-day period. Future work should examine the differentiation potential of attached and harvested BMSCs cultured over longer periods of time as recent research suggest varying potential depending on polymeric content.

We developed a novel method of creating two different surface roughnesses on PCL microcarriers using different impeller designs during the w/o/w process. How these designs resulted in significantly different roughnesses should be investigated. Again, differentiation potential was retained along the osteogenic and adipogenic lineages of

harvested BMSC which were cultured on PCL microcarriers of different microstructure. Future work should evaluate the potential of harvested BMSCs cultured over longer periods on surfaces of different roughness.

The effect of shear stress on BMSC growth on microcarriers was evaluated within spinner flasks. The effect of impeller design on cell growth should be evaluated in order to optimise mixing and cell growth. Two experimental groups of similar shear stress were found to have different BMSC proliferation rates. The explanation may lie with microcarrier-microcarrier collision frequency and this should be examined as a competing factor with shear stress on cell growth. It is suggested that the multipotency of BMSC growth be evaluated at different stages of cell culture to provide information on the variation of cell density and differentiation potential on the growth cycle.

7.6 Concluding Remarks

The studies described in this thesis contributed to the further understanding of spinner flask microcarrier technology. PHBV microcarriers proved a superior scaffold to PCL and PLGA, and comparable to Cytodex 1 in terms of BMSC proliferation rates. The lower density PHBV microcarriers may yet prove superior to Cytodex 1. Two impeller designs employed during the w/o/w process of microcarrier synthesis resulted in PCL microcarriers of two different levels of microstructure. BMSC expansion was superior on rough PCL microcarriers.

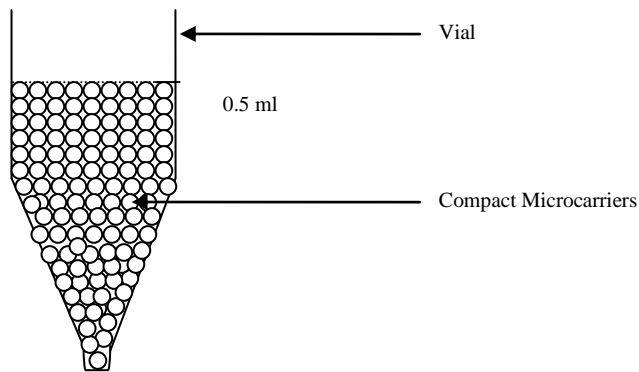
A novel use of Cytodex 1 microcarriers as tracers within PIV systems was demonstrated. PIV has once again been demonstrated as an invaluable tool in understanding cell expansion. Shear stress was evaluated within a 100 ml spinner flask bioreactor and it was found that 80% of the shear stress was localised within the

impeller region, which accounted for 55% of the working volume. Lower microcarrier concentration and impeller rotational rates favoured BMSC proliferation. Despite the many novel facts revealed by this thesis, further investigation is necessary to achieve the promises of spinner flask microcarrier technology.

8 Appendices

8.1 Sample calculation of Microcarrier Surface Area

Microcarriers were sieved into the 212-300 μm range. Hence, the average diameter of the microsphere = $(212 + 300)/2 \mu\text{m} = 256 \mu\text{m}$.



In the case of PLGA microcarriers, one of the three consecutive measurements revealed that 0.0594g PLGA occupied 0.5 ml of an eppendorf vial (sketch above). The microcarriers were compacted prior to weight measurement.

The volume of 1 microcarrier of diameter, 256 μm , or alternatively, radius 256/2 μm , = $(4/3) (22/7) (256/2 \mu\text{m})^3 \approx 8788066 \mu\text{m}^3 \approx 8.8 \times 10^{-6} \text{cm}^3 = 8.8 \times 10^{-6} \text{ml}$. The number of microcarriers in a 0.5 ml vial = $0.5 \text{ml} / 8.8 \times 10^{-6} \text{ml} = 56895$ microcarriers.

The surface area of 56895 microcarriers = $56895 \times [(4) (22/7) (256/2 \mu\text{m})^2] \approx 117.0 \times 10^8 \mu\text{m}^2 = 117 \text{cm}^2$. Finally, if the 117 cm^2 area of PLGA microcarriers weighed 0.0594g, then the surface area of PLGA microcarriers is $(117/0.0594) \text{cm}^2/\text{g} \approx 1973 \text{cm}^2/\text{g}$. The standard deviation was calculated based on the three consecutive measurements. The range of diameters is illustrated in Figure 64.

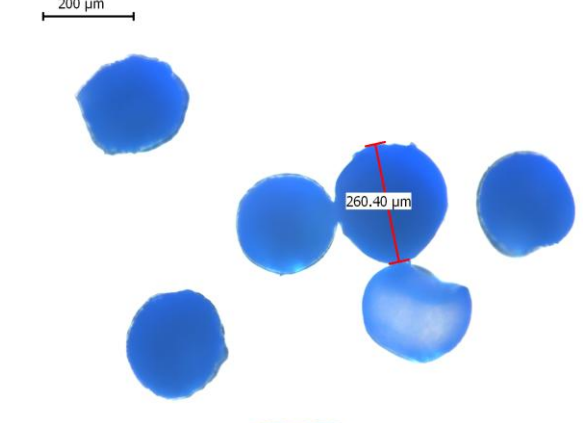
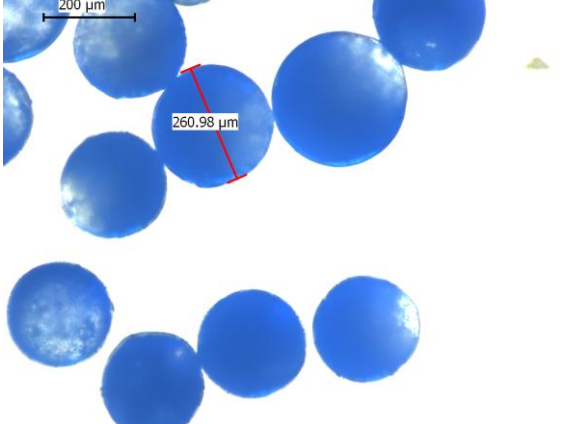
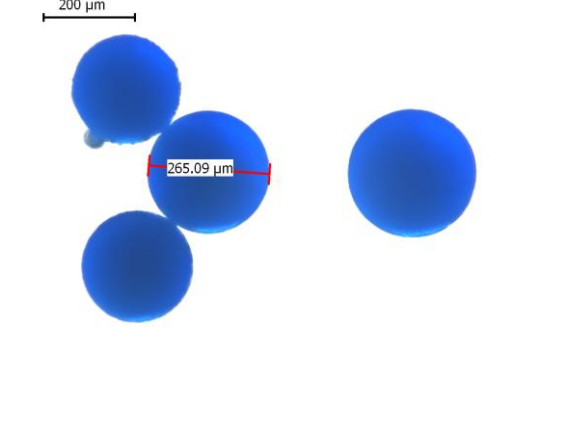
Polymer Type	Light Micrograph
<p style="text-align: center;">PHBV</p>	
<p style="text-align: center;">PCL</p>	
<p style="text-align: center;">PLGA</p>	

Figure 64: Light micrograph images of microcarriers sieved into the 212 -300 μm diameter ranges, illustrating the range of diameters measured by Leica Application Software (LAS).

8.2 Pilot Study quantitatively assessing the growth of Goat BMSCs on PHBV, PCL and PLGA microcarriers

This pilot study was conducted to examine the growth of goat BMSCs on PHBV, PCL and PLGA microcarriers. Two passage 9 goat BMSC donors were used for this study and the materials and methods were exactly the same as for chapter 3, with the exclusion of the differentiation protocols. Key observations from this pilot study included:

- (1) General linear, rather than exponential, growth of goat BMSCs (Figure 66).
- (2) No significant differences in proliferation rates were observed among the different scaffold types (Figure 67 and Figure 68), with the exception of a significant difference between Cytodex 1 and PHBV; Cytodex 1 was superior.
- (3) Using the human BMSC harvest protocol on the expanding cells on the microcarriers yielded no live goat BMSCs.

These pilot studies influenced the cell numbers used to construct the standard curve for the quantification of human cell numbers through the alamarBlue™ assay (appendix 8.3). Given the linear, rather than exponential growth of the goat BMSCs and coupled with the fact that they proliferate faster than human BMSCs, the static culture time of 120 hours was deemed sufficient for human cell culture studies.

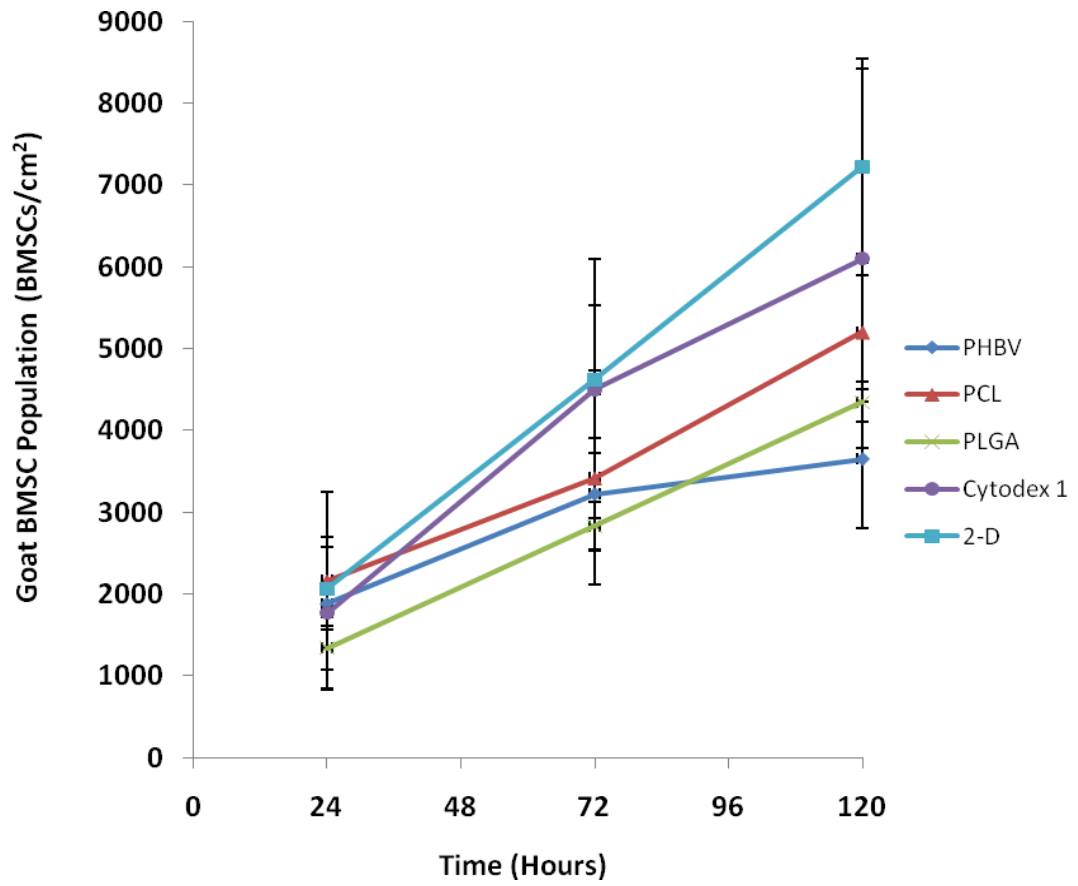


Figure 65: Goat BMSC expansion on different scaffold types over a 120-hour period. Seeding was performed at time 0 hours at a density of 2000 BMSCs/cm².

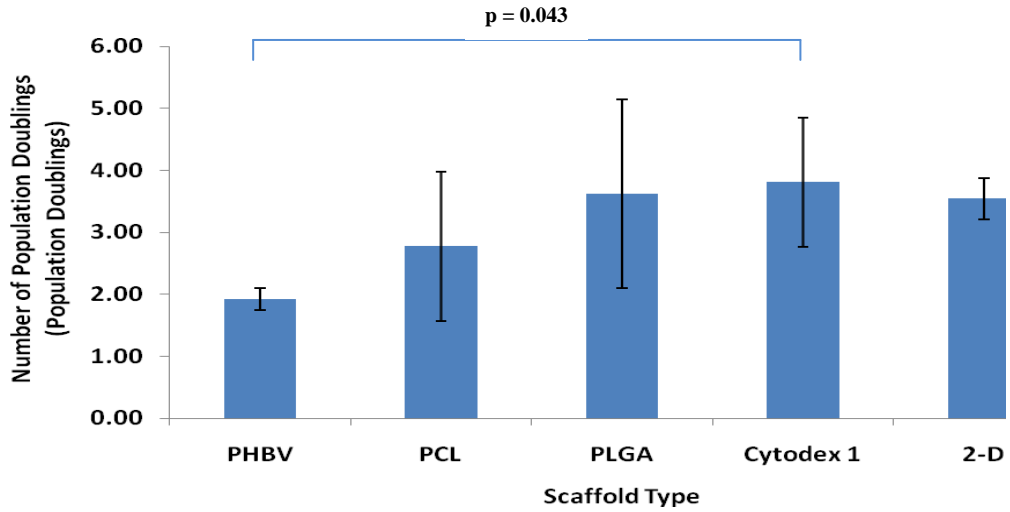


Figure 66: Number of Population Doublings using Goat BMSC population numbers from time-points 24 and 120 hours.

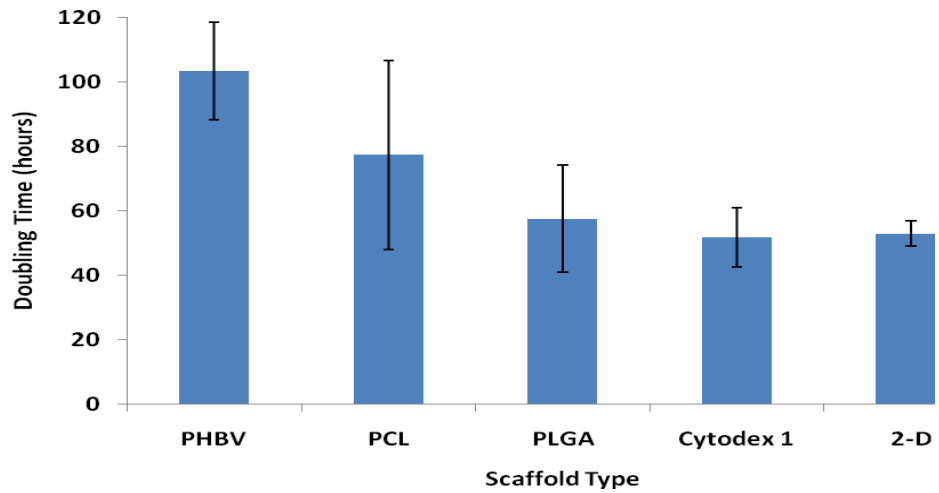


Figure 67: BMSC doubling times on the scaffold types using Goat BMSC population numbers from time-points 24 and 120 hours.

8.3 The alamarBlue™ assay to construct a Standard Curve for the quantification of cell numbers

According to the catalogue information (catalogue number DAL1025) of Biosource International Inc, USA and the technical datasheet (catalogue number BUF012B) of AbD Serotec, United Kingdom, the alamarBlue™ assay is a metabolic assay which monitors the proliferation of cells. The alamarBlue™ assay is non-toxic and may be used to monitor cell proliferation over a period of time, without having to detach or kill cells. The alamarBlue™ acts as an electron acceptor, as it is reduced by FMNH₂, FADH₂, NADH, NADPH and cytochromes of cells. Essentially, alamarBlue™ is a detector of reduction of all elements of the electron transport chain. As it accepts electrons, it changes colour from oxidised indigo blue to the reduced fluorescent pink state. The level of this reduction is measured by the fluorimeter, which is expressed in wavelength. Essentially, this assay measures the metabolic activity. The standard curve is based on the metabolic activity of proliferating cells on tissue culture plastic, which is subsequently converted into cell numbers. To improve the accuracy of cell quantification, the standard curve was constructed for given a passage number for a given human donor.

At time-point 0 hours, for passage 1 human BMSCs from a given donor, 6 different numbers of BMSCs were plated into each well of a 6-well plate. These numbers were determined (pre-determined by pilot studies) so that the BMSC numbers derived from the wavelengths of the experimental and control groups were interpolated, and not extrapolated, from the standard curve. This 6-well plate was subjected to the exact medium replenishment regime as the experimental and control groups. At time 120 hours, the alamarBlue™ assay was applied as per experimental and control groups. The

fluorimeter measurement the alamarBlueTM reduction and the output was expressed as wavelength. The BMSCs in the 6-well plate were then washed with pre-warmed PBS. They were harvested using 0.25% trypsin-EDTA. The harvested BMSCs were counted using the haemocytometer (Burker-Turk, Germany). A standard curve was constructed, plotting wavelength versus cell number. From this standard curve, the wavelengths from the experimental and control groups were interpolated. Hence, the cell numbers were determined for these groups.

8.4 Rough and Smooth Microcarriers

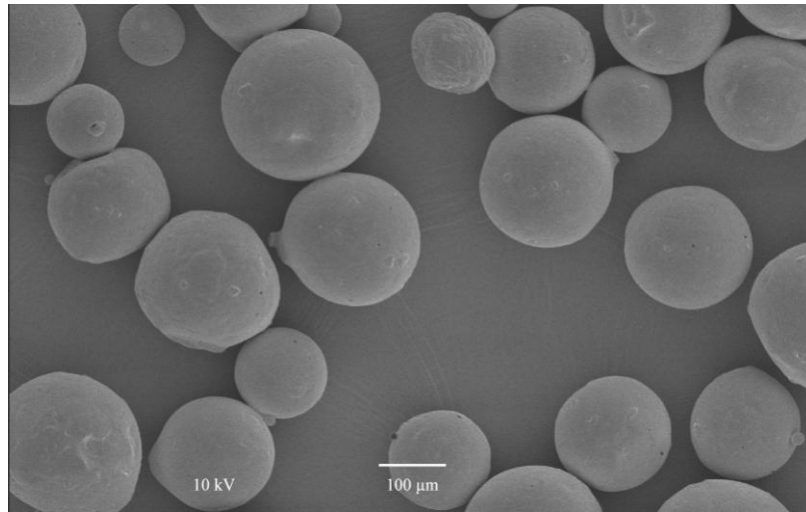


Figure 68: SEM micrograph of unsieved PCL-s microcarriers. They all appear smooth for a variety of diameters.

As seen in Figure 68, the PCL-s microcarriers show smooth surfaces across different diameters. In comparison to Figure 69, the majority of PCL-r microcarriers appear rough. It appears that the PCL-r microcarriers with larger diameters appear rougher than those with smaller diameters. Figure 70 illustrates the difference in roughness of PCL-s and PCL-r.

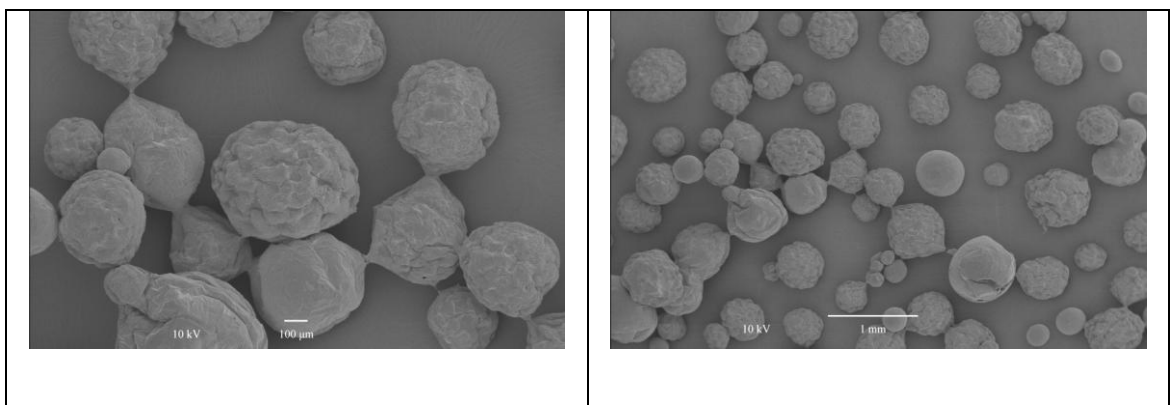


Figure 69: SEM micrographs of unsieved PCL-r microcarriers. It appears that surface roughness increases as microcarrier diameter increases.

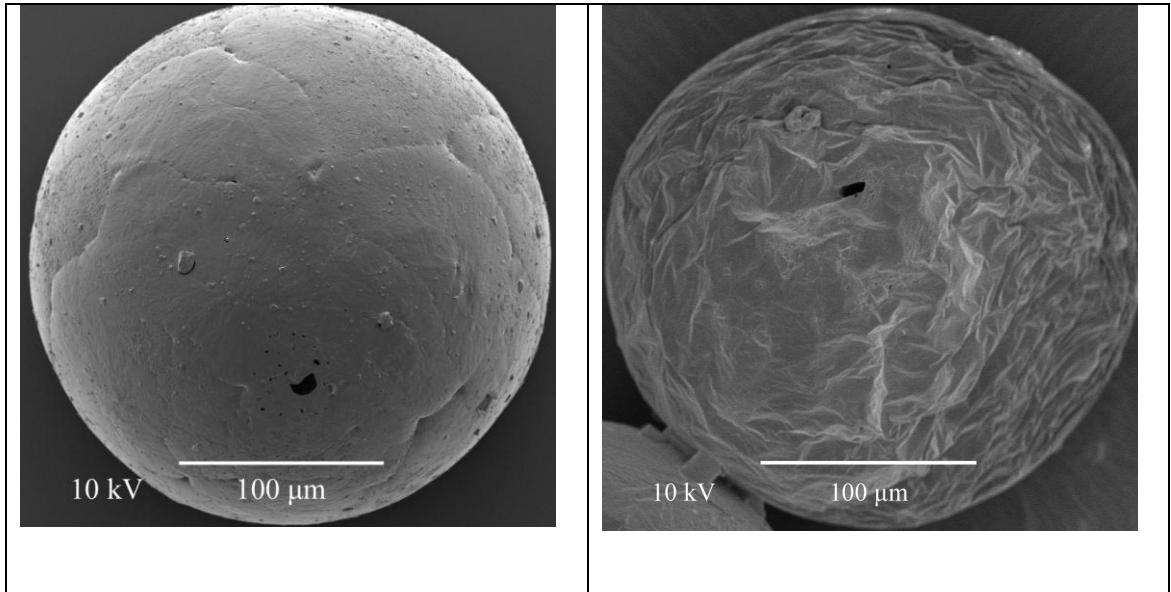


Figure 70: SEM images of PCL-s (left) and PCL-r (right) microcarriers within the 212-300 µm range.

In order to measure surface roughness, a laser profilometer was used. The microcarriers were placed onto a stage and placed into a focus using a camera. The roughness of PCL-s and PCL-r microcarriers ($n = 6$) were measured through scans as seen in Figure 71. For each microcarrier, as seen in Figure 71 in the top left-hand corner scan (aerial scan), a 100 µm x 100 µm square window area was drawn (ensuring that no part of this window did not cover outside of the microcarrier), area loaded and a surface filter of “1” was applied. From this square window, the software calculated the R_a , R_z and R_{zDIN} values. As 6 microcarriers were used to obtain the values, the surface roughness was calculated based on the average and standard deviation.

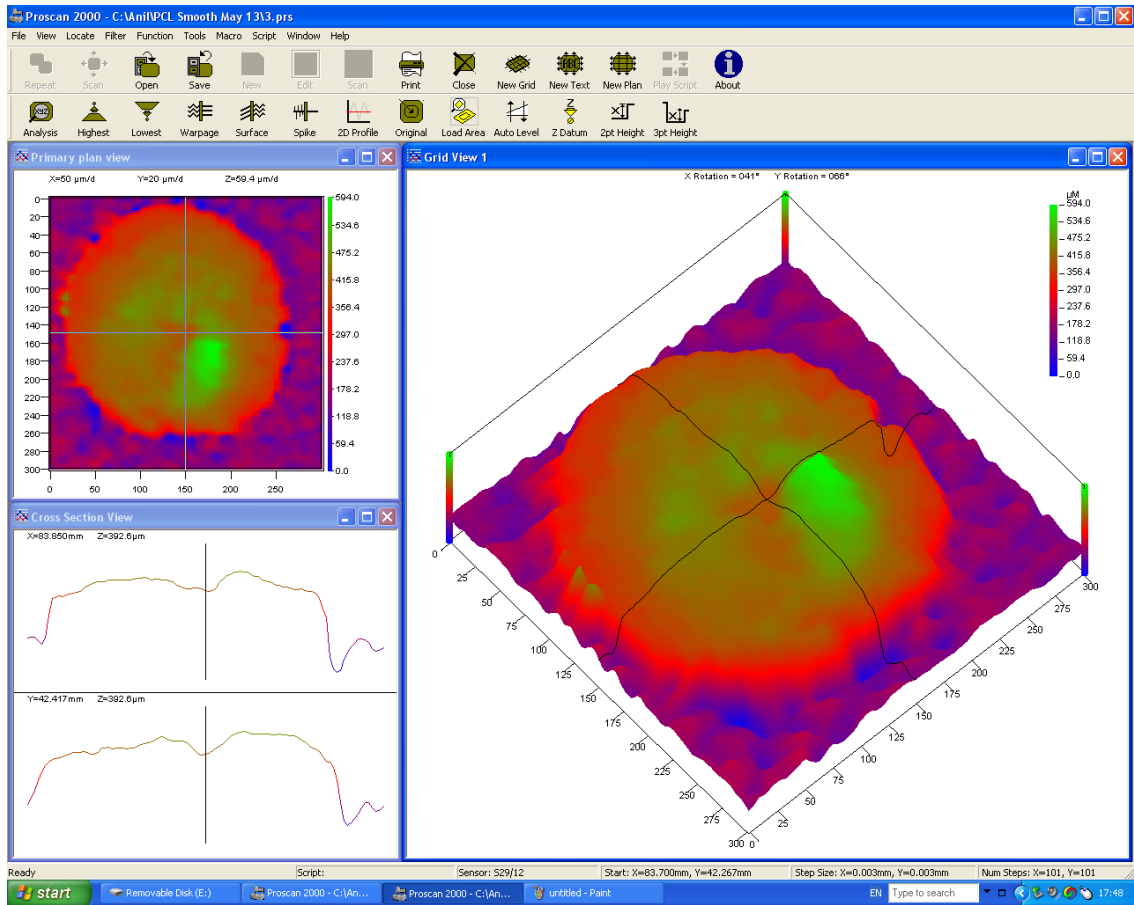


Figure 71: Snapshot of the software when measuring the surface roughness of the microcarriers.

8.5 Data for two other donors supplementary to chapter 3

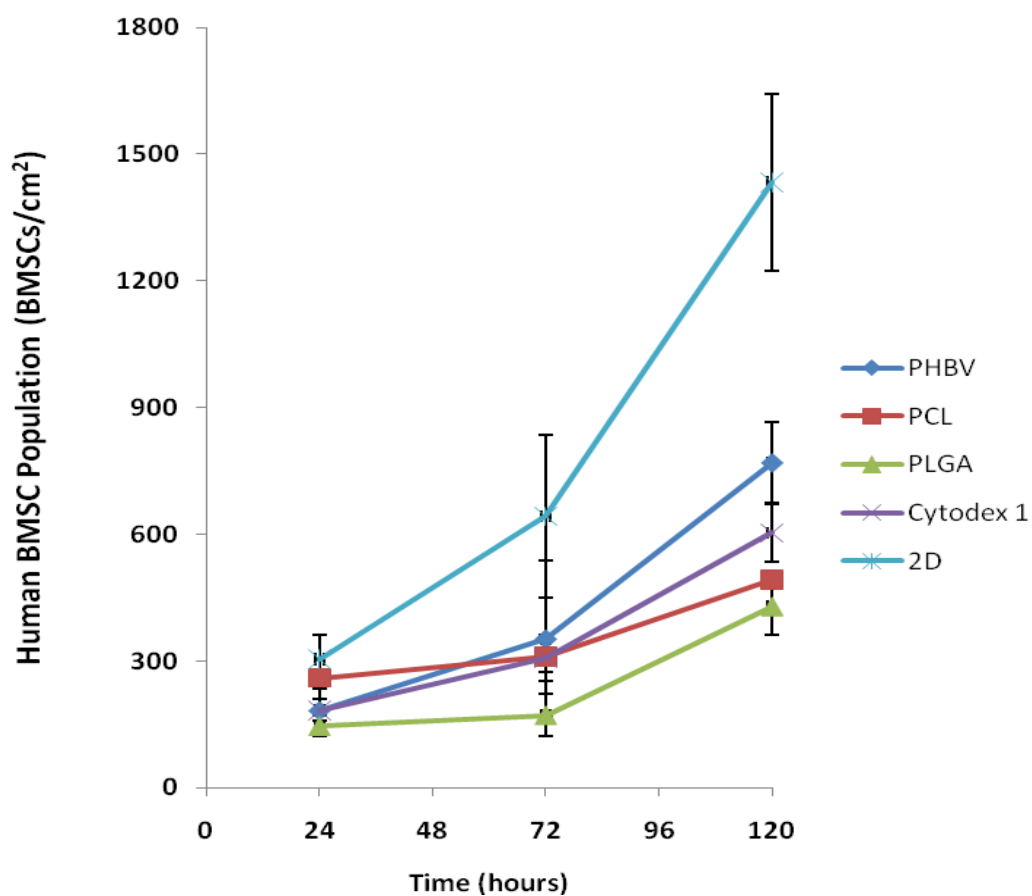


Figure 72: Human BMSC growth (donor 2) on the different scaffold types over a 120-hour period. Note that the seeding density applied was 2000 BMSCs/cm² at time 0 hours.

Growth data for donor 2 (Figure 72, Figure 73 and Figure 74) and donor 3 (Figure 75, Figure 76 and Figure 77) are listed in this section. BMSC growth is superior on PHBV microcarriers as compared to PCL and PLGA microcarriers. No significant difference in growth rates were observed among PHBV, Cytodex 1 and tissue culture plastic (2D).

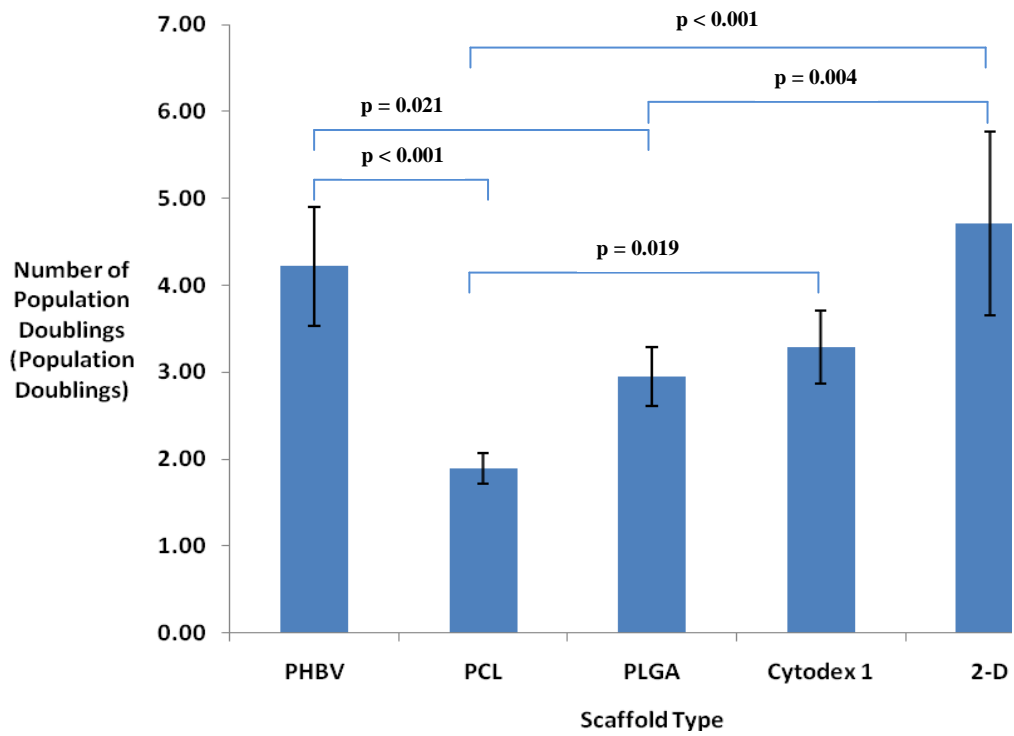


Figure 73: Human BMSC Population Doublings (donor 2) on the scaffold types. The data was calculated utilising BMSC population numbers at time-points 24 and 120 hours.

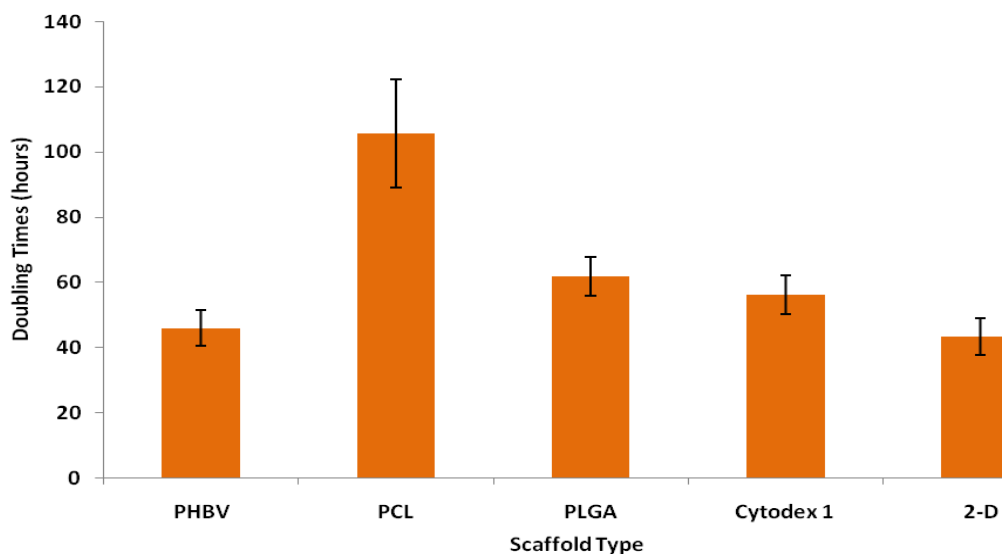


Figure 74: Human BMSC doubling times (donor 2) on the scaffold types. The data was calculated utilising BMSC population numbers at time-points 24 and 120 hours.

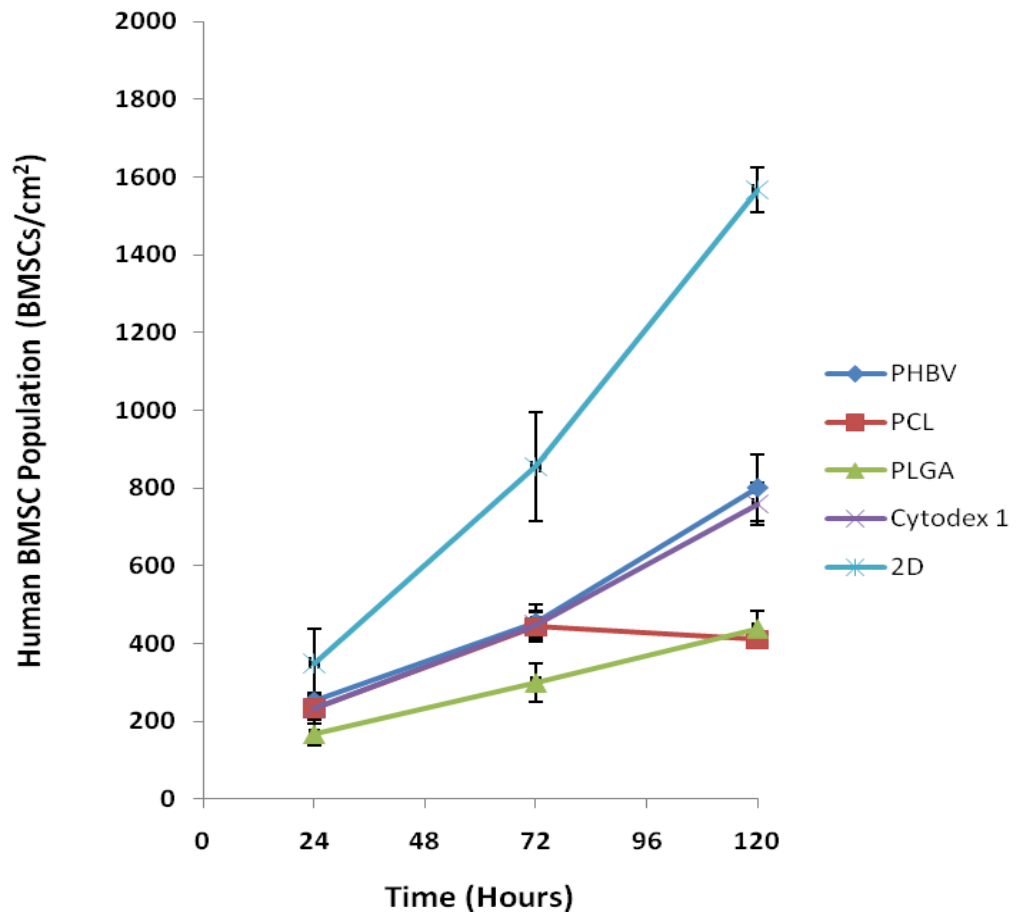


Figure 75: Human BMSC growth (donor 3) on the different scaffold types over a 120-hour period.

Note that the seeding density applied was 2000 BMSCs/cm² at time 0 hours.

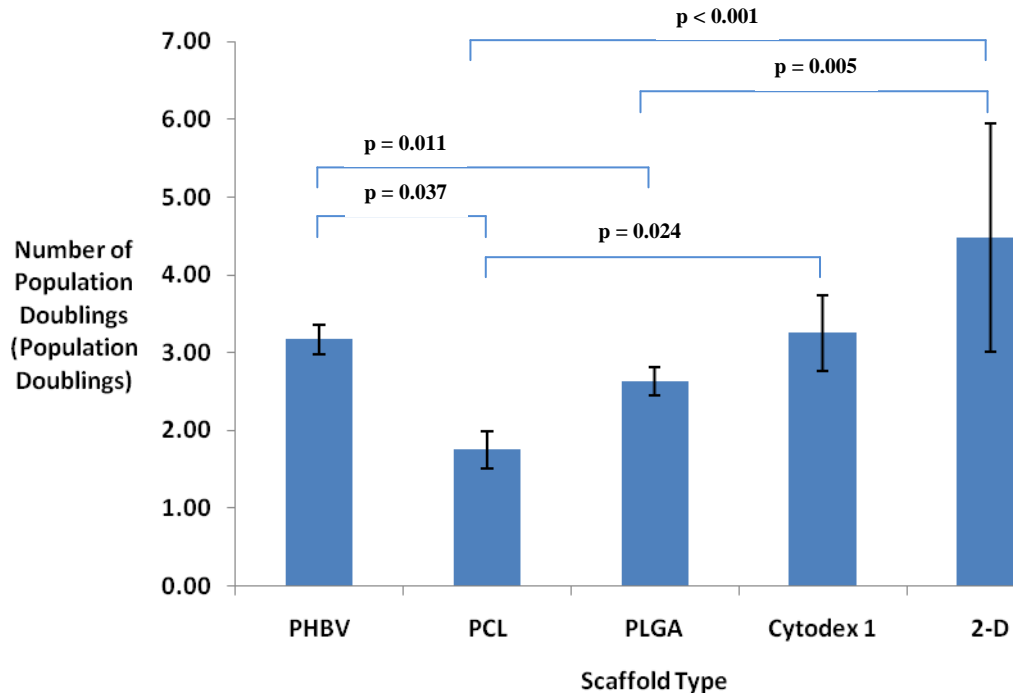


Figure 76: Human BMSC Population Doublings (donor 3) on the scaffold types. The data was calculated utilising BMSC population numbers at time-points 24 and 120 hours.

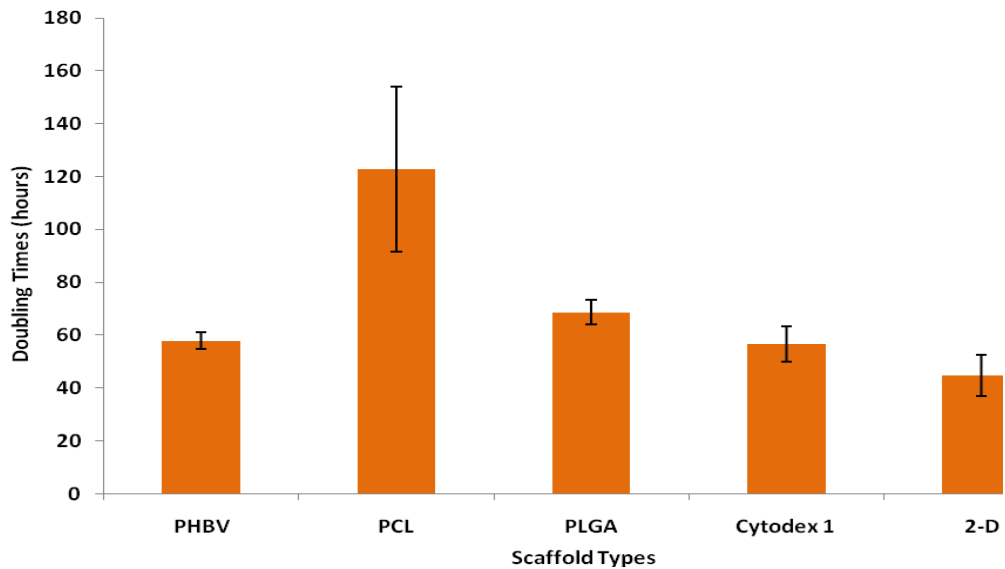


Figure 77: Human BMSC doubling times (donor 3) on the scaffold types. The data was calculated utilising BMSC population numbers at time-points 24 and 120 hours.

8.6 Data for two other donors supplementary to chapter 4

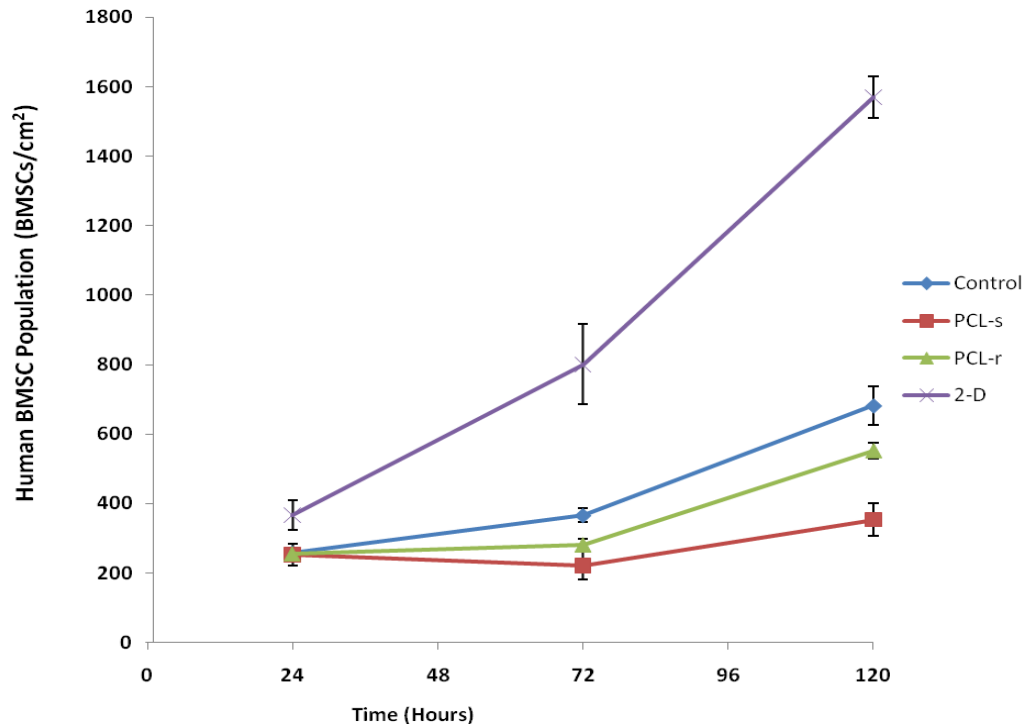


Figure 78: Human BMSC populations (donor 2) on the different scaffold types over a 120-hour period. Cytodex 1 is the 3D control and well-plates are the 2D control. The seeding density of 2000 BMSCs/cm² was applied at time 0 hours.

Growth data for donor 2 (Figure 78, Figure 79 and Figure 80) and donor 3 (Figure 81, Figure 82 and Figure 83) are shown within this section. BMSC growth on PCL-r are superior to PCL-s for all three donors.

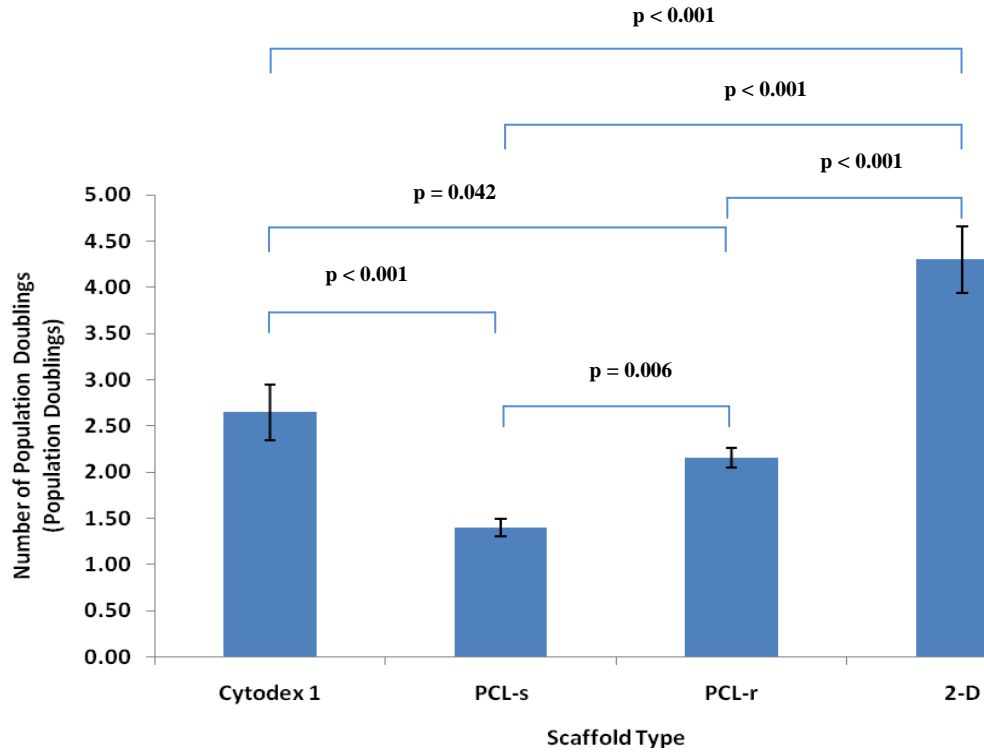


Figure 79: Human BMSC Population Doublings (donor 2) on the scaffold types. The data was calculated utilising BMSC population numbers at time-points 24 and 120 hours.

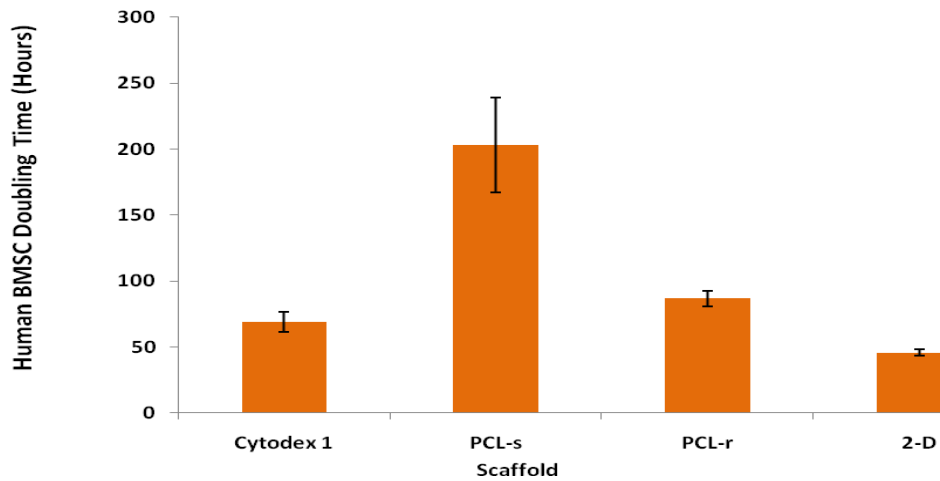


Figure 80: Human BMSC doubling times (donor 2) on the scaffold types. The data was calculated utilising BMSC population numbers at time-points 24 and 120 hours.

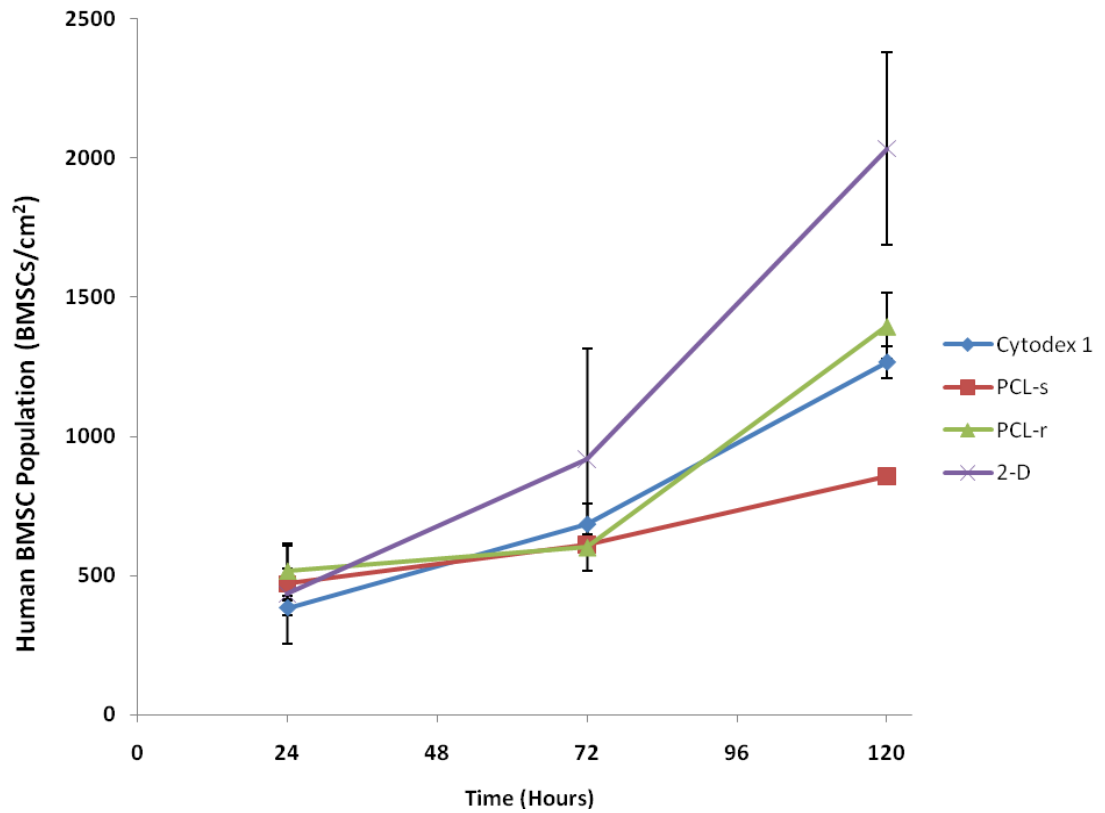


Figure 81: Human BMSC populations (donor 3) on the different scaffold types over a 120-hour period. Cytodex 1 is the 3D control and well-plates are the 2D control. The seeding density of 2000 BMSCs/cm² was applied at time 0 hours.

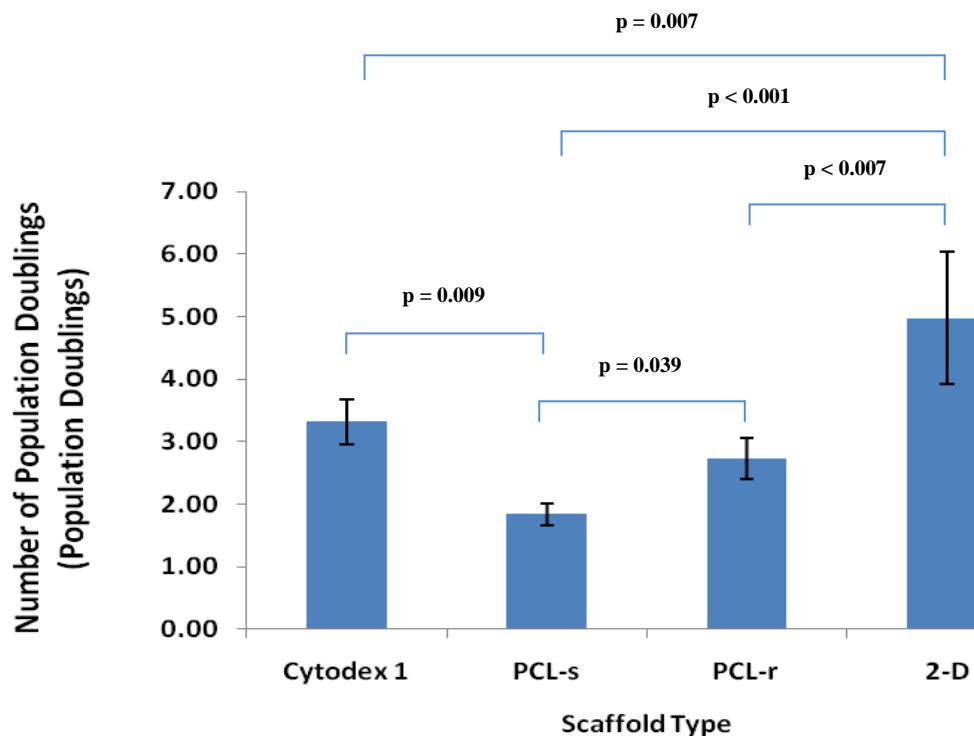


Figure 82: Human BMSC Population Doublings (donor 3) on the scaffold types. The data was calculated utilising BMSC population numbers at time-points 24 and 120 hours.

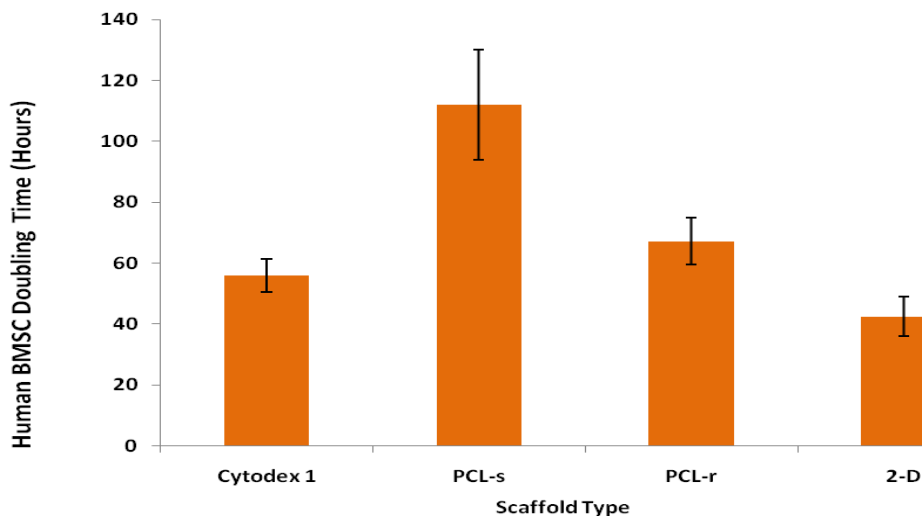


Figure 83: Human BMSC doubling times (donor 3) on the scaffold types. The data was calculated utilising BMSC population numbers at time-points 24 and 120 hours.

8.7 Analysis of raw PIV data

This section supplements the details of the analysis of raw PIV data as described in section 5.3.7. Using the Insight 3G software, for each image of a given impeller position for a given level of the PIV replica ($n = 100$), a “processing mask” (region of interest - ROI) was defined. This was done to ensure that data gathering covered regions where laser scatter was possible (Figure 47). The PIV processor setup included a grid engine (RecursiveNyquistGrid), a correlation engine (FFTCorrelator), a peak engine (GaussianPeak), frame spot starting and final dimensions of 64 and 32 respectively and maximum displacement of $dx = dy = 0.25$. The post-processing was used to validate fluid flow vectors (Raw data → image → processing → post-processing → setup → local validation → method → median test → remove vector field conditioning → start).

Using raw data images, a data list was created by clicking the following on the Insight 3G software: macro editor, “image source”, “calibration”, “masks” (ROI), “kernel processor” to verify information held, “execute”. The large volume of data warranted overnight processing.

Using Matlab, Matlab → Load data → Analysis → Spatial toolbox → Arrow size → Ensemble (for more than one image only) → Contour (Variable e.g. strain rate, + Type e.g. Flood) → Colour bar. In order to calculate the shear stress values (mean and standard deviation), the following Matlab programming was employed, where ProcessedDatalist is the processed overnight data, L = Level, A = Impeller Position and Pos = Positive values:

- L6A=ProcessedDatalist (ProcessedDatalist ~=0);

[This is done to allow Matlab to recognise the numerical figures; this is in the form of an excel spreadsheet of 15,000 cells owing to the size of the ROI; the zero values all fall outside of the ROI; L6A represent the strain rates]

- `viscosity = 0.9325;`

[This defines the viscosity]

- `PosL6A = sqrt(L6A^2);`

[Matlab has recognised approximately 15,000 positive and negative values owing to different directions of fluid. In order to accurately calculate mean and standard deviation values, all negative value are converted into positive values]

- `shearstressL6A = PosL6A.* viscosity;`

[Newton's law of viscosity to calculate shear stress]

- `mean(shearstressL6A);`
- `std(shearstressL6A);`

9 Promotion of Research

9.1 List of Award Shortlists

1. IChemE Awards for innovation and excellence 2010 in association with tce magazine, WSP/CEL Bioprocess Award, “Spinner Flask Bioreactor Shear Stress”, 4th November 2010, Palace Hotel, Manchester, UK, [http://cms.icheme.org/MainWebSite/General-
Baraec56ff8bc017325.aspx?Map=1FA4EFEF3C2B379373F641BFF51673FB](http://cms.icheme.org/MainWebSite/General-
Baraec56ff8bc017325.aspx?Map=1FA4EFEF3C2B379373F641BFF51673FB)

9.2 List of Publications

1. Ramlogan A.S., Gardner C., De Bruijn J.D., The Effect of Spinner Flask Bioreactor Shear on BMSC Growth, *Biotechnology & Bioengineering* (In submission).
2. Ramlogan A.S., More Spin, Less Shear, *TCE: The Chemical Engineer*, Flavell-White C., Forsdyke D. editors, November 2010, Issue 833:58
3. Wilkop T., Ramlogan A.S., Alberts I.L., De Bruijn J.D., Ray A.K., Surface Plasmon Resonance Imaging for Medical and Biosensing, *IEEE Conference Proceedings*, 2009, Vol 1-3:1493-1496.
4. Ramlogan A.S., De Bruijn J.D., Polymeric Microspheres composed of PHBV, PCL and PLGA support the attachment and proliferation of Stem Cells, *Tissue Engineering*. 2007, 13(7):1741.

9.3 List of Presentations (*presenting author)

1. Thomas Wilkop, Anil Shiva Ramlogan, Joost de Bruijn, Ian L. Alberts, Asim K. Ray*, Oral Presentation on “Surface Plasmon Resonance Imaging for Medical and Biosensing”, IEEE Sensors 2009, Christchurch Convention Centre, Christchurch, New Zealand, Oct 25th - 28th 2009.
2. Anil Shiva Ramlogan*, Raheleh Ahmadi*, Inés Jiménez Palomar*, Cheen Peen Khoo*, Kruba Shankar*, Oral Presentation on “Business Plan on BioSmart Technologies Ltd.”, Biotechnology Young Entrepreneurs Scheme (YES) 2009, Jury’s Inn Newcastle, United Kingdom, Oct 21st - 24th 2008.
3. Anil Shiva Ramlogan*, Joost de Bruijn. Poster Presentation on “Bone marrow-derived stromal cell Expansion on Microspheres: The Effect of Surface Microstructure”, World Biomaterials Congress 2008, Amsterdam, The Netherlands, May 28th – June 1st 2008.
4. Anil Shiva Ramlogan*, Joost de Bruijn. Poster Presentation on “Polymeric Microspheres composed of PHBV, PCL and PLGA support the attachment and proliferation of Bone marrow-derived stromal cells”, European Society for Biomaterials 2008, Brighton, United Kingdom, Sep 9th – 13th 2007.
5. Anil Shiva Ramlogan*, Joost de Bruijn. Oral Presentation on “Polymeric Microspheres composed of PHBV, PCL and PLGA support the attachment and proliferation of Bone marrow-derived stromal cells”, Termis-Eu 2008, Brighton, United Kingdom, Sep 4th – 7th 2007.

6. Progentix BV, Queen Mary University of London, Raheleh Ahmadi*, Anil Shiva Ramlogan*, Riemke van Dijkhuizen*, Frank W. Janssen*, Joost D. de Bruijn. Poster Presentation on “Bone Tissue Engineering and Adult Stem Cell Technology” to the London Technology Network at Whitehall, London (United Kingdom), 28th March 2007.
7. Anil Shiva Ramlogan*, Joost de Bruijn. Poster Presentation on “Stem Cell Expansion and Bioreactor Development” to the School of Engineering and Materials Science at Queen Mary, University of London (United Kingdom), 28th November 2006.
8. Anil Shiva Ramlogan*, Joost de Bruijn. Oral Presentation on “Stem Cell Expansion and Bioreactor Development” to the research group of Prof. Dietmar W. Hutmacher (Division of Bioengineering, National University of Singapore) at the Defence Science Organisation (Singapore), 10th November 2006.
9. Anil Shiva Ramlogan*, Joost de Bruijn. Oral Presentation on “Stem Cell Expansion and Bioreactor Development” to the School of Engineering and Materials Science Department of Queen Mary, University of London (United Kingdom), 16th October 2006.

9.4 List of Travel Grant Awards

1. Queen Mary University of London £450
2. Armourers and Brasiers Company £900
3. IOM³ Andrew Carnegie Research Fund £250

4. Armourers and Brasiers Company and Corus £300
5. Armourers and Brasiers Company £400
6. IOM³ Andrew Carnegie Research Fund £250
7. Royal Academy of Engineering International Travel Grant £500
8. Society of Chemical Industry Bursary (Messel Fund) £100

9.5 Student Research Management

1. Supervisor to Ian L. Alberts, Medical Student Research Intern, on experimental research project “Investigation of Cellular Events in Osseointegration by Surface Plasmon Resonance” (July 2009 – August 2009).
2. Supervisor to Daniel Rivilla, B.Eng student, on experimental research project “Mesenchymal stem cell Expansion on Microspheres: The Effect of Surface Microstructure” (August 2007 – April 2008).
3. Supervisor to Noor Latif, B.Eng student, on experimental research project “Mesenchymal stem cell Expansion on Microspheres: The Effect of Surface Microstructure” (August 2007 – April 2008).
4. Supervisor to Amir Taheri, B.Eng student, on experimental research project “Mesenchymal stem cell Expansion on polymeric microspheres” (August 2006 – April 2007).

5. Supervisor to Sharadha Wisidagama, B.Eng student, on experimental research project “Scaffold Development and Cell Expansion in Regenerative Medicine” (August 2006 – April 2007).
6. Supervisor to 11 undergraduates, on problem-based learning group “Designing bio-artificial Cartilage using Embryonic Stem cells and Poly-L-Lactic acid Scaffolds”. (November 2007 – December 2007).
7. Supervisor to 10 undergraduates, Ajayi Bisola, Baloch Faisal Ali, Bhairav Patel, Bukhari Farhat Syeda, Elmadani Esam, Muzaffar Danish, Pirvani Madiha, Siddiqui Adel Zia and Theocharopoulos Antonios, on problem-based learning group “Mesenchymal stem cells for Therapeutic Applications”. (September 2006 – December 2006).
8. Supervisor to 10 undergraduates, Anick Akbar, Saleh Hassan, Alex El-Kheir, Samantha Low, Usman Mahmood, Manoochehr Rasekh, Orly Selouk and Anas Sherif, on problem-based learning group “Expansion of Mesenchymal stem cells for Cell Therapy”. (September 2006 – December 2006).
9. Supervisor to 8 undergraduates, Bisola Ajayi, Bilal Ahmad, Dominique Strasdin, Kalaivani Sekar, Mohammad Akbar, Marayam Tanko, Taranjot Paneser and Thomas White, on problem-based learning group “Strategy for Cartilage Replacement”. (October 2005 – December 2005).

10 References

- Ahmadi R, Burns AJ, de Bruijn JD. 2009. Chitosan-based hydrogels do not induce angiogenesis. *Journal of Tissue Engineering and Regenerative Medicine* 4(4):309-315.
- Ahmadi R, de Bruijn JD. 2008. Biocompatibility and gelation of chitosan-glycerol phosphate hydrogels. *J Biomed Mater Res A* 86(3):824-32.
- Alison MR, Poulosom R, Forbes S, Wright NA. 2002. An introduction to stem cells. *J Pathol* 197(4):419-23.
- Altman DG, Bland JM. 2005. Standard deviations and standard errors. *BMJ* 331(7521):903.
- Ashton BA, Allen TD, Howlett CR, Eaglesom CC, Hattori A, Owen M. 1980. Formation of bone and cartilage by marrow stromal cells in diffusion chambers in vivo. *Clin Orthop Relat Res*(151):294-307.
- Aubin J, Le Sauze N, Bertrand J, Fletcher DF, Xuereb C. 2004. PIV measurements of flow in an aerated tank stirred by a down- and an up-pumping axial flow impeller. *Experimental Thermal and Fluid Science* 28(5):447-456.
- Bakker AD, Soejima K, Klein-Nulend J, Burger EH. 2001. The production of nitric oxide and prostaglandin E-2 by primary bone cells is shear stress dependent. *Journal of Biomechanics* 34(5):671-677.
- Balasundaram G, Sato M, Webster TJ. 2006. Using hydroxyapatite nanoparticles and decreased crystallinity to promote osteoblast adhesion similar to functionalizing with RGD. *Biomaterials* 27(14):2798-805.
- Bancroft GN, Sikavitsas VI, Mikos AG. 2003. Design of a flow perfusion bioreactor system for bone tissue-engineering applications. *Tissue Eng* 9(3):549-54.
- Bancroft GN, Sikavitsas VI, van den Dolder J, Sheffield TL, Ambrose CG, Jansen JA, Mikos AG. 2002. Fluid flow increases mineralized matrix deposition in 3D perfusion culture of marrow stromal osteoblasts in a dose-dependent manner. *Proc Natl Acad Sci U S A* 99(20):12600-5.
- Bartl R, Frisch B. 2003. Normal bone marrow: histology, histochemistry and immunohistochemistry. In: Wickramasinghe SN, McCullough J, editors. *Blood and Bone Marrow Pathology*. 1st ed. London: Elsevier Ltd. p 53-69.
- Bilgen B, Barabino GA. 2007. Location of scaffolds in bioreactors modulates the hydrodynamic environment experienced by engineered tissues. *Biotechnol Bioeng* 98(1):282-94.
- Bilgen B, Sucusky P, Neitzel GP, Barabino GA. 2006. Flow characterization of a wavy-walled bioreactor for cartilage tissue engineering. *Biotechnol Bioeng* 95(6):1009-22.
- Bird A. 2007. Perceptions of epigenetics. *Nature* 447(7143):396-8.
- Bluman A. 2008. The Normal Distribution. In: Bluman A, editor. *Elementary Statistics: A Step by Step Approach A Brief Version*. New York: McGraw-Hill. p 320.
- Both SK, van der Muijsenberg AJ, van Blitterswijk CA, de Boer J, de Bruijn JD. 2007. A rapid and efficient method for expansion of human mesenchymal stem cells. *Tissue Eng* 13(1):3-9.
- Braccini A, Wendt D, Jaquiere C, Jakob M, Heberer M, Kenins L, Wodnar-Filipowicz A, Quarto R, Martin I. 2005. Three-dimensional perfusion culture of human

References

- bone marrow cells and generation of osteoinductive grafts. *Stem Cells* 23(8):1066-72.
- Bruder SP, Jaiswal N, Haynesworth SE. 1997. Growth kinetics, self-renewal, and the osteogenic potential of purified human mesenchymal stem cells during extensive subcultivation and following cryopreservation. *J Cell Biochem* 64(2):278-94.
- Bussolati B, Bruno S, Grange C, Ferrando U, Camussi G. 2008. Identification of a tumor-initiating stem cell population in human renal carcinomas. *Faseb J* 22(10):3696-705.
- Cameron CM, Hu WS, Kaufman DS. 2006. Improved development of human embryonic stem cell-derived embryoid bodies by stirred vessel cultivation. *Biotechnol Bioeng* 94(5):938-48.
- Campbell JJ, Lee DA, Bader DL. 2006. Dynamic compressive strain influences chondrogenic gene expression in human mesenchymal stem cells. *Biorheology* 43(3-4):455-70.
- Cao Y, Vacanti JP, Paige KT, Upton J, Vacanti CA. 1997. Transplantation of chondrocytes utilizing a polymer-cell construct to produce tissue-engineered cartilage in the shape of a human ear. *Plast Reconstr Surg* 100(2):297-302; discussion 303-4.
- Caplan AI. 1991. Mesenchymal stem cells. *J Orthop Res* 9(5):641-50.
- Caplan AI. 1994. The mesengenic process. *Clin Plast Surg* 21(3):429-35.
- Caplan AI. 2005. Review: mesenchymal stem cells: cell-based reconstructive therapy in orthopedics. *Tissue Eng* 11(7-8):1198-211.
- Caplan AI, Bruder SP. 2001. Mesenchymal stem cells: building blocks for molecular medicine in the 21st century. *Trends Mol Med* 7(6):259-64.
- Caplan AI, Syftestad G, Osdoby P. 1983. The development of embryonic bone and cartilage in tissue culture. *Clin Orthop Relat Res*(174):243-63.
- Çatiker E, Gümüşcedderelioglu M, Güner A. 2000. Degradation of PLA, PLGA homo- and copolymers in the presence of serum albumin: a spectroscopic investigation. *Polymer International* 49(7):728-734.
- Cherry RS. 1993. Animal-Cells in Turbulent Fluids - Details of the Physical Stimulus and the Biological Response. *Biotechnology Advances* 11(2):279-299.
- Cherry RS, Kwon KY. 1990. Transient shear stresses on a suspension cell in turbulence. *Biotechnol Bioeng* 36(6):563-71.
- Cherry RS, Papoutsakis ET. 1986. Hydrodynamic Effects on Cells in Agitated Tissue-Culture Reactors. *Bioprocess Engineering* 1(1):29-41.
- Cherry RS, Papoutsakis ET. 1988. Physical mechanisms of cell damage in microcarrier cell culture bioreactors. *Biotechnol Bioeng* 32(8):1001-14.
- Cherry RS, Papoutsakis ET. 1989a. Growth and Death Rates of Bovine Embryonic Kidney-Cells in Turbulent Microcarrier Bioreactors. *Bioprocess Engineering* 4(2):81-89.
- Cherry RS, Papoutsakis ET. 1989b. Modeling of contact-inhibited animal cell growth on flat surfaces and spheres. *Biotechnol Bioeng* 33(3):300-5.
- Chia SM, Lin PC, Quek CH, Yin C, Mao HQ, Leong KW, Xu X, Goh CH, Ng ML, Yu H. 2005. Engineering microenvironment for expansion of sensitive anchorage-dependent mammalian cells. *J Biotechnol* 118(4):434-47.
- Chua LP, Ong KS, Song G. 2008. Study of velocity and shear stress distributions in the impeller passages and the volute of a bio-centrifugal ventricular assist device. *Artif Organs* 32(5):376-87.

References

- Chun KW, Yoo HS, Yoon JJ, Park TG. 2004. Biodegradable PLGA microcarriers for injectable delivery of chondrocytes: effect of surface modification on cell attachment and function. *Biotechnol Prog* 20(6):1797-801.
- Clarotti G, Schue F, Sledz J, Ait Ben Aoumar A, Geckeler KE, Orsetti A, Paleirac G. 1992. Modification of the biocompatible and haemocompatible properties of polymer substrates by plasma-deposited fluorocarbon coatings. *Biomaterials* 13(12):832-40.
- Colter DC, Class R, DiGirolamo CM, Prockop DJ. 2000. Rapid expansion of recycling stem cells in cultures of plastic-adherent cells from human bone marrow. *Proc Natl Acad Sci U S A* 97(7):3213-8.
- Conget PA, Minguell JJ. 1999. Phenotypical and functional properties of human bone marrow mesenchymal progenitor cells. *J Cell Physiol* 181(1):67-73.
- Coulson J, Richardson J. 1999. Flow of Liquids in Pipes and Open Channels. *Chemical Engineering*. 6th ed. Oxford: Butterworth-Heinemann. p 59-62.
- Coulson JM, Richardson JF, Backhurst JR, Harker JH. 1999. Liquid Mixing. In: Coulson JM, Richardson JF, Backhurst JR, Harker JH, editors. *Coulson & Richardson's Chemical Engineering*. 6th ed. Oxford: Butterworth-Heinemann. p 283-285.
- Crotts G, Park TG. 1998. Protein delivery from poly(lactic-co-glycolic acid) biodegradable microspheres: release kinetics and stability issues. *J Microencapsul* 15(6):699-713.
- Croughan MS, Hamel JF, Wang DI. 1988. Effects of microcarrier concentration in animal cell culture. *Biotechnol Bioeng* 32(8):975-82.
- Curran JM, Tang Z, Hunt JA. 2009. PLGA doping of PCL affects the plastic potential of human mesenchymal stem cells, both in the presence and absence of biological stimuli. *J Biomed Mater Res A* 89(1):1-12.
- Czarnecki JS, Lafdi K, Tsonis PA. 2008. A novel approach to control growth, orientation, and shape of human osteoblasts. *Tissue Eng Part A* 14(2):255-65.
- Dai NT, Williamson MR, Khammo N, Adams EF, Coombes AG. 2004. Composite cell support membranes based on collagen and polycaprolactone for tissue engineering of skin. *Biomaterials* 25(18):4263-71.
- Dang SM, Gerecht-Nir S, Chen J, Itskovitz-Eldor J, Zandstra PW. 2004. Controlled, scalable embryonic stem cell differentiation culture. *Stem Cells* 22(3):275-82.
- De Bari C, Dell'Accio F, Tylzanowski P, Luyten FP. 2001. Multipotent mesenchymal stem cells from adult human synovial membrane. *Arthritis Rheum* 44(8):1928-42.
- Degasne I, Baslé MF, Demais V, Huré G, Lesourd M, Grolleau B, Mercier L, Chappard D. 1999. Effects of Roughness, Fibronectin and Vitronectin on Attachment, Spreading, and Proliferation of Human Osteoblast-Like Cells (Saos-2) on Titanium Surfaces. *Calcified Tissue International* 64(6):499-507.
- Deligianni DD, Katsala N, Ladas S, Sotiropoulou D, Amedee J, Missirlis YF. 2001a. Effect of surface roughness of the titanium alloy Ti-6Al-4V on human bone marrow cell response and on protein adsorption. *Biomaterials* 22(11):1241-1251.
- Deligianni DD, Katsala ND, Koutsoukos PG, Missirlis YF. 2001b. Effect of surface roughness of hydroxyapatite on human bone marrow cell adhesion, proliferation, differentiation and detachment strength. *Biomaterials* 22(1):87-96.
- Delorme B, Ringe J, Pontikoglou C, Gaillard J, Langonne A, Sensebe L, Noel D, Jorgensen C, Haupl T, Charbord P. 2009. Specific lineage-priming of bone

- marrow mesenchymal stem cells provides the molecular framework for their plasticity. *Stem Cells* 27(5):1142-51.
- Deng Y, Zhao K, Zhang XF, Hu P, Chen GQ. 2002. Study on the three-dimensional proliferation of rabbit articular cartilage-derived chondrocytes on polyhydroxyalkanoate scaffolds. *Biomaterials* 23(20):4049-56.
- Dominici M, Le Blanc K, Mueller I, Slaper-Cortenbach I, Marini F, Krause D, Deans R, Keating A, Prockop D, Horwitz E. 2006. Minimal criteria for defining multipotent mesenchymal stromal cells. The International Society for Cellular Therapy position statement. *Cytotherapy* 8(4):315-7.
- Doran P. 2002. *Bioprocess Engineering Principles*. London: Academic Press Limited. p 132-383.
- Doyle C, Tanner ET, Bonfield W. 1991. In vitro and in vivo evaluation of polyhydroxybutyrate and of polyhydroxybutyrate reinforced with hydroxyapatite. *Biomaterials* 12(9):841-7.
- Drife JM, BA. 2004. Human Embryogenesis. In: Drife JM, BA., editor. *Clinical Obstetrics and Gynaecology*. 1st ed. London: Elsevier Limited. p 57.
- Dusting J, Sheridan J, Hourigan K. 2006. A fluid dynamics approach to bioreactor design for cell and tissue culture. *Biotechnol Bioeng* 94(6):1196-208.
- Eibl R, Eibl D, Eibl R, Werner S, Eibl D. 2010. Bag Bioreactor Based on Wave-Induced Motion: Characteristics and Applications. *Disposable Bioreactors*: Springer Berlin / Heidelberg. p 55-87.
- Ellis M, Jarman-Smith. M, Chaudhuri J. 2005. Bioreactor Systems for Tissue Engineering: A Four-Dimensional Challenge. In: Chaudhuri JM, AR., editor. *Bioreactors for Tissue Engineering*. Dordrecht: Springer. p 3.
- Ferrari G, Cusella-De Angelis G, Coletta M, Paolucci E, Stornaiuolo A, Cossu G, Mavilio F. 1998. Muscle regeneration by bone marrow-derived myogenic progenitors. *Science* 279(5356):1528-30.
- Fischer EM, Layrolle P, Van Blitterswijk CA, De Bruijn JD. 2003. Bone formation by mesenchymal progenitor cells cultured on dense and microporous hydroxyapatite particles. *Tissue Eng* 9(6):1179-88.
- Fischman J. 1999. How to build a body part. *Time* 153(8):54-5.
- Fok EY, Zandstra PW. 2005. Shear-controlled single-step mouse embryonic stem cell expansion and embryoid body-based differentiation. *Stem Cells* 23(9):1333-42.
- Fong WJ, Tan HL, Choo A, Oh SK. 2005. Perfusion cultures of human embryonic stem cells. *Bioprocess Biosyst Eng* 27(6):381-7.
- Frauenschuh S, Reichmann E, Ibold Y, Goetz PM, Sittinger M, Ringe J. 2007. A microcarrier-based cultivation system for expansion of primary mesenchymal stem cells. *Biotechnol Prog* 23(1):187-93.
- Freedman D, Pisani R, Purves R. 1998. The Average and the Standard Deviation. In: Freedman D, Pisani R, Purves R, editors. *Statistics*. 3rd ed. New York: W. W. Norton & Company, Inc. p 57-77.
- Freshney R. 2000a. Contamination. In: Freshney R, editor. *Culture of Animal Cells: A Manual of Basic Techniques*. 4th ed. New York: Wiley-Liss, Inc. p 285-288.
- Freshney R. 2000b. Culture Vessels. In: Freshney R, editor. *Culture of Animal Cells: A Manual of Basic Techniques*. 4th ed. New York: Wiley-Liss, Inc. p 77-87.
- Freshney R. 2005. Culture of Specific Cell Types. In: Freshney R, editor. *Culture of Animal Cells: A manual of basic techniques*. 5th ed. Hoboken, New Jersey: John Wiley & Sons Inc. p 400.

References

- Friedenstein AJ, Chailakhjan RK, Lalykina KS. 1970. The development of fibroblast colonies in monolayer cultures of guinea-pig bone marrow and spleen cells. *Cell Tissue Kinet* 3(4):393-403.
- Friedenstein AJ, Piatetzky S, II, Petrakova KV. 1966. Osteogenesis in transplants of bone marrow cells. *J Embryol Exp Morphol* 16(3):381-90.
- Gauthaman K, Venugopal JR, Yee FC, Peh GSL, Ramakrishna S, Bongso A. 2009. Nanofibrous substrates support colony formation and maintain stemness of human embryonic stem cells. *Journal of Cellular and Molecular Medicine* 13(9b):3475-3484.
- George W. 1987. Spectroscopic Analysis of Organic Compounds. In: George W, editor. *Infrared Spectroscopy*: Wiley. p 299.
- Gilding D. 1981. Biodegradable polymers. 209 – 232 p.
- Goldstein AS, Juarez TM, Helmke CD, Gustin MC, Mikos AG. 2001. Effect of convection on osteoblastic cell growth and function in biodegradable polymer foam scaffolds. *Biomaterials* 22(11):1279-88.
- Gomes ME, Bossano CM, Johnston CM, Reis RL, Mikos AG. 2006. In vitro localization of bone growth factors in constructs of biodegradable scaffolds seeded with marrow stromal cells and cultured in a flow perfusion bioreactor. *Tissue Eng* 12(1):177-88.
- Gomes ME, Sikavitsas VI, Behravesh E, Reis RL, Mikos AG. 2003. Effect of flow perfusion on the osteogenic differentiation of bone marrow stromal cells cultured on starch-based three-dimensional scaffolds. *J Biomed Mater Res A* 67(1):87-95.
- Goodwin TJ, Prewett TL, Wolf DA, Spaulding GF. 1993a. Reduced shear stress: a major component in the ability of mammalian tissues to form three-dimensional assemblies in simulated microgravity. *J Cell Biochem* 51(3):301-11.
- Goodwin TJ, Schroeder WF, Wolf DA, Moyer MP. 1993b. Rotating-wall vessel coculture of small intestine as a prelude to tissue modeling: aspects of simulated microgravity. *Proc Soc Exp Biol Med* 202(2):181-92.
- Gotherstrom C, Ringden O, Westgren M, Tammik C, Le Blanc K. 2003. Immunomodulatory effects of human foetal liver-derived mesenchymal stem cells. *Bone Marrow Transplant* 32(3):265-72.
- Grellier M, Bareille R, Bourget C, Amedee J. 2009. Responsiveness of human bone marrow stromal cells to shear stress. *J Tissue Eng Regen Med* 3(4):302-9.
- Grove JE, Bruscia E, Krause DS. 2004. Plasticity of bone marrow-derived stem cells. *Stem Cells* 22(4):487-500.
- Hammond TG, Hammond JM. 2001. Optimized suspension culture: the rotating-wall vessel. *Am J Physiol Renal Physiol* 281(1):F12-25.
- Hayflick L. 1979. The cell biology of aging. *J Invest Dermatol* 73(1):8-14.
- Higuera G, Schop D, Janssen F, van Dijkhuizen-Radersma R, van Boxtel T, van Blitterswijk CA. 2009. Quantifying in vitro growth and metabolism kinetics of human mesenchymal stem cells using a mathematical model. *Tissue Eng Part A* 15(9):2653-63.
- Hillsley MV, Frangos JA. 1994. Bone tissue engineering: the role of interstitial fluid flow. *Biotechnol Bioeng* 43(7):573-81.
- Hines WW, Montgomery DC, Goldsman DM, Borrer CM. 2003. Statistics and Sampling Distributions. In: Anderson W, Welter J, editors. *Probability and Statistics in Engineering*. 4th ed. New Jersey: John Wiley & Sons, Inc. p 203.

References

- Hirtenstein M, Clark J, Lindgren G, Vretblad P. 1980. Microcarriers for animal cell culture: a brief review of theory and practice. *Dev Biol Stand* 46:109-16.
- Hooke R. 1667. *Micrographia: or some physiological descriptions of minute bodies made by magnifying glasses : with observations and inquiries thereupon.* London: John Martin. 246 p.
- Hooker BS, Lee JM, An G. 1990. Cultivation of plant cells in a stirred vessel: Effect of impeller design. *Biotechnol Bioeng* 35(3):296-304.
- Horwitz EM, Gordon PL, Koo WK, Marx JC, Neel MD, McNall RY, Muul L, Hofmann T. 2002. Isolated allogeneic bone marrow-derived mesenchymal cells engraft and stimulate growth in children with osteogenesis imperfecta: Implications for cell therapy of bone. *Proc Natl Acad Sci U S A* 99(13):8932-7.
- Hutmacher DW, Schantz T, Zein I, Ng KW, Teoh SH, Tan KC. 2001. Mechanical properties and cell cultural response of polycaprolactone scaffolds designed and fabricated via fused deposition modeling. *J Biomed Mater Res* 55(2):203-16.
- In 't Anker PS, Scherjon SA, Kleijburg-van der Keur C, Noort WA, Claas FH, Willemze R, Fibbe WE, Kanhai HH. 2003. Amniotic fluid as a novel source of mesenchymal stem cells for therapeutic transplantation. *Blood* 102(4):1548-9.
- Jabbarzadeh E, Jiang T, Deng M, Nair LS, Khan YM, Laurencin CT. 2007. Human endothelial cell growth and phenotypic expression on three dimensional poly(lactide-co-glycolide) sintered microsphere scaffolds for bone tissue engineering. *Biotechnol Bioeng* 98(5):1094-102.
- Jackson KA, Mi T, Goodell MA. 1999. Hematopoietic potential of stem cells isolated from murine skeletal muscle. *Proc Natl Acad Sci U S A* 96(25):14482-6.
- Jacobs T. 2001. Full stem ahead. *Newsweek* 137(7):63-5.
- Jaiswal N, Haynesworth SE, Caplan AI, Bruder SP. 1997. Osteogenic differentiation of purified, culture-expanded human mesenchymal stem cells in vitro. *J Cell Biochem* 64(2):295-312.
- Jiang S, Ji X, An L, Jiang B. 2001. Crystallization behavior of PCL in hybrid confined environment. *Polymer* 42(8):3901-3907.
- Jiang Y, Jahagirdar BN, Reinhardt RL, Schwartz RE, Keene CD, Ortiz-Gonzalez XR, Reyes M, Lenvik T, Lund T, Blackstad M and others. 2002. Pluripotency of mesenchymal stem cells derived from adult marrow. *Nature* 418(6893):41-9.
- Jukes J, Both S, Post J, Van Blitterswijk CA, Karperien M, De Boer J. 2008. Stem Cells. In: Van Blitterswijk CA, editor. *Tissue Engineering*. 1st ed. London: Elsevier Inc. p 3.
- Kang B, Kang K, Lee Y. 2005. Biocompatibility and Long-Term Toxicity of InnoPol® Implant, a Biodegradable Polymer Scaffold. *Experimental Animals/ Japanese Association for Laboratory Animal Science* 54(1):37-52.
- Kapur S, Baylink DJ, Lau KH. 2003. Fluid flow shear stress stimulates human osteoblast proliferation and differentiation through multiple interacting and competing signal transduction pathways. *Bone* 32(3):241-51.
- Kaye GWC, Laby TH. 1995. Mechanical Properties of Materials. In: Kaye GWC, Laby TH, editors. *Tables of Physical and Chemical Constants*. 16th ed. Essex: Longman Group. p 52.
- Kim BS, Lee CC, Christensen JE, Huser TR, Chan JW, Tarantal AF. 2008. Growth, differentiation, and biochemical signatures of rhesus monkey mesenchymal stem cells. *Stem Cells Dev* 17(1):185-98.

References

- Kim HJ, Kim UJ, Leisk GG, Bayan C, Georgakoudi I, Kaplan DL. 2007. Bone regeneration on macroporous aqueous-derived silk 3-D scaffolds. *Macromol Biosci* 7(5):643-55.
- Klee D, Höcker H, Eastmond G. 1999. *Advances in Polymer Science*. Berlin Heidelberg: Springer-Verlag Berlin Heidelberg. 67-69 p.
- Kogame M, Matsuo S, Nakatani M, Kurisaki A, Nishitani H, Tsuchida K, Sugino H. 2006. ALK7 is a novel marker for adipocyte differentiation. *J Med Invest* 53(3-4):238-45.
- Koopman R, Schaart G, Hesselink MK. 2001. Optimisation of oil red O staining permits combination with immunofluorescence and automated quantification of lipids. *Histochem Cell Biol* 116(1):63-8.
- Kose GT, Korkusuz F, Korkusuz P, Purali N, Ozkul A, Hasirci V. 2003. Bone generation on PHBV matrices: an in vitro study. *Biomaterials* 24(27):4999-5007.
- Kose GT, Korkusuz F, Ozkul A, Soysal Y, Ozdemir T, Yildiz C, Hasirci V. 2005. Tissue engineered cartilage on collagen and PHBV matrices. *Biomaterials* 26(25):5187-97.
- Kumarasuriyar A, Jackson RA, Grondahl L, Trau M, Nurcombe V, Cool SM. 2005. Poly(beta-hydroxybutyrate-co-beta-hydroxyvalerate) supports in vitro osteogenesis. *Tissue Eng* 11(7-8):1281-95.
- Lagasse E, Connors H, Al-Dhalimy M, Reitsma M, Dohse M, Osborne L, Wang X, Finegold M, Weissman IL, Grompe M. 2000. Purified hematopoietic stem cells can differentiate into hepatocytes in vivo. *Nat Med* 6(11):1229-34.
- Langer R, Vacanti JP. 1993. Tissue engineering. *Science* 260(5110):920-6.
- Langer RS, Vacanti JP. 1999. Tissue engineering: the challenges ahead. *Sci Am* 280(4):86-9.
- Lanza R, Langer R, Vacanti J. 2000. *Principles of Tissue Engineering*. San Diego: Academic Press USA.
- Larson BL, Ylostalo J, Prockop DJ. 2008. Human multipotent stromal cells undergo sharp transition from division to development in culture. *Stem Cells* 26(1):193-201.
- Lee OK, Kuo TK, Chen WM, Lee KD, Hsieh SL, Chen TH. 2004. Isolation of multipotent mesenchymal stem cells from umbilical cord blood. *Blood* 103(5):1669-75.
- Lemare F, Steimberg N, Le Griel C, Demignot S, Adolphe M. 1998. Dedifferentiated chondrocytes cultured in alginate beads: restoration of the differentiated phenotype and of the metabolic responses to interleukin-1beta. *J Cell Physiol* 176(2):303-13.
- Levine EM, Becker Y, Boone CW, Eagle H. 1965. Contact Inhibition, Macromolecular Synthesis, and Polyribosomes in Cultured Human Diploid Fibroblasts. *Proc Natl Acad Sci U S A* 53:350-6.
- Li WJ, Laurencin CT, Caterson EJ, Tuan RS, Ko FK. 2002. Electrospun nanofibrous structure: a novel scaffold for tissue engineering. *J Biomed Mater Res* 60(4):613-21.
- Lincks J, Boyan BD, Blanchard CR, Lohmann CH, Liu Y, Cochran DL, Dean DD, Schwartz Z. 1998. Response of MG63 osteoblast-like cells to titanium and titanium alloy is dependent on surface roughness and composition. *Biomaterials* 19(23):2219-32.

References

- Lohmann CH, Sagun R, Jr., Sylvia VL, Cochran DL, Dean DD, Boyan BD, Schwartz Z. 1999. Surface roughness modulates the response of MG63 osteoblast-like cells to 1,25-(OH)₂D₃ through regulation of phospholipase A₂ activity and activation of protein kinase A. *J Biomed Mater Res* 47(2):139-51.
- Lu L, Mikos A. 1996. The importance of new processing techniques in tissue engineering. *Mater Res Soc Bull* 21:28-32.
- Macdonald JM, Xu A, Kubota H, LeCluye E, Hamilton G, Liu H, Rong Y, Moss N, Lodestro C, Luntz T and others. 2002. Liver Cell Culture. In: Atala A, Lanza RP, editors. *Methods of Tissue Engineering*. California: Elsevier. p 153.
- Majumdar MK, Keane-Moore M, Buyaner D, Hardy WB, Moorman MA, McIntosh KR, Mosca JD. 2003. Characterization and functionality of cell surface molecules on human mesenchymal stem cells. *J Biomed Sci* 10(2):228-41.
- Malda J, Frondoza CG. 2006. Microcarriers in the engineering of cartilage and bone. *Trends Biotechnol* 24(7):299-304.
- Malm T, Bowald S, Bylock A, Busch C. 1992. Prevention of postoperative pericardial adhesions by closure of the pericardium with absorbable polymer patches. An experimental study. *J Thorac Cardiovasc Surg* 104(3):600-7.
- Malm T, Bowald S, Bylock A, Busch C, Saldeen T. 1994. Enlargement of the right ventricular outflow tract and the pulmonary artery with a new biodegradable patch in transannular position. *Eur Surg Res* 26(5):298-308.
- Marletta G, Ciapetti G, Satriano C, Perut F, Salerno M, Baldini N. 2007. Improved osteogenic differentiation of human marrow stromal cells cultured on ion-induced chemically structured poly-epsilon-caprolactone. *Biomaterials* 28(6):1132-40.
- Martin JY, Schwartz Z, Hummert TW, Schraub DM, Simpson J, Lankford J, Jr., Dean DD, Cochran DL, Boyan BD. 1995. Effect of titanium surface roughness on proliferation, differentiation, and protein synthesis of human osteoblast-like cells (MG63). *J Biomed Mater Res* 29(3):389-401.
- Meijer GJ, de Bruijn JD, Koole R, van Blitterswijk CA. 2007. Cell-based bone tissue engineering. *PLoS Med* 4(2):e9.
- Meisenberg G, Simmons WH. 2006a. Carbohydrate Metabolism. In: Stibbe A, Gruliow R, editors. *Principles of Medical Biochemistry*. 2nd ed. Philadelphia: Mosby Elsevier. p 407-409.
- Meisenberg G, Simmons WH. 2006b. Glycolysis, Tricarboxylic Acid Cycle, and Oxidative Phosphorylation. In: Stibbe A, Gruliow R, editors. *Principles of Medical Biochemistry*. 2nd ed. Philadelphia: Mosby Elsevier. p 383.
- Melton DA, Cowan C. 2004. "Stemness": Definitions, Criteria and Standards. In: Lanza R, Gearhart J, Hogan B, Melton D, Pedersen R, Thomson J, West M, editors. *Handbook of Stem Cells*. Burlington, USA: Elsevier Inc. p xxv-xxxi.
- Mendes SC, Van Den Brink I, De Bruijn JD, Van Blitterswijk CA. 1998. In vivo bone formation by human bone marrow cells: effect of osteogenic culture supplements and cell densities. *J Mater Sci Mater Med* 9(12):855-8.
- Micheletti M, Yianneskis M. 2004. Study of fluid velocity characteristics in stirred solid-liquid suspensions with a refractive index matching technique. *Proceedings of the Institution of Mechanical Engineers Part E-Journal of Process Mechanical Engineering* 218(E4):191-204.
- Moioli EK, Hong L, Mao JJ. 2007. Inhibition of osteogenic differentiation of human mesenchymal stem cells. *Wound Repair Regen* 15(3):413-21.

References

- Moore GF, Saunders SM. 1998. The search for Biodegradable Polymers. Shropshire: iSmithers Rapra Publishing. Report nr 1859571182. 14-16 p.
- Moore KA, Lemischka IR. 2006. Stem cells and their niches. *Science* 311(5769):1880-5.
- Mueller S, Llewellyn EW, Mader HM. 2010. The rheology of suspensions of solid particles. *Proceedings of the Royal Society a-Mathematical Physical and Engineering Sciences* 466(2116):1201-1228.
- Muschler GF, Nakamoto C, Griffith LG. 2004. Engineering principles of clinical cell-based tissue engineering. *J Bone Joint Surg Am* 86-A(7):1541-58.
- Nakanishi K. 1962a. Band Positions and Intensity. In: Nakanishi K, editor. *Infrared Absorption Spectroscopy*. Tokyo: Nankodo Company Limited. p 44.
- Nakanishi K. 1962b. Tables of Characteristic Frequencies. In: Nakanishi K, editor. *Infrared Absorption Spectroscopy*. Tokyo: Nankodo Company Limited. p 20.
- Nakanishi K, and Solomon, P.H. 1977a. Tables of Characteristic Frequencies. *Infrared Absorption Spectroscopy*. San Francisco: Holden-Day, Inc. p 31.
- Nakanishi K, and Solomon, P.H. 1977b. Tables of Characteristic Frequencies. *Infrared Absorption Spectroscopy*. San Francisco: Holden-Day, Inc. p 14.
- Neuhuber B, Swanger SA, Howard L, Mackay A, Fischer I. 2008. Effects of plating density and culture time on bone marrow stromal cell characteristics. *Exp Hematol* 36(9):1176-85.
- Noth U, Osyczka AM, Tuli R, Hickok NJ, Danielson KG, Tuan RS. 2002. Multilineage mesenchymal differentiation potential of human trabecular bone-derived cells. *J Orthop Res* 20(5):1060-9.
- Odabas S, Sayar F, Güven G, Yanıkkaya-Demirel G, Piskin E. 2008. Separation of mesenchymal stem cells with magnetic nanosorbents carrying CD105 and CD73 antibodies in flow-through and batch systems. *Journal of Chromatography B* 861(1):74-80.
- Ohlstein B, Kai T, Decotto E, Spradling A. 2004. The stem cell niche: theme and variations. *Curr Opin Cell Biol* 16(6):693-9.
- Osdoby P, Caplan AI. 1979. Osteogenesis in cultures of limb mesenchymal cells. *Dev Biol* 73(1):84-102.
- Osdoby P, Caplan AI. 1981. Characterization of a bone-specific alkaline phosphatase in chick limb mesenchymal cell cultures. *Dev Biol* 86(1):136-46.
- Papoutsakis ET. 1991. Fluid-mechanical damage of animal cells in bioreactors. *Trends Biotechnol* 9(12):427-37.
- Park A, Cima LG. 1996. In vitro cell response to differences in poly-L-lactide crystallinity. *J Biomed Mater Res* 31(1):117-30.
- Park A, Wu B, Griffith LG. 1998. Integration of surface modification and 3D fabrication techniques to prepare patterned poly(L-lactide) substrates allowing regionally selective cell adhesion. *J Biomater Sci Polym Ed* 9(2):89-110.
- Pitt C, Andrady A, Bao Y, Sarnuei N. 1987. Estimation of the rate of drug diffusion in polymers. *American Chemical Society* 348:49-77.
- Pittenger MF, Mackay AM, Beck SC, Jaiswal RK, Douglas R, Mosca JD, Moorman MA, Simonetti DW, Craig S, Marshak DR. 1999. Multilineage potential of adult human mesenchymal stem cells. *Science* 284(5411):143-7.
- Poole AR, Kojima T, Yasuda T, Mwale F, Kobayashi M, Lavery S. 2001. Composition and structure of articular cartilage: a template for tissue repair. *Clin Orthop Relat Res*(391 Suppl):S26-33.

References

- Provin C, Takano K, Sakai Y, Fujii T, Shirakashi R. 2008. A method for the design of 3D scaffolds for high-density cell attachment and determination of optimum perfusion culture conditions. *J Biomech* 41(7):1436-49.
- Qiu Q, Ducheyne P, Gao H, Ayyaswamy P. 1998. Formation and differentiation of three-dimensional rat marrow stromal cell culture on microcarriers in a rotating-wall vessel. *Tissue Eng* 4(1):19-34.
- Raffel M, Willert C, Wereley S, Kompenhans J. 2007. Particle Image Velocimetry. Raffel M, Willert C, Wereley S, Kompenhans J, editors. Berlin: Springer. 448 p.
- Rai B, Teoh SH, Ho KH, Hutmacher DW, Cao T, Chen F, Yacob K. 2004. The effect of rhBMP-2 on canine osteoblasts seeded onto 3D bioactive polycaprolactone scaffolds. *Biomaterials* 25(24):5499-506.
- Reh TA, Nagy T, Gretton H. 1987. Retinal pigmented epithelial cells induced to transdifferentiate to neurons by laminin. *Nature* 330(6143):68-71.
- Ren T, Ren J, Jia X, Pan K. 2005. The bone formation in vitro and mandibular defect repair using PLGA porous scaffolds. *J Biomed Mater Res A* 74(4):562-9.
- Riddle RC, Taylor AF, Genetos DC, Donahue HJ. 2006. MAP kinase and calcium signaling mediate fluid flow-induced human mesenchymal stem cell proliferation. *Am J Physiol Cell Physiol* 290(3):C776-84.
- Russo VEA, Martienssen RA, Riggs AD. 1996. Epigenetic Mechanisms of Gene Regulation. Russo VEA, Martienssen RA, Riggs AD, editors. New York: Cold Spring Harbor Laboratory Press. 692 p.
- Saito T, Tomita K, Juni K, Ooba K. 1991. In vivo and in vitro degradation of poly(3-hydroxybutyrate) in rat. *Biomaterials* 12(3):309-12.
- Salgado AJ, Coutinho OP, Reis RL. 2004. Bone tissue engineering: state of the art and future trends. *Macromol Biosci* 4(8):743-65.
- Salingcarnboriboon R, Yoshitake H, Tsuji K, Obinata M, Amagasa T, Nifuji A, Noda M. 2003. Establishment of tendon-derived cell lines exhibiting pluripotent mesenchymal stem cell-like property. *Exp Cell Res* 287(2):289-300.
- Saunders MM, You J, Zhou Z, Li Z, Yellowley CE, Kunze EL, Jacobs CR, Donahue HJ. 2003. Fluid flow-induced prostaglandin E2 response of osteoblastic ROS 17/2.8 cells is gap junction-mediated and independent of cytosolic calcium. *Bone* 32(4):350-356.
- Sawae Y, Shelton JC, Bader DL, Knight MM. 2004. Confocal analysis of local and cellular strains in chondrocyte-agarose constructs subjected to mechanical shear. *Ann Biomed Eng* 32(6):860-70.
- Schlaeppli JM, Henke M, Mahnke M, Hartmann S, Schmitz R, Pouliquen Y, Kerins B, Weber E, Kolbinger F, Kocher HP. 2006. A semi-automated large-scale process for the production of recombinant tagged proteins in the Baculovirus expression system. *Protein Expr Purif* 50(2):185-95.
- Schofield R. 1978. The relationship between the spleen colony-forming cell and the haemopoietic stem cell. *Blood Cells* 4(1-2):7-25.
- Schop D, Janssen FW, Borgart E, de Bruijn JD, van Dijkhuizen-Radersma R. 2008. Expansion of mesenchymal stem cells using a microcarrier-based cultivation system: growth and metabolism. *J Tissue Eng Regen Med* 2(2-3):126-35.
- Schop D, Janssen FW, van Rijn LD, Fernandes H, Bloem RM, de Bruijn JD, van Dijkhuizen-Radersma R. 2009a. Growth, metabolism, and growth inhibitors of mesenchymal stem cells. *Tissue Eng Part A* 15(8):1877-86.
- Schop D, van Dijkhuizen-Radersma R, Borgart E, Janssen FW, Rozemuller H, Prins HJ, de Bruijn JD. 2009b. Expansion of human mesenchymal stromal cells on

References

- microcarriers: growth and metabolism. *Journal of Tissue Engineering and Regenerative Medicine* 4(2):131-140.
- Schroeder M, Niebruegge S, Werner A, Willbold E, Burg M, Ruediger M, Field LJ, Lehmann J, Zweigerdt R. 2005. Differentiation and lineage selection of mouse embryonic stem cells in a stirred bench scale bioreactor with automated process control. *Biotechnol Bioeng* 92(7):920-33.
- Sekiya I, Larson BL, Smith JR, Pochampally R, Cui JG, Prockop DJ. 2002. Expansion of human adult stem cells from bone marrow stroma: conditions that maximize the yields of early progenitors and evaluate their quality. *Stem Cells* 20(6):530-41.
- Sen A, Kallos MS, Behie LA. 2002. Expansion of mammalian neural stem cells in bioreactors: effect of power input and medium viscosity. *Brain Res Dev Brain Res* 134(1-2):103-13.
- Senuma Y, Franceschin S, Hilborn JG, Tissieres P, Bisson I, Frey P. 2000. Bioresorbable microspheres by spinning disk atomization as injectable cell carrier: from preparation to in vitro evaluation. *Biomaterials* 21(11):1135-44.
- Shao X, Goh JC, Hutmacher DW, Lee EH, Zigang G. 2006. Repair of large articular osteochondral defects using hybrid scaffolds and bone marrow-derived mesenchymal stem cells in a rabbit model. *Tissue Eng* 12(6):1539-51.
- Shen FH, Zeng Q, Lv Q, Choi L, Balian G, Li X, Laurencin CT. 2006. Osteogenic differentiation of adipose-derived stromal cells treated with GDF-5 cultured on a novel three-dimensional sintered microsphere matrix. *Spine J* 6(6):615-23.
- Shepard N, Mitchell N. 1976. The localization of proteoglycan by light and electron microscopy using safranin O. A study of epiphyseal cartilage. *J Ultrastruct Res* 54(3):451-60.
- Sikavitsas VI, Bancroft GN, Holtorf HL, Jansen JA, Mikos AG. 2003. Mineralized matrix deposition by marrow stromal osteoblasts in 3D perfusion culture increases with increasing fluid shear forces. *Proc Natl Acad Sci U S A* 100(25):14683-8.
- Sikavitsas VI, Bancroft GN, Mikos AG. 2002. Formation of three-dimensional cell/polymer constructs for bone tissue engineering in a spinner flask and a rotating wall vessel bioreactor. *J Biomed Mater Res* 62(1):136-48.
- Sittinger M, Reitzel D, Dauner M, Hierlemann H, Hammer C, Kastenbauer E, Planck H, Burmester GR, Bujia J. 1996. Resorbable polyesters in cartilage engineering: affinity and biocompatibility of polymer fiber structures to chondrocytes. *J Biomed Mater Res* 33(2):57-63.
- Skalak R, Fox C. *Tissue Engineering*. In: Skalak R, Fox C, editors; 1988; Lake Tahoe, California, USA. Alan R Liss Inc. p 343.
- Slack JM, Tosh D. 2001. Transdifferentiation and metaplasia--switching cell types. *Curr Opin Genet Dev* 11(5):581-6.
- Slayton W, Spangrude G. 2004. Adult Stem Cell Plasticity. In: Turksen K, editor. *Adult Stem Cells*. Totowa, New Jersey: Humana Press Inc. p 5.
- Smiler D, Soltan M, Albitar M. 2008. Toward the identification of mesenchymal stem cells in bone marrow and peripheral blood for bone regeneration. *Implant Dent* 17(3):236-47.
- Somerscales EFC, Papyrin AN, Soloukin RI. 1981. Tracer Methods. In: Emrich RJ, editor. *Fluid Dynamics*. London: Academic Press, Inc. (London) LTD. p 1-64.
- Stathopoulos NA, Hellums JD. 1985. Shear stress effects on human embryonic kidney cells in Vitro. *Biotechnol Bioeng* 27(7):1021-6.

References

- Stiehler M, Bunker C, Baatrup A, Lind M, Kassem M, Mygind T. 2009. Effect of dynamic 3-D culture on proliferation, distribution, and osteogenic differentiation of human mesenchymal stem cells. *J Biomed Mater Res A* 89(1):96-107.
- Storrie H, Stupp SI. 2005. Cellular response to zinc-containing organoapatite: an in vitro study of proliferation, alkaline phosphatase activity and biomineralization. *Biomaterials* 26(27):5492-9.
- Sucosky P, Osorio DF, Brown JB, Neitzel GP. 2004. Fluid mechanics of a spinner-flask bioreactor. *Biotechnol Bioeng* 85(1):34-46.
- Takahashi M, Kamei Y, Ezaki O. 2005. Mest/Peg1 imprinted gene enlarges adipocytes and is a marker of adipocyte size. *Am J Physiol Endocrinol Metab* 288(1):E117-24.
- Tang XJ, Wu QY. 2006. Mesenchymal stem cellular adhesion and cytotoxicity study of random biopolyester scaffolds for tissue engineering. *J Mater Sci Mater Med* 17(7):627-32.
- Tepliashin AS, Chupikova NI, Korzhikova SV, Sharifullina SZ, Rostovskaia MS, Topchiashvili ZA, Savchenkova IP. 2005. [Comparative analysis of cell populations with a phenotype similar to that of mesenchymal stem cells derived from subcutaneous fat]. *Tsitologiya* 47(7):637-43.
- Terada N, Hamazaki T, Oka M, Hoki M, Mastalerz DM, Nakano Y, Meyer EM, Morel L, Petersen BE, Scott EW. 2002. Bone marrow cells adopt the phenotype of other cells by spontaneous cell fusion. *Nature* 416(6880):542-5.
- Tewes F, Boury F, Benoit J. 2006. Biodegradable Microspheres: Advances in Production Technology. In: Benita S, editor. *Microencapsulation*. 2nd ed. Boca Raton, Florida: Taylor & Francis Group, LLC. p 31.
- Thissen H, Chang KY, Tebb TA, Tsai WB, Glattauer V, Ramshaw JA, Werkmeister JA. 2006. Synthetic biodegradable microparticles for articular cartilage tissue engineering. *J Biomed Mater Res A* 77(3):590-8.
- Till JE, McCulloch EA, Siminovitch L. 1964. A Stochastic Model of Stem Cell Proliferation, Based on the Growth of Spleen Colony-Forming Cells. *Proc Natl Acad Sci U S A* 51:29-36.
- Tonomura A, Sumita Y, Ando Y, Iejima D, Kagami H, Honda MJ, Ueda M. 2007. Differential inducibility of human and porcine dental pulp-derived cells into odontoblasts. *Connect Tissue Res* 48(5):229-38.
- Uematsu K, Hattori K, Ishimoto Y, Yamauchi J, Habata T, Takakura Y, Ohgushi H, Fukuchi T, Sato M. 2005. Cartilage regeneration using mesenchymal stem cells and a three-dimensional poly-lactic-glycolic acid (PLGA) scaffold. *Biomaterials* 26(20):4273-9.
- Vacanti CA. 2006. History of tissue engineering and a glimpse into its future. *Tissue Eng* 12(5):1137-42.
- van den Dolder J, Bancroft GN, Sikavitsas VI, Spauwen PH, Jansen JA, Mikos AG. 2003. Flow perfusion culture of marrow stromal osteoblasts in titanium fiber mesh. *J Biomed Mater Res A* 64(2):235-41.
- van Dijkhuizen-Radersma R, Moroni L, van Apeldoorn A, Zhang Z, Grijpma D. 2008. Degradable Polymers for Tissue Engineering. In: Van Blitterswijk CA, editor. *Tissue Engineering*. 1st ed. London: Elsevier Inc. p 201-204.
- Van Exan RJ, Hardy MH. 1980. A spatial relationship between innervation and the early differentiation of vibrissa follicles in the embryonic mouse. *J Anat* 131(Pt 4):643-56.

References

- Venkat RV, Stock LR, Chalmers JJ. 1996. Study of hydrodynamics in microcarrier culture spinner vessels: A particle tracking velocimetry approach. *Biotechnol Bioeng* 49(4):456-66.
- Visser S, Hergenrother R, Cooper S. 1996. Polymers. In: Ratner BD HA, Schoen FJ, Lemons JE, editor. *Biomaterials Science*. San Diego: Academic Press, USA. p 484.
- von der Mark K, Gauss V, von der Mark H, Muller P. 1977. Relationship between cell shape and type of collagen synthesised as chondrocytes lose their cartilage phenotype in culture. *Nature* 267(5611):531-2.
- Waddington CH. 1962. *Principles of Embryology*. Waddington CH, editor. Norwich: Jarrold and Sons Ltd. 510 p.
- Waddington CH. 1966. *Principles of Development and Differentiation*. Giles NH, Kenworthy W, Torrey JG, editors. Ontario, Canada: The Macmillan Company. 115 p.
- Wan C, He Q, Li G. 2006. Allogenic peripheral blood derived mesenchymal stem cells (MSCs) enhance bone regeneration in rabbit ulna critical-sized bone defect model. *J Orthop Res* 24(4):610-8.
- Wan Y, Qu X, Lu J, Zhu C, Wan L, Yang J, Bei J, Wang S. 2004. Characterization of surface property of poly(lactide-co-glycolide) after oxygen plasma treatment. *Biomaterials* 25(19):4777-83.
- Wang L, Chaw CS, Yang YY, Mochhala SM, Zhao B, Ng S, Heller J. 2004. Preparation, characterization, and in vitro evaluation of physostigmine-loaded poly(ortho ester) and poly(ortho ester)/poly(D,L-lactide-co-glycolide) blend microspheres fabricated by spray drying. *Biomaterials* 25(16):3275-82.
- Weber C, Pohl S, Portner R, Wallrapp C, Kassem M, Geigle P, Czermak P. 2007. Expansion and Harvesting of hMSC-TERT. *Open Biomed Eng J* 1:38-46.
- Westerweel J. 1994. Efficient Detection of Spurious Vectors in Particle Image Velocimetry Data. *Experiments in Fluids* 16(3-4):236-247.
- Wieland M, Sittig, C., Brunette, M., Textor, M., Spencer, N.D. 1999. Measurement and Evaluation of the Chemical Composition and Topography of Titanium Implant Surfaces. In: Davies JE, editor. *Bone Engineering*. 1st ed. Toronto: em squared incorporated. p 172.
- Xin X, Hussain M, Mao JJ. 2007. Continuing differentiation of human mesenchymal stem cells and induced chondrogenic and osteogenic lineages in electrospun PLGA nanofiber scaffold. *Biomaterials* 28(2):316-25.
- Yagmurlu MF, Korkusuz F, Gursel I, Korkusuz P, Ors U, Hasirci V. 1999. Sulbactam-cefoperazone polyhydroxybutyrate-co-hydroxyvalerate (PHBV) local antibiotic delivery system: in vivo effectiveness and biocompatibility in the treatment of implant-related experimental osteomyelitis. *J Biomed Mater Res* 46(4):494-503.
- Yan Chen GYaQC. 2002. Solid-state NMR study on the structure and mobility of the noncrystalline region of poly(3-hydroxybutyrate) and poly(3-hydroxybutyrate-co-3-hydroxyvalerate). *Polymer* 43(7):2095.
- Yang Y-Y, Chung T-S, Bai X-L, Chan W-K. 2000. Effect of preparation conditions on morphology and release profiles of biodegradable polymeric microspheres containing protein fabricated by double-emulsion method. *Chemical Engineering Science* 55(12):2223-2236.
- Yang YY, Chung TS, Ng NP. 2001. Morphology, drug distribution, and in vitro release profiles of biodegradable polymeric microspheres containing protein fabricated

- by double-emulsion solvent extraction/evaporation method. *Biomaterials* 22(3):231-41.
- Yin T, Li L. 2006. The stem cell niches in bone. *J Clin Invest* 116(5):1195-201.
- Ying QL, Nichols J, Evans EP, Smith AG. 2002. Changing potency by spontaneous fusion. *Nature* 416(6880):545-8.
- You J, Reilly GC, Zhen X, Yellowley CE, Chen Q, Donahue HJ, Jacobs CR. 2001. Osteopontin gene regulation by oscillatory fluid flow via intracellular calcium mobilization and activation of mitogen-activated protein kinase in MC3T3-E1 osteoblasts. *J Biol Chem* 276(16):13365-71.
- Zeng L, Xiao Q, Margariti A, Zhang Z, Zampetaki A, Patel S, Capogrossi MC, Hu Y, Xu Q. 2006. HDAC3 is crucial in shear- and VEGF-induced stem cell differentiation toward endothelial cells. *J Cell Biol* 174(7):1059-69.
- Zeng L, Zhang Y, Chien S, Liu X, Shyy JY. 2003. The role of p53 deacetylation in p21Waf1 regulation by laminar flow. *J Biol Chem* 278(27):24594-9.
- Zhao F, Chella R, Ma T. 2007. Effects of shear stress on 3-D human mesenchymal stem cell construct development in a perfusion bioreactor system: Experiments and hydrodynamic modeling. *Biotechnol Bioeng* 96(3):584-95.
- Zhao F, Ma T. 2005. Perfusion bioreactor system for human mesenchymal stem cell tissue engineering: dynamic cell seeding and construct development. *Biotechnol Bioeng* 91(4):482-93.
- Zheng Z, Bei FF, Tian HL, Chen GQ. 2005. Effects of crystallization of polyhydroxyalkanoate blend on surface physicochemical properties and interactions with rabbit articular cartilage chondrocytes. *Biomaterials* 26(17):3537-48.
- Zhu XH, Gan SK, Wang CH, Tong YW. 2007a. Proteins combination on PHBV microsphere scaffold to regulate Hep3B cells activity and functionality: a model of liver tissue engineering system. *J Biomed Mater Res A* 83(3):606-16.
- Zhu XH, Wang C-H, Tong YW. 2007b. Growing tissue-like constructs with Hep3B/HepG2 liver cells on PHBV microspheres of different sizes. *Journal of Biomedical Materials Research Part B: Applied Biomaterials* 82B(1):7-16.
- Zhu XH, Wang CH, Tong YW. 2009. In vitro characterization of hepatocyte growth factor release from PHBV/PLGA microsphere scaffold. *J Biomed Mater Res A* 89(2):411-23.
- Zimmermann S, Voss M, Kaiser S, Kapp U, Waller CF, Martens UM. 2003. Lack of telomerase activity in human mesenchymal stem cells. *Leukemia* 17(6):1146-9.
- Zitoun KB, Sastry SK, Guezennec Y. 2001. Investigation of three dimensional interstitial velocity, solid motion, and orientation in solid-liquid flow using particle tracking velocimetry. *Int J Multiphase Flow* 27(8):1397-1414.
- Zuk PA, Zhu M, Ashjian P, De Ugarte DA, Huang JI, Mizuno H, Alfonso ZC, Fraser JK, Benhaim P, Hedrick MH. 2002. Human adipose tissue is a source of multipotent stem cells. *Mol Biol Cell* 13(12):4279-95.